DOTTORATO DI RICERCA IN CHIMICA

Convenzione tra
UNIVERSITÀ DEGLI STUDI DI TRIESTE
e
UNIVERSITÀ CA' FOSCARI DI VENEZIA

CICLO XXX

Development of titanium dioxide based photocatalytic systems for CO_2 photoreduction

Settore scientifico-disciplinare: **CHIM/04**

DOTTORANDO
ALBERTO OLIVO

COORDINATORE
PROF. MAURO STENER

SUPERVISORE DI TESI
PROF. MICHELA SIGNORETTO

CO-SUPERVISORE DI TESI
DOTT. ELENA GHEDINI

ANNO ACCADEMICO 2016/2017

Ever tried
Ever fail
No matter
Try again
Fail again
Fail better

Samuel Becket

Summary

1 General Introduction

1.1 Environmental Issues

1.1.1 Atmosphere and greenhouse effect

The bond between mankind and its environment was, and still is, an extremely important feature of human history. In fact, throughout its evolution, earth produced the perfect conditions for life to flourish and mankind to thrive: billions of years ago, geological activity enriched the most superficial layers of atmosphere with relatively heavy gases (steam, carbon dioxide and ammonia), substrates for photosynthesis and nitrogen fixation, which provided a method for solar energy storage and the production of molecules for life sustenance [1]. Moreover, this biochemical process enriched atmosphere in nitrogen and oxygen, leading to actual air composition. This modification lead to the flourishing of biological microorganisms energetically sustaining on aerobic respiration, i.e. the transformation of carbon-based molecules oxidation to carbon dioxide and water [2,3]. Therefore, since their appearance on earth's surface, living organisms have been influencing the environment they settle in, atmosphere included [4].

After initial modifications in atmosphere in Archean and Proterozoic eras, atmosphere has been remained oxygenated from Cambrian period for almost half a billion years [5,6]. The presence of some of these gases involved in origin of life and its maintenance (water vapour, methane, ozone and carbon dioxide in particular) due to their favourable properties in temperature and radiation control on the surface. In fact, short-wave ultraviolet radiation emitted by the sun is potentially harmful to life, but these gases absorb UV-C radiation (wavelength < 280 nm) [7]. At the same time and most importantly, they also effectively absorb thermal infrared radiation from Earth's surface, trapping it and provide thermal energy dissipation [8]. In fact, it was estimated that Earth's mean surface temperature, 14 °C, would have dropped to -19 °C in absence of these components of atmosphere. For these reasons, these gases are called greenhouse gases (GHGs), due to their ability to trap heat within the surface-troposphere system [9].

The presence of these gases in atmosphere composition naturally undergoes little fluctuations over time, leading to climate alternation of warm and glacial periods in

geological history. This variability was related also to natural factors such as sunlight intensity, ocean currents, volcanic activity: therefore, climate variability is something natural and recurrent [10]. From this point of view, it would seem that the changes in climate during the industrial era (from 1750 to today) is a natural phenomenon.

However, the features of the climate change we have been experiencing recently has many differences with those that happened in the past. Nowadays we are observing what has been called an "*abrupt climate change*" because the rate of this process is faster than the cause [11]. Usually a 5 or 6 °C naturally global-mean temperature change occurs during the ice-age cycles while in the twentieth century, a thermal anomaly of 1 °C was measured by US National Aeronautics and Space Administration (NASA) [12], while the duration of ice-age cycle is measured in thousands of years [13].

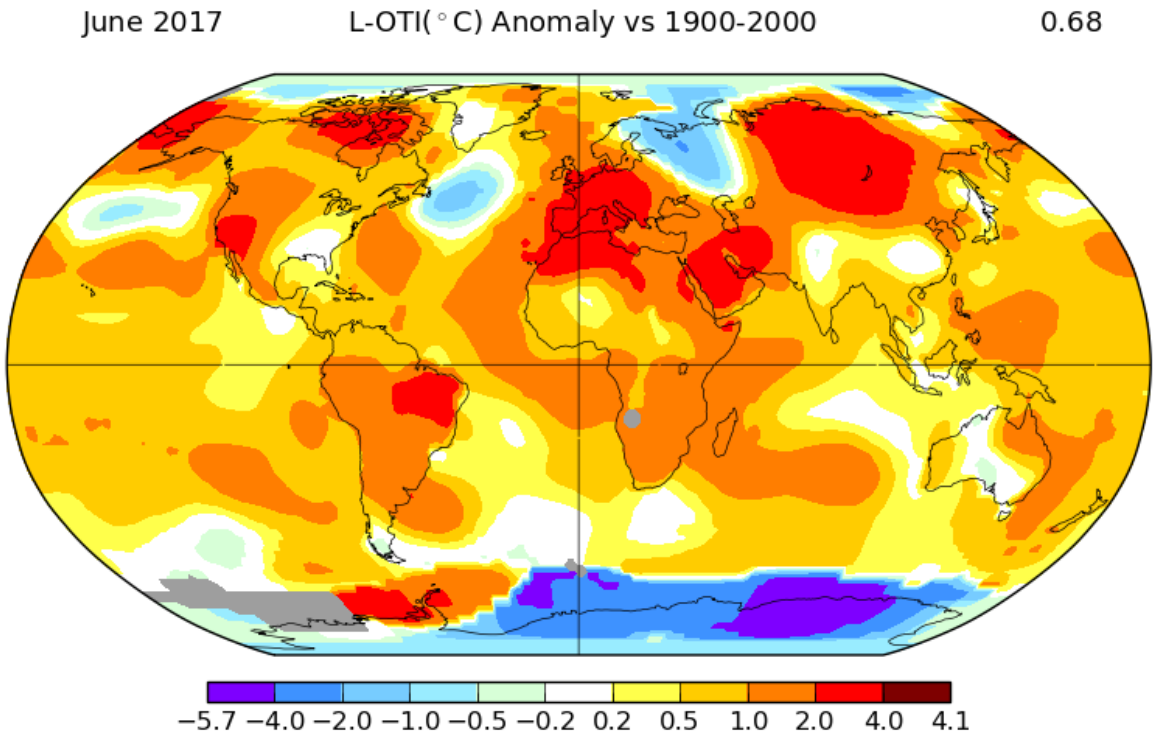

Figure 1.1 2017 Global thermal anomaly based on 20th century mean temperature [12].

This abrupt change in temperatures has led to different modifications in climate from area to area, such as desertification in tropical regions, the intensifications of hurricanes in

southern areas of United States of America, floods in Southeast Asia, topicalisation of the Mediterranean Sea, sea level rise and summertime melting of Arctic sea-ice [14-18], with huge consequences both for men and environment.

For example, according to Levermann and co-workers, global sea-level has risen from 18 to 22 cm in the last 100 years, and it will rapidly increase by 2.3 m per 1 °C of warming during the 21st century [19] with severe consequences for coastal flora, fauna and humanity. Moreover, caused by a combination of a warming-induced decline in oxygen solubility and reduced ventilation of the deep ocean, ocean nutrient cycles and the marine habitat might be affected, with potentially detrimental consequences for fisheries and coastal economies [20]. In some way, similarly to what happened at the first steps of life on Earth, current modifications in climate are ascribable to living beings, but, in this particular case, to human activities [21]. It has also been well established that the emissions of greenhouse gases have been playing an important role in this phenomenon due to their ability to modulate Earth temperature.

1.1.2 Greenhouse gases

According to IPCC, the International Panel on Climate Change [22], the eight primary greenhouse gases, whose presence have a direct effect on Earth's radiation adsorption, are:

- Water vapor (H_2O)
- Carbon dioxide (CO_2)
- Methane (CH_4)
- Nitrous oxide (N_2O)
- Ozone (O_3)
- Chlorofluorocarbons (CFC_s)
- Hydrofluorocarbons (HFCs)
- Sulphur hexafluoride (SF_6)

In recent years, other gases, such as carbon monoxide (CO) and volatile organic compounds (VOCs) have been classified as indirect greenhouse gases [23]: in fact, these molecules are not able to adsorb Earth's radiation but, in their atmospheric degradation, are converted in greenhouse effective gases, such as ozone, water and carbon dioxide.

The effectiveness in trapping Earth's radiation is measured by radiative forcing, defined as "*the change in net irradiance at the tropopause after allowing for stratospheric temperatures to readjust to radiative equilibrium, but with the surface and tropospheric temperatures and state held fixed at the unperturbed values*"[24]. This value indicates the relevancy of a factor in climate change: the bigger is the radiative forcing, the bigger is the effect of a greenhouse gas. It is usually given as relative to pre-industrial conditions (before 1750) and in 2007 IPCC esteemed that human activities caused a radiative forcing of +1,6 $W \cdot m^{-2}$ (from +0,6 $W \cdot m^{-2}$ to +2,4 $W \cdot m^{-2}$).

At first sight, it can be said without any doubt that some of them, if not all, were present in the atmosphere even before manhood, though not in the concentrations we are experiencing in these days [25]. Moreover, each gas has different chemical properties leading to a different radiative forcing and a different effect on the environment. For this reason, among the international scientific community, it was introduced a new parameter, the CO_2 equivalent ($CO_{2\text{-}eq}$) emission that is defined by IPCC [26] as the amount of CO_2 emission that would cause the same time-integrate radiative forcing over a given time horizon, as an emitted amount of a long-lived GHGs or a mixture of GHGs. This value is calculated according to the following equation:

$$CO_{2\text{-}eq} = emission \cdot GWP$$

Equation 1.1

where **emission** stands for the actual GHG emission while **GWP** is the global warming potential, another important parameter for the purpose. High GWP values indicate a major effect on the environment. This factor is usually considered on different time horizons (20, 100 and 500 years). In addition to that, it is important not only to consider the effect each

GHG has, but also its lifetime in the atmosphere. In Table 1.1, GWP and atmosphere lifetime of the main GHGs are reported.

			Global Warming Potential for given time horizon		
Industrial Designation or Common name	Chemical Formula	Lifetime (years)	20-years	100-years	500-years
Carbon Dioxide	CO_2		1	1	1
Methane	CH_4	12	72	25	7,6
Nitrous Oxide	N_2O	114	310	289	153
HFC-23	CHF_3	270	12000	14800	12200
HFC-125	CHF_2CF_3	29	6350	3500	1100
HFC-134	CH_2FCF_3	14	3830	1430	435
HFC-143	CH_3CF_3	52	5890	4470	1590
HFC-152	CH_3CHF_2	1,4	437	124	38
PCF-14	CF_4	50000	5210	7390	11200
PCF-116	C_2F_6	10000	8630	12200	18200
Sulphur Hexafluoride	SF_6	3200	16300	22800	32600

Table 1.1 Lifetime and Global Warming Potential of the most common greenhouse gases [26].

In this table water vapour and ozone are not mentioned for different reasons: water vapour effect is considered in methane GWP because it is formed by methane and other hydrocarbons oxidation [27], while ozone has different effects according to geographical and atmospheric factors [28]. Recently, some studies introduced the use of GWP also for some volatile organic compounds (VOC) because they are not directly responsible for global warming, but bring about substances that affect global warming such as carbon dioxide and water during decomposition in atmosphere [29].

A more comprehensive and representative metric was endorsed by Shine and co-workers [9]: this is the global temperature change potential (GTP), defined as the global-mean temperature change realised at a given time horizon from a pulse emission of 1 kg of gas. This parameter, though not used by governmental organisms due to higher uncertainty depending on the specific assumptions being made, takes into account environment response to a radiative forcing, providing a more representative effect of greenhouse gases [29].

The choice to use carbon dioxide as a benchmark greenhouse gas for both GWP and GTP, reflects the importance of this gas for global warming. From both these metrics, it might seem that carbon dioxide effect on global warming is lower than other substances, especially compared to hydrofluorocarbons (HFCs) and chlorofluorocarbons (CFCs). Due to their great effect, their use was internationally banned by the Montreal Protocol [30], ratified by 197 countries in 1987. This treaty was aimed at the reduction hydrochlorofluorocarbons (HCFCs), more for their ozone-depleting effect than for their effect on global warming. Nowadays, their emission is extremely low, with an extremely low effect compared to carbon dioxide: in fact, HCFCs emissions represents only 0.77 $GtCO_2$-eq/y during 2007−2012 [31]. To provide a comparison with actual CO_2 emissions, year 2016 broke the record for the greatest CO_2 emissions, that reached the highest value ever, above 40 Gt of carbon dioxide were emitted all over the world and it is supposed to increase in the next future [32].

Therefore, in this historical moment, CO_2 represents the most important threat to atmosphere and environment and the scientific community is struggling to understand global warming phenomenon and to provide mitigation protocols.

1.1.3 Carbon dioxide in atmosphere: environmental scenario and remediation strategies

The significance of carbon dioxide for environmental issues is related to the proportions of its human activities (i.e. the use of fossil fuels for energy and transportation) and of related emission in atmosphere [33] compared to environmental conditions before industrialisation.

In fact, from its appearance on Earth's surface (4 million years ago) to the beginning of industrialisation, mankind experienced an atmosphere in which CO_2 level was ranging between 220 ppm to 340 ppm [34]. Since it is quite difficult to acquire historical data on annual carbon dioxide and direct CO_2 measurements were performed since 1958, such data can be obtained indirectly from air bubbles in ice cores in location with no summer melting, such as Antarctica [35].

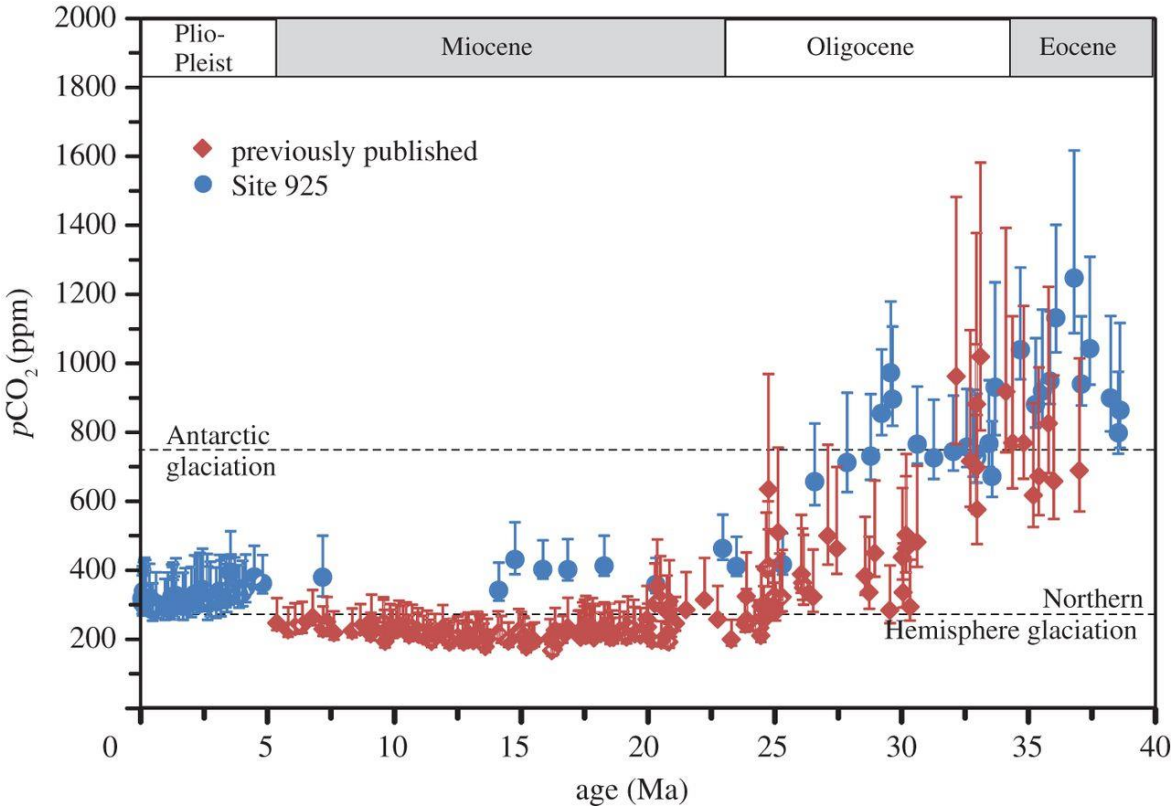

Figure 1.2 Carbon dioxide concentration in atmosphere the last 40 million years [36].

Since 1750 onwards, CO_2 levels in atmosphere have steadily increased, at an extremely high rate compared those observed over geological eras. This trend has become even more pronounced after World War II economic growth. Despite the environmental policies taken, global fossil fuels related CO_2 emissions grew approximately 25% in the period between 1990 and 2004 [37]. More recent studies affirm that this concentration has grown in the last years: in May 2013 carbon dioxide concentration reached 400 ppm, which was considered as limit value, since these concentrations had never been reached before [38].

In December 2017, CO_2 concentration reached 408 ppm, the highest observed value in human history and this value will grow to by 2.8 ppm/year in the foreseeable future [39].

From the comparison of trends in carbon dioxide concentrations and temperatures in the 20th century, it is evident that these two environmental parameters are strictly connected and in the last decade scientific community agreed that global warming main cause is the increase in CO_2 concentrations due to human activities [40].

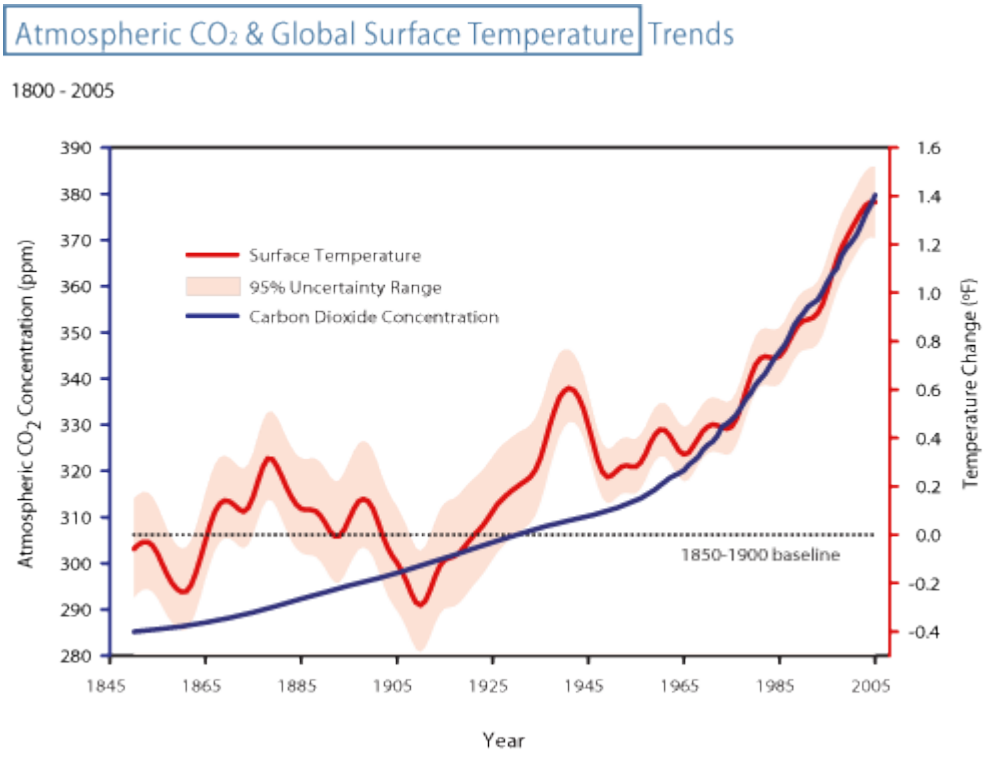

Figure 1.3 Correlation between CO_2 concentration and temperature change [40].

Due to the anthropogenic origin of these huge environmental phenomena, the word *Anthropocene* was coined to describe this particular historical moment we are living in. According to Crutzen, the Anthropocene has started in the 1960s, when human activities effect on climate and environment became relevant [41]. In the last decades attention to the environment has grown into an important feature of western society and its preservation still represents a challenge. How – or whether – to respond to the warming effects from greenhouse gases is an issue of intense debate in the public sphere [42].

From the late '90s policy makers committed themselves to find solid solution to the environmental threat of carbon dioxide. The first real political effort to overcome the climate change is the Kyoto Protocol [43], that was signed in 1997 by 192 countries and is still a landmark in environmental policies. One of the most important commitments is the reduction of greenhouse gases: more specifically, countries that have rectified this document, decided to put effort into "reducing their overall emission of these gases *per capita* by at least 5% below 1990 levels in the commitment period from 2008 to 2012". Their effort has been recently renewed by the Paris Agreement in December 2015, a treaty endorsed by 194 countries aimed at keeping world average temperature increase below 2 °C [44]. There are several strategies to pursue this aim [45]:

- to decrease the carbon intensity of the economic system;
- to increase the efficiency in energy production and consumption processes;
- to improve the ability to capture and sequester CO_2 from atmosphere and its utilisation.

The first one would require replacement of fossil fuels, which the world is depending on for 80 % of energy production [46]: this would mean a complete change of the paradigm of energy and transportation technologies. Much attention has been given to alternative energy sources such as biomass and hydrogen economy, but, despite some demonstrative infrastructures, a real worldwide distribution network and hydrogen fueled devices are still long to be used [47]. Whereas, reduction of economy carbon intensity represents an important strategy that has been pursued and endorsed by national and international governments. In fact, the word carbon footprint, was coined and defined as the regenerative forest capacity required to sequester the anthropogenic carbon dioxide emissions [48], has grown an important parameter to assess processes sustainability. However, the reduction of carbon footprint is not able to eliminate at the root CO_2 emissions, but only to reduce them.

In the third approach CO_2 is not considered neither as a waste not to emit in atmosphere nor to be avoided, but as useful source for chemicals and fuels. This strategy has a two-

folded main advantage: on one side, environmental remediation related to CO_2 emissions avoidance and, on the other, production of highly requested products. In fact, it must be remembered that fossil fuels are meant to be extinguished [49] and mankind is strenuously seeking for alternative and sustainable sources of energy, therefore it is extremely important to study new technologies for this purpose.

1.1.4 CO_2 industrial utilisation

Carbon dioxide finds several industrial applications already, using CO_2 either as a reagent or solvent, as shown in the figure below.

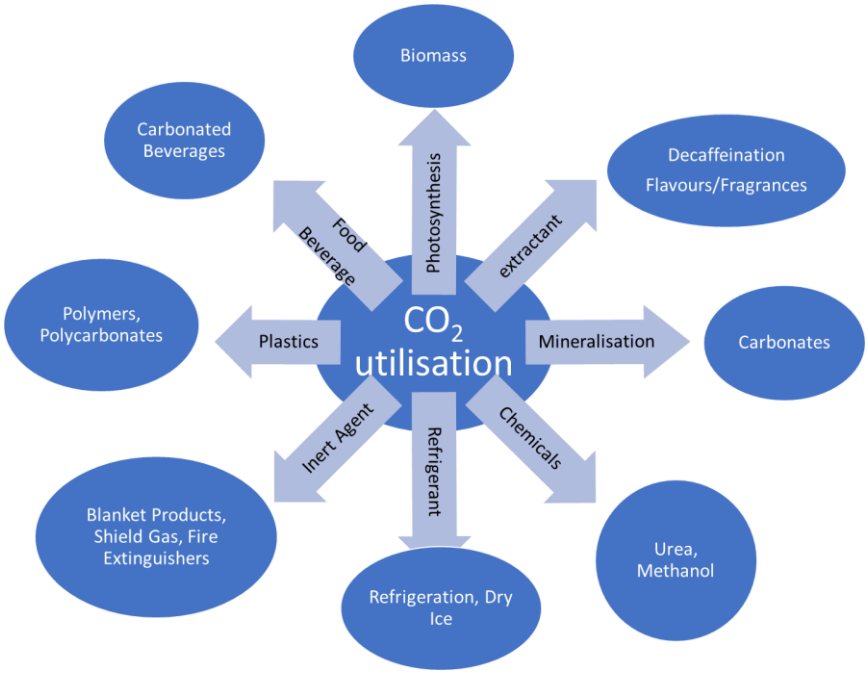

Figure 1.4 Main CO_2 utilisation applications, data from US Department of Energy [50].

The earliest process involving CO_2 is urea production, which has been working since 1882 [51] and yields to this important fertilizer from ammonia and carbon dioxide at 200 °C and 250 bar with 4:1 NH_3/CO_2 molar ratio [52].

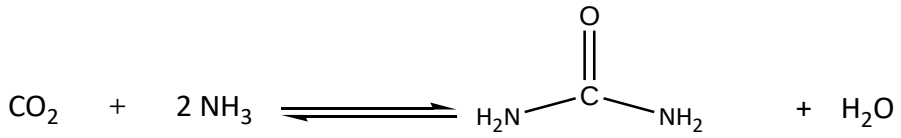

Equation 1.2

This process has in impact on carbon dioxide emissions from ammonia plants. However, due to high NH_3/CO_2 molar ratio, reduces only partially ammonia production's carbon footprint. CO_2 can also be used in other industrial/commercial applications such as a shielding gas as a refrigerating agent [53], in welding manufacture [54], as a flame-extinguishing agent [55], in food packaging [56] and as a carbonating additive for soft-drinks [57].

Due to favourable physicochemical properties, carbon dioxide in the form of supercritical fluid (sc-CO_2) finds applications as an extracting agent in food industry for its relatively inertness, inexpensiveness, non-toxicity, non-flammability, recyclability. A breakthrough process is the decaffeination of coffee beans patented by Hag in 1978 in Western Germany [58]. Another application is the extraction of natural aromas and fragrances in both food and perfume industry. Moreover, sc-CO_2 is a good solvent in homogeneous catalysis due to complete miscibility with gaseous reactants, fast mass transfer and easy products removal [59], opening new possibilities about homogeneous catalysts recover and reuse.

In chemical processing, CO_2 finds application as green carbon source in organic synthesis, despite it is a kinetically and thermodynamically stable molecule [60]. As a matter of fact, it shows affinity toward nucleophiles and electron-donating reagents. Carbon dioxide can be used in the production of organic carbonates and carbamates to substitute highly hazardous phosgene: for example, dimethyl carbonate (DMC), a fuel additive and a monomer for polycarbonates, can be synthesised from CO_2. In polymer chemistry, CO_2 and epoxies alternation in polymerization leads to materials characterised by lower oxygen permeability and higher biodegradability than polystyrene. CO_2 finds also application in the synthesis of acrylic acid derivatives and in the carboxylation of organic halides or, industrially, in salicylic acid synthesis from phenol [61] with high atom efficiency.

Though all these established and new fields of application for carbon dioxide chemical use have been exploited, they are still not able to represent a solid way of exploitation of the

magnitude of this pollutant emissions. In particular, target products should find utilisation as fuels since their worldwide consumption is two orders of magnitude higher than that of chemicals [62].

1.1.5 CO_2 capture and storage for carbon remediation

Among possible solutions for CO_2 remediation, Carbon Dioxide Capture and Storage (CCS) represents a leading technology to assist the transition from fossil fuels based economy to the use of alternative energy sources [63]: this is a mid-term solution to reduce fossil fuels' environmental impact until renewable energy sources are available [64]. Therefore, it represents the most likely tool for the reduction of current fossil fuels derived CO_2 emissions.

CCS technologies are supposed to be used in plants run by fossil fuels and they are aimed at collecting and generating pure carbon dioxide flues in order to avoid their emission in the atmosphere from stationary sources, storing them in geological or oceanic suitable sites [65].

Such processes, engineering differences aside, consist of three phases:

1. Carbon dioxide capture
2. Transportation
3. Storage

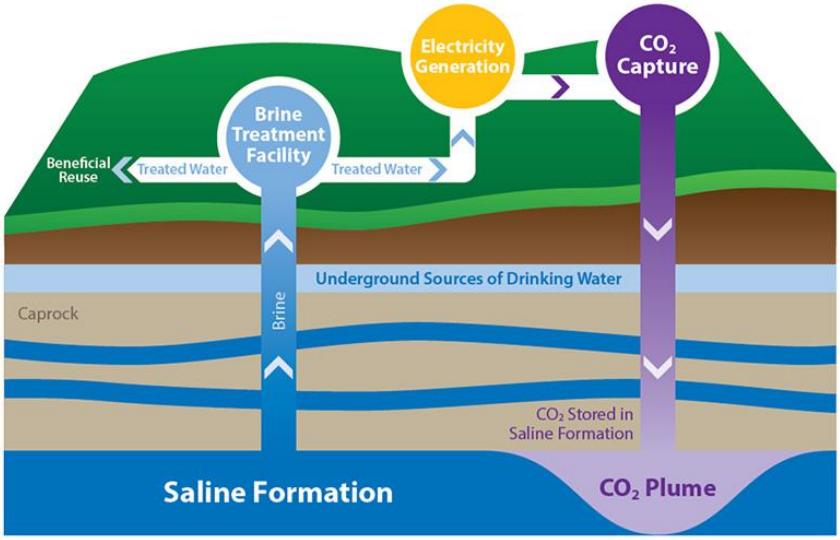

Figure 1.5 Schematic view of CCS processes [50].

In the first step, post-combustion carbon dioxide capture, can be performed following several methods, which differ in engineering, performances and cost. CO_2 capture at power plants and other large point sources CCS is not a new concept since it is used, for example, in hydrogen purification.

The classical post-combustion approach is the exploitation of carbon dioxide chemical adsorption on monoethanolamine (MEA). Despite maturity, this technology has some disadvantages such as low carbon dioxide loading capacity, high corrosion rate and MEA degradation by SO_2, NO_2, O_2 and HCl. Alternative absorbents have been studied like N-methyldiethanolamine (MDEA), 2-(butylamino)ethanolamine (BEA) [66] improving absorption capacity and rate. In all cases, amine and carbon dioxide are converted into carbamates and carbonates that release reactants back at higher temperature composition.

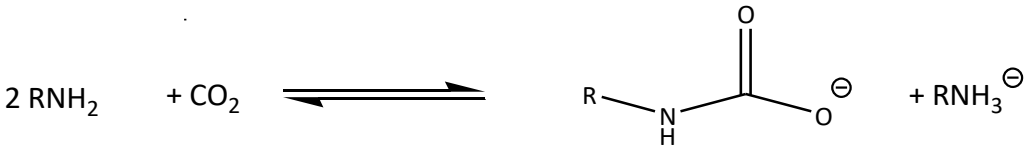

Equation 1.3

Equation 1.4

Due to amine's corrosiveness, instability and cost, solid gained wider attention adsorbents for their lower cost, less corrosion, greater stability and greater adaptability. Zeolites, also known as molecular sieves, are believed to be very efficient and adaptable to different engineering approaches. In fact, these inorganic supports, when treated with amines, are particularly interesting for this purpose [67]. An innovative adsorbent system employs a mesoporous MCM-41 silica impregnated with polyethyleneimine, that is called "molecular basket" [68].

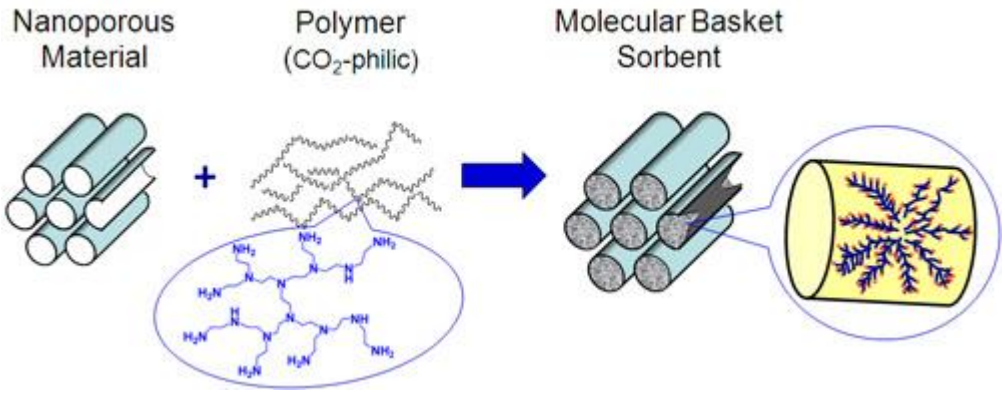

Figure 1.6 Molecular basket structure [68].

After the separation from other flue gases, by pipelines or shipping, CO_2 is transported to storage sites [69]. Carbon dioxide is usually moved in supercritical form because of the higher density than gas phase and the rather high pressure drops, but new solutions are under consideration to avoid supercriticality [70]. Alkali resin polymers were also tested and it was found that they can be regenerated at low temperature (45 °C) with a water vapour in a so-called "moisture swing absorption system", which releases CO_2 and the resin using a low energy input [71].

Captured CO_2 is stored usually in geological sequestration sites while ocean storage at great depths is less common choice since CO_2 causes water acidification with consequences on marine life [72]. The chosen sites require long-term geological stability, minimum environmental impact and prolonged liability.

The first commercial scale CCS plants was developed in Canada in the province of Saskatchewan and it has been operative by year 2000; since then, other full scale rigs were built throughout the country, which dramatically reduces the number of possible sites. [73]. Conversely, in Europe there are not currently any commercial operating CCS plants for several reasons such as: lack of political will, low CO_2 price, lack of commercial drivers to capture and store CO_2, and public opposition to the proposed facilities [74]. The European Union is financing projects to establish this technology, and, up to now, the only working CCS plant is Statoil's Snøhvit and Sleipner offshore gas plant in Norway since 1996 [75], while in Scotland (UK) Peterhead power station is the world's first demonstrative gas-fired power station to host a full-chain carbon capture and storage (CCS) project on a commercial scale, whose efficiency in capturing CO_2 has reached 90 %. [76]. The most common

application of captured CO_2 is the use for enhanced oil recovery (EOR) in depleting fossil fuel reservoirs and it has been used in real sites, like in North Sea oil rigs [77].

Despite the beneficial effects of this technology in reducing energy production carbon footprint, some technical aspects need to be tailored, such as CO_2 adsorbents formulation, overall process energetic efficiency and avoidance of CO_2 leakage through displacement of rock strata and from oceanic reservoirs.

However, the most critical objection to CCS is that CO_2 is still considered as a pollutant not to emit instead of being considered as an alternative carbon source. Very recently, attention shifted from CCS to carbon capture and utilisation technologies (CCU), capable of transforming this waste in useful products.

1.1.6 Possible CO_2 utilisation in the future

The utilisation of CO_2 to obtain fuels, energy storage media and chemicals is attracting interest from industry and policy makers [78]. CCU technologies play a potential role in the decarbonisation of our society but key issues that still need to be addressed include economic competitiveness and, most importantly, overall the carbon balance considering both direct and indirect CO_2 emissions [79]. The contribution of CO_2 utilisation to CO_2 emissions reduction objectives depends on the rate of penetration of CO_2-derived products in the market.

Most importantly, CO_2 utilisation could be a significant opportunity for innovative industrial processes, as already been demonstrated by many recent initiatives in, for example, chemical and cement industries. This strategy would fit also Circular Economy dictamens, providing a concrete integration of economic activities and social and environmental wellbeing in a sustainable way [80].

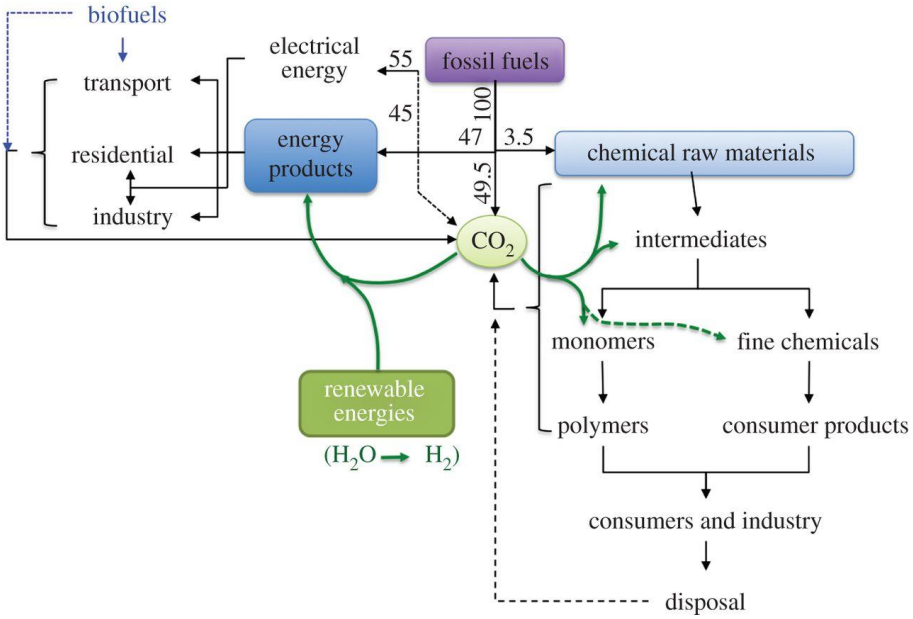

Figure 1.7 Integrate circular carbon economy [81].

Bearing these considerations in mind, the conversion to fuels looks more suitable than chemicals production. First of all, fossil fuels use implies the use of hydrocarbons (obtained by geological processes in millions of years) by combustion at a rate which is way faster than their formation [82]. This means that carbon cycle is not closing, accumulating carbon as CO_2 in atmosphere [83]. Secondly, the fossil fuels cannot be considered sustainable, since they are meant to be extinguished [84]. Finally, the amount of CO_2 to be converted is extremely high and worldwide fuels demand is two orders of magnitude higher than that of chemicals [85].

In general, any carbon dioxide conversion reaction exploits its two main physicochemical properties, i.e. either acidity or high oxidation state. In order to obtain energy fuels, carbon dioxide must be reduced to either CO or formaldehyde or oxalic acid or dimethyl ether or methanol or methane.

$$\boldsymbol{CO_2 + 4H_2 \xrightarrow{cat} CH_4 + 2H_2O}$$

Equation 1.5

These kind of processes, generally called *methanations*, occur at a temperature ranging between 150 °C and 500 °C and pressures up to 100 bars in presence of a nickel based catalyst [86]. Despite their effectiveness, there are two main drawbacks to these processes:

1- hydrogen is produced by fossil hydrocarbons steam reforming, so the sustainability problem is not completely outplayed. When H_2 comes from renewables, such biomass steam reforming [87], this technology will be independent from fossil fuels;

2- heating, in most cases, derives from fossil fuels combustion, leading to non-negative overall CO_2 emissions.

To overcome these intrinsic methanations drawbacks, other technologies should be applied such as photocatalytic CO_2 reduction. This process is usually referred to as artificial photosynthesis, due to its great similarities to the natural plants-sustaining mechanism.

$$\boldsymbol{CO_2 + H_2O \xrightarrow{cat} solar\ fuels + O_2}$$

Equation 1.6

In both cases, primary energy input is light (which, in a sustainable process, should be provided by the sun) and high energy molecules are obtained [88]. Reaction products are gaseous or liquid hydrocarbons, usually called *solar fuels*, that can be used in stationary and mobile applications without further processing, since they are equivalent to the fossil ones. Recycling carbon dioxide from solar hydrocarbons combustion closes carbon circle in non-biological process without involving biomass and, in the case of first generation biomass, dealing with ethical issues and competition for agricultural land [89]. Moreover, water can substitute hydrogen and be used as a reductant and proton source [90]: this extremely important feature allows to set CO_2 photoreduction free also from indirect CO_2 emission and improve the sustainability of the whole process.

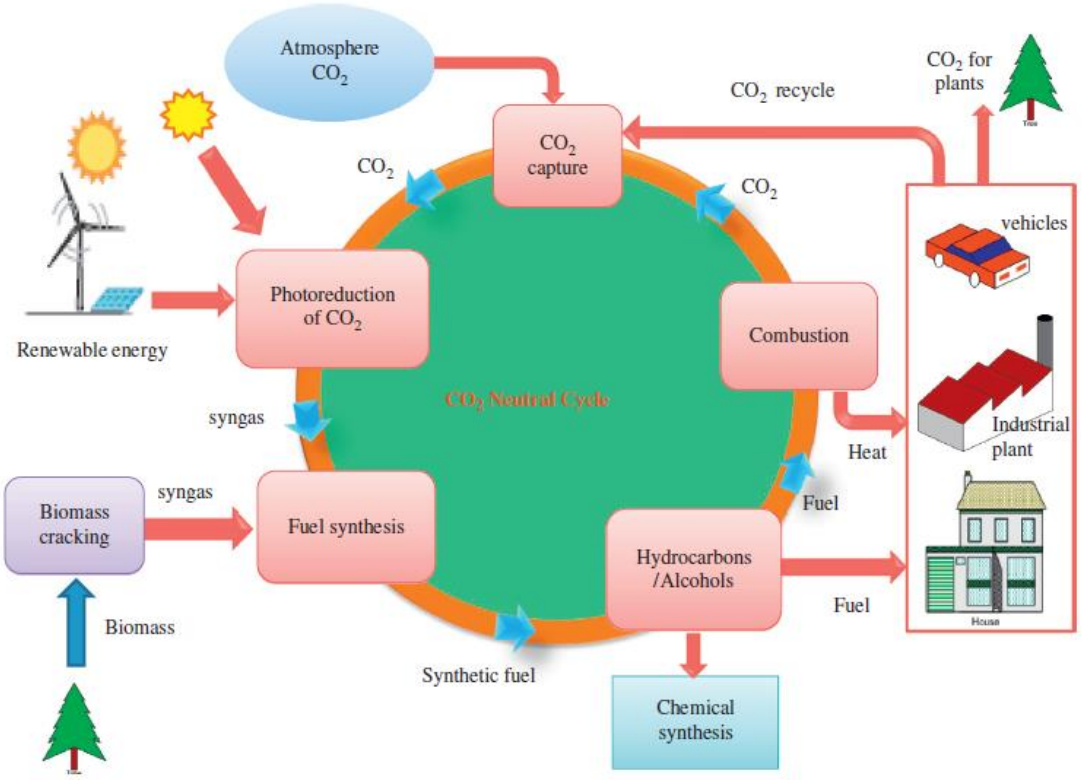

Figure 1.8 Carbon dioxide neutral cycle with renewable solar fuels production [91].

Therefore, CO_2 photoreduction is a key technology for the development of C-based industry that is independent from fossil fuels and drives mankind from Anthropocene to *Sustainocene*, an era in which economic and social wealth meets a wise and responsible use of environmental resources [92]; for this reasons CO_2 photoreduction has been chosen as a topic for this Ph.D. thesis and discussed afterwards.

1.2 Carbon Dioxide Photoreduction

1.2.1 Fundamentals in photocatalysis

The International Union for Pure and Applied Chemistry (IUPAC) defines photocatalysis as a "*Change in the rate of a chemical reaction or its initiation under the action of ultraviolet, visible, or infrared radiation in the presence of a substance—the photocatalyst —that absorbs light and is involved in the chemical transformation of the reaction partners*" [93]. The first article on photocatalysis was published by Fujishima and Honda in 1972, in which irradiated TiO_2 assisted water splitting into hydrogen and oxygen was presented [94], and

from the beginning this technology seemed appropriate for alternative energy production [95]. The first study on carbon dioxide reduction over different photocatalyst appeared on *Nature* by T. Inoue *et al.* in 1979 [96]: however, at that time it seemed more an unconventional variation on photocatalytic water splitting. In fact, according to the authors, in this reaction, *in situ* formed hydrogen reduces carbon dioxide leading to methane and all possible by-products due to partial reduction like formic acid, formaldehyde.

$$\boldsymbol{H_2O + h\nu \xrightarrow{cat} H_2 + {}^{1}/_{2}\, O_2}$$

Equation 1.7

$$\boldsymbol{CO_2 + H_2 \xrightarrow{cat} CH_xO_y + H_2O}$$

Equation 1.8

Further studies showed that reaction mechanism is far more complicated than that [97], but this topic will be discussed afterwards.

In photocatalysis, and in catalysis in general, the choice of the photocatalyst is fundamental. Homogeneous catalysts have been investigated mimicking natural photosynthetic systems. Iron, nickel and rhenium organometallic complexes proved to be photoactive in carbon dioxide reduction [98-100]. However, heterogeneous catalysts are preferred in industrial practice because of their inexpensiveness, great photostability and easy recovery.

Various semiconductive inorganic materials were tested in carbon dioxide photoreduction, like cadmium sulphide (CdS), gallium arsenide (GaAs), gallium phosphide (GaP), zinc sulphide (ZnS), zinc oxide (ZnO), tungsten trioxide (WO_3) and zirconia (ZrO_2) [101,102]. However, the most studied material is titanium dioxide TiO_2 due to its potentialities to make this process an industrial mean to pursue CO_2 abatement.

All these semiconductors are characterized by an intermediate electron conductivity between those of conductors and insulating materials. This property relies on materials physicochemical and, in particular, in the electronic interaction between the atoms that

lattice is made up of. In fact, the linear combination of an extremely high number of discrete atomic orbitals in the lattice yields to energetically close molecular orbitals, which can be approximated to continuous bands. Electronic properties depend on the difference of energy between valence band (VB), or the highest occupied molecular orbital (HOMO), and conduction band (CB), or the lowest occupied molecular orbital (LUMO). This difference, the band gap (BG) is the amount of energy to supply to a semiconductor for an electric current to flow [103]. When it happens, the ionic couple electron-hole (e^--h^+) is generated: then the vacancy in the valence bond allows electron movement from neighboring atoms generating the current. If in a material this energetic difference is lower than Brownian motion energy (k_BT) or the conduction band is partially occupied, it is called a conductor, while, if this difference is higher than 9 eV, the material is an insulator. If the material's band gap lies between these two limit values, it is called a semiconductor [104].

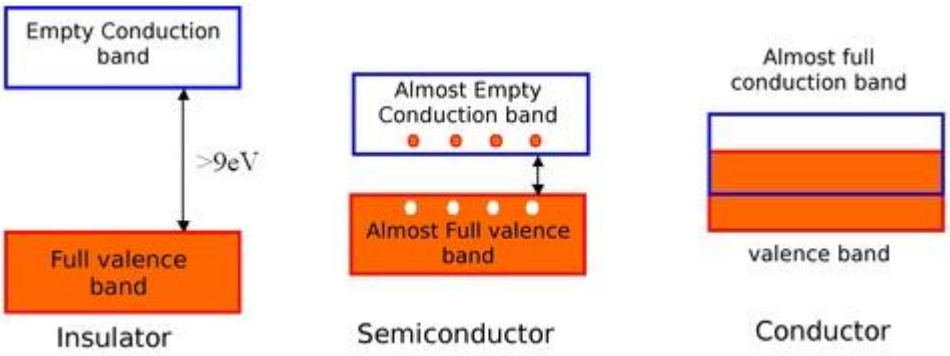

Figure 1.9 Valence bond (VB) and conduction band (CB) in insulators, semiconductors and conductors.

The energy input for electron promotion from VB to CB can be provided by a light source as long as irradiation photon energy is equal to or higher than material's band gap. These charge separation and migration on the surface allows oxidation reactions with the positive hole in the valence band while reduction can occur in the conduction band, where there is an extra-electron, without any modification on photoactive semiconductor [105].

In heterogeneous photocatalytic processes, two physicochemical parameters must be considered:

- Band Gap, since it is connected to maximum radiation wavelength for semiconductors irradiation by this equation [106]:

$$BG = \frac{h \cdot c}{\lambda}$$

Equation 1.9

where h is Planck constant, c is speed of light and λ is radiation wavelength. The lower is the band gap, the minor is the energy required for electron circulation;

- Recombination phenomena: in fact, electron-hole lifetime should be as long as possible for substrates to interact photoactivated surface sites; to do so, this charge separation has to last more than few nanoseconds generally [107]. In fact, it is very likely that photoexcited electron undergoes relaxation from CB to VB releasing energy either emitting light or producing heat [108].

These physicochemical properties are the parameters to be taken into account in the choice of a photocatalyst, since it affects required radiation and substrate activation mechanism. Up to now, the most frequently used photocatalyst is titanium dioxide due to its favourable properties, which will be discussed in the following section.

1.2.2 Titanium dioxide general features

Generally called titania, titanium dioxide is an inorganic material that has been known for centuries. Titania ores are located in different countries, such as USA, Canada, Russia and China, where its main metal impurities are iron, manganese, magnesium, aluminium, silicon, chromium, niobium, etcetera [109]: thus TiO_2 needs further purifications to be used. Industrially, two processes are employed, depending on TiO_2 content in the raw

mineral. The oldest and best-known process is the so-called sulphate process, which is suitable for raw materials containing less than 75 wt. % of titania, like ilmenite. In this process, minerals are digested in concentrated sulphuric acid and then in cold water titanium sulphate, $Ti(SO_4)_2$, precipitates as a wet cake while impurities remain in solution. Afterwards, pure $Ti(SO_4)_2$ is hydrolysed with water steam at 100 °C, dried and calcined to obtain pure TiO_2. The other process, the chloride process, which is employed when TiO_2 content in raw material is up to 96 wt. %, requires Ti(IV) reduction with carbon to Ti (0) that afterwards reacts with chlorine to yield titanium tetrachloride. $TiCl_4$ is then distilled and treated with pure oxygen giving pure titania and chlorine back.

In 2015, 6 million tons of titania were produced [110] covering a 13,7 billion US $ world market where the average price ranges between 1 and 3 US $/kg in 2016 [111]. This material is widely used in coatings and plastics industry for its chemical stability, non-toxicity and favourable price/effect ratio. Due to its very high refractive index (2.8 for rutile and 2.55 for anatase crystal phase), titania has been applied in several sectors such as paints, coating materials, plastics, fibres, printing inks, papers, construction materials, enamel, ceramics and cosmetics. Moreover, the use of titania as a pigment (E171 code) is allowed by US Food and Drug Administration (FDA) in food if its concentration is below 1 wt. % [112] for white opaque finish to candies or as a whiteness enhancer in non-diary creamers, or in salad dressings and similar [113]. Moreover, new titania-based materials have been formulated for pharmaceutical applications, such as matrixes in oral drug delivery systems and as implant material for cardiovascular stents, joint replacements, bone and dental implants, etcetera [114].

Titanium dioxide has also been used in catalysis for decades as a support for metal particles like nickel [115], iron [116], rhodium [117], palladium, platinum [118] and also gold [119]. However, titania itself can be used as a photocatalyst. In fact atoms and molecules (H_2, O_2, H_2O, CO, CO_2, NH_3 and also organic compounds) can be adsorbed on titanium dioxide surface where dissociations and chemical reactions can occur [120]. It is clear that this phenomenon is deeply influenced by structural and surface characteristics.

Crystallographic configuration has an impact on titania catalytic behaviour and thus this parameter must be considered. In nature titanium dioxide occurs in three different crystal phases: rutile, anatase and brookite [121]. The first two structures are described by a

tetragonal geometry but they differ for their space group ($P4_2/mnm$ for rutile and $I4_1/amd$ for anatase). In both structures, titanium is octahedrally coordinated to six oxygen atoms, that in turn are bridging two metallic centres, but in rutile octahedra share one corner along, whilst anatase's octahedra are connected by edges. Differently to these two, brookite, the rarest crystal phase, has a rhombohedral structure (Pbca space group).
All the three structures are shown in Figure 1.10 and Figure 1.11.

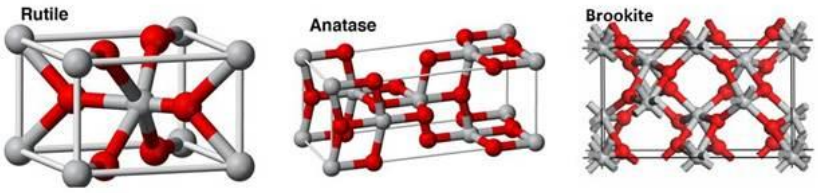

Figure 1.10 Balls and sticks structures of rutile, anatase and brookite.

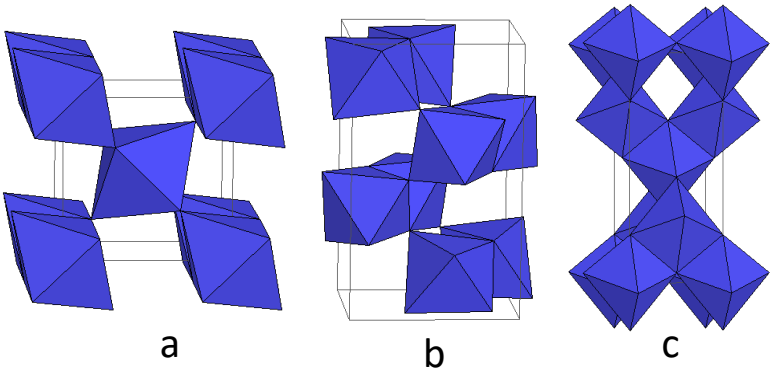

Figure 1.11 Octahedra structure of rutile (a), anatase (b) and brookite (c).

From thermodynamic data, rutile is the most stable phase [122]: however, free energy differences between the three crystallographic phases are very small (4-20 kJ/mol). Therefore, at normal values of temperature and pressure, anatase and brookite might be considered as stable as rutile.
In addition to that, it is well known that at room temperature titanium dioxide shows n-type semiconducting properties. This peculiarity is due to titania tendency for oxygen deficiency. This characteristic is explained by either oxygen vacancies or titanium interstitials [123]. It was observed both theoretically and experimentally that band gap depends on crystallographic structure. In fact, band gap is 3.03 eV for rutile, 3.20 eV for

anatase and 3.26 eV for brookite [124]. In other terms, required incident light must have a wavelength minor than or equal to 410 nm for rutile, 388 nm for anatase and 381 nm for brookite, whose values are in the border region between ultraviolet (200-400 nm) and visible light (400-800 nm). Since solar spectrum is mainly composed by visible and ultraviolet light, the use of titania as a material for photoreduction are potentially fitting with a complete exploitation of solar radiations.

Crystallinity affects also another important aspect of the photocatalytic phenomenon, i.e. recombination rate. In fact, electron-hole lifetime should be long at least few nanoseconds in order to be photocatalytically active [125]. In titanium dioxide, some punctual defects in the lattice like both titanium and oxygen vacancies and also titanium interstitial atoms were observed and these deviations from ideal structure are more energetically feasible in the case of anatase rather than in those of rutile and brookite: this means that excited states are more stable when titanium dioxide displays the anatase structure [126]. In fact, while rutile TiO_2 is a direct semiconductor, anatase is an indirect semiconductor, where electrons stabilisation at the lowest level in CB enables longer electron-hole life and greater mobility [127]. Summing up these two factors, it is possible to state that, though rutile has a lower (and closer to the visible region of the electromagnetic spectrum) band gap, anatase phase is generally preferred for titania photocatalysts because of its lower electron-hole recombination.

1.2.3 Titanium dioxide photocatalytic applications

Titanium dioxide has found already photocatalytic commercial application, especially for environmental pollutant remediation, but also in other markets.

In the case of pollutants abatement, inorganic, organic compounds and microorganisms are decomposed on titanium dioxide in either liquid or gaseous phase. Volatile organic compounds (VOCs) oxidation has been investigated in the last two decades [128]. According to the World Health Organization (WHO), these substances, that show a boiling point in the range 50-260 °C (such as methanol, formaldehyde, aromatic compounds, chlorinated hydrocarbons, etcetera) can have either carcinogenic, mutagenic or teratogenic properties and thence be harmful for human health. Photocatalytic oxidation (PCO), performed on titania catalyst, seems to be the most feasible technology to abate

VOCs at run temperature and atmospheric pressure and it is efficient even when these pollutants are present in low concentrations, generally in the ppb range [129]. Among the inorganic pollutants, the most investigated for photoconversion are nitrogen oxides (NOx), whose anthropogenic emission is basically related to fuels combustion and some industrial processes, such as Haber-Bosch process and nitric acid production [130] with negative effects for both men and environment.

The application of the photocatalytic technology to materials in the green building industry seem a good way to solve these environmental issues and, at the same time, increase inhabitants' wellness. In fact, photocatalytic concrete, that is concrete containing titanium dioxide, is able to adsorb atmospheric NOx and transform them in calcium nitrate which is not harmful at all [131]. Then innocuous nitrates are washed away by rain. These materials can also have a possible effect on VOCs abatement, since titania can oxidize them directly to carbon dioxide [132] which is non-toxic for men but definitely harmful for the environment.

These technologies have also been translated to pollutants in liquid systems such as VOCs and organic pesticides in ground and surface waters. In particular, interest has been focalized on water disinfection from different types of bacteria like *Micrococcus Lyrae, Staphylococcus Aureus* and *Escherichia Coli* [133]. In the market, there are already some titania products with photocatalytic activity. The most important material is P25 by the German Evonik Corporation [134], which over the years has become a benchmark material in all literature papers concerning photocatalysis.

Recently, some works about hygiene and medical applications have been published. In fact, titania can be used in coatings to sterilize door handles, toilet flushes and bed frames reducing the spread of infections in places like hospitals and hotels, and unpleasant odours can be removed at the same time [135]. In addition to that, it has been discovered that, under UV irradiation, titania particles, through oxidation reaction, suppress cancer cell growth and, in some cases, completely degrade them [136]. Tests were performed on sarcoma cells *in vitro*, *in vivo* and *ex vivo* with extremely positive results: the positive effect on sarcoma is accompanied with no harm for normal cells.

Considering all its environmental and medical applications, titanium dioxide is an efficient and versatile photocatalytic material, that, for some applications, has been formulated to specific purposes and put into the market.

1.2.4 Possibilities and challenges in CO_2 Photoreduction on TiO_2

Since the pioneering work by T. Inoue *et al.* in 1979 [96], many other researchers put their effort in the development of an efficient CO_2 photoreduction. However, until the early 1990s, this reaction was considered more as a particular reaction to prove materials photoactivity than an exploitable technology: in the last two decades, the environmental sensitivity has grown bringing about all the potentials from this reaction and then more energy has been spent on the issue. From Scopus database [137] the number of publications on carbon dioxide photoreduction has exponentially grown in the las ten years, indicating the importance and efforts within scientific community to this topic. In 2017, 111 papers were published on this topic and this value is supposed to grow even more in 2018.

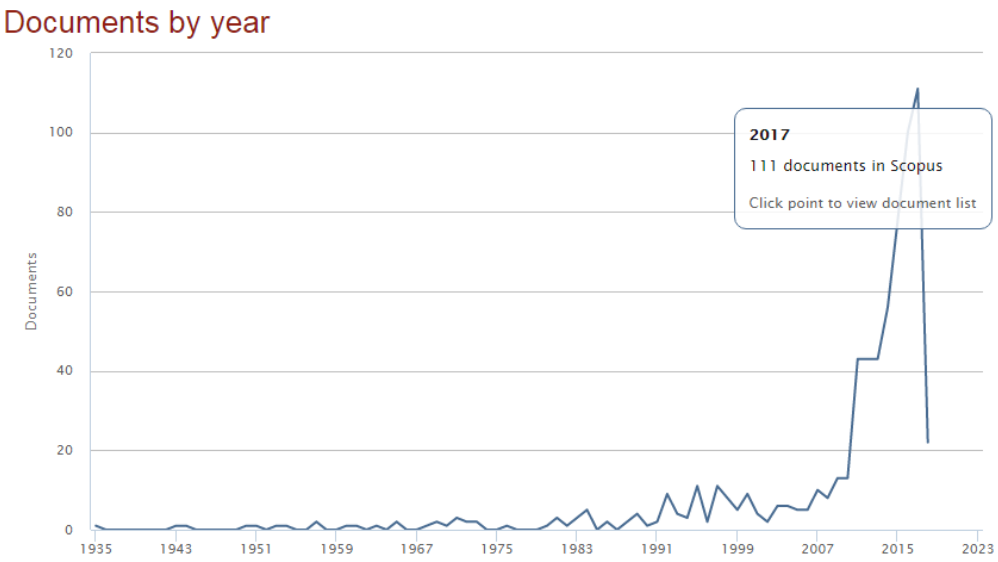

Figure 1.12 Number of publications per year on carbon dioxide photoreduction (source: https://www.scopus.com).

In fact, many reasons can be provided to explain the many environmental and economic advantages that explain the growing interest in this reaction [62]:

- environmentally friendly public image for the contribution to the conversion a greenhouse gas to valuable chemicals or fuels;
- decrease in CO_2 disposal costs;
- use of a feedstock with low or even negative value;
- production of high density liquid and gaseous fuels from CO_2 compatible with existing infrastructures.

CO_2 photoreduction is defined as an *uphill* process, since products energy is higher compared to reagents: in fact, if we consider Gibbs free energy of formation for most simple C1 compounds (reported in Figure 1.13), CO_2 is characterised by the lowest value of all molecules, indicating that any transformation requires energy. In the case of photoreduction, this energy is provided by a light source, which in the future could be free and sustainable sunlight.

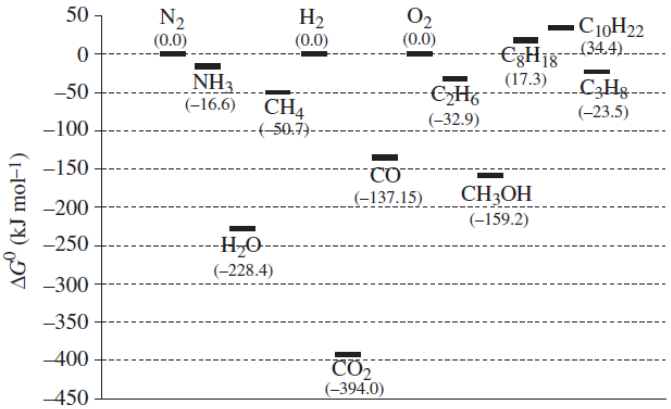

Figure 1.13 Gibbs free energy of formation for selected chemicals [138].

Whilst electronic hole in VB oxidises water, it has not been clarified yet whether CB's photoexcited electrons reduce CO_2 or H^+ from water, which, on its turn, reduces CO_2 [97,139-140]. In fact, in this reaction hydrogen transfer from oxygen to carbon occurs and it is not clear if hydrogen binds to carbon either as H^+ or $H\cdot$ or H^-.

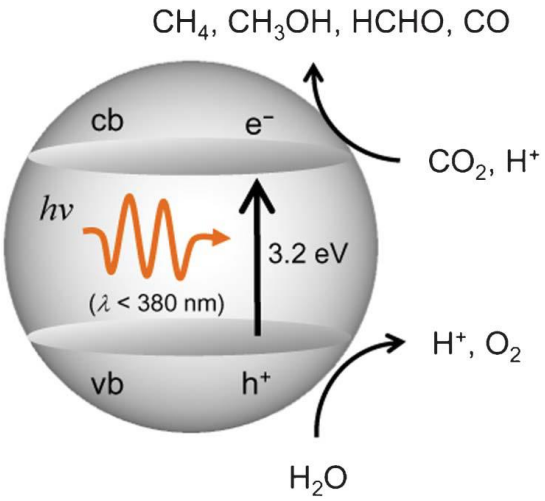

Figure 1.14 General mechanism for CO_2 photoreduction [141]

Due to all the variables involved in this process, among all proposed reaction mechanisms, none of them has been unanimously accepted yet. Moreover, the complexity of physicochemical processes within CO_2 photoreduction make this task extremely difficult. For these reasons, improvement in CO_2 photoreduction efficiency in solar fuels production is largely dependent on two factors that are interconnected one to the other, namely catalysts' physicochemical properties and reactor design. Both these aspects will be considered in the following paragraphs and throughout the whole thesis.

1.2.5 Titanium dioxide modification

Despite its great potentialities as a photocatalyst, titanium dioxide needs modification to adjust its properties for this reaction. First of all, adsorption, a preliminary phenomenon to any heterogeneous reaction, should be improved. In fact, Ti^{4+} centres are strong Lewis acid sites while O^{2-} is a weak Lewis base [140]: carbon dioxide can bind by oxygen to coordinatively unsaturated titanium sites or it can occupy oxygen vacancies by carbon. Unfortunately, in both cases the interaction with CO_2 is weak, while water vapour adsorption is way more intense [142]. Water is able to displace adsorbed CO_2 but prevents other carbon dioxide molecules to adsorb. In this way protons are reduced to molecular hydrogen instead of carbon by water splitting reaction [143]. Despite the great utility of

water splitting for sustainable hydrogen production, it does not provide any carbon dioxide transformation and then it is not desirable for these purposes.

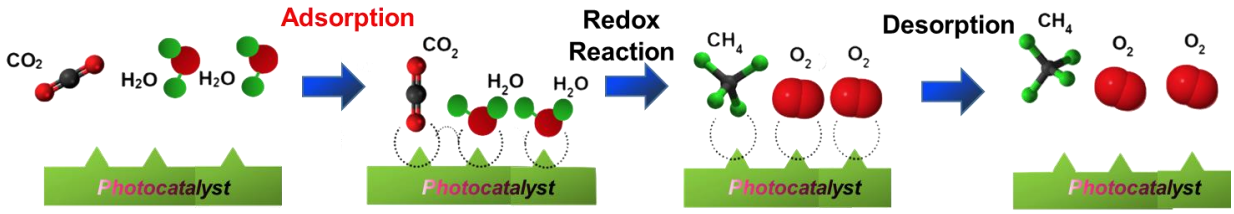

Figure 1.15 General heterogeneous CO_2 photoreduction process (rielaboration from ref. 142)

Once both reactants adsorption on adjacent sites has occurred, a multiple electrons transfer takes place through, despite it has not been clarified wheter it is a single multielectronic step or multiple mono-electronic steps [144]. Anyways, the amount of required electrons is extremely high and makes doping a useful and necessary upgrade for titania photocatalysts, in order to increase photoexcited electrons stability.

Reaction (25 °C and pH 7)	E° (V vs. NHE)
$CO_2 + 2H^+ + 2e^- \longrightarrow HCOOH$	-0,61
$CO_2 + 2H^+ + 2e^- \longrightarrow CO + H_2O$	-0,53
$CO_2 + 4H^+ + 4e^- \longrightarrow HCHO + H_2O$	-0,48
$CO_2 + 6H^+ + 6e^- \longrightarrow CH_3OH + H_2O$	-0,38
$CO_2 + 8H^+ + 8e^- \longrightarrow CH_4 + 2\,H_2O$	-0,24
$2H_2O + 4h^+ \longrightarrow O_2 + 4H^+$	+0,81

Table 1.2 Semireactions electrons required and redox potentials [145].

Noble transition metals like platinum [146], silver [147] and gold [148] were tested as promoters to stabilise and fasten separation of photoexcited charge carriers. In all the published papers, metal loading is very low, generally minor than 2 wt. %, since it acts only as a doping agent: moreover, generally high metal fractions are detrimental to titanium dioxide photoactivity. Even in this case, in the last years, greater attention has been put on less noble metals like nickel and copper [149].

1.2.6 Photoreactor design

The choice of the reactor design and process conditions is not a trivial matter, but it is responsible for substrates and photons delivery to the photocatalytic surface. While mass transfer is commonly considered in conventional catalysis processes, in photocatalysis also photons transfer must be addressed too. In fact, it is necessary for both reactants and photons to reach the surface for a photocatalytic reaction to take place.

As already mentioned, first studies focused on photoreaction in liquid systems [96]. In this case, the solvent, that is water, acts as a reductant as well and this strategy has been pursued ever since [144]. In this case several phenomena should be taken into account for mass transfer such as solubility, diffusion, convection and migration. CO_2 solubility in aqueous phase system, (0.03 M at 25 °C and 1 atm) [150], must be considered as a possible limiting step for the reaction in liquid phase, whereas in gas phase mixability is not an issue to be considered. In gas phase, migration can be excluded too since, in this case, only neutral species are involved in mass transfer, while in liquid phase the presence of charged catalytic surfaces and (bi)carbonates species can affect migration processes [151]. Therefore, only mass transport by diffusion and convection are considered. Usually gas phase reactions are performed in CO_2 excess and water vapour diffusion in CO_2 constant is relatively high (0.138 $cm^2 \cdot s^{-1}$), making possible to assume that the mass transport in gas phase CO_2 photoreduction is determined by convection only. High pressure is required to increase carbon dioxide solubility in the reaction medium [152], whereas in gas phase is not required.

The other important process parameter to be considered is light energy input. Despite generally photocatalytic technologies' main aim is the use of visible light, high CO_2 reduction potential and available semiconductors' CB energy levels limit the exploitation

of visible light as a source of energy and most published papers focus on this reaction under UV irradiation [153].

In addition to that, also the amount of irradiated photons is a fundamental parameter to be considered for an overall understanding of a photocatalytic process, since irradiation is the main force that drives it. This important parameter is considered by irradiance, which is defined by IUPAC "*as the radiant power, P, of all wavelengths incident from all upward directions on surface divided by the area of the element*" [93].

$$Irr = \frac{P}{illuminated\ area}$$

Equation 1.10

This metric is connected to the number of photons by the equation 4:

$$Photons\ (Einstein) = \frac{Irr \cdot illuminated\ area \cdot time \cdot \lambda}{N_A \cdot h \cdot c}$$

Equation 1.11

where λ is radiation wavelength, N_A is Avogadro's number, h Planck's constant and c speed of light.

Among photocatalytic researchers, the effect of irradiance has been scarcely investigated. As reported by Hermann, products formation generally increases with photons input [154]. However, in the case of CO_2 photoreduction, it is not clear whether irradiance enhances only photoactivity or drives also other parasitic reactions, such as water splitting and products degradation.

1.3 Aim of the work

Since growing CO_2 emissions represent a significant environmental issue, carbon dioxide transformation into high energy products seems the most suitable option to solve two critical issues of the twenty-first century, i.e. anthropogenic global warming and research for alternative and sustainable fuels. Among possible option, photoreduction, known also as artificial photosynthesis, represents one of the most promising in terms of sustainability.

For these reasons, this thesis will focus on understanding the key aspects involved in carbon dioxide photoreduction process and on assessing which are the most suitable catalysts and process conditions for and efficient conversion to solar fuels. In fact, the development of an efficient technology for carbon dioxide conversion into solar fuel relies on an interdisciplinary "catalysis by design" approach covering different expertise areas, such as fundamental and applied science. Up to now, published research papers address this topic either by focusing on materials development or by reaction parameters investigation, without much interest in considering both aspects at the same time. This "classical" approach does not allow to appreciate, for example different effect of catalyst promotion depending on experimental conditions or variations in light harvesting properties. For this reason, this thesis will investigate carbon dioxide photoreduction considering both photocatalysts formulation and reaction conditions impact on process effectiveness.

The work reported in this thesis can be divided in two parts, which are strictly connected one to the other. The first one will deal with materials formulation and in particular on the development of an efficient titanium dioxide based material: in this part will be investigated how materials' physicochemical properties affect reactant adsorption and light harvesting in CO_2 photoreduction. In the second part, focusing more on reactor engineering and reaction conditions, the best materials will be tested in different conditions in order to understand the effect of reaction medium and irradiance on solar fuels production.

The experimental work will be divided in six chapters:

- in chapter 2 the development of the lab-scale rig, which will be used for materials screening, will be presented;
- in chapter 3 titanium dioxide adsorption properties are modulated by synthetic route and basic oxides introduction;
- in chapter 4 metal particles introduction on titanium dioxide are studied to increase materials light harvesting;
- in chapter 5 materials are tested in liquid and gas phase lab-scale rigs in order to assess reaction medium effect;

- in chapter 6 materials are tested in different irradiance conditions, in order to get an insight of light source effect by a design of experiments approach;
- in chapter 7 general conclusions will be provided.

For the sake of clarity, a flow diagram is reported in Figure 1.16, in which the connection between the chapters is described.

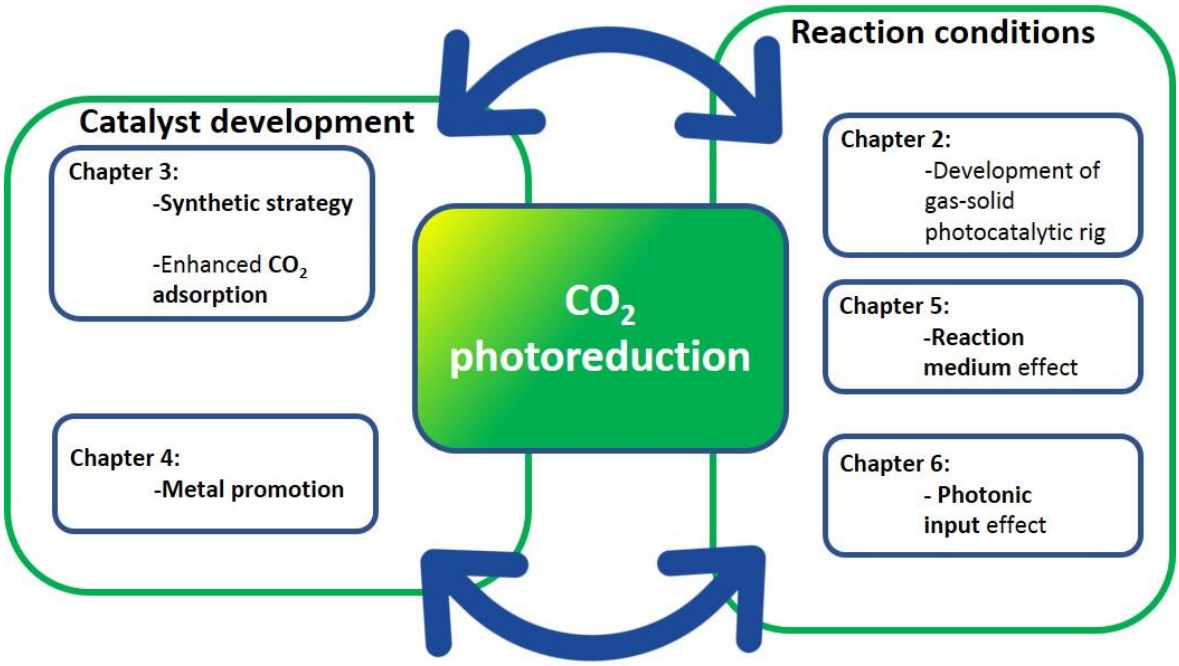

Figure 1.16 Flow diagram describing thesis outline.

At the end of this work, it would be possible to state which is the most promising catalyst modification and which are the most suitable reactor engineering conditions to increase CO_2 photoreduction effectiveness.

1.4 References

[1] E.M. Galimov, Geochemistry International 55 (2017) 401-417.

[2] C.T. Reinard, N.J. Planavsky, S.L. Olson, T.W. Lyons, D.H. Erwin, Proceedings of the National Academy of Sciences of the United States of America 113 (2016) 8933-8938.

[3] N.H. Sleep, D.K. Bird, Philosophical Transaction of the Royal Society B 363 (2008) 2651-2664.

[4] M.H. Hart, Icarus 33 (1978) 23-29.

[5] M.W. Wallace, A.S. Hood, A. Shuster, A. Greig, N.J. Planavsky, C.P. Reed, Earth and Planetary Letters 466 (2017) 12-19.

[6] S.A. Crowe, L.N. Døssing, N.J. Beukes, M. Bau, S.J. Kruger, R. Frei, D.E. Canfield, Nature 501 (2013) 535-539.

[7] J.H. Carver, Nature 292 (1981) 136- 138.

[8] A. Costa, M. Guarino, Atmospheric Environment 43 (2009) 1548-1566.

[9] K.P. Shine, J.S. Fuglestvedt, K. Hailemariam, N. Stuber, Climatic Change 68 (2005) 281-302.

[10] G.A. Florides, P. Christodoulides, Environment International 35 (2009) 390-401.

[11] R.B. Alley, J. Marotzke, W.D. Nordhaus, J.T. Overpeck, D.M. Peteet, R.A. Rielke, R.T. Pierrehumbert, P.B. Rhines, T.F. Stocker, L.D. Talley, J.M. Wallace, Nature 299 (2003) 2005-2010.

[12] GISTEMP Team, 2016: GISS Surface Temperature Analysis (GISTEMP). NASA Goddard Institute for Space Studies. Dataset accessed 2017-08-07 at https://data.giss.nasa.gov/gistemp/.

[13] P.U. Clark, A.S. Dyke, J.D. Shakun, A.E. Carlson, J. Clark, B. Wolfarth, J.X. Mitrovica, S.W. Hostetles, A.M. McCabe, Science 325 (2009)710-714.

[14] C.J. Barrow, International Encyclopedia of Human Geography, 1st ed. Elsevier 2009 Oxford UK.

[15] L. Kantha, Ocean Engeneering 70 (2013) 124-128.

[16] M. Monirul Qader Mirza, Global Environmental Change 12 (2002) 127-138.

[17] D.E. Raitsos, G. Beaugrand, D. Georgopoulos, A. Zenetos, A.M. Pancucci-Papadopoulou, A. Theocharis, E. Papathanassiou, Limnology and Oceanography Journal 55 (2010) 1478-1484.

[18] K. Brysse, N. Oreskes, J. O'Reilly, M. Oppenheimer, Global Environmental Change 23 (2013) 327-337.

[19] A. Levermann, P.U. Clark, B. Marzeion, G.A. Milne, D. Pollard, V. Radic, A. Robinson, Proceedings of the National Academy of Sciences of the United States of America 110 (2013) 13745-13750.

[20] S. Schmidtko, L. Stramma, M. Visbeck, Nature 252 (2017) 335-339.

[21] K. Stanislawka, K. Krawiec, Z.W. Kundzewicz, Computer and Mathematics with Applications 64 (2012) 3717-3728.

[22] A.P.P. Baede, P. van der Linden, A. Verbruggen, Annex II to IPCC 2014 Report, available at http://www.ipcc.ch/pdf/assessment-report/ar4/syr/ar4_syr_appendix.pdf

[23] R.G. Derwent, W.J. Collins, C.E. Johnson, D.S. Stevenson, Climatic Change 49 (2001) 463-487.

[24] G.A. Folberth, S.T. Rumbold, W.J. Collins, T.M. Butler, Urban Climate 1 (2012) 4-19.

[25] D.M. Kammen, B.D. Marino, Chemosphere 26 (1993) 69-86.

[26] 4th IPCC 4th assessment 2007, available at http://www.ipcc.ch/pdf/assessment-report/ar4/syr/ar4_syr.pdf

[27] D.T. Shindell, G. Favulegi, D.M. Koch, G.A. Schmidt, N. Unger, S.E. Bauer, Nature 326 (2009) 716-718.

[28] T.K. Berntsen, j.S. Fuglentvedt, M.M. Joshi, k.P. Shine, N. Stuber, M. Ponater, R. Sausen, D.A. Hauglustaine, L. Li, Tellus B 57 (2005) 283-304.

[29] O. Boucher, P. Friedlingstein, B. Collins, K.P. Shine, Environmental Research Letters 4 (2009) 1-5.

[30] G.J.M. Velders, S.O. Andersen, J.S. Daniels, D.W. Fahey, M. McFarland, Proceedings of the National Academy of Sciences 104 (2007) 4814-4819.

[31] S.A. Monntzka, M. McFarland, S.O. Andersen, B.R. Miller, D. W. Fahey, B.D. Hall, L. Hu, C. Siso, J.W. Elkins, Journal of Physical Chemistry A 119 (2015) 4439-4449.

[32] C. Figueres, H.J. Schellnhuber, G. W. J. Rockström, A. Hobley, S. Rahmstorf, Nature 546 (2017) 593-595.

[33] E. Benhal, G. Zahedi, E. Shamsaei, A. Bahadori, Journal of Cleaner Production 51 (2013) 142-161.

[34] P.N. Pearson, M.R. Palmer, Nature 406 (2000) 695-699.

[35] T. Blunier, T.M. Jenk, Encyclopedia of Quaternary Science, 2nd ed. Elsevier 2013 Oxford UK.

[36] Y.G. Zhang, M. Pagani, Z. Liu, S.M. Bohaty, R. DeConto, Philosophical Transaction of the Royal Society A 371 (2013) 1-20.

[37] G.P. Peters, E.G. Hertwich, Climatic Change 86 (2008) 51-66.

[38] J.G.J. Olivier, G. Janssens-Maenhout, M. Muntean, J.A.H.W. Peters, Trends in Global CO_2 emissions: 2013 Report, 1st ed. PBL Press 2013 The Hague The Netherland.

[39] Data from Global Monitory Division of US National Oceanic and Atmospheric Administration, available at https://www.esrl.noaa.gov/gmd/trends/monthly.html

[40] A. Indermüle, T.F. Stocker, F. Joos, H. Fisher, H.J. Smith, M. Wahlen, B. Deck, D. Mastroianni, J. Tschumi, T. Blunier, R. Meyer, B. Stauffer, Nature 398 (2000) 121-126.

[41] P.J. Crutzen, Nature 415 (2002) 23.

[42] A.J. Porter, T.R. Kuhn, B. Nerlich, Organization Studies 38 (2017) 1-26.

[43] Kyoto Protocol, full text available at https://www.unfccc.int

[44] United Nations Framework Convention on Climate Change (UNFCCC) Adoption of the Paris Agreement, 21st Conference of the Parties, 2015 Paris.

[45] H. Arawaka, M. Aresta, J.N. Armor, M.A. Barteau, E.J. Beckman, A.T. Bell, J.E. Bercaw, C. Creutz, E. Dinjus, D.A. Dixon, K. Domen, D.L. Dubois, J. Eckert, E. Fujita, D.H. Gibson, W.A. Goddard, D.W. Goodman, J. Keller, G.J. Kubas, H.H. Kung, J.E. Lyons, L.E. Manzer, T.J. Marks, K. Morukuma, K.M. Nicholas, R. Periana, L. Que, J. Rostrup-Nielsen, W.M.H. Sachter, L.D. Schmidt, A. Sen, G.A. Somorjai, P.C. Star, B.R. Stults, W. Tumas, Chemical Reviews 101 (2001) 953-996.

[46] C. McGlade, P. Ekins, Nature 517 (2015) 187-190.

[47] T. da Silva Veras, T. Simonato Mozer, D. da Costa Rubim Messeder dos Santos, A. da Silva Cesar, International Journal of Hydrogen Economy 42 (2017) 2018-2033.

[48] M.S. Mancini, A. Galli, V. Nicolucci, D. Lin, S. Bastianoni, M. Wackernagel, N. Marchettini, Ecological Indicators 61 (2016) 390-403.

[49] P.B. Weisz, Physics Today 57 (2004) 47-52.

[50] United States Department of Energy, National Energy Technology Laboratory website https://netl.doe.gov

[51] N.W. Krase, V.L. Gaddy, The Journal of Industrial and Enigneering Chemistry 7 (1922) 611-616.

[52] K.H. Büchel, H.H. Moretto, P. Woditsch, Industrial Inorganic Chemistry 2nd ed. Wiley 2000 Weinheim Germany.

[53] A. Pearson, International Journal of Refrigeration 28 (2005) 1140-1148.

[54] S. Zielińska, F. Valensi, N. Pellerin, S. Pellerin, K. Musioł, C. de Izarra, F. Briand, Journal of Material Processing Technology, 209 (2009) 3581-3591.

[55] V.R. Katta, F. Takahashi, G.T. Linteris, Combustion and Flame 137 (2004) 506-522.

[56] M. Jakobsen, J. Risbo, Journal of Food Engineering 92 (2009) 285-290.

[57] G. Calderone, C. Guillou, F. Reniero, N. Naulet, Food Research International 40 (2207) 324-331.

[58] M.V. Palmer, S.S.T. Ting, Food Chemistry 52 (1995)345-352.

[59] P.G. Jessop, Journal of Supercritical Fluids 38 (2006) 211-231.

[60] T. Sakakura, J.C. Choi, H. Yasud, Chemical Reviews 107 (2007) 2365-2387.

[61] T. Iijima, T. Yamaguchi, Tetrahedron Letters 48 (2007) 5309-5311.

[62] G. Centi, S. Perathoner, Catalysis Today 148 (2009) 191-205.

[63] M. E. Boot-Handford, J. C. Abanades, E. J. Anthony, M. J. Blunt, S. Brandani, N. Mac Dowell, J. R. Fernandez, M.-C. Ferrari, R. Gross, J. P. Hallett, R. S. Haszeldine, P. Heptonstall, A. Lyngfelt, Z. Makuch, E. Mangano, R. T. J. Porter, M. Pourkashanian, G. T. Rochelle, N. Shah, J. G. Yao, P. S. Fennell, Energy and Environmental Science 7 (2014) 130–189.

[64] H. Yang, Z. Xu, M. Fan, R. Gupta, R.B. Slimane, A.E. Bland, I. Wright, Journal of Environmental Sciences 20 (2008) 14-27.

[65] A. Sanna, M. Uibu, G. Caramanna, R. Kuusik, M. Maroto-Valer, Chemical Society Reviews 43 (2014) 8049-8080.

[66] S. Ma'mun, H.F. Svendsen, K.A. Hoff, O. Juliussen, Energy Conversion and Management 48 (2007) 251-258.

[67] G.P. Knowles, J.V. Graham, S.W. Delaney, A.L. Chaffee, Fuel Processing Technology, 86 (2005) 1435-1448.

[68] X. Ma, X. Wang, C. Song, Journal of American Chemical Society 131 (2009) 5777-5783.

[69] J.C.M. Pires, F.G. Martins, M.C.M. Alvim-Ferraz, M. Simões, Chemical Engineering Research and Design 89 (2011) 1146-1160.

[70] G.J. Collie, M. Nazeri, A. Jahabakhsh, C.W. Lin, M. Maroto-Valer, Greenhouse Gas Science and Technology 7 (2017) 10-28.

[71] G. Holmes, K. Nold, T. Walsh, K. Heidel, M.A. Henderson, J. Ritchie, P. Klavins, a. Singh, D.W. Keith, Energy Procedia 37 (2013) 6079-6095.

[72] IPCC, Special Report on Carbon Dioxide Capture and Storage, 1st ed. Cambridge University press 2005 Cambridge UK.

[73] M. Mitrovic, A. Malone, Energy Procedia 4 (2011) 5685-5691.

[74] R. Lofstedt, Journal of Risk Research 18 (2015) 675-691.

[75] O. Eiken, P. Ringrose, C. Hermanrud, B. Nazarian, T.A. Torp, L. Høier, Energy Procedia 4 (2011) 5541-5548.

[76] B. Spence, D. Horan, O. Tucker, Energy Procedia 63 (2014) 6258-6266.

[77] H. Zangeneh, S. Jamshidi, M. Saltanieh, International Journal of Greenhouse Gas Control 17 (2013) 515-522.

[78] J. van Heek, K. Arning, M. Ziefle, Energy Policy 105 (2017) 53–66.

[79] J. Nässén, J. Holmberg, A. Wadeskog, M. Nyman, Energy 32 (2007) 1593-1602.

[80] A. Murray, K. Skene, K. Haynes, Journal of Business Ethics 140 (2017) 369-380.

[81] C. Ampelli, S. Perathoner, G. Centi, Philosophical Transactions of the Royal Society 373 (2015) 1-34.

[82] M. Höök, X. Tang, Energy Policy 52 (2013) 797-809.

[83] P. Falkowski, R. J. Scholes, E. Boyle, J. Canadell, D. Canfield, J. Elser; N. Gruber, K. Hibbard, P. Högberg, S. Linder, F. T. Mackenzie, B. Moore III, T. Pedersen, Y. Rosenthal, S. Seitzinger, Nature 290 (2000) 291-296.

[84] P.B. Weisz, Physics Today 57 (2004) 47-52.

[85] G. Centi, S. Perathoner, Catalysis Today 148 (2009) 191-205.

[86] M. Younas, L.L. Kong, M.J.K. Bashir, H. Nadeem, A. Shehzad, S. Sethupathu, Energy and Fuels 30 (2016) 8815-8831.

[87] N. Muradov, International Journal of Hydrogen Economy 42 (2017) 14058-14088.

[88] C. Graves, S.D. Ebbesen, M. Morgensen, K.S. Lackner, Renewable and Sustainable Energy Reviews 15 (2011) 1-23.

[89] T. Faunce, Procedia Engineering 49 (2012) 348-356.

[90] A. Dhakshinamoorthy, S. Navalon, A. Corma, H. Garcia, Energy and Environmental Science 5 (2012) 9217-9233.

[91] M. Tahir, N. Amin, Renewable and Sustainable Energy Reviews 25 (2013) 560-579.

[92] D.R. MacFarlane, X. Zhang, M. Kar, Green Chemistry 18 (2016) 5689-5692.

[93] S.E. Braslavsky, A.M. Braun, A.E. Cassano, A.V. Emeline, M.I. Litter, L. Palmisano, V.N. Parmon, N. Serpone, Pure and Applied Chemistry 83 (2011) 931-1014.

[94] A. Fujishima, K. Honda, Nature, 238 (1972) 37-38.

[95] A.J. Bard, Journal of Photochemistry 10 (1979) 59-75.

[96] T. Inoue, A. Fujishima, S. Konishi, K. Honda, Nature 277 (1979) 637-638.

[97] L. Liu, Aerosol and Air Quality Research 2 (2014) 453-469.

[98] J. Bonin, M. Robert, M. Routier, Journal of American Chemical Society 136 (2014) 16768-16771.

[99] J. Song, E.L. Klein, F. Neese, S. Ye, Inorganic Chemistry 53 (2014) 7500-7507.

[100] H. Kawanami, D.C. Grills, T. Ishizaka, m. Chatterejee, A. Sukuzi, Journal of CO_2 utilization 3-4 (2013) 93-97.

[101] P. Usubharatawana, D. McMartin, A. Veawab, T. Tontiwachwuthikul, Industrial Engineering Chemistry Research 45 (2006) 2558-2568.

[102] K. Kočì, L. Obalová, Z. Lacný, Chemical Papers 62 (2008) 1-9.

[103] J. Schneider, M. Matsuoka, M. Takeuchi, J. Zhang, Y. Horichi, M. Anpo, D.W. Bahnemann, Chemical Reviews 114 (2014) 9919-9986.

[104] A.R. West, Basic State Solid Chemistry, 2nd ed. Wiley 1988 New York USA.

[105] J.M. Hermann, Applied Catalysis B: Environmental 99 (2010) 461-468.

[106] O. Carp, C.L. Huisman, A. Reller, Progress in Solid State Chemistry 32 (2004) 33-177.

[107] A.L. Linsebigler, G. Lu, J.T. Yates, Chemistry Review 95 (1995) 753-758.

[108] J. Tauc, Semiconductors and Semimetals 21 (1984) 299-327.

[109] K.H. Büchel, H.H. Moretto, P. Woditsch, Industrial Inorganic Chemistry 2nd ed., Wiley 2000 Weinheim Germany.

[110] G.M. Bedinger, 2016 United States Geological Survey Mineral Reports, available at https://www.usgs.gov/

[111] Hexa Research, Titanium Dioxide, Market Size and Forecast, By Manufacturing Process (Chloride Route, Sulfate Process), By product (Anatase, Rutile), By Application (Paints & Coatings, Plastics, Paper, Ink, Specialties) And Trend Analysis, 2014 – 2024 1st ed. Hexa Research Press Felton CA, USA 2017.

[112]US Food and Drugs Administration official site: http://www.fda.gov

[113] J. Smith, L. Long-Shum, Food Additives Data Book, 1st ed. Blackwell Publishing Company 2003 Oxford UK.

[114] H. H. Behrei, K.R. Mohamed, G. T. El-Bassyouni, Ceramics International 35 (2009) 1991-1997.

[115] J. Van de Loosdrecht, A.M. Van der Kraan, A.J. Van Dillen, J.W. Geus, Journal of Catalysis, 170 (1997) 217-226.

[116] J. Deng, D. Wang, X. Wei, R. Zhai, H. Wang, Surface Science 249 (1991) 213-222.

[117] A. Berkò, G. Menesi, F. Solymosi, Surface Science 372 (1997) 202-210.

[118] I.R. Galindo, J.A. de los Reyes, Fuel Processing Technology 88 (2007) 859-863.

[119] F. Menegazzo, M. Signoretto, F. Pinna, M. Manzoli, V. Aina, G. Cerrato, F. Boccuzzi, Journal of Catalysis 309 (2004) 241-247.

[120] U. Diebold, Surface Science Reports 48 (2003) 53-229.

[121] F.A. Cotton, G. Wilkinson, Advanced Inorganic Chemistry, 3rd ed. Wiley 1972 New York USA.

[122] A. Narotsky, J.C. Jamieson, O.J. Kleppa, Science, 158 (1967) 338-389.

[123] M.K. Nowotny, P. Bogdanoff, T. Dittrich, S. Fiechter, A. Fujishima, H. Tributsch, Material Letters 64 (2010) 928-930.

[124] T. Shibata, H. Irie, M. Ohmori, A. Nakajima, T. Watanabe, K. Hashimoto, Physical Chemistry Chemical Physics 6 (2004) 1359-1362.

[125] A.L. Linsebigler, G. Lu, J.T. Yates, Chemistry Review 95 (1995) 753-758.

[126] A. Kubacka, M. Fernández-García, G. Colón, Chemical Reviews 112 (2012) 1555-1614.

[127] N. Daude, C. Gout, C. Jouanin, Physical Review B 15 (1977) 3299-3235.

[128] W.K. Jo, J.H. Park, H.D. Chun, Journal of Photochemistry and Photobiology A: Chemistry 148 (2002) 109-119.

[129] S. Wang, H.M. Ang, M.O. Tade, Environment International 33 (2007) 694-705.

[130] V. Trevisan, A. Olivo, F. Pinna, M. Signoretto, F. Vindigni, G. Cerrato, C.L. Bianchi, Applied Catalysis B: Environmental 319 (2014) 61-70.

[131] A. Olivo, M. Signoretto, E. Ghedini, F. Pinna, D. Marchese, G. Cruciani, M. Manzoli, Chemistry Select 2 (2017) 728-739.

[132] L. Zou, Y. Luo, M. Hooper, E. Hu, Chemical Engineering and Processing 45 (2006) 959-964.

[133] M. Pelaez, N.T. Nolan, S.C. Pillai, M.K. Seery, P. Falaras, A.G. Kontos, P.S.M. Dunlop, J.W.J. Hamilton, J.A. Byrne, K. O'Shea, M.H. Entezari, D.D. Dionysiou, Applied Catalysis B: Environmental 125 (2012) 331-349.

[134] Evonic Corporation official site: http://www.corporate.evonik.de

[135] S. Noimark, C.W. Dunnill, I.P. Parkin, Advanced Drug Delivery Reviews 65 (2013) 570-580.

[136] A. Stefanou, A. Evangelou, P. Falaras, Catalysis Today 151 (2010) 58-63.

[137] Scopus database website https://scopus.com

[138] Z. Jiang, T. Xiao, V. Kuznetsov, P.P. Edwards, Philosophical Transactions of the Royal Society A 368 (2010) 3343-3364.

[139] E. Karamian, S. Sharifnia, Journal of CO_2 Utilization 16 (2016) 194-203.

[140] M. Anpo, H Yamashita, Y. Ichihashi, S. Ehara, Journal of Electroanalytical Chemistry 396 (1995) 21-26.

[141] K. Mori, H. Yamashita, M. Anpo, RCS Advances 2 (2012) 3165-3172.

[142] L.L. Tan, W.J. Ong, S.P. Chai, A.M. Rahman, Chemical Engineering Journal 308 (2017) 248-255.

[143] M. Li, M.K.H. Leung, D.Y.C. Leung, K. Sumathy, Renewable and Sustainable Energy Reviews 11 (2007) 401-425.

[144] G. Liu, N. Hoivik, K. Wang, H. Jakobsen, Solar Energy Materials and Solar Cells 105 (2012) 53-68.

[145] K. Li, X. An, H. Park, M. Khraisheh, J. Tang, Catalysis Today 224 (2013) 3-12.

[146] J. Mao, L. Ye, K. Li, X. Zhang, J. Liu, T. Peng, L. Zan, Applied Catalysis B: Environmental 144 (2014) 855-862.

[147] D. Kong, J.Z.Y. Tan, F. Yang, J. Zeng, X. Zhang, Applied Surface Science 277 (2013) 105-110.

[148] A. Corma, H. Garcia, Journal of Catalysis 308 (2013) 168-175.

[149] Q. Zhang, T. Gao, J.M. Andino, Y. Li, Applied Catalysis B: Environmental 123 (2012) 257-264.

[150] R.H. Perry, D.W. Green, Perry's Chemical Engineers' Handbook, 7th ed. McGraw-Hill 1997 New York USA.

[151] A. Dhakshinamoorthy, S. Navalon, A. Corma, H. Garcia, Energy and Environmental Science 5 (2012) 9217-9233.

[152] P. Usubharatana, D. McMartin, A. Veawab, P. Tontiwachwuthikul, Industrial Engineering Chemical Research 45 (2006) 2558-2568.

[153] S. Roy, O. Varghese, M. Paulose, C.A. Grimes, ACS Nano 4 (2010) 1259-1278.

[154] J. Hermann, Catalysis Today 53 (1999) 115-129.

2 Design of a Photocatalytic Process for CO_2 Reduction

This chapter will provide an overlook on all different experimental setups for photocatalytic carbon dioxide photoreduction, considering their strengths and weaknesses related to physical and chemical phenomena involved in this process. From these considerations, all the choices, that were made, will be rationally explained and the final experimental setup will be explained.

Finally, commercial titanium dioxide materials will be tested in the lab-scale rig to validate its effectiveness. In this part, catalyst introduction method will be considered too, investigating which method is the most suitable. The preliminary assessment of reaction conditions and reactor design displayed in this chapter will be used in the further chapters on photocatalysts formulation.

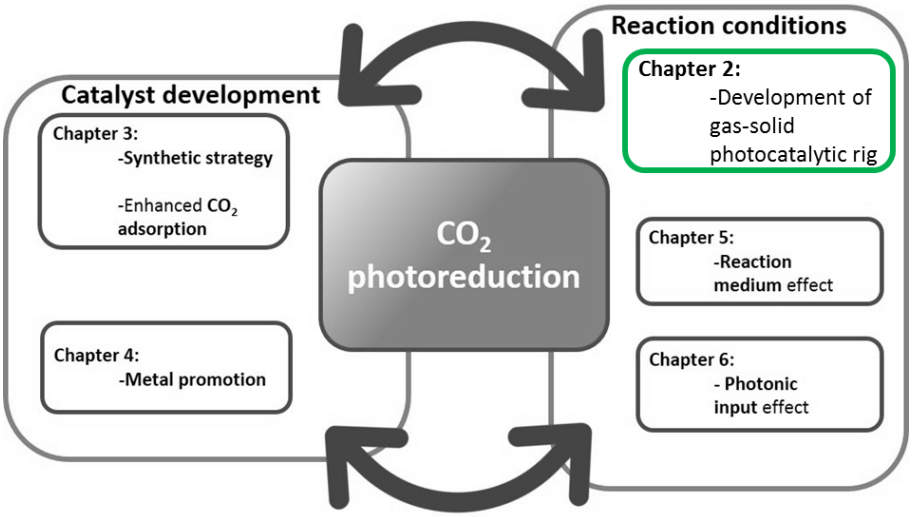

Figure 2.1 Sketch representing this chapter connection to the others in this thesis.

2.1 Literature review on photoreactors

2.1.1 Three phases photocatalytic systems

From an historical point of view, the first developed photoreactors for CO_2 reduction were batch reactors where the catalyst was suspended in a liquid medium, usually

water, and carbon dioxide was bubbled through reaction medium and light reached reaction medium through quartz windows [1-4].

This choice of three-phases slurry reactors was, and still is, widely used due to many advantages. First of all, these experimental rigs are similar to those used for carbon dioxide photoelectrocatalytic reduction [5,6] and, most importantly, they have been widely used in photooxidation processes, which, in some cases, are available on a commercial scale [7,8].

In addition to that, catalyst does not require any casting or shaping procedure before its use, so it can be used as a powder without further modification. Mass transfer is achieved by mixing, either magnetically or mechanically, providing homogeneity in reaction medium.

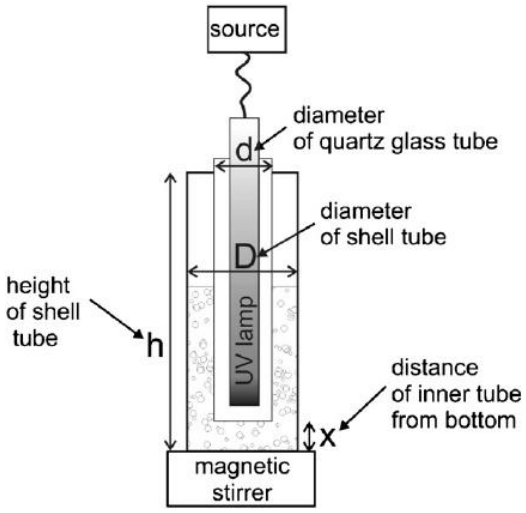

Figure 2.2 Example of a three phases batch reactor [9].

For example, Reli and co-workers used a batch reactor (reported in Figure 2.2) that was characterised by annular geometry: the UV lamp is cast at the centre of the reactor to maximise light harvesting efficiency and it irradiates the aqueous catalyst suspension and CO_2 is bubbled through it to reach saturation [9].

However, liquid phase setups are affected by experimental drawbacks that need to be overcome. The first one, as mentioned in Chapter 1, i.e. extremely low CO_2 solubility in

water, is extremely important and limits reagents availability. Being water usually exceeding to carbon dioxide, water splitting becomes an important side reaction, which implies reductants consumption without carbon dioxide conversion.

Several solutions to this problem have been reported in literature. The most common strategy is the introduction of a base to improve CO_2 solubility. Many authors use basic solutions as reaction media which lead to the formation of more soluble and stable carbonates and bicarbonate species in solution [10]. Generally, the most used base is sodium hydroxide [11,12], but use of other bases is reported, such as sodium bicarbonate [13], potassium biphosphate [14] and triethanolamine (TEA) [15].

Whereas, Quin and co-workers did not use water as a reaction medium, but used methanol, whose CO_2 solubility is way higher [16] and observed that the main product was methyl formate which was obtained by esterification of the solvent and formic acid from CO_2 reduction. Alternatively, Liu and co-workers used isopropanol as a solvent increasing CO_2 solubility leading to similar results [17].

However, it has been observed that these solvents can act as sacrificial agent and be oxidised in TiO_2's valence band instead of water [18]. This means a minor sustainability of the process because, in these photocatalytic systems, the reductant is more expensive and industrially derived from fossil sources (mainly natural gas or coal gasification).

Whereas, Rossetti *et al.* reported that the use of a pressurised photoreactor increases carbon dioxide dissolution in aqueous media yielding higher catalytic activity in methane production avoiding chemical absorption as carbonates in high pH conditions [19], which might lead to reactor walls corrosion. Alternatively, Kaneco and co-workers performed photoreduction in liquid CO_2 overcoming solubility problems [20] at 20 °C, but, compared to common photocatalytic reactions, pressure is extremely high (6.5 MPa) in order to maintain CO_2 in liquid phase.

The second issue to face in three phases batch reactors is light transfer. In fact, photons are required to travel from light source through reaction medium to the photocatalyst surface, where they are absorbed and activate the photocatalyst. By the refractive index

n, defined as the ratio between speed of light in vacuum (c_0) to speed of light in any medium (c), it is possible to compare reaction media permeability to photons.

$$n = \frac{c_0}{c}$$

Equation 2.1

At 293 K with and 361 nm light wavelength, water refractive index is 1.34795, whereas refractive index value is 1.000464 for CO_2 and 1.000256 for water vapour [21,22]: it means that light transfer in aqueous solutions is much more difficult in liquid media compared to gas phase systems.

Finally, the use of fine suspended catalyst might lead to fouling of radiation source, lower active surface contact area and higher separation cost for products collection. Despite technological advances, some of these issues such as high refractive index and poor solubility cannot be completely eliminated, reducing the potentialities of these systems.

2.1.2 Gas-solid photocatalytic systems

Over the years, gas-solid photoreactors have become popular in literature. This solution allows finally to solve issues related to CO_2 solubility in water. In fact, as any gas, water vapour and carbon dioxide are perfectly mixable, allowing thus to tune reactants ratio and perform photoreduction in CO_2 excess avoiding water splitting. Moreover, separation is easier since reagents and products are in gas phase while the catalyst is solid.

Despite all these advantages, still some technological issues need to be addressed to reach a real breakthrough in CO_2 photoreduction. In fact, the end goal is to design a flow process in which continuously reagents reach the catalyst and products are formed. However, due to thermodynamic limitations and technical inexperience, batch processes are generally reported in literature, due to high contact time between catalyst and reagents [10], despite recently some papers on flow reaction have appeared [23].

The first concern is the control of CO_2/H_2O ratio. For example, Bazzo and Urawaka reported the use of moist quartz wool to generate water vapour *in situ* [24]. However, in this case, the amount of water in the gas phase is not controlled leading to differences in the CO_2/H_2O ratio calculations. Collado and co-workers used a controlled evaporator mixture to maintain reactants ratio [25], whereas other authors, such as Tahir and Amin [26] or Cybula *et al.* [27], employ a water bubbler to saturate flowing CO_2 with water vapour. In this way it is possible to tune water amount controlling temperature, pressure and carbon dioxide flow, as indicated in equation 2. However, temperature is not controlled, though it affects water vapour pressure and thus CO_2/H_2O ratio, leading to a lower tests reproducibility.

$$H_2O\ flow = \frac{\left(H_2O_{vapour\ pressure}\right)_{T,p} \cdot CO_2 flow}{p_{TOT} - \left(H_2O_{vapour\ pressure}\right)_{T,p}}$$

Equation 2.2

Gas-solid systems allows also a great choice in catalyst introduction techniques. Packed bed reactor design is the easiest technological solution, since low pressure drops can be achieved controlling catalyst particle size providing promising results [28]. However, it suffers from a low irradiated surface area to volume ratio, that negatively affect photon harvesting and thus light absorption and scattering [29]. According to Kočí and co-workers [30], annular reactor, where the catalyst in embedded within two concentric cylinders and the radiation source is in the centre, improved irradiation homogeneity, despite issues in gases mixing due to small cross-section.

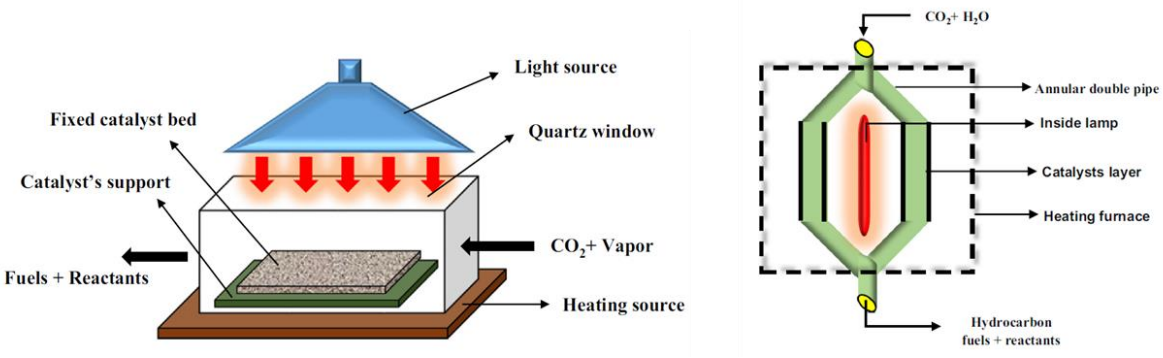

Figure 2.3 Schematic of a fixed bed photoreactor (left) and annular reactor (right) [31].

To overcome inhomogeneous irradiance, several solutions were developed. The use of optical fibres instead of a single light source provides high transmission and irradiation uniformity [32]. This kind of irradiation is generally coupled with the use of honeycomb monoliths, which also minimise pressure drops. The catalyst is layered within monolith inner walls by wash-coating or, as reported by Ola and Maroto-Valer [33], it is synthesised *in situ* by sol-gel method.

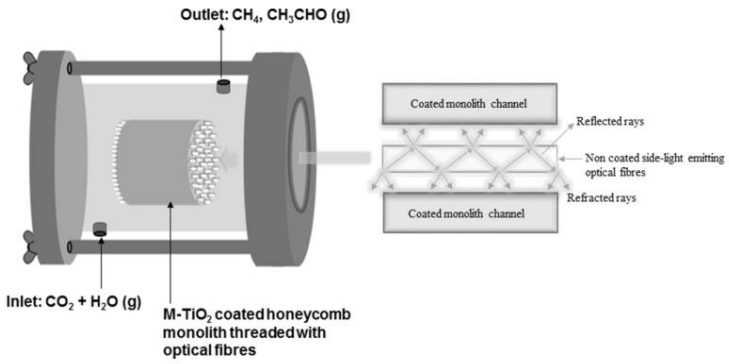

Figure 2.4 Schematic of a TiO_2 coated monolith reactor illuminated by optical fibres [33].

However, in these systems mass transfer of reagents and products to and from the catalytic sites might be too critical and channels opacity might decrease light harvesting efficiency [34]. Finally, another possibility for gas-solid reactor for thin film is thin film reactors. In this configuration, the photocatalyst is not immobilised onto beads, fibres or monoliths, but it is deposited on a plate or, even better on photoreactors surface. In this case, irradiation and light distribution are influenced by geometry and light source with great effects on global photoactivity [35]. Several geometries were reported in literature: for example, Pathak *at al.* used nafion membranes to support photocatalyst film [36], whereas Tan and co-workers used a quartz rod within the photoreactor [37].

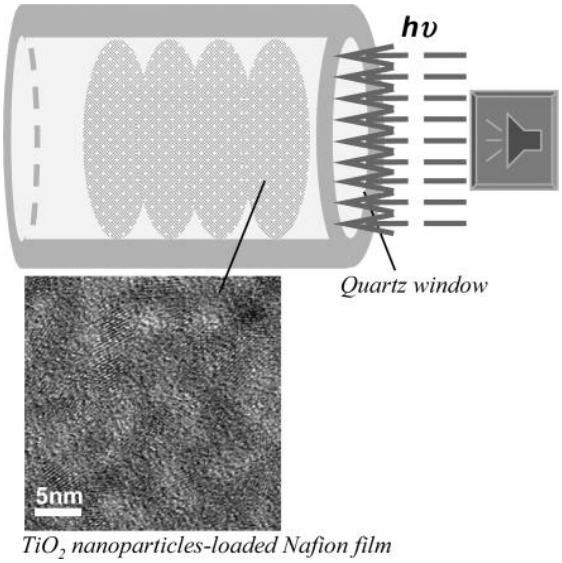

Figure 2.5 Nafion immobilised TiO_2 on gas-solid photoreactor [36].

2.2 From phenomena to process design

Ideally, a solar light driven photoreactors must have [31]:

- high coverage area for catalyst holding and spectral distribution;
- a support with small-through channels allowing high CO_2 velocity and high mass transfer;
- no flow routes through the reactor where the catalysts remain without light irradiation;
- an efficient reflector to harvest maximum illumination and intensity.

Comparing both three-phases and two-phases photoreactors (summarised in Table 2.1), gas-solid systems are most suitable option for the design of a photoreactor due to their flexibility in process development and smaller limitations to mass-related physical phenomena (i.e. CO_2 adsorption and light scattering through reaction medium).

	Issue	Solution
Three-phases Photoreactors	CO_2 solubility	Basic reaction medium Alternative solvent High pressure
	Water Splitting	Sacrificial agent
	Light scattering	Efficient Stirring Wise reactor geometry
	Fouling	Preformed catalyst
	Separation	Preformed catalyst
Gas-solid Photoreactors	Variable CO_2/H_2O ratio	Control of reactants feed
	High contact time	Batch reactor
	Irradiation inhomogeneity	Geometry Optic fibres Catalyst immobilisation

Table 2.1 Summary of features to consider in CO_2 photoreactors design.

Considering reactants feed, bubbling gaseous CO_2 seems the easiest yet efficient way to obtain CO_2-rich reactants mixture avoiding the use of sacrificial agents. Moreover, by a careful control of carbon dioxide flow and bubbler temperature, is possible to obtain a stable and constant CO_2/H_2O ratio.

Secondly, light harvesting should be taken into account. Energy input should be as low as possible. As mentioned in Chapter 1, due to involved reactions redox potentials, visible light use is very challenging [38]; therefore light sources intensity must be tuned by irradiance. Generally, irradiance ranges from 200 $W \cdot m^{-2}$ to 3000 $W \cdot m^{-2}$ [39,40] despite average UV sun irradiance is 50 $W \cdot m^{-2}$. Moreover, also reactor shape affects light harvesting. In order to maximise catalyst irradiation and thus photons absorption on photocatalytic surface, the highest fraction of the catalyst must be exposed. For this reason, high area to volume ratio is required, regardless catalyst introduction method.

Finally, also detection method should be considered. In order to avoid contamination from air, and in particular oxygen, in-line systems are generally preferred. A variety of

analytical choices are reported in literature, but the most used analytical techniques for gas-solid reactors are gas chromatography and mass spectrometry [41,42].

All these considerations were taken into account to develop a lab-scale photocatalytic rig, which will be discussed in this chapter. Moreover, two different commercial titanium dioxide materials will be tested and compared in order to understand which physicochemical phenomena are crucial for an efficient CO_2 photoreduction.

2.3 TiO_2 Reference materials

For this study, two reference TiO_2 material were considered. The first one is P25 from Evonik GmbH [43], the most commonly used titanium dioxide for reference and comparison with the literature data. The second is MIRKAT 211, which has been purchased by Euro Support sro. [44] which is characterised by high surface area and anatase crystal phase, the most appropriate titania phase for photocatalytic applications.

2.4 Materials characterisations

2.4.1 Nitrogen physisorption

Through this technique, information on surface area, pore volume and pore size distribution was collected. These morphological properties affect reagents and products diffusion to and from superficial active sites respectively, thus affecting photocatalytic performances.

IUPAC categorised porous materials according average pore diameter [45] and divided them in:

- microporous materials when average pore diameter is below 2 nm;
- mesoporous materials if it is between 2 and 50 nm;
- macroporous materials if it is larger than 50 nm.

By this analytical analysis, the weak non-selective and reversible interaction between surfaces gaseous molecules through dipole-dipole interactions or Van der Waals forces is observed. Experimentally, adsorbed and desorbed nitrogen volume is measured at different relative pressures (p/p_0). From these data, collected at the same temperature (-196 °C), two curves, called isotherms, can be sketched.

IUPAC [46] classified six different isotherms (reported in Figure 2.6), which refer to six different ideal surface structures.

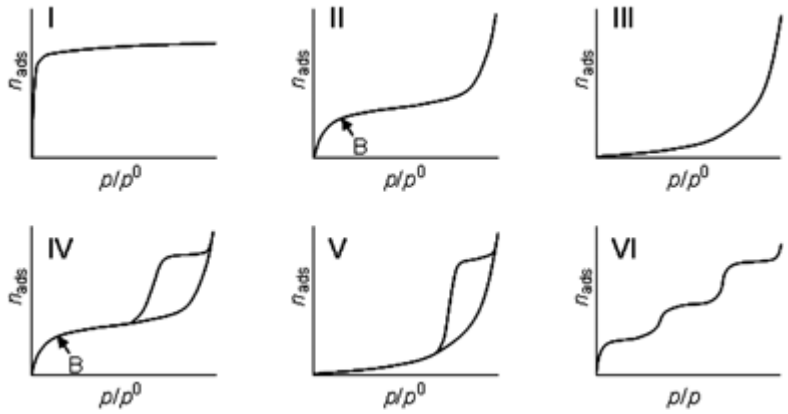

Figure 2.6 IUPAC classification for physisorption isotherms

Type I isotherm is typical for microporous systems, type II for macroporous or non-porous materials, type IV for mesoporous material. Type III and type V are usually uncommon and indicate an extremely weak interaction between surface and adsorbate while type VI reveal a multi-layer adsorption.

Different from other isotherms, in type IV and V isotherms adsorption and desorption branches are characterised by different trends leading to a hysteresis loop. In fact, at relative pressures higher than 0.4, mesoporous materials adsorb more gas than they can desorb: in fact, capillary condensation in mesopores limits uptake over a range of high relative pressure. However, hysteresis shape gives further information on mesopores structure. According to IUPAC, four types of hysteresis loops can be observed and they are reported in Figure 2.7.

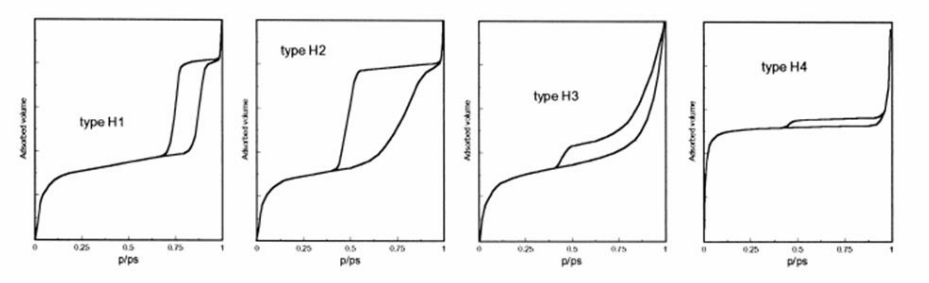

Figure 2.7 IUPAC hystereses classification

H1 hysteresis corresponds to porous materials made up of agglomerates or formed by approximately uniform spheres with narrow size distribution; surface properties are similar when H2 hysteresis is observed, but pore size is more irregular. Finally, H3 and H4 types indicate the presence of slit-shaped pores.

For this study physisorption measurements, a Micromeritics ASAP 2000 Analyser was used. Before measurements all the calcined samples have been thermally treated at 200 °C for 2 hours under vacuum in order to get rid of water and other adsorbate species on porous surface, which might provide misleading results.

Qualitative information aside, from collected data processing precise information about surface area and pore distribution can be obtained. Specific surface area can be calculated by the BET model proposed by Brunauer, Emmett and Teller [47]. This model is based on several assumptions, among whom the most important are [48]:

- physisorption is the only physical phenomenon observed;
- adsorption sites are well-defined and only one adsorbate molecule is adsorbed on each site and there is no interaction between adsorbed molecules;
- each adsorbed molecule can act as a single site leading to multi-layer adsorption;
- adsorption and desorption rates are similar in the uppermost layer, so adsorbed molecules and gas phase are in equilibrium;
- for all layers, apart from the first one where the adsorbent is directly in contact with the solid surface, heat of adsorption is assumed equal to heat of liquefaction;
- molecule layers number tends to infinity at saturation pressure.

By these assumptions, through BET equation, the volume of monolayered adsorbed gas can be calculated:

$$\frac{p}{V_{ads}(p_0-p)} = \frac{1}{V_m \cdot C} + \frac{C-1}{V_m \cdot C} \cdot \frac{p}{p_0}$$

Equation 2.3

where is p is gas pressure, p_0 is saturation pressure, V_{ads} is measured volume of adsorbed gas, C is the BET constant and V_m is the gas volume of a gas monolayer on the investigated surface. From V_m and the volume occupied by a nitrogen molecule (16.2 $Å^2$), surface area can be calculated. This equation in valid only when p/p_0 is lower than 0,3, since capillary condensation cannot happen at low relative pressures.

Whereas, BJH model, proposed by Barret, Joyner and Halenda takes information from capillary condensation phenomenon and gives information on average pore size and pore size distribution [49]. This model is the application of Kelvin equation to mesoporous systems and gives a relation between relative pressure and pore diameter d:

$$d = \frac{-4\sigma V_L}{RT \ln\left(\frac{p}{p_0}\right)} + 2t$$

Equation 2.4

where σ is surface tension, V_L is liquid molar volume and t is adsorbed layer thickness. Average pore diameter and distribution can be obtained plotting adsorbed gas versus diameter.

2.4.2 X-ray diffraction (XRD)

X-Ray Diffraction technique was used to determine crystal structure. In particular, three important parameters can be measured: crystal phase, their relative abundance and crystallite dimensions. For this work's purposes, crystal phase is crucial and this method allows to know whether in the synthesised samples titanium dioxide is amorphous, or crystalline in anatase, rutile or brookite phase.

X-rays, due to their highly energy, are able to penetrate solid matter, since their wavelength is similar to atomic dimensions. In any X-ray irradiated material, each atom acts like radiation generator and emits part of the incident radiation. In crystal solids, which are characterised by modular order in atoms disposition, radiation waves undergo either constructive or destructive interferences depending to diffraction angle 2θ [50]. Each crystal phase is identified by a peculiar X-ray diffractogram which is connected to material's structure.

In particular, through the Bragg's law it is possible to calculate the distance between crystal planes characterised by the same Miller's indexes h k l (d_{hkl}):

$$\boldsymbol{n\lambda = 2d_{hkl} \cdot sin\,\theta}$$

Equation 2.5

where λ is the incident wavelength and n the order of diffraction. From these data, it is possible to calculate lattice parameters. Moreover, crystallite average dimensions are obtained using the Scherrer's equation that correlates average diameter D_{hkl}, peak width Δ(2θ) and its position.

$$\boldsymbol{D_{hkl} = \frac{const \cdot \lambda}{\Delta(2\theta) \cdot cos\,\theta}}$$

Equation 2.6

To obtain such information wide angle x-ray scattering (WAXS) was used. XRD analyses were performed in the Department of Earth Sciences at the University of Ferrara in collaboration with Prof. Giuseppe Cruciani. A Bruker D8 Advance powder diffractometer, whose emitted radiation is $CuK\alpha_{1,2}$, that works at 40 kV and 40 mA, was used. Instrumental parameters are reported here:

- Stepsize: 0,02 °
- Antiscatter: 1/2 °, 0,1 mm, 1/2 °
- 2θ range: 5-80 °
- Time/step: 3 s

2.5 Gas-solid photocatalytic rig and photoreactors

In the development of the photocatalytic rig, all considerations from sections 2.1 and 2.2 were taken into consideration. As mentioned, due to operational flexibility, both carbon dioxide and water were introduced in gas phase. In particular, the mixture was made passing a compressed CO_2 (99.99 %) flow through a water bubbler. For a fine control of CO_2/H_2O ratio, CO_2 flow was controlled by a mass flow controller, whereas bubbler temperature was regulated by an oil bath. A sketch of the rig is reported in Figure 2.8.

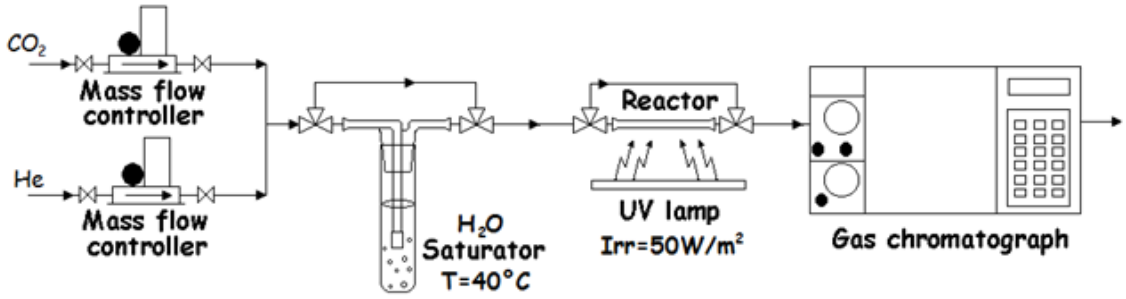

Figure 2.8 Sketch of developed photocatalytic rig for CO_2 photoreduction.

To compare catalyst introduction methods and geometry in gas-solid systems, two different photoreactors were considered, namely a fixed bed reactor and a thin film reactor, which are shown in Figure 2.9.

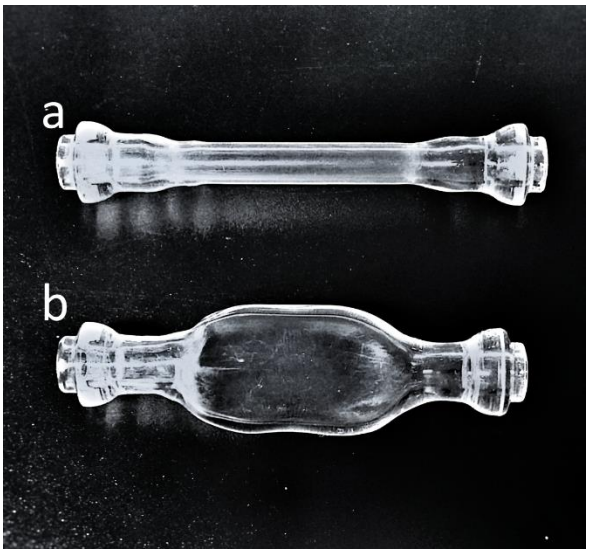

Figure 2.9 Fixed bed (a) and thin film (b) reactors.

The fist reactor is a tubular borate glass fixed bed reactor (length 40 mm, diameter 4 mm) where the catalyst (400 mg) was introduced as small particles with controlled size ranging between 0.2-0.3 mm (corresponding to 50-70 mesh). The second one is borate glass thin film reactor (length 33 mm, height 18 mm, thickness 2 mm). In this case the catalyst (10 mg) was introduced by deposition of the catalyst suspended in 2-propanol on the light-exposed side of the reactor. Since 2-propanol acts as a hydrogen donor [18], leading to data misinterpretation, the photocatalytic film had been dried at 110 °C for one hour before use and this treatment completely eliminated all residues of dispersing agent.

The samples were illuminated using a 125 W mercury UVA lamp (purchased from Helios Italquartz s.r.l. with emission range 315–400 shielded by a special tubular quartz, to select the 365 nm wavelength), yielding an average irradiance of 50 $W \cdot m^{-2}$. This value was chosen considering average solar radiation of 1000 $W \cdot m^{-2}$ and UV fraction in solar light (ca. 5 %). Comparing with literature data, irradiance is extremely low, but in these conditions it is possible to appreciate differences in materials' ability to absorb photons. Reactor materials wise, it was observed that irradiance in front of the reactor is the same as behind it, indicating that the reactor walls light adsorption is neglectable. In performed tests, neither heating nor cooling is used: in fact, UV lamp provides a stable and constant temperature of 40 °C on the photocatalytic surface. Once the gaseous mixture of carbon dioxide and water vapour is formed, it flowed through the reactor. Compressed CO_2 (99.99%) regulated by a mass flow controller was carried through a water bubbler kept at 40 °C to generate CO_2 and H_2O vapour mixture (13.3 CO_2/H_2O molar ratio). The reactor was sealed when the system reached the equilibrium state and this moment was considered as the beginning of the reaction. Therefore, the reaction was not performed under a continuous gas flow, but it took place in static conditions. Thus, at the beginning of the reaction, 9.2 µmol of CO_2 and 0.7 µmol of H_2O were present in reaction medium. In all catalytic tests, the reaction time was six hours.

The reaction products were injected in an in-line gas chromatograph (HP 6890) by means of a 250 µL C-10WE automatic valve. Products separation was performed with a 2 m long Porapak Q column (a mixture of polydivinylbenzene and polyethyldivinylbenzene)

on a 30 mL·min^{-1} helium flow. Oven temperature was kept at 40 °C for 2 minutes and then raised at 120 °C for five minutes (heating rate 50 °C·min^{-1}). Identification and quantification was performed by a thermal conductivity detector (TCD). Activity results were expressed in turn over numbers (TONs) in μmol·g_{cat}^{-1}, as commonly used in literature [51,52]. To assure repeatability and reproducibility, photocatalytic tests were performed at least three times to enable error analysis. For all samples, error margin is about ± 10 % of obtained value both for TON and TOF results.

Photonic yield (Φ), a useful metric to appreciate photons uptake for reactants conversion, was calculated according to IUPAC recommendations [53]:

$$\Phi\ (\%) = \frac{required\ e^{-}=8*CH_4(mol)}{incident\ photons\ (einstein)} \cdot 100$$

Equation 2.7

$$\Phi\ (\%) = \frac{8 \cdot CH_4(mol) \cdot Irr\ (W \cdot m^{-2}) \cdot t\ (s) \cdot A\ (m^2) \cdot \lambda\ (m) \cdot N_A(mol^{-1})}{h\ (J \cdot s) \cdot c\ (m \cdot s^{-1})} \cdot 100$$

Equation 2.8

where 8 is the number of required electrons for CO_2 reduction to CH_4, Irr is the irradiance, t is reaction time, A is the illuminated area, λ radiation wavelength, N_A is Avogadro's number, h is Planck's constant and c is speed of light.

The choice of turnover number and frequency and photonic yield among all IUPAC recommended metrics was carefully decided to measure and compare different features of a photocatalytic process: in fact, turnover number (TON) and frequency (TOF) take in consideration the effectiveness of a catalyst in obtaining one or more products and therefore allow to compare materials photoactivity; whereas, photonic yield is dependent on photons input so as to assess and compare the effectiveness in light harvesting and this feature allows to compare different photoreactors' effectiveness in delivering photons to the catalyst.

2.6 Results and discussion

Materials were tested in CO_2 photoreduction in developed photocatalytic rig using two different reactors, a fixed bed reactor and a thin film reactor, in order to investigate reactor design effect on photocatalytic performances.

Before performing the activity runs, blank tests were carried out with both reactors in order to avoid any bias in data collection and interpretation. In fact, traces of organic species can definitely lead to misleading results [60]. In fact, they could had been still present deriving from photocatalyst manipulation and, in the case of thin film reactor, from dispersing agent. For this reason, several blank tests were performed: without light, catalyst, or reactants. In none of these cases any hydrocarbon formation was observed. Also, a test with catalyst, light, and water (so, without CO_2 only) was performed, and also in this test no C-based product was detected: from these evidences, the absence of carbonaceous species on the surface was confirmed. Thus, it is possible to state, first of all, that this reaction is not a photochemical reaction, but a photocatalytic one and the photocatalyst is necessary to have CO_2 photoreduction. Moreover, catalysts are photostable and do not contain any trace of carbon from their manipulation, and collected data are not affected by carbonaceous species on the photocatalytic surface.

After positive results in blank tests, materials performances after six hours reaction are reported in Table 2.2 and in Figure 2.10.

	FIXED BED REACTOR		*THIN FILM REACTOR*	
	CH_4 ($\mu mol \cdot g_{cat}^{-1}$)	H_2 ($\mu mol \cdot g_{cat}^{-1}$)	CH_4 ($\mu mol \cdot g_{cat}^{-1}$)	H_2 ($\mu mol \cdot g_{cat}^{-1}$)
P25	0.01	n.d.	8.7	0.3
MIRKAT 211	0.03	n.d.	14.0	0.1

Table 2.2 P25 and MIRKAT 211 photocatalytic performances in CO_2 photoreduction.

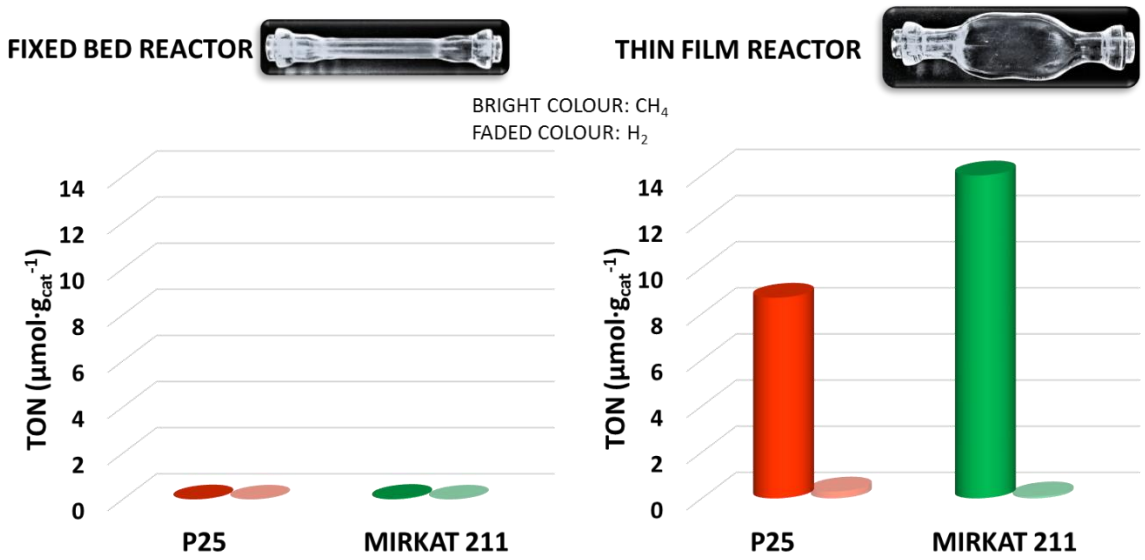

Figure 2.10 P25, MIRKAT 211, $TiO_{2\text{-}PREC}$ and $TiO_{2\text{-}SG}$ photocatalytic performances in CO_2 photoreduction.

From chart and graphs, it is evident that, for both reference TiO_2 based materials, the thin film reactor enormously boosts titania effectiveness in the CO_2 conversion by roughly three orders of magnitude in the same experimental conditions, but in two different photocatalytic reactors. To understand this extremely satisfactory result, several factors contributes should be taken into account. In fact, this result cannot be ascribed to the different amount of catalyst employed for each test. Indeed, in the thin film reactor the amount of catalyst is reduced from 400 mg in fixed bed reactor to 10 mg and, most importantly, to expose all the employed catalyst to incident light: thus the catalyst is more available to incident photons to provide the photocatalytic effect. In fact methane photonic yield, which is independent from catalyst loading, is enormously increased for all samples by three orders of magnitude as well.

	FIXED BED REACTOR photonic YIELD (%)	*THIN FILM REACTOR photonic YIELD (%)*
P25	$2.31 \cdot 10^{-4}$	0.11
MIRKAT 211	$6.93 \cdot 10^{-4}$	0.18

Table 2.3 P25, MIRKAT 211, $TiO_{2\text{-}PREC}$ and $TiO_{2\text{-}SG}$ photonic yield for methane production

Moreover, the use of a thin film promotes adsorption of reagents on the active sites and also products desorption, which needs to be as fast as possible to make catalytic sites available for new carbon dioxide molecules to adsorb again.

Considering overall effects in thin film reactors, it was possible to obtain photocatalytic performances close to data reported in literature [31,54] despite reactions are considerably milder. It must be remembered that these tests were performed at room temperature, atmospheric pressure and, most importantly, low irradiance, corresponding to UV fraction in solar light.

Using both reactors, the only detected products are methane, from complete CO_2 reduction, and hydrogen, from water splitting. All samples showed a higher selectivity to methane than hydrogen (more than 90 % all samples): this might be attributed to the high CO_2/H_2O ratio which was achievable only by introducing both water and carbon dioxide in gas phase.

Photocatalytic tests were performed in static conditions and for a relatively long time (six hours): so it can be easily supposed that, in this case, thermodynamically favoured products are more likely to be formed than kinetic favoured ones [55]. As a matter of fact, conversion to methane, which requires the greatest amount of photoexcited electrons, is also the most probable event compared to the conversion to CO, formaldehyde or methanol. However, in the case of the results obtained in the fixed bed reactor, it is extremely difficult to appreciate differences between photocatalyst in methane production and it was possible to detect hydrogen but not to quantify it.

In the case of thin film reactor, differences in photoactivity in CO_2 photoreduction are appreciable and in detail MIRKAT 211 performed considerably better than P25 and this behaviour can be correlated to materials different physicochemical properties. According to nitrogen physisorption analyses (reported in Figure 2.11), P25 is characterised by the lowest surface area (50 $m^2 \cdot g^{-1}$) and an average pore size of 25 nm, whilst MIRKAT 211 has a much higher surface area (217 $m^2 \cdot g^{-1}$) and a lower pore size dimension centred a 7.5 nm.

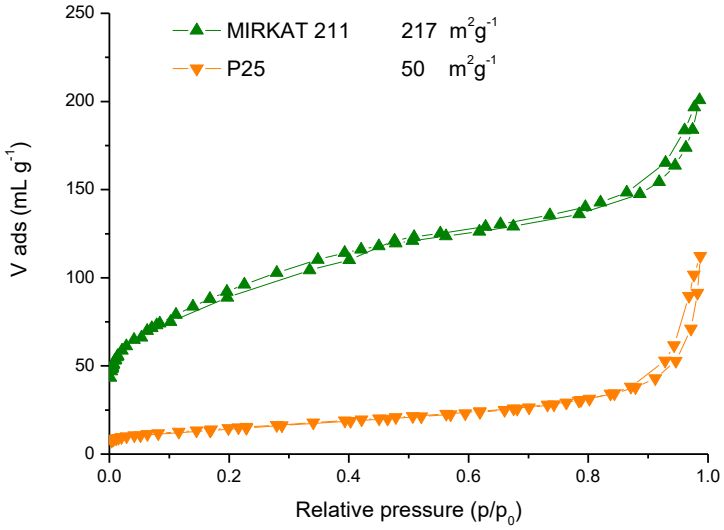

Figure 2.11 P25 and MIRKAT 211 nitrogen physisorption isotherms.

However, despite being an important parameter, surface area is not the only explanation for photocatalytic trends. In fact, crystallinity was investigated and X-ray diffraction measurements were performed and from XRD patterns, reported in Figure 2.12, and there are some differences in crystallinity and crystal phases observed.

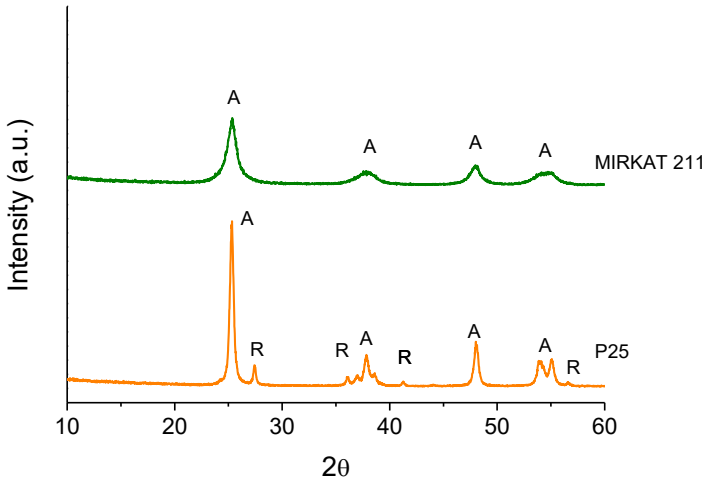

Figure 2.12 P25 and MIRKAT 211 XRD profiles.

Differently from all other three samples, P25's XRD profile shows not only anatase-related peaks in (JCPDS card no. 00-002-0387), but also rutile-related ones (JCPDS card

no. 76-1940). In fact, it is known that this material consists in a mixture of these two crystal structures in a ca. 75/25 anatase/rutile ratio [56]. Rutile alone is not the best photocatalytic phase due to great instability of lattice trapping sites, which lead to fast electron-hole recombination [57] and thus lower photoactivity. Whereas, in the other reference commercial sample MIRKAT 211 the only observed crystal phase is tetragonal anatase, since all detected peaks correspond to this crystalline phase, which is the most suitable phase for photocatalytic purposes [58]. Unfortunately, diffraction peaks are very broad and not well defined: according to manufacturer's data [44], only 40 wt. % of the reference material is crystalline and in the anatase phase, whereas the remaining fraction is amorphous. The presence of amorphous is related to the presence of surface defects, which can act as charge recombination centres, reducing photocatalytic effectiveness [59].

Therefore, best performing titanium dioxide based materials in CO_2 photoreduction must be characterised by two different features: relatively high surface area and crystallinity in anatase phase only and materials formulation must be devoted.

2.7 Conclusion

Throughout this chapter, it was shown how a lab-scale rig for CO_2 photoreduction was developed from physical phenomena understanding to benchmark materials testing. The choice to introduce reactants in gas phase allowed to overcome critical issues typical of this reaction in liquid medium, namely light scattering and poor CO_2 solubility and adsorption on the photocatalyst in reaction medium. In fact, through a careful control of rig design and experimental parameters, it was possible to obtain highly favourable carbon dioxide rich reactant mixture and high C-based product selectivity.

Within gas medium rigs, thin film reactor proved to enhance enormously photocatalytic activity compared to more commonly used fixed bed reactor. In fact, light harvesting is more efficient due to higher irradiated catalyst fraction, and this was confirmed both by photocatalyst performances and photonic yield, which increased by three orders of magnitude from fixed bed to thin film reactor. Moreover, developed photocatalytic process operates in mild conditions compared to other CO_2 photoreduction processes

reported in literature, especially in terms of pressure and irradiance, which is similar to UV irradiance within average solar light irradiation.

Finally, from these preliminary tests with commercial benchmark materials, it was possible to understand which physicochemical and textural properties are necessary for a performant photocatalyst for CO_2 photoreduction and, in particular, the co-presence of surface and textural properties. Surface area proved to be an important feature despite alongside crystallinity in anatase phase are necessary to improve photoactivity.

In the next chapters, the formulation of photocatalytic materials will be reported, aimed at modifying materials behaviour in two extremely important phenomena involved in CO_2 heterogeneous photoreduction: surface CO_2 adsorption and electron transfer.

2.8 Reference

[1] T. Inoue, A. Fujishima, S. Konishi, K. Honda, Nature 277 (1979) 637–638.

[2] R.L. Cook, R.C. MacDuff, A.F. Sammells, Journal of the Electrochemical Society 135 (1988) 3069–3070.

[3] G. Dey, A. Belapurkar, K. Kishore, Journal of Photochemistry and Photobiology A: Chemistry 163 (2004) 503–508.

[4] K. Kočí, L. Obalová, Z. Lacný, Chemistry Papers 62 (2008) 1–9.

[5] S. Ichikawa, R. Doi, Catalysis Today 27 (1996) 271-277.

[6] R. Hasan, S.B.A. Hamid, W.J. Basirun, Z.Z. Chowdhury, A.E. Kandjani, S.K. Bhargava, New Journal of Chemistry 39 (2015) 369-376.

[7] K.L. Gering, Photoreactor with self-contained photocatalyst recapture, US patent US6827911 B1.

[8] K.H. Funken, C. Sattler, J. Ortner, L. de Oliveira, Solar photoreactor, US patent US6633042 B1.

[9] M. Reli, O. Kozák, Z. Lacný, D. Plachá, L. Obalová, Catalysis Today 176 (2011) 212-214.

[10] O. Ola, M. Maroto-Valer, Journal of Photochemistry and Photobiology C: Chemistry Reviews 24 (2015) 16-42.

[11] T. Mizuno, A. Kengi, O. Kiyohisa, S. Akira, Journal of Photochemistry and Photobiology A: Chemistry 98 (1996) 87–90.

[12] X. Li, J. Chen, H. Li, J. Li, Y. Xu, Y. Liu, J. Zhou, Journal of Natural Gas Chemistry 20 (2011) 413–417.

[13] Q.D. Truong, J.-L. Liu, C.-C. Chung, Y.-C. Ling, Catalysis Communications 19 (2012) 85–89.

[14] M. Halmann, Nature 275 (1978) 115–116.

[15] H. Fujiwara, H. Hosokawa, K. Murakoshi, Y. Wada, S. Yanagida, T. Okada, S. Yanagida, Journal of Physical Chemistry B 101 (1997) 8270–8278.

[16] S. Qin, F. Xin, Y. Liu, X. Yin, W. Ma, Journal of Colloid and Interface Science 356 (2011) 257-261.

[17] B.-J. Liu, T. Torimoto, H. Yoneyama, Journal of Photochemistry and Photobiology A: Chemistry 113 (1998)93-97.

[18] S. Kaneco, Y. Shimizu, K. Ohta, T. Mizuno, Journal of Photochemistry and Photobiology A: Chemistry 115 (1998) 223-226.

[19] I. Rossetti, A. Villa, M. Compagnoni, L. Prati, G. Ramis, C. Pirola, C.L. Bianchi, W. Wang, D. Wang, Catalysis Science and Technology 5 (2015) 4481-4487.

[20] S. Kaneco, H. Kurimoto, K. Ohta, T. Mizuno, A. Saji, Journal of Photochemistry and Photobiology A: Chemistry 109 (1997) 59-63.

[21] A. Bideau-Mehu, Y. Guern, R. Abjean, A. Johannin-Gilles, Optics Communications 9 (1973) 432-434.

[22] D. R. Lide, CRC Handbook of Chemistry and Physics, 89th ed. CRC Press 2005 Boca Raton USA.

[23] F. Rechberger, M. Niederberger, Marials Horizons 4 (2017) 1115-1121.

[24] A. Bazzo, A. Urawaka, ChemSusChem 6 (2013) 2095-2102.

[25] L. Collado, P. Jana, B. Sierra, J.M. Coronado, P. Pizarro, D.P. Serrano, V.A. de la Peña O'Shea, Chemical Engineering Journal 224 (2013) 128-135.

[26] M. Tahir, N. Amin, Applied Catalysis B: Environmental 162 (2015) 98-109.

[27] A. Cybula, M. Klein, A. Zaleska, Applied Catalysis B: Environmental 164 (2015) 433-442.

[28] M. Tahir, N. Amin, Energy Conversion Management 76 (2013) 194–214.

[29] G.A. Raupp, J.A. Nico, S. Annagi, R. Changrani, R. Annapragada, American Institute of Chemical Engineering Journal 43 (1997) 792-801.

[30] K. Kočí, M. Reli, O. Kozák, Z. Lacný, D. Plachá, P. Plaus, L. Obalová, Catalysis Today 176 (2011) 212-214.

[31] S. Das, W. Wan Daud, Renewable and Sustainable Energy Reviews 39 (2014) 765-805.

[32] J. Wu, H.M. Lin, International Journal of Photoenergy 7 (2005) 115–119.

[33] O. Ola, M. Maroto-Valer, Chemical Engineering Journal 283 (2016) 1244-1253.

[34] T. Van Gerven, G. Mul, J. Moulijn, A. Stankiewicz, Chemical Engineering and Processing 46 (2007) 781-789.

[35] R. Howe, Developments in Chemical Engineering and Mineral Processes 6 (1998) 55–84.

[36] P. Pathak, M.J. Meziani, Y. Li, L.T. Cureton, Y.P. Sun, Chemical Communications 10 (2004) 1234-1235.

[37] L. Tan, W. Ong, S. Chai, A. Rahman, Chemical Engineering Journal 308 (2017) 248-255.

[38] K. Li, X. An, H. Park, M. Khraisheh, J. Tang, Catalysis Today 224 (2013) 3-12.

[39] B. Vijayan, N.M. Dimitrijevic, Rajh, K. Gray, Journa of Physical Chemistr 114 (2010) 12994-13002.

[40] M. Tahir, B. Tahir, N. Amin, Applied Catalysis B: Environmental 204 (2017) 548-560.

[41] M. Manzanares, C. Fàbrega, J. Oriol Ossó, L.F. Vega, T. Andreu, J.R. Morante, Applied Catalysis B: Environmental 150-151 (2014) 57-62.

[42] O. Ola, M. Maroto-Valer, Journal of Catalysis 309 (2014) 300-308.

[43] Evonik's datasheet, available at https://www.aerosil.com/sites/lists/RE/DocumentsSI/TI-1243-Titanium-Dioxide-as-Photocatalyst-EN.pdf

[44] Eurosupport's datasheet, available at http://www.eurosupport.nl/pdf/catalytic_titanias.pdf.

[45] J. Rouquerol, D. Avnir, C.W. Fairbridge, D.H. Everett, J.H. Haynes, N. Pernicone, J.D.F. Ramsay, K.S.W. Sing, K.K. Unger, Pure and Applied Chemistry 66 (1994) 1739-17358.

[46] K.S.W. Sing, D.H. Everett, R.A.W. Haul, l. Moscou, R.A. Pierotti, J. Rouquérol, T. Siemieniewska, Pure & Applied Chemistry 67 (1985) 603-619.

[47] S. Brunauer, P.H. Emmett, E. Teller, Journal of American Chemical Society 60 (1938) 309-319.

[48] K.S.W. Sing, Advances in Colloid and Interface Science 76-77 (1998) 3-11.

[49] E.P. Barrett, L.S. Joyner, P.P. Halenda, Journal of American Chemical Society 73 (1951), 373-380.

[50] B.D. Cullity, Elements of X-Ray Diffraction, 1st ed. Addison-Wesley Pubblishing Company 1956 Reading PA USA.

[51] D. Liu, Y. Fernandez, O. Ola, M. Maroto-Valer, C.M.A. Parlett, A.F. Lee, J.C.S Wu, Catalysis Communication 25 (2012) 78-82.

[52] M. Tahir, N.S. Amin, Applied Catalysis B: Environmental 142-143 (2013) 512-522.

[53] S. E. Braslavsky, A.M. Braun, A.E. Cassano, A.V. Emeline, M.I. Litter, L. Palmisano, V.N. Parmon, N. Serpone, Pure and Applied Chemistry 83 (2011) 931-1014.

[54] D. Chen, X. Zhang, A. Lee, Journal of Materials Chemistry 3 (2015) 14487-14516.

[55] K. Li, X. An, H. Park, M. Khraisheh, J. Tang, Catalysis Today 224 (2014) 3-12.

[56] Z. Ding, G.Q. Lu, P.F. Greenfield, Journal of Physical Chemistry B 104 (2000) 4815-4820.

[57] D.C. Hurum, A.G. Agrios, K.A. Gray, T. Rajh, M.C. Thurnauer, Journal of Physical Chemistry B 107 (2003) 4545-4549.

[58] M. Janus, M. Inagaki, B. Tryba, M. Toyoda, A.W. Morawski, Applied Catalysis B: Environmental 63 (2006) 272-276.

[59] K. Yanagisawa, J. Overstone, Journal of Physical Chemistry B 103 (1999) 7798-7787.

3 Titanium dioxide synthetic strategy and enhanced CO_2 adsorption by basic oxides promotion

In this chapter materials formulation is considered to address one of the most crucial step in solar fuels production, i.e. carbon dioxide adsorption on photocatalytic surface. According to literature review on this topic, the most suitable synthetic approach for titanium dioxide was considered preliminarily and furthermore modification was chosen and promoted catalysts formulation was performed, correlating materials' physicochemical properties with photocatalytic results obtained using the thin film reactor developed in the previous chapter.

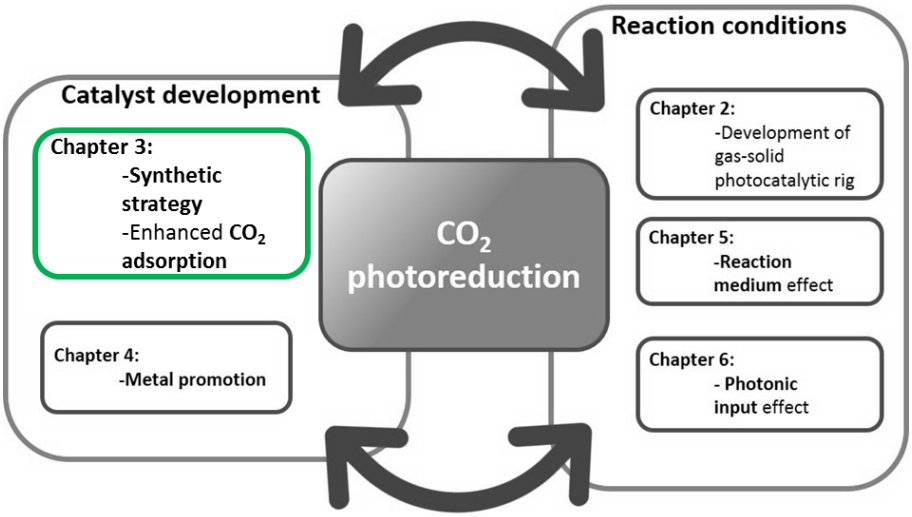

Figure 3.1 Sketch representing this chapter connection to the others in this thesis.

3.1 Introduction

3.1.1 Synthetic strategies for carbon dioxide

As already mentioned in the general introduction, for any photocatalytic application of titanium dioxide, texture and surface properties deeply affect materials effectiveness. To tune physicochemical features, catalysts synthetic pathway must be carefully considered. In the case of carbon dioxide photoreduction, evidences from preliminary

tests performed with commercial samples, which have been reported in the previous chapter and examples in literature [1,2] indicate that the two features to be considered are high surface area and crystallinity.

To synthesise titanium dioxide with suitable properties, in literature many synthetic procedures are reported, such as hydrothermal and solvothermal methods [3-6], chemical vapour deposition [7,8], physical vapour deposition [9], electrodeposition [10], microwave assisted methods [11], etcetera. However, the two most commonly used synthetic approaches to prepare titanium dioxide are precipitation and sol-gel process, due to their facility in performing them and final materials properties easily tunable by experimental conditions [12].

The precipitation of hydroxides occurs by the addition of a basic solution (NaOH, aqueous ammonia, urea) to a precursor that usually is either titanyl sulphate $TiOSO_4$, or titanium sulphate $Ti(SO_4)_2$ or titanium tetrachloride $TiCl_4$ [13,14]. From an extremely acidic aqueous solution of one of these precursors, by means of a basic precipitating agent, pH is increased, $Ti(OH)_4$ nuclei are formed, which can happen by OH- ions adsorption on the surface or by increasing particle size. Smaller particle size can be achieved when nucleation is faster than nuclei growth, whereas bigger ones will be obtained when growth is preferred. The rates of these two processes are affected by precursor concentration, pH of the solution and temperature. Precipitation always must be followed by calcination, which allows transition from titanium hydroxide to oxide and, if temperature is sufficiently high, phase transition from amorphous to crystalline. As observed in previous studies, this synthetic strategy allows to tune surface area and phase transition temperatures [15] and, as a consequence, photocatalytic performances. Alternative to precipitation, sol-gel process has been widely reported in literature due to the possibility to synthesise nanometres-sized crystallised TiO_2 powders of high purity at relatively low temperatures [16]. Sol–gel process consists in reactions of hydrolysis and polycondensation of metal alkoxides, $M(OR)_x$, to form oxopolymers, which are then converted into an oxide network [12] (from Equation 3.1 to Equation 3.3).

$$M(OR)_n + H_2O \rightleftharpoons M(OR)_{n-1}(OH) + ROH$$

Equation 3.1

$$M(OR)_n + M(OR)_{n-1}(OH) \rightleftharpoons M(OR)_{n-1} - O - M(OR)_{n-1} + ROH$$

Equation 3.2

$$2\,M(OR)_{n-1}(OH) \rightleftharpoons M(OR)_{n-1} - O - M(OR)_{n-1} + H_2O$$

Equation 3.3

In the case of titanium dioxide synthesis by sol-gel, due to Ti^{4+} low electronegativity, hydrolysis reaction is so fast that it might lead to $Ti(OH)_4$ precipitation. To overcome this issue, several chelating agents can be used, such as diols, (di)carboxylic acids or diketonate compounds [12].

Despite precise control of experimental conditions in precipitation and sol-gel synthesis might improve titanium dioxide properties, however it is not sufficient to assure satisfying results in CO_2 photoreduction. To reach them, materials modification is a resourceful tool, but it is necessary to understand physicochemical phenomena involved in this process.

3.1.2 CO_2 adsorption on TiO_2: a critical yet necessary step for solar fuels production

As any heterogeneous catalytic process, also CO_2 photoreduction consists in three different steps:

1. reactants adsorption and photons absorption on the photocatalyst;
2. heterogeneously catalysed chemical reaction;
3. products desorption.

The first step is fundamental because it allows both reactants to interact with each other with the suitable orientation for the redox reaction to happen. In fact, as observed experimentally in blank tests reported in the previous chapter and reported from theoretical and spectroscopic studies, carbon dioxide and water vapour, can interact

with each other [17]: oxygen lone pairs in H_2O can interact with anti-bonding $2\pi_u$ at central carbon atom in CO_2, leading to the formation of van der Waals complexes [18]. However, without any catalyst or photocatalyst, any conversion, even to carbon acid, cannot happen due to high energy barrier in gas phase (> 200 $kJ \cdot mol^{-1}$) [19].

In literature, it is well reported that both carbon dioxide and vapour can be adsorbed on titanium dioxide [20-22], but its adsorption is weaker for the former than the latter. It was reported by Henderson that oxygen vacancies on titanium dioxide surface binds CO_2 slightly more strongly than five-coordinated Ti^{4+} sites [23] and usually carbon dioxide is linearly coordinated [24]. On the same oxygen vacancies, water is dissociated into stable bridging OH groups, which can be desorbed increasing temperature [25].

CO_2 adsorption on TiO_2 follows Freundlich model, which is generally used for non-ideal sorption processes [26]:

$$q = k_f p^{1/n}$$

Equation 3.4

where q is adsorbed gas (mmol of gas /g of adsorbent), p is pressure ad equilibrium, while k_f and n are Freundlich constants. Calculated 1/n value, 0.4, indicates that predominant CO_2 adsorption mechanism is chemical adsorption rather than physical adsorption.

However, when carbon dioxide and water competitive adsorption occurs, CO_2 adsorption is blocked by the presence of preadsorbed water on titanium dioxide surface, while, weakly adsorbed CO_2 is displaced by postdosed H_2O, and there is little or no evidence for bicarbonate formation in either case [25]. This TiO_2 physicochemical property affects process selectivity: preferential water adsorption might lead to hydrogen production from water splitting into molecular hydrogen and oxygen [27]. This side-reaction, for the purposes of the work, is detrimental and undesired because decreases process selectivity and, at the same time, lead to reductant consumption. Ikeue and co-workers observed that adsorption is favoured on irradiated photocatalysts [28] but, several adjustments can be considered to improve adsorption. For example, as

reported in the previous chapter, high CO_2 relative pressure in reaction mixture improves its adsorption, improving C-based products in photoreduction process.

In addition to process design, materials formulation might be helpful to boost photoactivity. Considering carbon dioxide slight acidity, the introduction of basic components might improve carbon dioxide adsorption. Some authors introduced basic amines on titanium dioxide surface to improve affinity toward carbon dioxide. For example Liao *et al.* functionalised TiO_2 with monoethanolamine [29], whilst Kapica-Kozar and co-workers tested CO_2 adsorption on TiO_2 modified with NaOH, KOH, ethylenediamine (EDA), triethylenetetramine (TETA) and tetraethylenepentamine (TEPA) [30]. However, in none of the cases reported in literature, the effect of organic species in reaction medium is reported nor promoter's stability.

Recently, Tan and co-workers found that the introduction of graphene oxide on titanium dioxide increases CO_2 adsorption on photocatalytic surface [31]. According to the authors, Langmuir-Hinshelwood mechanism suitably describes substrates adsorption mechanism: carbon dioxide and water competitively adsorb on adjacent surface sites and then react to form solar fuels. It was calculated that carbon dioxide adsorption on titanium dioxide surface is 400 times weaker than water. However, graphene oxide is still an expensive material, which might limit large scale applications of carbon dioxide photoreduction.

An alternative strategy to enhance CO_2 adsorption could be the introduction of inexpensive and stable basic metal oxides, such as calcium or magnesium oxides [32]. For this application, the use of an inorganic base, instead of organic amines or graphene-derived materials, provides important advantages:

- magnesium and calcium oxide are considerably more stable, abundant, inexpensive and safe compared to organic amines;
- simple methods, such as incipient wetness impregnation, can be used for their introduction on titanium dioxide surface;
- most importantly, photocatalytic results are not affected by the presence of organic promoters, which can undergo reduction in reaction conditions.

In literature, some applications of alkali-earth promoted titania for photocatalytic oxidations of acidic substrates are reported. For example, Al-Salim *et al.* used these photocatalytic systems for oxalic acid photooxidations observing an improvement in efficiency due to increased oxalate adsorption [33]. Similar results were obtained by Pozan and Kambur on photocatalytic 4-chlorophenol oxidation [34]. For these reasons, it was supposed that such modification would enhance carbon dioxide adsorption too.

Therefore, this section of the work is devoted to the development of TiO_2-based catalysts characterised by high, or total selectivity to CO_2 photoreduction. After considering the most efficient synthetic approach for bare titanium dioxide, calcium and magnesium oxides will be introduced on the best performing bare titanium dioxide from preliminary tests in the previous chapter. The effect of promoter loading will also be considered introducing different amount of promoter (from 0.5 to 2.0 wt. %). Physicochemical properties effect on photoactivity was evaluated by an in-depth characterisation, specially aimed at understanding the interaction between carbon dioxide toward the photocatalytic surface.

3.2 Materials syntheses

3.2.1 Titanium dioxide synthesis by precipitation and sol-gel

Two lab-made samples were prepared for comparison using two different methods: precipitation and sol-gel process, which differ for the chemical reactions involved and thus for TiO_2 precursor and experimental conditions.

For the precipitation method, in 250 mL beaker a 1.2 M titanyl sulphate solution was prepared dissolving 34.55 g of $TiOSO_4$ (Sigma-Aldrich Ti assay > 29 wt. %) in 100 mL of deionised water. At the same time, a 9.0 M NaOH solution is prepared in a volumetric flask (36 g of NaOH, Carlo Erba assay > 97 wt. %, in 100 mL of deionised water in ice bath to overcome extreme exothermicity). Both solutions were added drop wise and simultaneously to 200 mL of distilled water under vigorous stirring (500 rpm), in order to keep a neutral pH, which was controlled by a Metrohm 691 pH meter. Obtained $Ti(OH)_4$ suspension was aged at 60 °C for 20 hours. Then, precipitated solid was filtered

and washed with deionised water until spare sulphate ions removal, which was verified by means of the barium chloride test [35]. Wet $Ti(OH)_4$ cake was dried overnight at 110 °C and calcined at 400 °C (heating rate 2 °C·min^{-1}) for 4 hours in air flow (30 mL·min^{-1}) to obtain TiO_2. This sample was labelled as $TiO_{2\text{-PREC}}$.

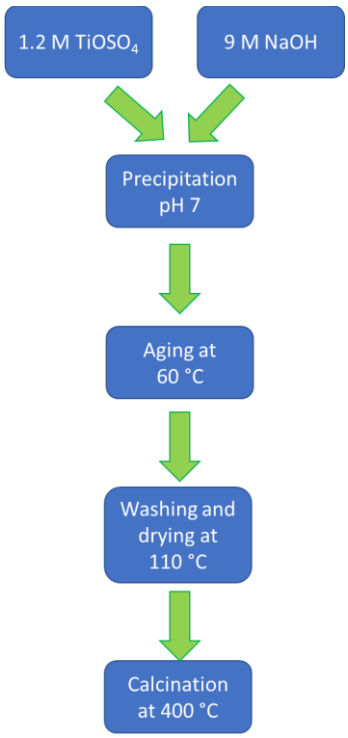

Figure 3.2 $TiO_{2\text{-PREC}}$ synthetic pathway.

Sol-gel sample was prepared from a different precursor, namely titanium butoxide ($Ti(OC_4H_9)_4$, Sigma-Aldrich assay > 97 wt. %). In a typical synthesis, 30 mL of $Ti(OC_4H_9)_4$ were solved in 30 mL of 1-butanol (Sigma-Aldrich, assay > 99 wt. %) in presence of 6.3 mL of acetylacetone (pentane-2,4-dione $C_5H_8O_2$, Fluka assay 99.5 wt.%) for at least 30 minutes in order to chelate titanium alkoxide molecules (Figure 3.3, reaction a).

The chelated titanium solution was slowly dropped (1.5 mL·min^{-1}) by means of a peristaltic pump into 600 mL of a 0.2 vol. % acetic acid (VWR, assay > 99.9 wt. %) solution in deionised water under vigorous stirring (500 rpm) and aged at room temperature and

atmospheric pressure for 3 hours to for the sol by hydrolysis and condensation (Figure 3.3, reactions b,c and d).

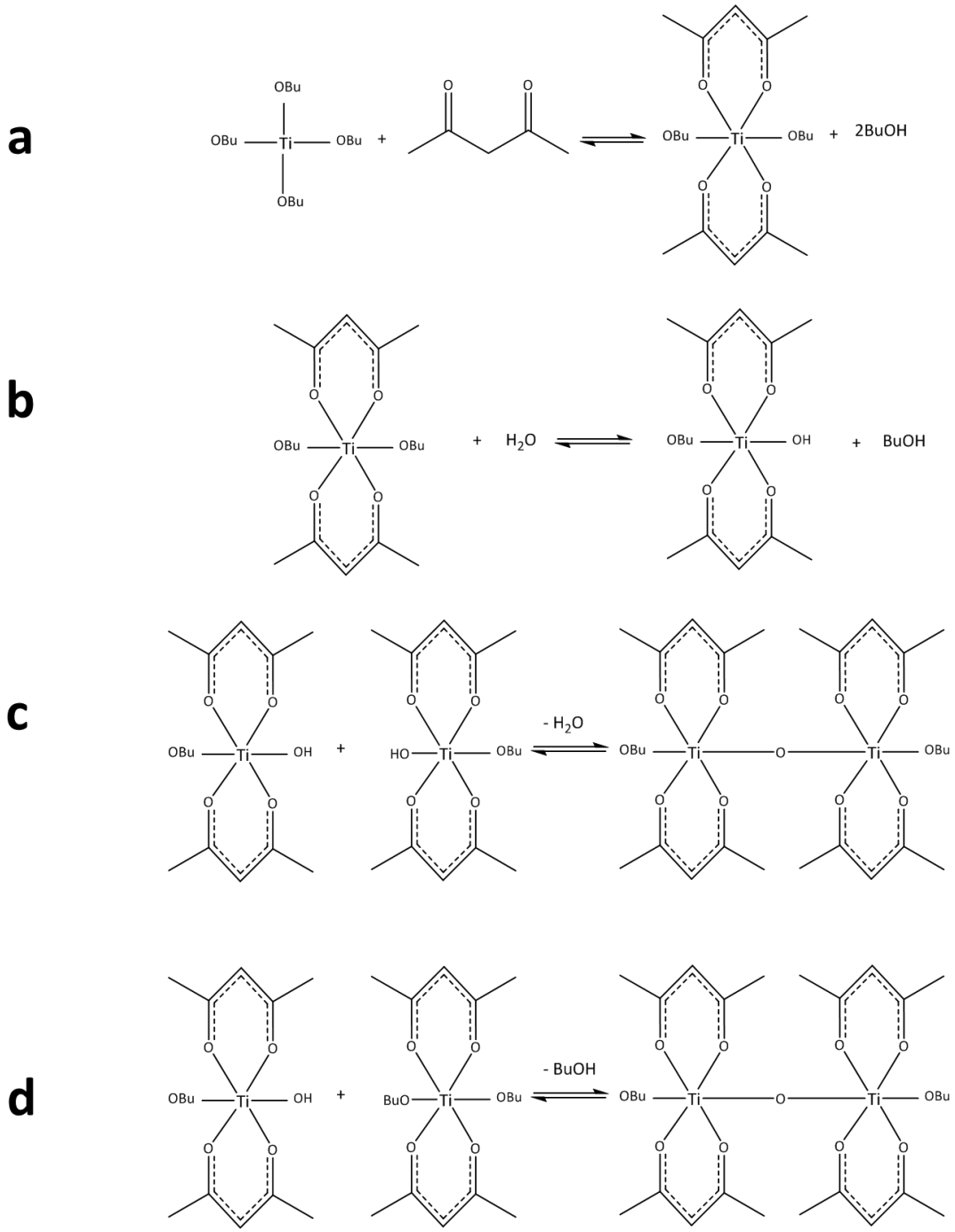

Figure 3.3 Reactions involved in sol-gel synthesis: a is titanium alkoxide chelation, b is its hydrolysis, c and d are condensation reactions.

Afterwards, the obtained sol was aged in a 1 L PTFE vessel at 90 °C for 40 h under autogenous pressure. Then solvent within obtained gel was eliminated by evaporation

at 90 °C overnight and calcined at 400 °C (heating rate 2 °C·min^{-1}) for 4 hours in air flow (30 mL·min^{-1}) to obtain TiO_2. This sample has been labelled as $TiO_{2\text{-}SG}$.

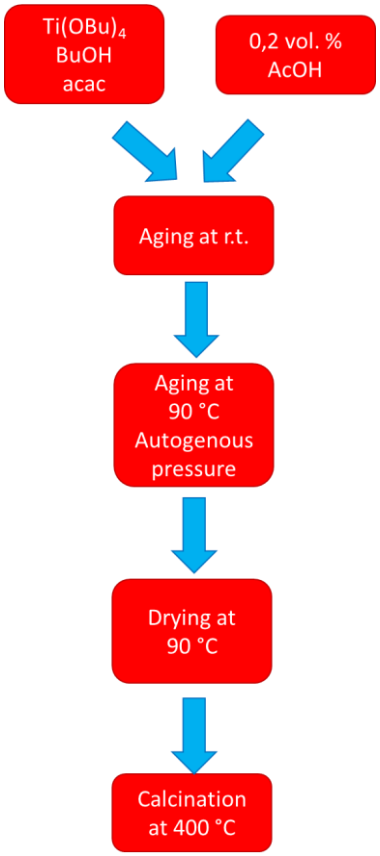

Figure 3.4 $TiO_{2\text{-}SG}$ synthetic pathway.

3.2.2 CaO and MgO introduction on TiO_2

Calcium and magnesium were introduced on dried $Ti(OH)_4$. Calcium and magnesium oxides were introduced by incipient wetness impregnation before calcination using nitrate salts as precursors ($Ca(NO_3)_2{\cdot}4H_2O$ Sigma Aldrich, assay > 99 % and $Mg(NO_3)_2{\cdot}6H_2O$ Sigma Aldrich, assay > 98 %). Three different alkaline earth metal amounts were chosen, i.e. 0.5, 1.0 and 2.0 metal wt. %. Finally, samples were calcined at 400 °C for 4 hours in air flow to obtain final materials. Samples were labelled as $xMTiO_{2\text{-}y}$, where x represents metal amount, M the alkali earth metal oxide (either Ca or Mg) and y stands for synthetic method. Unpromoted sample was used as reference, and

also chosen benchmark materials, namely P25 purchased from EVONIK gmbh and MIRKAT 211 from Eurosupport sro.

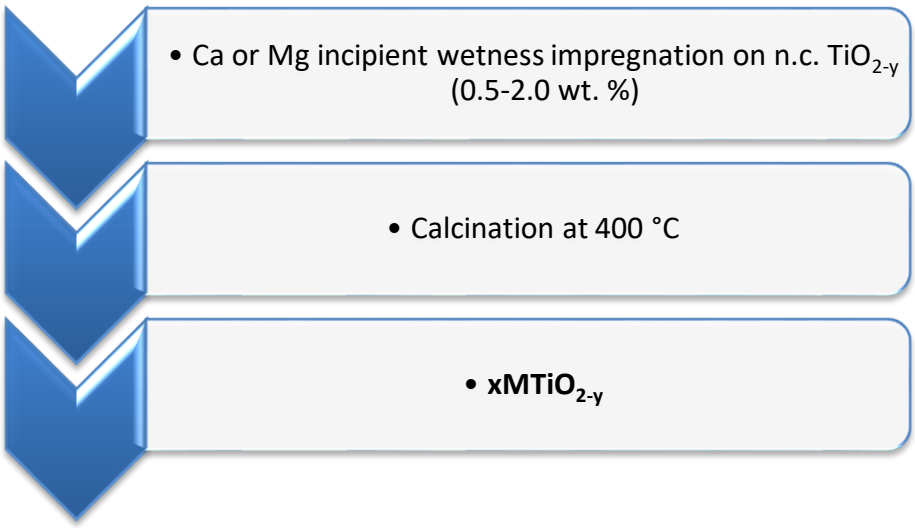

Figure 3.5 General synthetic pathway for alkali-earth promoted TiO_{2-y}.

3.3 Characterisations

3.3.1 Thermal Gravimetric/Differential Thermal Analysis (TG/DTA)

Thermal gravimetric analysis coupled with differential thermal analysis (TG/DTA) investigates phenomena that happen when samples undergo heating under an air flow. Weight loss and exchanged heat are measured and this technique reveals physicochemical processes involved in calcination to decide the best conditions for it.

From thermal gravimetry it is possible to determine sample weight loss during a heating treatment: from this analysis, the necessary temperature for either adsorbed molecules desorption (e.g. water or other solvents) or for oxidation reactions is measured. Differently, DTA measures enthalpy variations during heating compared to a reference (generally alumina) and thermal differences between the two materials is monitored throughout the whole analysis.

The combinations of these two analyses is useful to understand temperature for required process and their thermal tonality. For example, a thermal variation associated with weight loss corresponds to species desorption from the sample or their oxidation, whereas it is ascribed to a phase transition if no weight loss is observed.

TG/DTA analyses were performed at the Department of Earth Sciences at University of Ferrara by Prof. Giuseppe Cruciani who is acknowledged for his collaboration. Simultaneous Netzsch Thermal Analyzer STA 409 in been used in air with a 10 °C/min heating during all the analysis.

3.3.2 X-ray diffraction (XRD)

Crystal structure was determined by X-Ray Diffraction (XRD) patterns were collected on a Bruker D8 Advance powder diffractometer with a sealed X-ray tube (copper anode; operating conditions, 40 kV and 40 mA) and a Si(Li) solid state detector (Sol-X) set to discriminate the Cu Kα radiation. Apertures of divergence, receiving and detector slits were 2.0 mm, 2.0 mm, and 0.2 mm, respectively. Data scans were performed in the 2θ range 5°–80° with 0.02° step size and counting times of 3 s/step. Quantitative phase analysis and crystallite size determination was performed using the Rietveld method as implemented in the TOPAS v.4 program (Bruker AXS) using the fundamental parameters approach for line-profile fitting.

3.3.3 Nitrogen physisorption

N_2 adsorption–desorption isotherms at -196 °C were performed using a MICROMERITICS ASAP 2000 analyser to obtain information on the surface properties. All samples were previously outgassed at 200 °C for 2 h in vacuum. The mesopores volume was measured as the adsorbed amount of N_2 after capillary condensation. The surface area was evaluated using the standard BET equation [36] and the pore size distribution was obtained using the BJH method [37] applied to the isotherm desorption branch.

3.3.4 Temperature Programmed Oxidation (TPO)

In temperature programmed oxidation, a chemical reaction, in this case oxidation, is monitored while temperature increases linearly with time [38]. Therefore, the presence of oxidable species, such as organic residues from synthetic procedure, is detected. This

is a very common analysis in catalyst characterisation since it can give a lot of qualitative and quantitative information.

In a typical experiment, 50 mg of sample was introduced in a quartz reactor, in which a 5 % O_2/He under a constant flow of 40 mL/min. Then, the sample is heated in oxidising atmosphere with a rate of 10 °C·min^{-1} up to 800 °C. Oxygen consumption, that is related to oxidation reactions, is monitored *via* thermal conductivity detector (TCD): when gas composition changes, i.e. oxygen is consumed, there is a signal variation. The instrumental apparatus is shown in Figure 3.6 with typical instrumental output plot of oxygen consumption versus temperature.

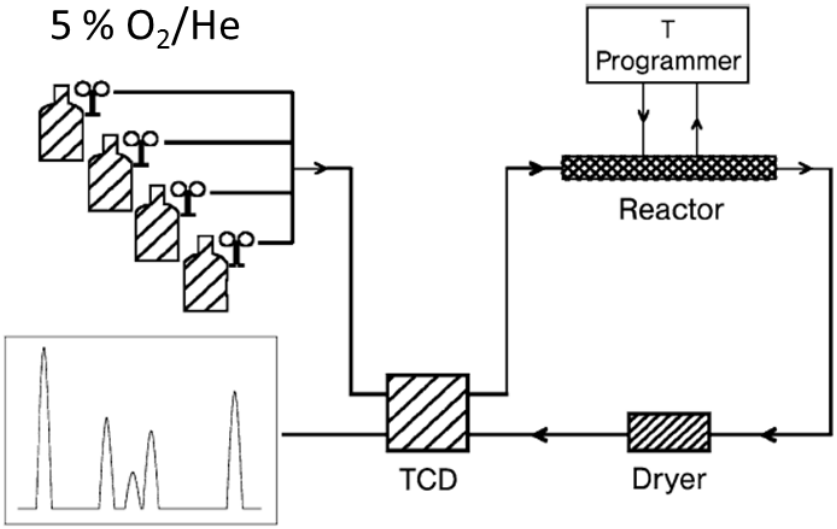

Figure 3.6 TPO technical apparatus [38].

From experimental data, it is possible to detect how many species were oxidised during thermal treatment and their oxidability. The lowest is the temperature of organic species oxidation, the highest is their oxidability.

TPO analyses might also provide quantitative information. Through a calibration method, it is possible to know the exact amount of oxygen employed during the reaction: then, knowing oxidation stoichiometry, it is possible to know the exact amount of residual carbon species on the sample. In this work, only qualitative considerations

will be made: in particular, the presence of organic species from synthetic protocols will be investigated.

3.3.5 CO_2 Temperature programmed desorption (CO_2-TPD)

Temperature programmed desorption (TPD) is an analytical thermal technique in which the desorption of a probe molecule from a surface is monitored while increasing temperature linearly. The interaction between probe molecule and surface is specific and the right combination of probe must be carefully considered.

CO_2 temperature programmed desorption (CO_2-TPD) is a commonly used technique in heterogeneous catalysis to evaluate surface basicity due to probe molecule's acidity [39]. In the specific case of carbon dioxide photoreduction, where CO_2 is the key reagent, this characterisation technique gives also indications about the interaction of this molecule with catalytic surface.

Generally, before the analysis materials surface is covered with CO_2 at a specific temperature, usually between 20 °C and 80 °C [40,41]: then samples are heated in order to desorb CO_2. The presence of desorption peaks indicates the presence of basic sites, which can bind carbon dioxide and can be characterised by different basic strength. The higher is desorption peak, the stronger is the basic site.

CO_2-TPD experiments were carried out in a lab-made equipment, reported in Figure 3.7, and procedure was developed.

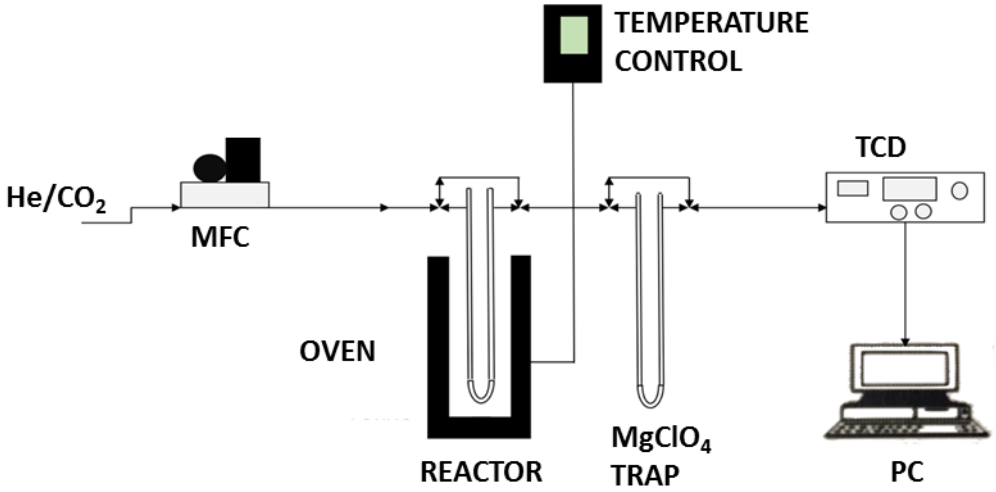

Figure 3.7 Experimental setup for CO_2-TPD analysis.

Samples (50 mg) were pre-treated at 110 °C for 30 minutes to clean materials' surface from adsorbed water, then CO_2 was sent to the sample at 40 °C using 0.5 mL loop until surface saturation. This temperature was chosen both as an average value within reported experimental procedures for CO_2-TPD in literature and to mimic adsorption in reaction conditions.

Finally, materials were heated at 10 °C/min from 40 °C to 800 °C under helium flow (40 mL/min STP). The effluent gases were analysed by a Gow-Mac TCD detector using a magnesium perchlorate trap to stop H_2O during the pre-treatment.

3.3.6 Photocatalytic tests

The photocatalytic tests were performed in the photocatalytic gas-solid rig developed in the previous chapter. To summarise briefly, reactor configuration and reaction conditions are reported in the chart below.

Reactants phase	both gaseous
water introduction method	bubbler at 40 °C
CO_2/H_2o ratio	13.3
reactor	thin film
temperature	40 °C
pressure	1 atm
irradiance	50 $W \cdot m^{-2}$

Table 3.1 Experimental conditions for CO_2 photoreduction tests.

3.4 Results and discussion

3.4.1 TiO_2 synthetic route effect on photoactivity

Before testing lab-made materials in carbon dioxide photoreduction, their physicochemical and textural properties must be analysed to assess their suitability.

In the case of lab-made samples, $TiO_{2\text{-PREC}}$ and $TiO_{2\text{-SG}}$, calcination process must provide the dehydration of $Ti(OH)_4$ to TiO_2, its crystallisation to the most suitable phase (i.e. anatase) and the complete oxidation of residual carbonaceous species if they are involved in the synthetic procedure. To do so, TG/DTA analysis was performed on not calcined (n.c.) $TiO_{2\text{-PREC}}$ and $TiO_{2\text{-SG}}$ lab-made samples and results are reported in Figure 3.8.

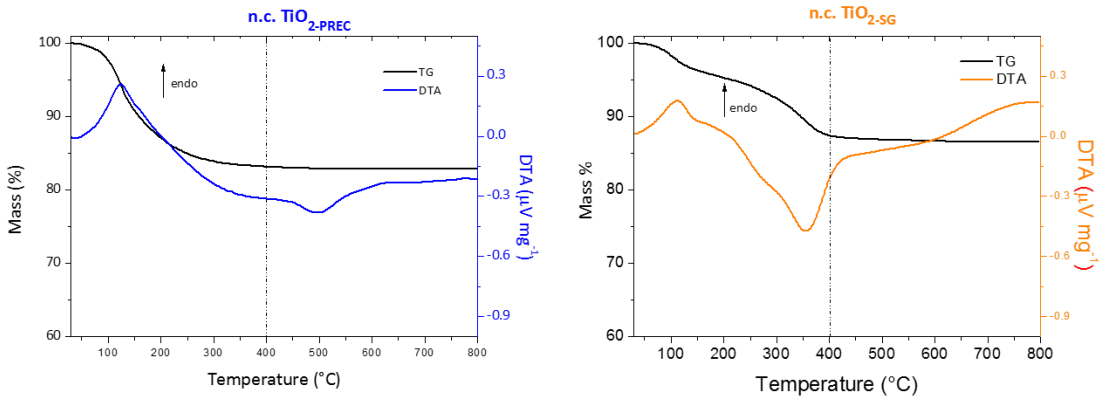

Figure 3.8 TG/DTA results from not calcined (n.c.) $TiO_{2\text{-PREC}}$ and $TiO_{2\text{-SG}}$ lab-made samples.

In both samples' TG curve, an endothermic weight loss takes place in a single stage from 60 °C to 120 °C was observed and it can be attributed to the loss of superficially adsorbed water. At higher temperature, exothermic processes were observed related to samples weight loss. In the case of n.c.$TiO_{2\text{-PREC}}$, this weight loss end at 300 °C, whereas in $TiO_{2\text{-PREC}}$ it finishes at 400° C.

In the former sample, this phenomenon can be ascribed to water loss and $Ti(OH)_4$ conversion in TiO_2. In this sample, organic species can be excluded because only inorganic salts were used in samples preparation and sulphate spare ions were eliminated completely by washing. Moreover, in this sample, another exothermic phenomenon without any weight loss was observed between 400 °C and 600 °C. According to literature data [42], this process is associated to the phase transition from amorphous to crystalline titania in the anatase phase.

In the latter, n.c.$TiO_{2\text{-SG}}$, weight loss is slower and this more exothermic process can be ascribed to oxidation of carbonaceous species. In fact, in this sample, organic residues are still present due to organic molecules involved in the synthetic process (i.e. 1-butanol, acetylacetone, acetic acid). Moreover, at the same temperature, phase transition to anatase might occur, providing its contribution to global exothermicity. Finally, in this sample it is possible to observe a structure rearrangement starting at 600 °C, whereas it is not detected for n.c.$TiO_{2\text{-SG}}$.

Considering the TG/DTA results, it was proposed that 400 °C calcination temperature could be an optimal compromise for both samples. In fact, n.c.$TiO_{2\text{-PREC}}$'s transition from amorphous happens at this temperature assuring a suitable crystal phase, whereas, in n.c.$TiO_{2\text{-SG}}$, all organic components are oxidised (and phase transition might happen as well). If carbonaceous species were not completely removed, altered catalytic results would have been obtained [43].

The absence of carbonaceous species in calcined sample was confirmed also by temperature programmed oxidation (TPO) relative to n.c.$TiO_{2\text{-SG}}$ and $TiO_{2\text{-SG}}$, reported in Figure 3.9. In fact, n.c.$TiO_{2\text{-SG}}$'s TPO profile a peak centred at 350 °C with a shoulder at 250 °C, both related to carbonaceous, whereas n.c.$TiO_{2\text{-SG}}$ TPO profile did not provide any oxygen consumption. Therefore, TPO analysis confirmed that calcination of n.c.$TiO_{2\text{-SG}}$ completely eliminated residual organic species from the sample.

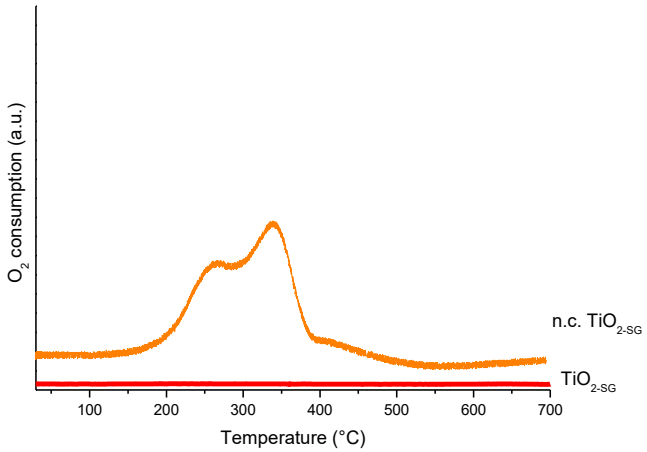

Figure 3.9 n.c.$TiO_{2\text{-}SG}$ and $TiO_{2\text{-}SG}$ TPO spectra.

Once it was confirmed, from TG/DTA and TPO analyses, that hydroxide to oxide conversion at 400 °C had occurred in both lab-made samples and that n.c.$TiO_{2\text{-}SG}$ does not contain any carbon trace, photocatalytic tests were performed and results after six hours reaction are reported in Table 3.2 and Figure 3.10.

	CH_4 PRODUCTION ($\mu mol \cdot g_{cat}^{-1}$)	**H_2 PRODUCTION ($\mu mol \cdot g_{cat}^{-1}$)**
P25	8.7	0.3
MIRKAT 211	14.0	0.1
$TIO_{2\text{-}PREC}$	20.0	0.2
$TIO_{2\text{-}SG}$	15.0	0.3

Table 3.2 P25, MIRKAT 211, $TiO_{2\text{-}PREC}$ and $TiO_{2\text{-}SG}$ photocatalytic performances in CO_2 photoreduction.

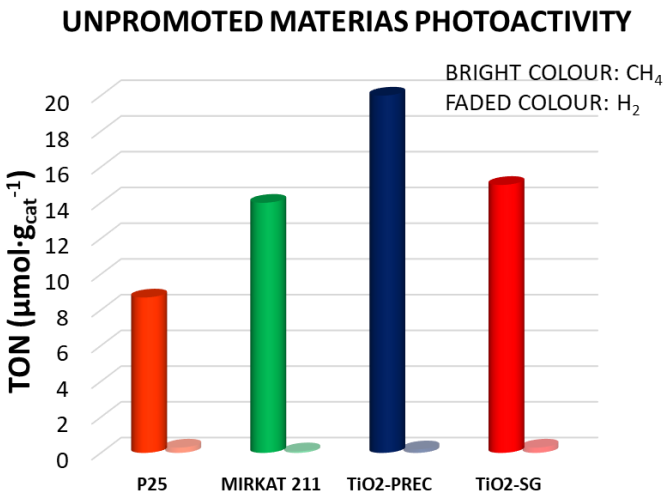

Figure 3.10 P25, MIRKAT 211, $TiO_{2\text{-}PREC}$ and $TiO_{2\text{-}SG}$ photocatalytic performances in CO_2 photoreduction.

From reported results, it is clear that both lab-made samples performed better than commercial benchmark materials, and in particular, $TiO_{2\text{-}PREC}$ provided better results than $TiO_{2\text{-}SG}$. This evidence indicates that the two different synthetic strategies actually yielded to different materials featured by different physicochemical properties. Considering the two aforementioned critical properties, namely surface area and crystallinity, physicochemical characterisation was performed.

High surface area, which assures the availability of a large number of photocatalytic sites available to both reactants and photons [44], is highly desirable and, to this purpose, nitrogen physisorption was carried out and isotherms are reported below. All samples provided type IV isotherms, but it is evident that there are noticeable differences in shape which are symptom of different surface properties.

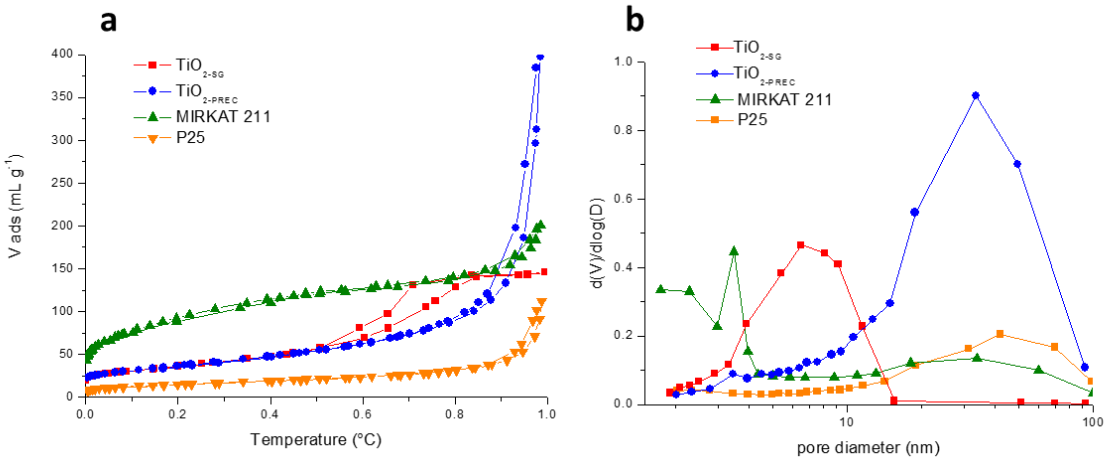

Figure 3.11 P25, MIRKAT 211, $TiO_{2\text{-}PREC}$ and $TiO_{2\text{-}SG}$ N_2 physisorption isotherms (a) and pore size distribution (b).

Among all samples, P25 is characterised by the lowest surface area (50 $m^2 \cdot g^{-1}$) and its isotherm shows a narrow H1 type hysteresis loop at high relative pressures (between 0.8 and 1 p/p_0), indicating a narrow distribution of pores with an average pore size of 25 nm. Whereas, MIRKAT 211 isotherm provides a higher nitrogen adsorption at low relative pressures indicating a much higher surface area (217 $m^2 \cdot g^{-1}$) and a wider H4 type hysteresis loop, corresponding to a wider and non-homogeneous pore size distribution. Comparing lab-made samples, they show a similar adsorption volume at low p/p_0 region indicating similar specific surface area (110 $m^2 \cdot g^{-1}$ for $TiO_{2\text{-}PREC}$ and 116 $m^2 \cdot g^{-1}$ for $TiO_{2\text{-}SG}$) while they differ in hysteresis loop shape. $TiO_{2\text{-}PREC}$'s H1 type hysteresis is shifted at high relative pressures. Differently, $TiO_{2\text{-}SG}$ isotherm can be classified as H2 type at lower relative pressures, indicating a pore size distribution centred at lower values and ranging between 3 and 15 nm. Taking into account all these considerations, all samples, apart from P25, provided are characterised by a surface area which is higher than 100 $m^2 \cdot g^{-1}$, which is generally considered a value typical of high surface area titanium dioxide materials.

P25, the sample characterised by the lowest surface area, provides the lowest photoactivity in CO_2 reduction, whereas other samples provided better results and the best performing catalyst is $TiO_{2\text{-}PREC}$, which, however, is not characterised by the highest

surface area. Therefore, despite being an important parameter, surface area is not a satisfactory explanation for photocatalytic trends since MIRKAT 211 is characterised by double the surface area of the most performing catalyst.

For this reason, crystallinity was investigated and X-ray diffraction measurements were performed and from XRD patterns, reported in Figure 3.12, all commercial and lab-made samples are crystalline, even though there are some differences in crystallinity and crystal phases observed.

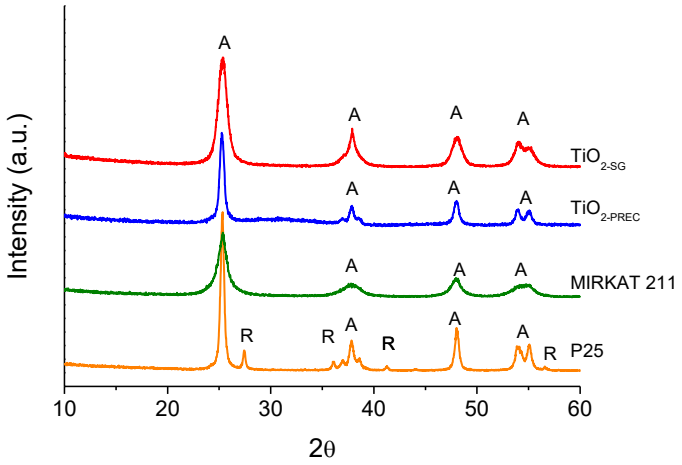

Figure 3.12 P25, MIRKAT 211, $TiO_{2\text{-}PREC}$ and $TiO_{2\text{-}SG}$ XRD profiles.

As already discussed in section 2.6, P25 shows the co-presence of both anatase and rutile in 75/25 ratio [45,46] (which is not ideal for this photocatalytic application), whilst in MIRKAT 211 anatase is the only observable crystal phase, despite XRD peak broadness confirms that only 40 % of this material is crystalline whilst the rest is amorphous [44].

Also $TiO_{2\text{-}PREC}$ and $TiO_{2\text{-}SG}$, the best performing materials, are characterised by anatase phase only and diffraction peaks are sharper than MIRKAT 211's ones. Comparing these two, peaks are less defined in sol-gel made sample compared to the best performing sample prepared by precipitation, indicating a lower crystallinity in $TiO_{2\text{-}SG}$.

Therefore, evidences from N_2 physisorption and XRD confirm what observed in the previous chapter, i.e. that relatively high surface area and high crystallinity in anatase phase are required features for an efficient photocatalyst.

3.4.2 CaO and MgO promoted samples

Once assessed the best synthetic method for titanium dioxide, i.e. precipitation, modification by calcium or magnesium oxide was performed in order to enhance CO_2 adsorption. CaO and MgO were used to this purpose, due to their basicity, abundance, inexpensiveness and easiness in introduction.

Considering their surface properties, all samples are mesoporous materials, as confirmed by type IV isotherm pattern in N_2 physisorption isotherms, which are very similar in shape to that obtained by unpromoted $TiO_{2\text{-PREC}}$ sample, despite a little decrease due to alkali-earth oxide introduction and, most probably, partial pores blockage of titanium dioxide porous structure. However, the amount of alkali earth promoters on surface area is very small, so the effect is not much significant, as observed in literature on similar materials [47,48]. Surface area values are listed in Table 3.3.

SAMPLE	**SURFACE AREA ($m^2 \cdot g^{-1}$)**
$TiO_{2\text{-PREC}}$	110
$0.5CaTiO_{2\text{-PREC}}$	109
$1CaTiO_{2\text{-PREC}}$	106
$2CaTiO_{2\text{-PREC}}$	99
$0.5MgTiO_{2\text{-PREC}}$	94
$1MgTiO_{2\text{-PREC}}$	91
$2MgTiO_{2\text{-PREC}}$	86

Table 3.3 Alkali-oxide material surface areas.

Looking more closely to surface area values, the magnesium oxide has a bigger impact on titanium dioxide surface than calcium oxide. In fact, comparing Mg^{2+}'s ionic radius (86 pm) and Ca^{2+}'s one (114 pm) [49], bivalent magnesium ions are much smaller than calcium ones, thus more easily introducible into titania's porosity during impregnation; then, during calcination, when precursors decomposition leads to correspondent oxides, promoter particles sinter and this is more probable with magnesium oxide. Thus this phenomenon provides more effective titania's pores blockage in the case of magnesium oxide promotion, leading to slightly lower surface areas.

Alkali-earth modified materials were tested in carbon dioxide photoreduction in the rig developed in the previous chapter and their results are reported alongside those from unpromoted titanium dioxide and commercial benchmark materials focusing on selectivity to methane or other C-based products. Photocatalytic results are reported in Figure 3.13 and Table 3.4.

All promoted samples showed a total selectivity to methane and no trace of hydrogen formation was observed regardless the dopant nature and its loading amount, indicating a beneficial effect of the introduction of an alkali earth oxide on titanium dioxide in titanium dioxide-based photocatalysts. Unfortunately, the increase in selectivity is accompanied by a decrease in photoactivity, as observed by the introduction of either CaO or MgO. This effect is more noticeable for MgO promotion compared to CaO. In this latter case, a correlation between CaO loading and photoactivity loss is observable.

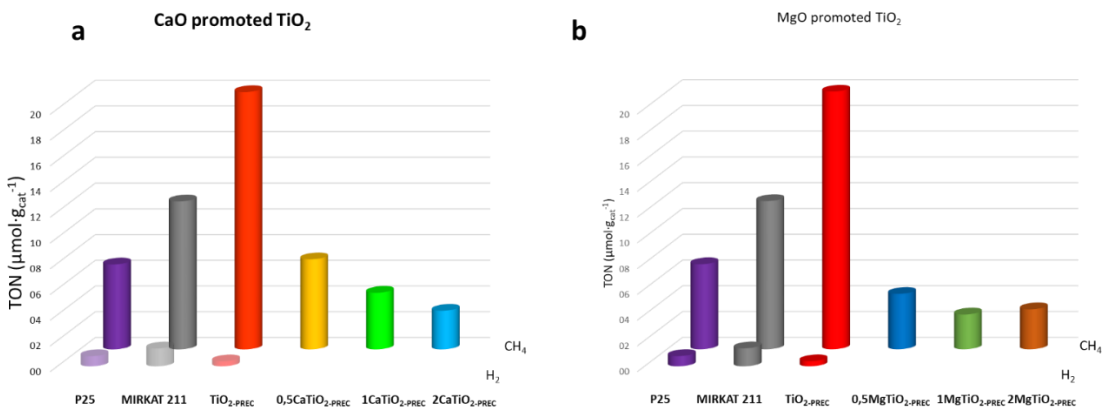

Figure 3.13 Photocatalytic tests results using CaO promoted sample (a) and MgO promoted ones (b).

	CH_4 ($\mu mol \cdot g_{cat}^{-1}$)	H_2 ($\mu mol \cdot g_{cat}^{-1}$)
P25	8.7	0.3
MIRKAT 211	14.0	0.1
$TiO_{2\text{-}prec}$	20.0	0.2
$0.5C_ATiO_{2\text{-}PREC}$	7.4	n.d.
$1CaTiO_{2\text{-}PREC}$	4.2	n.d.
$2C_ATiO_{2\text{-}PREC}$	2.9	n.d.
$0.5MgTiO_{2\text{-}PREC}$	4.3	n.d.
$1MgTiO_{2\text{-}PREC}$	2.7	n.d.
$2M_GTiO_{2\text{-}PREC}$	3.1	n.d.

Table 3.4 Alkali-earth promoted samples photocatalytic performances in CO_2 photoreduction compared to unpromoted one and commercial benchmarks.

From photocatalytic results, it is therefore clear that, in some way, the introduction of alkali-earth oxides modified the interaction between the reagents, and in particular carbon dioxide and the photocatalytic surface. To investigate this phenomenon, CO_2-TPD analyses, reported in Figure 3.14, were performed and allowed to understand the interactions between carbon dioxide and the different photocatalytic surfaces.

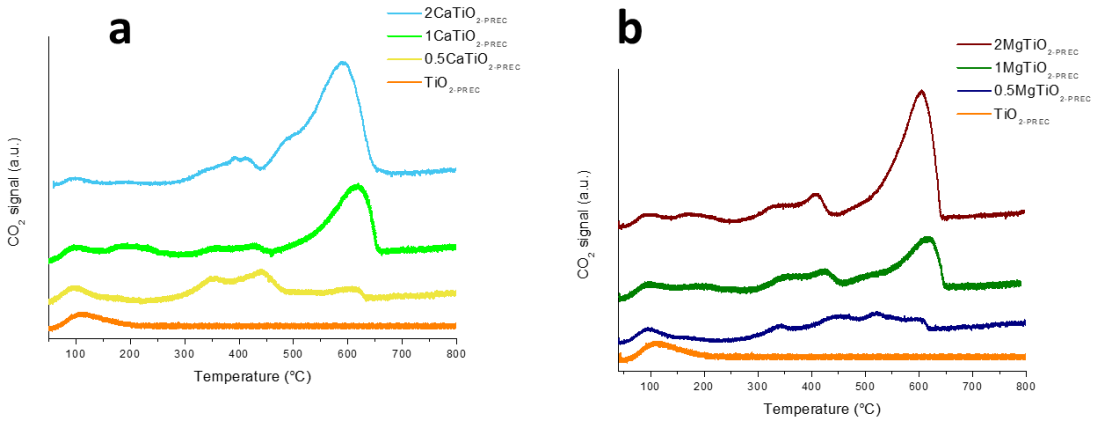

Figure 3.14 CaO promoted sample (a) and MgO promoted ones (b) CO_2-TPD patterns.

$TiO_{2\text{-PREC}}$'s CO_2-TPD pattern shows only a small peak between 80 °C and 120 °C ascribable to CO_2 weakly adsorbed on titanium dioxide surface, and this signal is observable also for all promoted samples. Considering $0.5CaTiO_{2\text{-PREC}}$, the most performant among promoted sample, and $0{,}5MgTiO_{2\text{-PREC}}$, multiple bands are observed: in the case of CaO promoted sample, desorption strongest band range between 300 °C and 450 °C, whereas for MgO promoted one this band is wider, ranging between 300 °C and 600 °C. In the case of samples with the 1 and 2 wt.% of either calcium and magnesium, there is a clear CO_2 desorption peak from 450 °C and 650 °C. All these peaks are ascribed to the CO_2 desorption from different carbonate species whose adsorption is stronger than weakly adsorbed CO_2 [50]. In particular, it can be observed that, increasing basic dopant loading, there is an increase of strongly adsorbed and thus stable carbonates.

According to DFT adsorption studies by Kwon and co-workers [51], due to lower ionic radius, electron transfer from MgO to adsorbed CO_2 (to form stable carbonates) is more efficient compared to CaO. This means that, even if CaO and MgO adsorb the same amount of CO_2 in TPD experiments the chemical nature of this bond is different. In fact, even a small amount of MgO is enough to almost completely suppress photoactivity, while milder CaO-CO_2 interaction leads to a gradual decrease in efficiency in CO_2 reduction.

Carbonate species are characterised by more negative reduction potentials than carbon dioxide and they are similar in value to titanium dioxide conduction band potentials. This means that their reduction on TiO_2 is thermodynamically less favoured, explaining photoactivity loss in promoted samples [52].

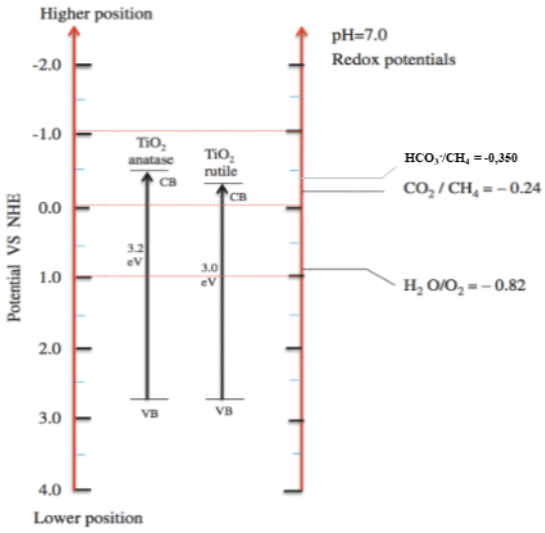

Figure 3.15 Carbon dioxide and carbonate species redox potentials compared to titanium dioxide valence and conduction bands (re-elaboration from ref. 52)

Therefore, from collected experimental data, the enhancement of carbon dioxide adsorption on photocatalytic surface as carbonates by alkali-earth metal doping was so strong to suppress photoactivity, indicating that a balance in CO_2 adsorption is needed.

3.5 Conclusion

Materials formulation proved to be an important strategy to modulate materials physicochemical properties and thus to modify photocatalysts' both activity and selectivity in carbon dioxide photoreduction with water.

From tests with commercial benchmark and lab-made not promoted materials, it was possible to understand which physicochemical and textural properties are necessary for a performant photocatalyst for CO_2 photoreduction and, in particular, the co-presence

of high surface area and textural properties. Surface area proved to be an important feature despite, among tested samples, the best performing material, a lab-made titanium dioxide prepared by precipitation, did not provide the highest surface area. In fact, it was proved that anatase phase and high crystallinity are necessary to improve photoactivity.

Not only process efficiency, but also selectivity is strictly connected to photocatalyst interaction with substrates. In particular, the most delicate phenomenon to control is carbon dioxide adsorption on photocatalyst in order to avoid water splitting side reaction, especially in presence of TiO_2 based materials.

Performing reaction in gas phase conditions allowed to increase selectivity using a high CO_2/H_2O ratio, but it is not sufficient to obtain a total selectivity to solar fuels. TiO_2 modification by bases proved to be effective in yielding a total selectivity to methane, which suppresses reductant consumption by water splitting and, in a possible application, might avoid separation processes. However, the improvement in selectivity was accompanied by activity loss, which was explained considering the interaction between reactants and surface by CO_2-TPD analyses. Thanks to this technique, it was observed that a too strong CO_2 adsorption on alkali-earth modified materials, poorly reducible carbonate species are formed, reducing materials photoactivity.

Therefore, for a selective yet active catalyst is necessary to balance adsorption properties: in fact, on one side, it is necessary to enhance carbon dioxide adsorption but, at the same time, it does not have to be too strong to avoid carbonate species formation.

3.6 References

[1] Z. Xiong, Y. Luo, Y. Zhao, J, Zhang, C. Zheng, J.C.S. Wu, Physical Chemistry Chemical Physics 18 (2016) 13186-13195.

[2] H. Zhao, F. Pan, Y. Li, Journal of Materiomics 3 (2017) 17-32.

[3] M. Andersson, L. Oesterlund, S. Ljungstroem, A.J. Palmqvist, Journal of Physical Chemistry B 106 (2002) 10674-10681.

[4] L. Kumaresan, A, Prahbu, M. Palanichamy, V. Murugesan, Materials Chemistry and Physics 126 (2010) 445-452.

[5] X. Feng, J. Zhai, L. Jiang, Angewandte Chemie International Edition 44 (2005) 5115-5118.

[6] X. Wang, J. Zhuang, Q. Peng, Y.D. Li, Nature 437 (2005) 121-124.

[7] X. Chen, S.S. Mao, Chemistry Reviews 107 (2007) 2891-2959.

[8] L.M. Hitchman, F. Tian, Journal of Electroanalytical Chemistry 538-539 (2002) 165-172.

[9] Z. Zhang, J. Goodall, D.J. Morgan, S. Brown, R. Clark, J. Knowles, N. Mordan, J. Evans, A. Carley, M. Bowker, J. Darr, Journal of the European Ceramic Society 29 (2009) 2343-2353.

[10] O. Carp, Progress in Solid State Chemistry 32 (2004) 33-177.

[11] S. Protti, A. Albini, N. Serpone, Physical Chemistry Chemical Physics 16 (2014) 19790-19827.

[12] C. Su, B.Y. Hong, C.M. Tseng, Catalysis Today 96 (2004) 119-126.

[13] S.K. Poznyak, A.I. Kokorin, A.I. Kulak, Journal of Electroanalytical Chemistry 442 (1998) 99-105.

[14] Y. Xie, C. Yuan, Materials Research Bulletin 39 (2004) 533-543.

[15] V. Trevisan, M. Signoretto, F. Pinna, G. Cruciani, G. Cerrato, Chemistry Today 30 (2012) 25-28.

[16] F. Peng, L. Cai, L. Huang, H. Yu, H. Wang, Journal of Physical Chemistry of Solids 69 (2008) 1657-1663.

[17] M.T. Nguyen, T.-K. Ha, Journal of American Chemical Society 106 (1984) 599-602.

[18] K.M. Merz Jr., Journal of American Chemical Society 112 (1990) 7973-7980.

[19] B. Jönsson, G. Karlström, H. Wennerström, S. Forsén, B. Ross, J. Almlöf, Journal of American Chemical Society 99 (1977) 4628-4632.

[20] M. Anpo, H. Yamashita, Y. Ichihashi, S. Ehara, Journal of Electroanalytical Chemistry 396 (1995) 21-26.

[21] U. Diebold, Surface Science Reports 48 (2003) 53-229.

[22] A. Markovits, A. Fahmi, C. Minot, Journal of Molecular Structure 371 (1996) 219-235.

[23] M.A. Henderson, Surface Science 400 (1998) 203-219.

[24] C. Morterra, A. Chiorino, F. Boccuzzi, E. Fisicaro, Zeitschrift für Physikalische Chemie 124 (1981) 211-222.

[25] S. Krischok, O. Höfft, V. Kempter, Surface Science 507-510 (2002) 67-73.

[26] B. Michalkiewicz, J. Majewska, G. Kądziołka, K. Bubacz, S. Mozia, A.W. Morawski, Journal of CO_2 utilization 5 (2014) 47-52.

[27] A. Dhakshinamoorthy, S. Navalon, A. Corma, H. Garcia, Energy and Environmental Science 5 (2012) 9217-9233.

[28] K. Ikeue, S. Nozaki, M. Ogawa, M. Anpo, Catalysis Today 74 (2002) 241-248.

[29] Y. Liao, S.W. Cao, Y. Yuan, Q. Gu, Z. Zhang, C. Xue, Chemistry European Journal 20 (2014) 10220-10222.

[30] J. Kapica-Kozar, E. Piróg, R.J. Wrobel, S. Mozia, E. Kusiak-Nejman, A.W. Morawski, U. Narkiewicz, B. Michalkiewicz, Microporous and Mesoporous Materials 231 (2016) 117-127.

[31] L.L. Tan, W.J. Ong, S.P. Chai, A.M Rahman, Chemical Engineering Journal 308 (2017) 248-255.

[32] W. Isahak, Z. Ramli, M.W. Ismail, K. Ismail, R.M. Yusop, M. Wahab, M. Hisham, M.A. Yarmo, Journal of CO_2 Utilization 2 (2013) 8-15.

[33] N.I. Al-Salim, S.A. Bagshaw, A. Bittar, T. Kemmitt, A.J. McQuilan, A.M. Mills, M.J. Ryan, Journal of Materials Chemistry 10 (2010) 2358-2363.

[34] G.S. Pozan, A. Kambur, Applied Catalysis B: Environmental 129 (2013) 409-415.

[35] M.A. Tabatabai, Environmental Letter 7 (1974) 237-243.

[36] S. Brunauer, P.H. Emmett, E. Teller, Journal of American Chemical Society 60 (1938) 309-319.

[37] E.P. Barrett, L.S. Joyner, P.P. Halenda, Journal of American Chemical Society 73 (1951), 373-380.

[38] J.W. Niemantsverdriet, Spectroscopy in Catalysis, 3rd ed. Wiley 2007 New York USA.

[39] V. Vishwanathan, H.-S. Roh, J.-W. Kim, K.-W. Jun, Catalysis Letters 96 (2004) 23-28.

[40] A. Azzouz, D. Nistor, D. Miron, A.V. Ursu, T. Sajin, F. Monette, P. Niquette, R. Hausler 449 (2006) 27-34.

[41] J. Mao, L. Ye, K. Li, X. Zhang, J. Liu, T.Peng, L. Zan, Applied Catalysis B: Environmental 144 (2014) 855-862.

[42] B.N. Shelimov, N.N. Tolkachev, O.P.Tkachenko, G.N.Baeve, K.V. Klementiev, A.Y. Stakheev, V.B. Kazansky, Journal of Photochemistry and Photobiology A 195(2008) 81–88.

[43] I. Grigioni, M.V. Dozzi, M. Bernareggi, G. Chiarello, E. Selli, Catalysis Today 281 (2017) 214-220,

[44] D.S. Kim, S.Y. Kwak, Applied Catalysis A: General 323 (2007) 110-118.

[45] Z. Ding, G.Q. Lu, P.F. Greenfield, Journal of Physical Chemistry B 104 (2000) 4815-4820.

[46] D.C. Hurum, A.G. Agrios, K.A. Gray, T. Rajh, M.C. Thurnauer, Journal of Physical Chemistry B 107 (2003) 4545-4549.

[47] N.I. Al-Salim, S.A. Bagshaw, A. Bittar, T. Kemmitt, A.J. McQuilan, A.M. Mills, M.J. Ryan, Journal of Materials Chemistry 10 (2000) 2538-2563.

[48] P. Panagiotopuplou, D.I. Kondarides, Applied Catalysis B: Environmental 101 (2011) 738-746.

[49] R.D. Shannon, Acta Crystallographica 32 (1976) 751-767.

[50] Y.C. Liu, J.F. Liu, H. He, Y.B. Yu, L. Xue, Chinese Science Bulletin 52 (2007) 2063-2071.

[51] S. Kwon, P. Liao, P.C. Stair, R.Q. Snurr, Catalysis Science and Technology 6 (2016) 7885-7895.

[52] M. Tahir, N. Amin, Energy Conversion and Management 76 (2013) 194-214.

4 Metal modified photocatalysts

Throughout this chapter, material modification continues focusing on actual photocatalytic redox reaction. The enhancement of electronic transfer from excited photocatalytic surface to carbon dioxide will be addressed, considering introduction by two promising strategies, namely semiconductors coupling and metal particles characterised by surface plasmonic resonance. After providing relevant state of the art on the topic, several materials were prepared and materials' physicochemical properties are reported and correlated with photocatalytic performances.

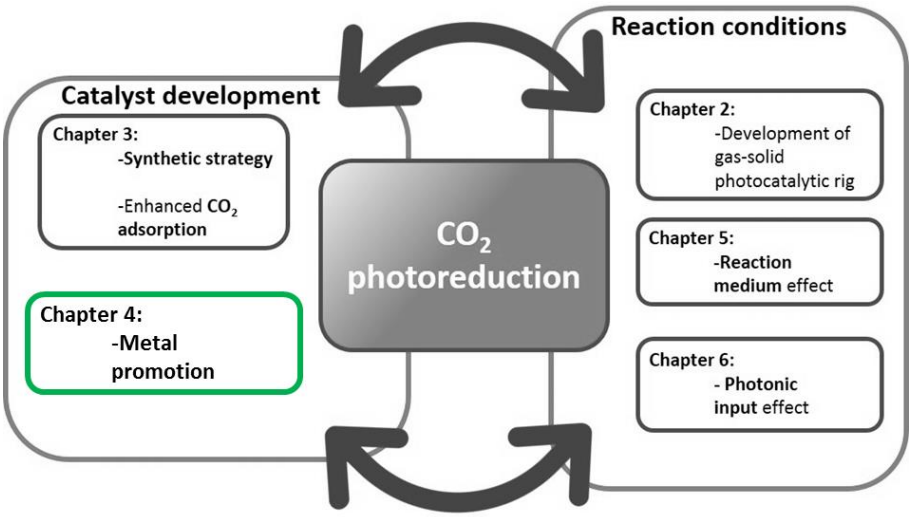

Figure 4.1 Sketch representing this chapter connection to the others in this thesis.

4.1 Metal modification on TiO_2 for CO_2 photoreduction: a state of the art

Electronic transfer from the catalyst to reactants and backwards is the backbone of photocatalytic processes and it covers great importance in CO_2 photoreduction, where desired products formation requires more than six electrons transfer.

Product Species	*Electrons to obtain product from CO_2 reduction*	*Redox potential (eV)*
CO	2	-0.53
HCOOH	2	-0.61
HCHO	4	-0.48
CH_3OH	6	-0.38
CH_4	8	-0.24

Table 4.1 Electrons required to reduce CO_2 to C_1 hydrocarbons [1,2].

For this reason, the metastability of electron-hole species should be as high as possible. In the case of titanium dioxide, charge carriers are characterised by different charge transfer rate: holes in valence band (VB) react faster with electron donors (10^{-12}-10^{-9} s), whilst conduction band (CB) excited electron transfer, which is the pivotal phenomenon in photoreduction processes, (10^{-5}-10^{-3} s), is slower [3]. Moreover, to transfer both charge carrier to reactant is essential for CB to be set at higher energy (which means a more negative potential) than electron acceptor, whereas for VB to be set at lower energy (more positive potential) than electron donor, thus allowing electron and holes flow [4].

Considering titanium dioxide bands position and desired redox potentials (reported in Figure 4.2), reduction in conduction band is extremely sensitive, since the most critical issue to be controlled and tuned is the fast electron-hole recombination at the photoexcited catalytic sites [5,6].

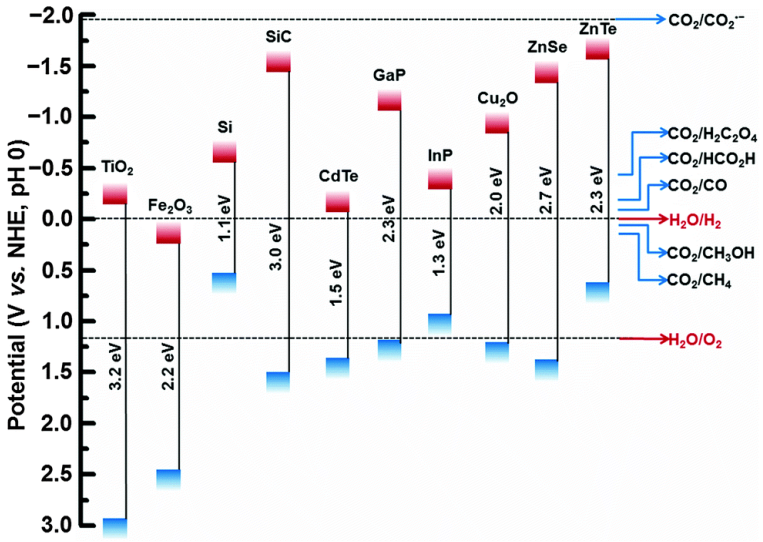

Figure 4.2 Comparison between reduction potentials and semiconductors bands position [7].

Considering these thermodynamic aspects, materials formulation should be designed to boost CB reactivity [8-11]. Considering bare titanium dioxide, anatase is the most suitable titania crystalline phase because of its slightly lower recombination rate, a feature highly required in this process [12-15]. Moreover, materials design, and in particular small particle size and reduced grain boundaries (such as in titanium dioxide nanotubes and nanorods) proved to be effective in exposing photocatalytic sites [2].

Crystal phase and particle structure aside, several different strategies can be pursued [16]:

- non-metal doping;
- dye sensitising;
- semiconductors coupling;
- metal doping;
- surface plasmon resonance.

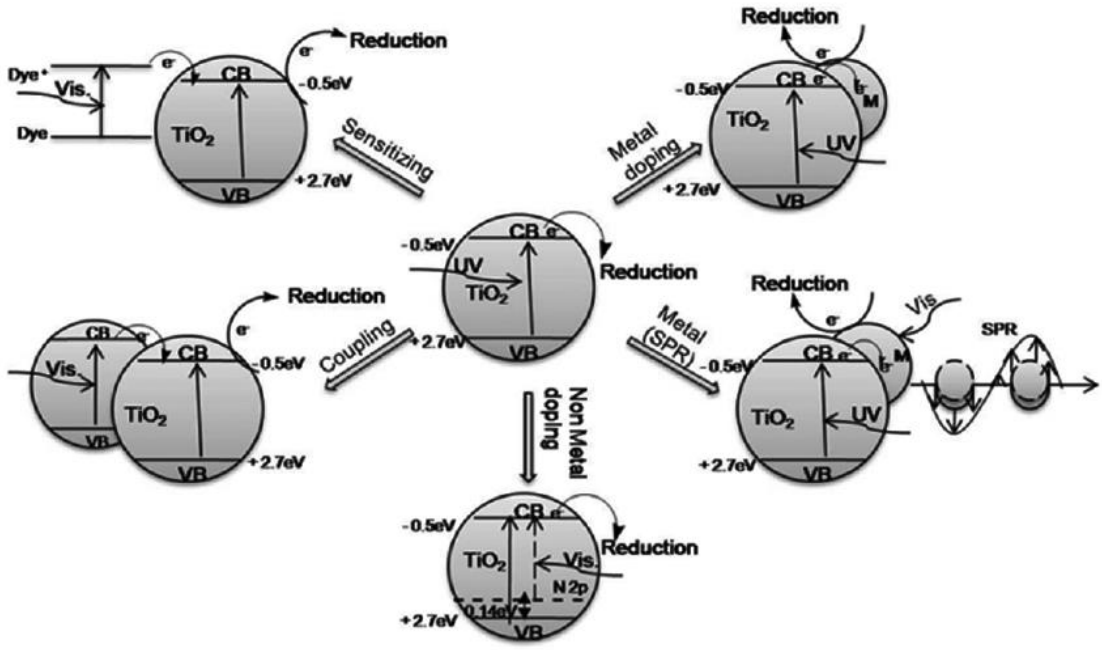

Figure 4.3 Possible routes for titanium dioxide modifications [16].

The introduction of a sensitiser (usually an organic dye) on the photocatalytic surface was reported by Graetzel *et al.* [17,18]. Though these systems are widely studied, they are affected by sensitizer degradation, a phenomenon, which should be avoided, especially in C-based solar fuels production [19].

Doping with non-metal, (such as boron, carbon, nitrogen and fluorine) has already found wide applications in photooxidation processes, such as NO_x removal and VOCs oxidation [20,21]. Considering electronic structure, these elements' 2p orbitals can either combine with titanium and oxygen orbitals, increasing VB energy [22], or create intermediate energetic levels between valence band and conduction band, but generally closer to VB [23]. Therefore, much modification occurs on conduction band electronic properties, thus non-metal modification is not suitable to improve stability of promoted electrons in CB.

The addition of another semiconductor as a co-catalyst has been applied to limit electron-hole recombination [24-26] and, at the same time, potentially to reduce photocorrosion of semiconductors resulting from charge carrier accumulation and thus improve photocatalysts stability [27]. However, choice in semiconductor is not uninfluential and should be considered carefully. In fact, the differences in energy levels

between VB and CB in the two semiconductors should allow an electron flow at the heterojunction of the two species, affecting the circulation of photoexcited electrons on the final material [28]. To obtain electrons injection into titania CB, the coupled semiconductor's Fermi level should be higher or, in other terms, have a more negative CB [29]. Semiconductors coupling can occur either *via* direct Z-scheme, where charge separation is achieved by electrons and hole injection to VB and CB of semiconductors occurs in opposite direction, or direct Z-scheme, where charge transfer occurs in the same direction without charge separation [30].

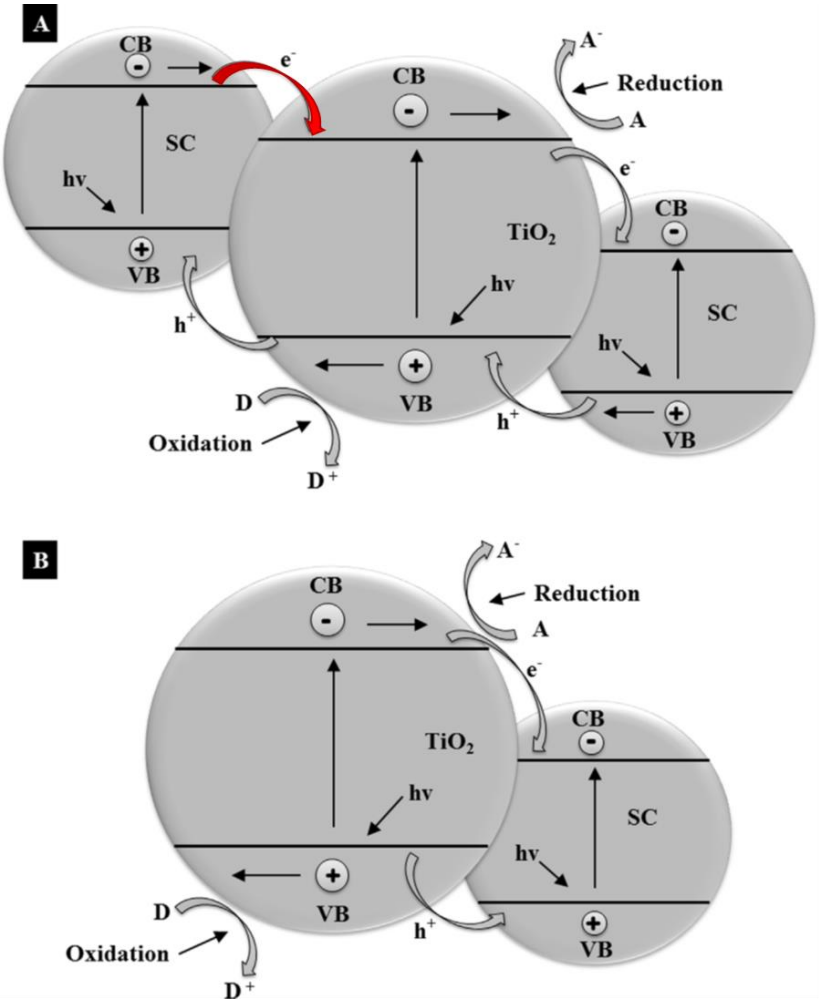

Figure 4.4 Coupling of TiO_2 with semiconductors by direct (A) and indirect (B) Z-scheme [31].

Copper(II) oxide appears as a good candidate as a co-catalyst due to its electronic properties, appropriate Fermi level, great availability and low cost [32]. Qin *et al.* reported that the introduction of surface copper species positively affects titania

photoactivity by enhanced separation of titanium dioxide strong oxidative holes and reductive electrons [33]. At the same time, electrons in TiO_2 CB could recombine with the holes in CuO with a VB close to the CB of TiO_2, retarding recombination on VB in TiO_2.

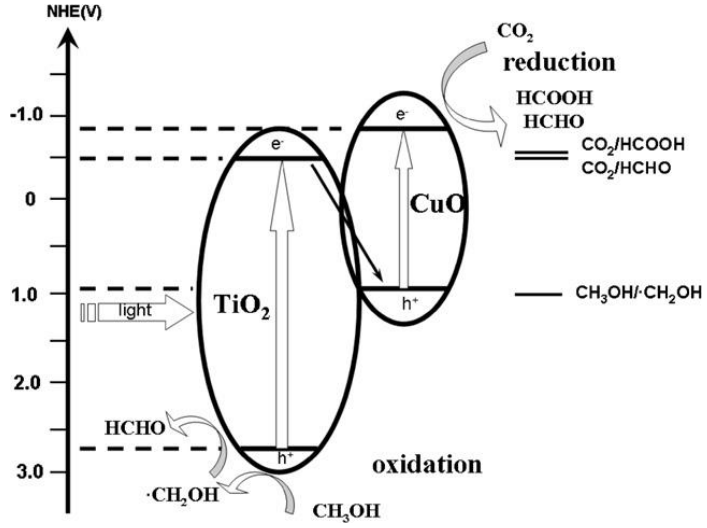

Figure 4.5 Band positions in CuO and TiO_2 compared to several redox reaction potentials.

Moreover, Isahak *et al.* reported that CuO is an efficient CO_2 adsorbent, favouring the interaction between substrates and the photocatalytic surface [34].

Another method to improve electron-hole stability is the introduction of noble or non-noble metal nanoparticles (such as nickel, ruthenium, platinum, silver and gold) on titania surface [35-38]. In these materials, the excited electrons flow from the semiconductor to the metal under light irradiation [39]. Due to this phenomenon, upward band bending formed due to an excess of positive charges in TiO_2 is originated at the interface between metal and semiconductor from the migrating electrons, which increases Fermi energy level. This interface, called Schottky barrier, between the titanium oxide and the metal nanoparticle, hinders electron flow back to titanium dioxide, preventing electron-hole recombination and thus acting as an electron trap [36,40-44].

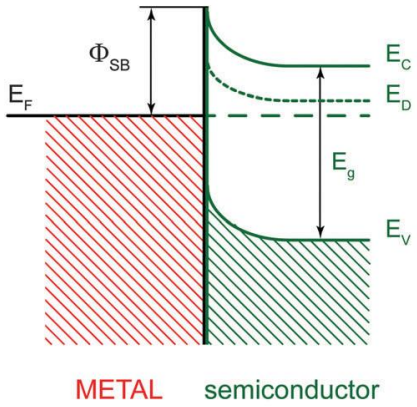

Figure 4.6 Scheme of a metal-semiconductor Schottky barrier (E_C = minimum energy for semiconductor CB, E_V = maximum energy for semiconductor VB, E_D = donor's energy level, E_g = bandgap, E_F = Fermi level, Φ_{SB} = Schottky barrier height) [45].

Beside these electron-trapping properties, gold and silver nanoparticles are also characterised by the surface plasmonic resonance (SPR) effect [46]. This phenomenon consists in the collective oscillation of valence electrons in metal atoms under irradiation, which causes electronic perturbation and thus light absorption (usually called plasmonic band) in the visible region [47]. The position and shape of the surface plasmon band is affected by several physical properties, such as particle size, shape of the particles and Coulombic charge of the nanoparticle among others [48].

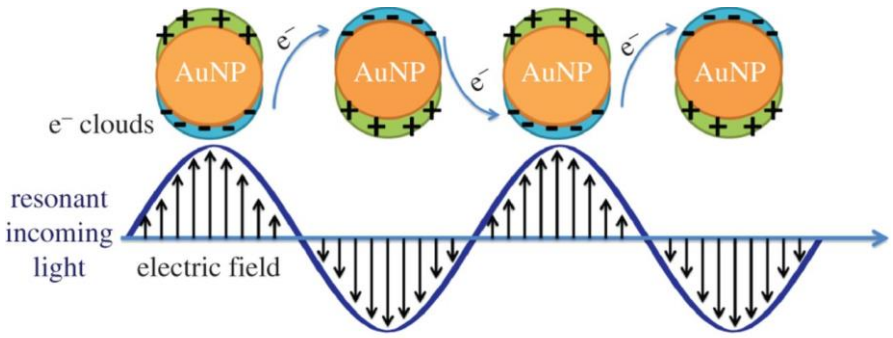

Figure 4.7 Surface plasmon oscillations in spherical gold nanoparticles [49].

In Au-TiO_2 systems, surface gold nanoparticles excited electrons can be ejected and thus populate the conduction band of this semiconductor, since the energy of the TiO_2 conduction band is lower than photoejected electrons [39]. In other terms, irradiation on TiO_2 materials coupled with gold causes a charge separation state with milder oxidation (positive gold) and same reduction (TiO_2 conduction band) potentials as TiO_2 and other photocatalysts [39]. This electronic modification should be extremely beneficial in CO_2 photoreduction, whose limiting step lies in TiO_2's CB reductive capability.

Since all these phenomena modify the overall electronic circulation by different mechanism, they might have different effects on the activity and selectivity displayed by titania in the CO_2 photoreduction, with consequences on the efficiency of the overall process. Actually, in order to make this process an efficient and sustainable technology, it is important to develop an active and selective photocatalytic process. Therefore, this section of the work will be devoted at investigating CO_2 photoreduction using CuO-TiO_2 and Au-TiO_2 photocatalytic materials for a sustainable process focusing on activity and selectivity, correlating catalytic performances with physicochemical modification induced by metal introduction.

4.2 Materials synthesis

Copper oxide and gold nanoparticles were introduced on $TiO_{2\text{-PREC}}$ sample, whose synthetic protocol was described in paragraph 2.3, since its compromise between relatively high surface area and anatase crystal phase provided the best photocatalytic results in CO_2 reduction.

4.2.1 Copper oxide introduction

Incipient wetness impregnation with a copper precursor, namely $Cu(NO_3)_2{\cdot}3H_2O$ (assay >99%, Sigma–Aldrich), was performed on dried $Ti(OH)_4$ (i.e. n.c. $TiO_{2\text{-PREC}}$). By this technique, copper precursor (to get a 0.2 wt. % on the final material) is dissolved into an amount of water that is equal to material's pore volume. Then the metal solution is dropped on the porous solid to impregnate while it is continuously stirred.

The main advantages of this method are:

- quantitative metal introduction;
- use of minimum required water;
- surface disposition of impregnated metal;
- rapidity and easiness.

Then the copper-impregnated sample was calcined at 400 °C in air flow in order to obtain the CuO-$TiO_{2\text{-PREC}}$ photocatalyst.

4.2.2 Gold nanoparticles introduction

In the case of gold nanoparticles, the incipient wetness method would not allow to deposit small gold nanoparticles on the titania surface [50]. Therefore, in order to obtain gold nanoparticles smaller than 10 nm, gold was added to titania by using the deposition–precipitation (DP) method [51]. This method, reported for the first time by Haruta and co-workers [52], by a careful control of pH from values below support isoelectronic point to values above allows to deposit gold almost quantitatively only on the support [53].

Titanium dioxide was suspended in an aqueous solution of $HAuCl_4 \cdot 3H_2O$ at 60 °C, whose pH is below 2, and then raised and maintained equal to 8.6 with 0.5 M NaOH (assay > 97% Carlo Erba) for 3 hours, while controlling the pH value by the addition of sodium hydroxide solution. Gold amount was 0.2 wt. %, the same as in the case of the CuO-TiO_2 photocatalyst, for comparison purposes (in the case of CuO, promoters amount was considered on metal basis). The sample was filtered and washed from chlorides with deionised water. The absence of chlorides was verified by the silver nitrate test. The samples were then dried at 35 °C overnight and finally calcined in air for 1 h at 400 °C. The final sample has been labelled Au-$TiO_{2\text{-PREC}}$.

4.3 Characterisations

4.3.1 X-ray diffraction (XRD)

By these technique, several information can be obtained on morphological structure modification induced by promoters: in particular, it is possible to detect whether promoting metal atoms enter TiO_2 structure modifying lattice parameters or they form heterostructures and, if they are crystalline, to calculate their size.

These analyses were carried out at the school of Engineering and Physical Sciences at Heriot Watt University (Edinburgh, UK) and Dr. Georgina Rosair is gratefully acknowledged for her help in conducting these measurements. XRD analyses were conducted using a Bruker Nonius X8-Apex2 CCD diffractometer with an Oxford Cryosystems Cryostream routinely running at 100K (copper anode; operating conditions, 40 kV and 40 mA) and a Si(Li) solid state detector (Sol-X) set to discriminate the Cu Kα radiation. Apertures of divergence, receiving and detector slits were 2.0 mm, 2.0 mm, and 0.2 mm, respectively. Data scans were performed in the 2θ range 5°–80° with 0.02° step size and counting times of 3 s/step.

4.3.2 Nitrogen physisorption

Information on the surface properties were obtained by N_2 adsorption–desorption at -196 °C analyses, which were carried out using a MICROMERITICS ASAP 2000. Before measurements, all samples had been outgassed at 200 °C for two hours in vacuum. The surface area was calculated by BET equation [54] and the pore size distribution was obtained using the BJH method [55] applied to the isotherm desorption branch.

4.3.3 Flame atomic absorption

This analytical technique helped to determine the exact amount of copper and gold introduced in doped samples. It exploits a property that every element has, that is to electron excitation from occupied orbital to unoccupied ones, that leads to light adsorption: since energetic gaps between orbitals change from atom to atom, adsorption spectrum provides both qualitative and quantitative elemental composition.

This phenomenon takes place when atoms are in the form of gaseous atoms: therefore, samples must be *atomised*. In this case flame atomization was used.

All the samples were prepared by solubilisation in an extremely acidic medium. 100 mg of each sample was solved in a solution made up of 5 mL milli-Q water, 1,5 mL of hydrofluoric acid and 3 mL of aqua regia (3:1 mixture of hydrochloric, HCl and nitric acid HNO_3) in a PTFE vessel using a Milestone 1600 Microwave Digester. Then, after cooling to run temperature, 5 mL of boric acid have been added to buffer unreacted HF. Then samples have been moved into 50 mL volumetric flasks and made up to volume with milli-Q water.

Analyses were performed using a Perkin-Elmer Aanalist 100 flame atomic absorption spectrometer where flame has been fed by a 1:3 acetylene:air mixture and a cathode made up of the element to investigate (i.e. either copper or gold) was employed. The instrumental parameters are:

- wavelength 324.8 nm for copper and 242.8 nm for gold;
- slit 0.7 nm;
- linearity range 0-5 ppm and 0-15 ppm for copper and gold respectively.

For metal quantification, absorbance was related to concentration C through the Lambert-Beer law [56]:

$$\boldsymbol{A = \varepsilon \cdot b \cdot C}$$

Equation 4.1

where ε is molar absorptivity and b is path length. Several standard copper and gold solutions were prepared in concentrations range for both elements.

4.3.4 Temperature programmed reduction (TPR)

Temperature programmed reduction gives information about metal species on their reducibility, oxidation state and interaction with a support. This technique consists in monitoring the presence of reducible species by means of hydrogen consumption, while

temperature increases linearly with time [57]. By this characterisation, it is possible to detect how many reducible metal species are present in a sample and have information on their reducibility. The lowest is the temperature of metal species reduction, the highest is their reducibility. Then, in the case that a metal can be present in the sample in more than one oxidation state, this analysis shows if different metal species are present and gives indications of metal interactions with the support.

TPR experiments were carried out in a lab-made equipment, similar to that described for temperature programmed oxidation and CO_2 desorption. Each sample (50 mg) was heated at 10 °C/min from 25 °C to 800 °C in a 5 % H_2/Ar reducing mixture (40 mL·min^{-1} STP). The effluent gases were analysed by a Gow-Mac TCD at 100 °C detector using a magnesium perchlorate trap to adsorb H_2O.

4.3.5 Diffuse reflectance UV–Visible-NearInfraRed Spectroscopy

Diffuse reflectance UV–Vis- NearInfraRed (NIR) spectroscopy allows to investigate how these materials interact with light and measure semiconductors band gap. Moreover, it is possible to observe metal promoters' interaction and whether the modify TiO_2's band gap or not.

Spectra were collected at r.t. on a Varian Cary 5000 spectrophotometer with an integrating sphere attachment using $BaSO_4$ powder as an internal reference, working in the 50000-4000 cm^{-1} range, corresponding to 200-2500 nm. Results will be displayed in both units: in fact, while the use of nanometres is more significant and generally used throughout photocatalysis scientific community, wavenumbers allows to appreciate even minimal differences in light absorption.

The layer of powder sample was made sufficiently thick such that all incident light was absorbed or scattered before reaching the back surface of the sample holder. A typical thickness of 1–3 mm was required. The samples in the form of powders were placed in a quartz cell, allowing treatments in controlled atmosphere and temperature.

UV–Vis-NIR spectra of the as prepared samples are reported in the Kubelka-Munk function (KM) [58];

$$\boldsymbol{KM = \frac{(1-R)^2}{2R}}$$

Equation 4.2

Wavelength λ can be transformed in the corresponding energy E through simple physics equations [59]:

$$\boldsymbol{E(eV) = h\nu = \frac{h \cdot c}{\lambda} = \frac{1240}{\lambda(nm)}}$$

Equation 4.3

where energy E is expressed in eV, h is Plank constant (6,626 $J \cdot s^{-1}$), ν is light frequency, c is the speed of light (2,998·10^8 $m \cdot s^{-1}$) and wavelength is expressed in nm. The band gap energy (BG) of the catalysts were determined by the intercept of a linear fit to the absorption edge and they can be estimated using Equation 4.3.

4.3.6 Fourier Transform InfraRed Spectroscopy (FTIR)

To understand how to carbon dioxide and water interact with the photocatalytic surface, FTIR were carried out. By this technique chemical heteroatomic bonds vibrations in molecules (such as CO, CO_2 and NO) and their variation in bond strength is detected [57]. Thus, from these data, it is possible to identify adsorbed species and which chemical bonds in these species are affected by adsorption onto the surface of the catalyst.

The FTIR analyses were performed at University of Turin in collaboration with Doc. Maela Manzoli using a Perkin Elmer 2000 spectrometer (equipped with a cryogenic MCT detector). For the analyses at increasing temperature, each sample, in the form of self-supporting pellet, was placed in an AABSPEC 2000 cell which allows to collect spectra in situ in controlled atmosphere and temperature. The samples were outgassed from room temperature up to 150°C.

In addition to these tests, CO_2 adsorption measurements at room temperature were performed. In this case, the samples were submitted to outgassing at r.t. for one hour

in order to remove water, that is adsorbed at the surface due to the exposition to air. The spectrum of the sample before the inlet of CO_2 was subtracted from each spectrum and all spectra were normalised with respect to the density of the pellets.

4.3.7 Scanning emission spectroscopy (SEM) and Energy Dispersive Spectroscopy (EDS)

By these microscopic analyses, morphological and textural properties, as long as samples' elemental composition, were investigated. From the interaction between specimen surface and a focused electronic beam, whose energies are in the range of 5 to 50 kV [60]. Backscattered electrons provide information on composition and topography of the sample, because heavy elements scattering is more efficient and thus they appear brighter in the image. Moreover, secondary electrons emitted from beam bombarded specimen surface are collected and their energy dispersion allows to obtain surface elemental composition (EDS mode).

Synthesised samples were analysed by SEM to identify average titanium dioxide grain size and, by EDS analysis, eventually to observe metal promoters presence on the surface and their distribution.

Analyses were carried out at the Institute of Petroleum Engineering at Heriot Watt University (Edinburgh, UK) and Doc. Jim Buckman is gratefully acknowledged for his collaboration for SEM-EDS analyses. A Philips/FEI XL30 Environmental SEM equipped with a LaB_6 gun at 30 kV, and an EDAX UTW energy dispersive X-ray detector was used. In each analysis a small amount of the sample (10 mg approximatively) was placed on conductive carbon adhesive discs (diameter 10 mm).

4.4 Photocatalytic tests

Catalytic CO_2 reduction tests were carried out in the photocatalytic gas-solid rig developed in the chapter 2. To summarise briefly, reactor configuration and reaction conditions are reported in the chart below.

Reactants phase	both gaseous
water introduction method	bubbler at 40 °C
CO_2/H_2o ratio	13.3
Reactor	thin film
Temperature	40 °C
Pressure	1 atm
Irradiance	50 $W \cdot m^{-2}$

Table 4.2 Experimental conditions for CO_2 photoreduction tests.

4.5 Results and discussion

4.5.1 Materials characterisation and photoactivity

In order to further improve the effectiveness of the titania photocatalyst, two different promoters, i.e. CuO and Au, were introduced into the TiO_2 sample. The choice of 0.2 wt. % amount of copper, as CuO, and gold nanoparticles was not arbitrary, but it was driven by a careful screening in literature of similar catalytic systems. As described by Tseng and co-workers [61] Cu loading can mask the TiO_2 surface, reducing the photoexciting capacity of TiO_2. Moreover, Liu *et al.* reported that 2-dimensional copper oxide islands facilitate rapid charge migration from titanium dioxide, whereas on 3-dimensional crystallites electron-hole recombination potential is minimised [62]. In addition to that, from a preliminary work [63] it was observed that 0.2 wt. % copper loading as CuO provided the best photocatalytic results. Similar trends were observed also for gold nanoparticles promotion on titanium dioxide, but, in this case, it was observed that an extremely high gold loading decreases gold-titania interphase area, leading to lower photoactivity [64,65]. For these reasons, the same amount (0.2 wt. % on metal base) of promoter was added, as confirmed by the FAAS analysis

Due to such low amount, it was observed that the addition of the promoter has a negligible effect on the specific surface area, as demonstrated by N_2 physisorption results reported in Table 4.3.

Photocatalyst	BET Specific Surface Area (m^2/g)
$TiO_{2\text{-PREC}}$	110
$CuO\text{-}TiO_{2\text{-PREC}}$	100
$Au\text{-}TiO_{2\text{-PREC}}$	100

Table 4.3 Specific Surface Areas of the examined photocatalysts obtained by N_2 physisorption analyses.

From SEM analyses, it is possible to observe that metal promoters introduction does not modify titanium dioxide morphology. In detail, in both $CuO\text{-}TiO_{2\text{-PREC}}$ and $Au\text{-}TiO_{2\text{-PREC}}$ titanium dioxide aggregates are characterised by granular texture with average size ranging from 150 µm to 250 µm where grain edges are well defined. The presence of metal promoter was detected only for $CuO\text{-}TiO_{2\text{-PREC}}$ as small grains on top of TiO_2 grains: in fact in EDS analysis on these small particles it is possible to observe the presence of peaks related to copper atoms. Whereas, gold nanoparticles are too small to be detected in $Au\text{-}TiO_{2\text{-PREC}}$ by SEM analysis and only titanium dioxide grains were detected similar in size and by EDS analysis only titanium related peaks were observed. In fact, according to what reported by Menegazzo *et al.* [51], chosen synthetic approach, namely deposition-precipitation method, allows to obtain nanoparticle smaller than 10 nm, which is way smaller than SEM magnifying potentialities.

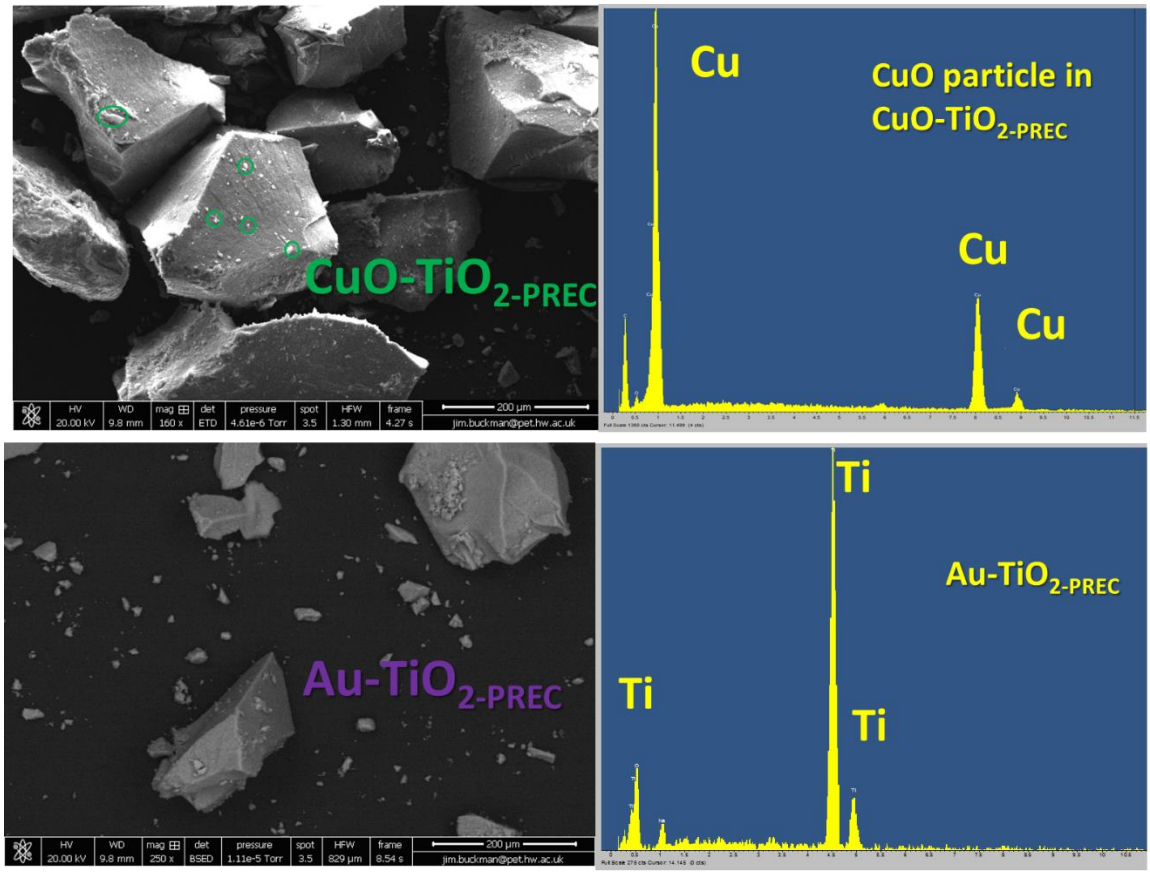

Figure 4.8 SEM (left) and EDX (right) analyses of CuO-$TiO_{2\text{-}PREC}$ (top) and CuO-$TiO_{2\text{-}PREC}$ (bottom).

The presence of promoters was not detected also by XRD analysis for any sample, where only anatase TiO_2 related peaks were detected (in accordance with JCPDS Card No. 00-002-0387). This might be ascribable either to low loading or promoter particles amorphous structure. While CuO-$TiO_{2\text{-}PREC}$ does not show any difference in peaks position to $TiO_{2\text{-}PREC}$, Au-$TiO_{2\text{-}PREC}$'s 101 plane peak, the most intense within anatase spectrum) is shifted toward lower angles (25.38° instead of 25.51°) and it is wider. This experimental evidence is related to gold nanoparticles ability to hinder TiO_2 crystallisation [66].

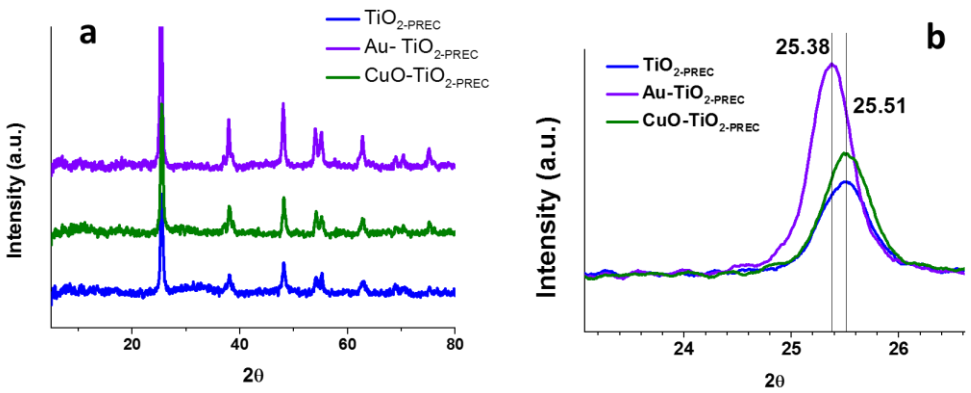

Figure 4.9 XRD spectra of investigated sample (a) and zoom on the peak related to 101 plane (b).

To investigate promoters' oxidation state, TPR analyses were carried on to have information on the oxidation state of copper and gold after insertion into the TiO_2 sample.

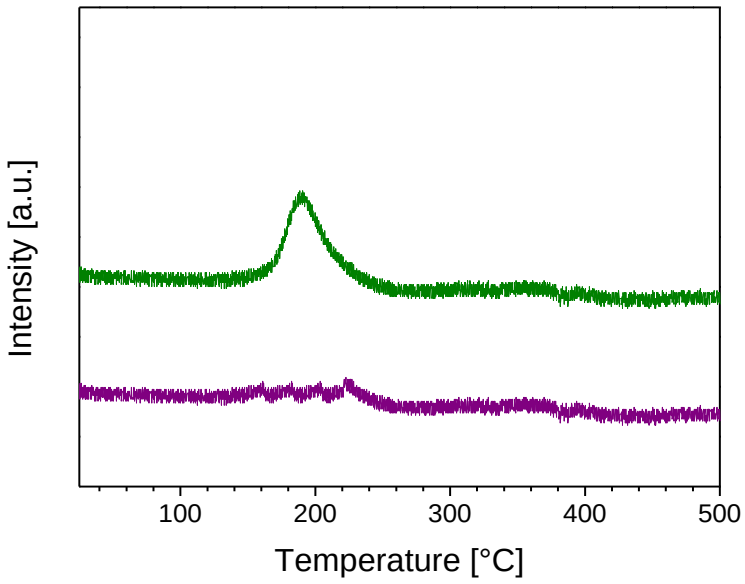

Figure 4.10 TPR analyses of CuO-$TiO_{2\text{-}PREC}$ sample (green curve) and Au-$TiO_{2\text{-}PREC}$ sample (violet curve).

TPR measurements revealed that copper is present as Cu(II), due to a single hydrogen consumption centred at 190 °C ascribable to Cu(II) reduction to Cu(0) (reported in Figure 4.10, green curve), in accordance with data in literature [67,68]. Differently, gold

nanoparticles are in their ground state, since hydrogen consumption was not observed (violet curve in Figure 4.10).

To finally assess the effect on interaction with light, diffuse reflectance UV-Vis-NIR spectra of the CuO-TiO_2 (green curve) and Au-TiO_2 (violet curve) photocatalysts are shown in Figure 4.11.

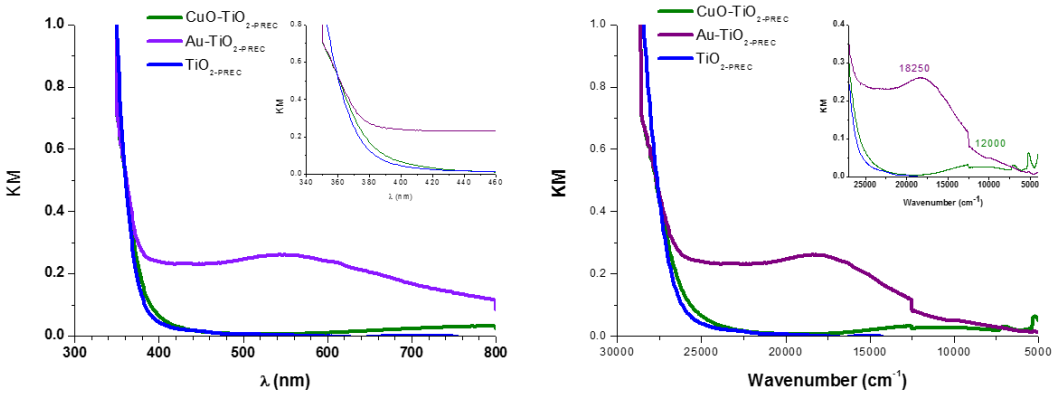

Figure 4.11 Diffuse reflectance UV-Vis-NIR spectra of TiO2-PREC (blue curve), CuO-$TiO_{2\text{-}PREC}$ (green curve) and Au-$TiO_{2\text{-}PREC}$ (violet curve) photocatalysts. Inset: zoom of the spectra in the Vis-NIR region.

The presence of the promoters does not seem to modify the titania electronic properties, since the absorption in the UV region was comparable and very small modification in the band gap value were observed: a value corresponding to 3,19 eV for CuO-$TiO_{2\text{-}PREC}$ and 3.16 eV for Au-$TiO_{2\text{-}PREC}$, which are slightly lower than the typical value for bare anatase titania $TiO_{2\text{-}PREC}$ (3.21 eV). Therefore, the presence of the promoters did not affect titania light absorption: in fact metal promoters species are supposed to reduce electron-hole recombination by modifying the TiO_2's excited electrons relaxation phenomena.

However, some differences were observed in the Vis-NIR region, as shown in the inset of Figure 4.11. In particular, a broad absorption peak, centred at 18250 cm^{-1} (corresponding to 548 nm), was observed in Au-$TiO_{2\text{-}PREC}$ sample and it can be ascribed to the plasmonic resonance of gold nanoparticles [69,70]. Differently, CuO-$TiO_{2\text{-}PREC}$ provided a weak absorption centred at 12000 cm^{-1} (corresponding to 830 nm),

attributed to d-d transition in Cu(II) species, confirming the presence of copper(II) oxide nanoparticles [71,72] on material's surface.

After having considered physicochemical properties of promoted photocatalysts, Au-$TiO_{2\text{-PREC}}$ and the CuO-$TiO_{2\text{-PREC}}$ samples were tested in the CO_2 photoreduction. The results are reported in Figure 4.12 and Table 4.4 with those already obtained for the unpromoted $TiO_{2\text{-PREC}}$ sample.

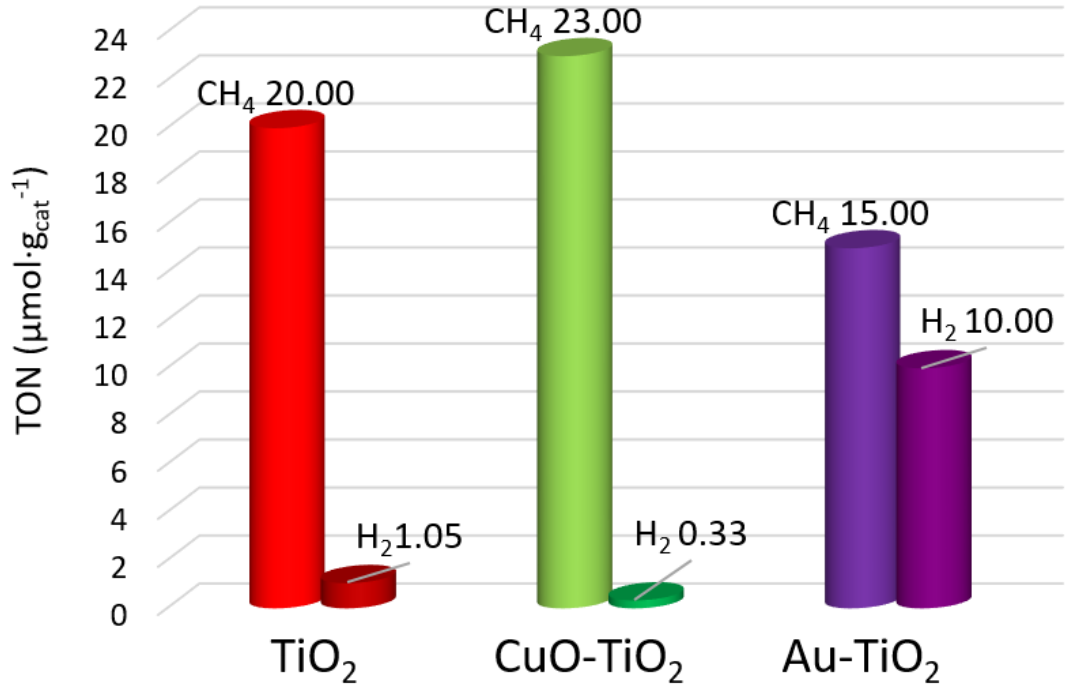

Figure 4.12 Photoactivity tests in the CO_2 photoreduction performed on unpromoted $TiO_{2\text{-PREC}}$ (left, blue columns), Au-$TiO_{2\text{-PREC}}$ (centre, violet columns) and CuO-$TiO_{2\text{-PREC}}$ (right, green columns).

	METHANE PRODUCTION (µmol·g_{cat}^{-1})	HYDROGEN PRODUCTION (µmol·g_{cat}^{-1})	SELECTIVITY TO METHANE (%)	METHANE RELATED PHOTONIC YIELD (%)
$TIO_{2\text{-PREC}}$	20.00	1.05	95	0.25
Au-$TIO_{2\text{-PREC}}$	15.00	10.00	60	0.19
CuO-$TIO_{2\text{-PREC}}$	23.00	0.33	98	0.29

Table 4.4 Productivity, selectivity and methane related photonic yield of investigated samples.

First of all, it was observed that in the presence of all three catalysts the only detected products are methane and hydrogen: the former derives from complete CO_2 photoreduction (Equation 4.4) and the latter comes from the water splitting reaction (Equation 4.5).

$$CO_2 + 2H_2O \rightleftharpoons CH_4 + 2O_2$$

Equation 4.4

$$2H_2O \rightleftharpoons 2H_2 + O_2$$

Equation 4.5

However, the presence of CuO and Au promoters affected activity as well as selectivity in the CO_2 photoreduction process. In particular, if compared to the unpromoted sample, the presence of CuO slightly increased the catalyst photoactivity in the formation of methane (from 20.00 for to 23.00 $\mu mol_{CH4} \cdot g_{cat}^{-1}$) and, at the same time, it reduced hydrogen production by water splitting even more. More specifically, selectivity to methane increased from 95 % for the undoped TiO_2 sample to 98 % for the CuO-$TiO_{2\text{-PREC}}$ sample. On the contrary, the sample containing Au nanoparticles provided the lowest methane production (15.00 $\mu mol_{CH4} \cdot g_{cat}^{-1}$), whereas the production of hydrogen was considerably higher (10.00 $\mu mol_{H2} \cdot g_{cat}^{-1}$), leading to only a 60 % selectivity to methane. In the same way, considering light harvesting for CO_2 photoreduction, copper introduction increased methane related photonic yield from 0.25 % for the undoped sample to 0.29 % for CuO-$TiO_{2\text{-PREC}}$ sample, whilst it decreased to 0.19 % for Au-$TiO_{2\text{-PREC}}$ sample.

The above results proved that the introduction of CuO on TiO_2 catalyst favoured CO_2 photoreduction and, on the contrary, the presence of Au nanoparticles increased the activity in water splitting reaction. To deeply understand these experimental data, it must be considered that the former reaction occurs only if the both carbon dioxide and water interact on the photoexcited catalytic surface [24]. Whereas, if only water is adsorbed on the surface, only water splitting reaction happens, since the CO_2 molecule is more difficultly adsorbed than water on the surface of titania [73]. To overcome this issue, this process was designed and performed in a large excess of CO_2, even though it

was not possible to suppress completely water splitting. The catalytic data indicate that the introduction of gold nanoparticles on the TiO_2 surface seems to increase the hydrophilicity of the photocatalyst and, as a consequence the capability of Au-TiO_2 to adsorb water was enhanced. Carneiro *et al.* reported that gold nanoparticles modify hydroxyl groups population on titania surface [74]. Thus, it can be supposed that different photocatalytic behaviour displayed by the two photocatalysts are affected by the different surface properties of CuO-TiO_2 and Au-TiO_2.

4.5.2 Influence of the surface and electronic properties on the photoactivity of CuO-TiO_2 and Au-TiO_2

In order to explain the differences in photocatalytic behaviour observed for the two promoted catalysts in the CO_2 photoreduction, FTIR measurements were performed on both CuO-$TiO_{2\text{-PREC}}$ and Au-$TiO_{2\text{-PREC}}$ samples.

The FTIR absorbance spectra collected on CuO-$TiO_{2\text{-PREC}}$ and Au-$TiO_{2\text{-PREC}}$ samples upon outgassing from room temperature up to 150 °C are reported in Figure 4.13. As specified in the experimental section, the spectra were normalised to the density of the pellets, in order to obtain semi-quantitative information: in this way, the intensity of the absorption bands can be taken as a measure of the amount of adsorbed species and of their stability to the outgassing at increasing temperature on the two photocatalysts. The intense absorption centred at about 3400 cm^{-1} and the peak at 1632 cm^{-1} and 1629 cm^{-1} observed on both CuO-$TiO_{2\text{-PREC}}$ and Au-$TiO_{2\text{-PREC}}$ are ascribed to the stretching and bending modes, respectively, of OH groups indicating the presence of adsorbed molecular water (navy curves). Most part of such molecules is easily removed upon degassing the samples at r.t. for 30 minutes (bold blue curves); however, it can be observed that a hydroxyl groups and water molecules monolayer still remains [75] and gradually decreases upon outgassing at increasing temperature, up to 150 °C (red curves), as confirmed by the peak at 3673 cm^{-1} with a weak shoulder at 3721 cm^{-1}, due to the stretching mode of two types of free hydroxyl groups [76,77] (see the insets in Figure 4.13). However, if compared with CuO-$TiO_{2\text{-PREC}}$, the Au-$TiO_{2\text{-PREC}}$ photocatalyst is characterised by a more hydrophilic surface since the intensity of the bands due to the presence of adsorbed water molecules is much higher than those related to carbonate

species and observed at lower frequencies (wavenumber < 1600 cm^{-1}) that will be discussed in detail afterwards. This behaviour at outgassing gives an idea of the behaviour of the catalyst at the surface during the CO_2 photoreduction, that is performed at room temperature in the presence of water: in fact, this preliminary FTIR analysis indicates that water is more strongly adsorbed on Au-$TiO_{2\text{-PREC}}$ than on CuO-$TiO_{2\text{-PREC}}$.

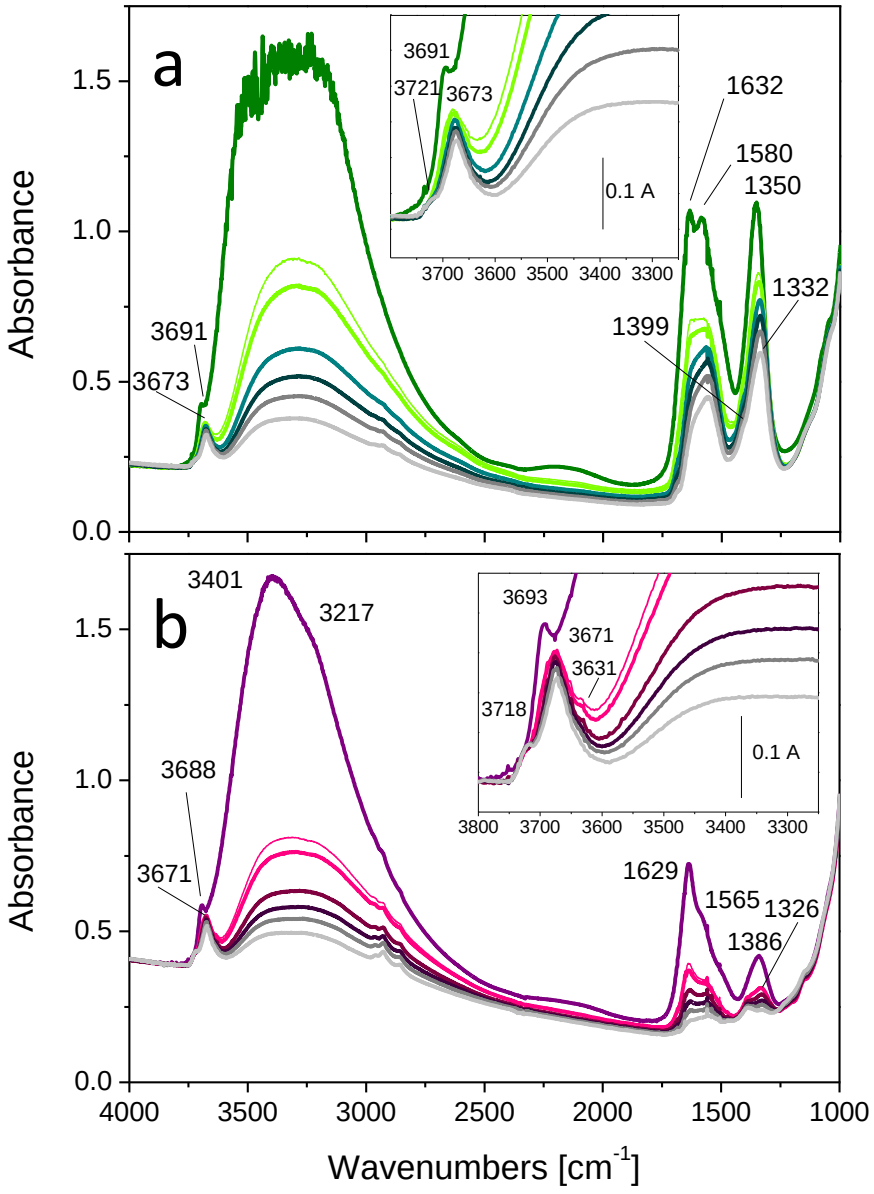

Figure 4.13FTIR absorbance spectra of CuO-$TiO_{2\text{-PREC}}$ (section a) and Au-$TiO_{2\text{-PREC}}$ (section b) in air (olive/purple curves), under 10 min (fine green/pink curves) and 30 min (bold green/pink curves) outgassing at r.t., at 80 °C (cyan/wine curves), at 100 °C (dark cyan/wine curves), at 120 °C (dark grey curves) and at 150 °C (light grey curves).

Looking more closely at FTIR spectra, a careful comparison among the spectra obtained from the two photocatalysts reveals some peculiarities. At wavenumbers lower than 2500 cm^{-1}, the addition of gold induced a modification in the spectra, ascribable to the erosion of an electronic absorption, occurring at all the temperatures here considered (violet curves vs. green curves in Figure 4.14). It is particularly noticeable that this electronic absorption is related to the presence of free electrons in titania conduction band: its erosion reflects the population of new energetic levels created when gold nanoparticles are introduced. In this case, the Schottky barrier between the metal nanoparticles and the oxide hinders electron flow to TiO_2, effectively behaving as an electron trap. This phenomenon is more pronounced in the case of Au-$TiO_{2\text{-PREC}}$ (violet curves) than in the case of CuO-$TiO_{2\text{-PREC}}$ (green curves) and these considerations are also in agreement with the DRUV-Vis results that point out a small difference in the titania band gap of the two samples (see Figure 4.11, insets).

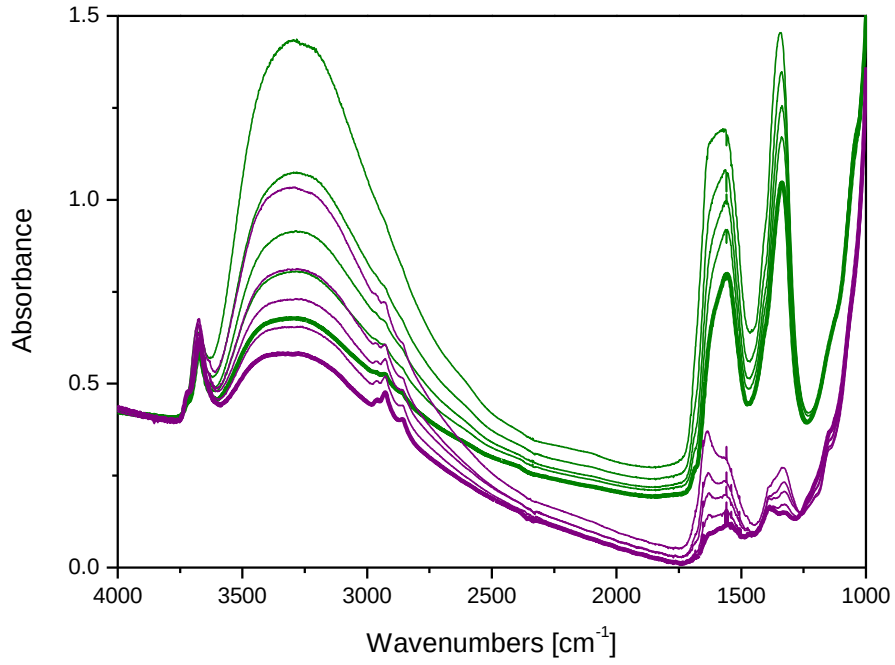

Figure 4.14Comparison among the normalised FTIR absorbance spectra of CuO-TiO_2 (green curves) and Au-TiO_2 (violet curves) reported in Figure 4.11. Spectra normalised to the pellet density.

Therefore, the above findings indicate that in the case of the gold-doped titania photocatalyst, a slightly less negative titania CB can be hypothesised, resulting in a less effective CO_2 reduction, that is the least thermodynamically favoured process [31]. Thus, despite gold insertion modified the electronic circulation on photocatalytic surface, it has a detrimental effect on the activity and selectivity displayed by titania in the CO_2 photoreduction if compared to CuO-promoted titania.

4.5.3 Interaction with CO_2 at room temperature: surface reactivity

On both samples CO_2adsorption at r.t. was performed to investigate the interaction between the most inert photoreduction reactant and the catalytic surfaces and the results are reported in *Figure 4.15*, section a. During preliminary treatment, the samples were outgassed from r.t. up to 150 °C for 10 minutes and then the temperature was decreased cooled to r.t. in outgassing conditions. This protocol assured the desorption of most weakly adsorbed water molecules on the surface, leaving only some residual of hydroxyl groups and adsorbed water molecules, as shown in section a. CuO-$TiO_{2\text{-PREC}}$'s and Au-$TiO_{2\text{-PREC}}$'s FTIR spectra before adsorption (green and violet curves respectively) provided several bands in the 2400-2250 cm^{-1} and 1800-1000 cm^{-1} regions (highlighted by dashed frames and enlarged in sections b and c, respectively) upon the inlet of 15 mbar CO_2 at room temperature (bold curves).

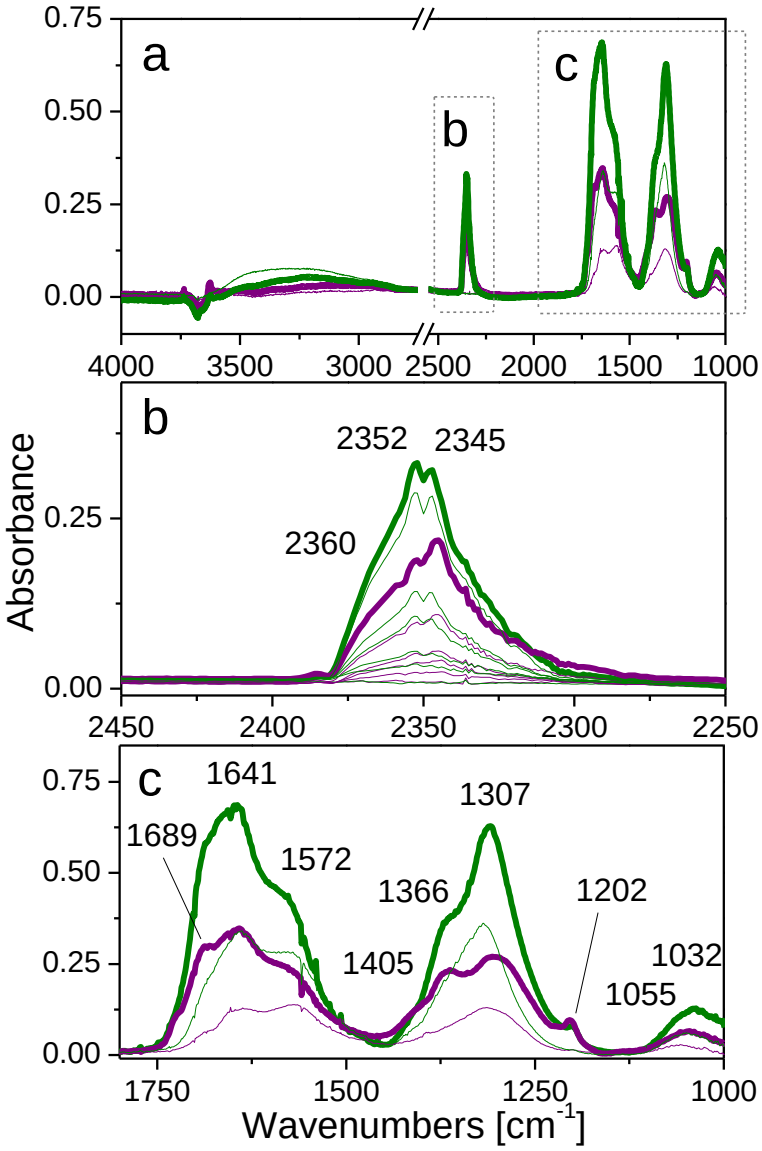

Figure 4.15 Section a: FTIR difference spectra collected on CuO-$TiO_{2\text{-}PREC}$ (green curves) and Au-$TiO_{2\text{-}PREC}$ (violet curves) after the inlet of 15 mbar CO_2 at r.t. (bold curves) and following outgassing at the same temperature for 30 minutes (fine curves). Section b: zoom on the 2450-2250 cm^{-1} spectral range in which the spectra collected at decreasing CO_2 pressure and under outgassing at r.t. (fine curves). Section c: zoom on the 1800-1000 cm^{-1} spectral range.

Two components at 2345 and 2352 cm^{-1} due to an asymmetric absorption, with a broad shoulder centred at 2360 cm^{-1}, was observed (section b, bold curves) and these signals are ascribable to carbon dioxide molecules linearly adsorbed on Ti^{4+} sites. These bands are gradually depleted when CO_2 pressure is decreased and even more after outgassing at r.t. (fine curves). Observed absorption intensity in the case of CuO-$TiO_{2\text{-}PREC}$ (green curves) is higher than compared to Au-$TiO_{2\text{-}PREC}$, indicating a bigger amount of linearly

adsorbed CO_2 on CuO-doped titania. Moreover, the shift of the Σ_u^+ band of adsorbed CO_2 molecules with respect to the gas phase (2343 cm^{-1}) is dependent on materials acidity and it increases with Lewis acid strength of the cationic surface sites [78]. Therefore, the presence of two defined peaks indicates that the CO_2 molecules are adsorbed on surface Ti^{4+} ions with different Lewis acid strength. In addition to these, other bands due to carbonate-like species by further reaction of linearly adsorbed CO_2 with O_2^- basic sites are observable in both spectra (section c, bold curves), but with different relative intensity. The production of carbonate-like species indicates the presence of surface Ti^{4+}-O^{2-} couples in which the basic O atom reacted with the central C atom in CO_2. More specifically, these considerations regard bands at 1641, 1307 and 1032 cm^{-1}, and at 1572, 1366 and about 1045 cm^{-1}, which are related to two different (chelate and/or bridged) bidentate adsorbed carbonate species [79]. From these experimental data, titania surface is characterised by several kinds of sites and the most relevant are those able to coordinate molecular CO_2 and those producing bidentate carbonate species. In Figure 4.16, a schematic representation of linearly and chelate CO_2 adsorbed species is reported.

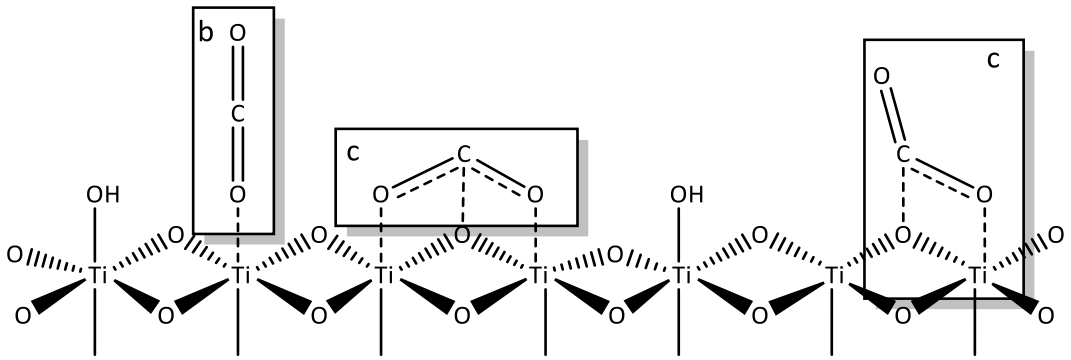

Figure 4.16 Schematic representation of possible bonds between CO_2 and TiO_2 surface: linear (b) and chelate species (c).

All these sites are more abundant on CuO-$TiO_{2\text{-PREC}}$ than on Au-$TiO_{2\text{-PREC}}$. Moreover, on the CuO-$TiO_{2\text{-PREC}}$ catalyst, the produced species are slightly more stable to the outgassing at r.t. than on Au-$TiO_{2\text{-PREC}}$, as revealed by the comparison between the initial

intensity (bold curves) and final intensity (fine curves) of the bands related to each sample.

Looking in details at bands located at 1689, 1405 and 1202 cm^{-1}, they almost have the same intensity for both samples, due to bicarbonate species produced by reaction of CO_2 with some surface basic –OH groups [78, 80]. The component at about 1730 cm^{-1}, more evident in the case of Au-$TiO_{2\text{-PREC}}$ and tentatively assigned to carboxylate species is also detected [81].

FTIR spectra of adsorbed CO_2 definitely showed that the surface of the CuO-$TiO_{2\text{-PREC}}$ photocatalyst is more efficient in adsorbing and reacting with CO_2, resulting in a stronger interaction between the CO_2 molecules and the photocatalytic surface [82], which represents the first step of carbon dioxide photoreduction. This physicochemical behaviour can righteously explain the differences in photocatalytic behaviour.

From all the experimental findings, it is possible to state that metal promotion affects not only electronic properties, but also surface ones and reactants adsorption (particularly for CO_2, the least adsorbable reactant) and, as a consequence, materials activity and selectivity in CO_2 photoreduction.

4.6 Conclusions

Throughout this chapter it was highlighted that titanium dioxide properties modification by metal promotion is a powerful tool to improve activity and to drive overall process selectivity. A careful consideration of possible material promotions allowed to select the most promising ones: copper oxide as a co-catalyst and gold nanoparticles as an electron-trap. However, there is much more than these physicochemical features to consider to fully understand photocatalytic behaviour.

Electronic properties modification enhanced charge separation. Unexpectedly, this feature in Au-$TiO_{2\text{-PREC}}$ seems to negatively affect activity, excessively suppressing electrons availability in titanium dioxide's conduction band. Moreover, a less negative conduction band was observed, which indicates a less efficient conduction band's reductant strength in CO_2 photoconversion. Conversely CuO promotion did not provide any negative effect.

However, electronic properties are not the only feature to consider in order to get a complete understanding of the overall process. As already mentioned in the previous chapter, CO_2 adsorption on catalytic surface represents a critical step that deserves great attention as developing greener and highly active catalysts. In fact, FTIR analyses confirmed that the interaction between the least reactive reagent and the photocatalytic surface is more efficient, indicating a higher activity in breaking C=O bond in CO_2.

Therefore, CuO-$TiO_{2\text{-PREC}}$ photocatalyst matches all these requirements, proving to be more active and selective than the Au-$TiO_{2\text{-PREC}}$ material. The reasons for the enhanced photoactivity can be related to the presence and the abundance of surface sites able to efficiently adsorb and react with the CO_2 reactant.

4.7 References

[1] V. Singh, I.J. Castellanos, Beltran, J. Casamada Ribot, P. Nagpal, NANO Letters 14 (2014) 597-603.

[2] K. Li, X. An, K.H. Park, M. Khraisheh, J. Tang, Catalysis Today 224 (2014) 3-12.

[3] A.L. Linsebigler, G. Lu, J.T. Yates, Chemistry Review 95 (1995) 753-758.

[4] A. V. Puga, Coordination Chemistry Reviews 315 (2016) 1-66.

[5] T. Sun, E. Liu, J. Fan, X. Hu, F.Wu, W. Hou, Chemical Engineering Journal 228 (2013) 896-906.

[6] A. Linsebigler, G. Lu, J. Yates, Chemical Reviews 95 (1995) 735-758.

[7] X. Chang, T. Wang, J. Gong, Energy Environmental Science 9 (2016) 2177-2196.

[8] G. Vereb, L. Manczinger, G. Bozso, A. Sienkiewicz, L. Forro, K. Mogyorosi, K. Hernadi, A. Dombi, Applied Catalysis B: Environmental 129 (2013) 566-574.

[9] R. Marshall, L. Wang, Catalysis Today 225 (2014) 111-135.

[10] M. Pelaez, N.T. Nolan, S.C Pillai, M.K. Seery, P. Falaras, A.G. Kontos, P.S.M. Dunlop, J.W.J. Hamilton, J.A. Byrne, K. O'Shea, M.H. Entezari, D.D Dionysiou, Applied Catalysis B: Environmental 125 (2012) 331–349.

[11] H. Xu, S. Ouyang, L. Liu, N. Umezawa, J. Ye, Journal of Materials Chemistry A 2 (2014) 12462-12661.

[12] M. Janus, M. Inagaki, B. Tryba, M. Toyoda, A.W. Morawski, Applied Catalysis B: Environmental 63 (2006) 272-276.

[13] I. Kang, Q. Zhang, S. Yin, T. Sato, F. Saito, Applied Catalysis B: Environmental 82 (2008) 81-87.

[14] S. Das, W. Wan Daud, Renewable and Sustainable Energy Reviews 39 (2014) 765-805.

[15] U. Diebold, Surface Science Reports 48 (2003) 53-229.

[16] V. Jeyalakshmi, R. Malahkshmi, K.R. Krishnamurthy, B. Viswanathan, Indian Journal of Chemistry 51 (2012) 1263-1283.

[17] O'Regan, M. Grätzel, Nature 353 (1991) 737-740.

[18] M. Grätzel, Nature 414 (2001) 338-344.

[19] D. Beydoun, R. Amal, G. Low, S. McEvoy, Journal of Nanoparticle Research 1 (4) (1999) 439–458.

[20] V. Trevisan, A. Olivo, F. Pinna, M. Signoretto, F. Vindigni, G. Cerrato, C.L. Bianchi, Applied Catalysis B: Environmental 160-161 (2014) 452-160.

[21] P. Wang, P.S. Yap, T.T. Lim, Applied Catalysis A: General 399 (2011) 252-261.

[22] R. Asahi, T. Morikawa, T. Ohwaki, K. Aoki, Y. Taga, Science 293 (2001) 269-271.

[23] M.V. Dozzi, E. Selli, Journal of Photochemistry and Photobiology C: Reviews 14 (2013) 13-28.

[24] X. Meng, S. Ouyang, T. Kako, P. Li, Q. Yu, T. Wang, J. Ye, Chemical Communications 50 (2014) 11517-11519.

[25] B. Ohtani, Inorganic Photochemistry 63 (2011) 395-430.

[26] S.C. Roy, O. K. Varghese, M. Paulose, C.A. Grimes, ACS Nano 4 (2010) 1259-1278.

[27] S. Bai, W. Yin, L. Wang, Z. Li, Y. Xiong, RCS Advances 6 (2016) 57446-57463.

[28] Y. Wang, B. Li, C. Zhang, L. Cui, S. Kang, X. Li, L. Zhou, Applied Catalysis B: Environmental 130-131 (2013) 277-284.

[29] S. Malato, P. Fernandez-Ibanez, M.I. Malodato, J. Blanco, W. Gerjakm, Catalysis Today 147 (2009) 1-59.

[30] Y. Ma, X. Wang, Y. Jia, X. Chen, H. Han, C. Li, Chemistry Reviews 114 (2014) 9987-70043.

[31] O. Ola, M. Maroto-Valer, Journal of Photochemistry and Photobiology C: Chemistry Reviews 24 (2015) 16-42.

[32] L. Liu, F. Gao, H, Zhao, Y. Li, Applied Catalysis B: Environmental 134-135 (2013) 349-358.

[33] S. Qin, F. Xin, Y. Liu, X. Yin, W. Ma, Journal of Colloid and Interface Science 356 (2011) 257-261.

[34] W.N.R.W. Isahak, Z. A.C. Ramli, M.W. Ismail, K. Ismail, R.M. Yosup, M.W.M. Hisham, M.A. Yarmo, Journal of CO_2 Utilization 2 (2013) 8-15.

[35] S.K. Ghosh, T. Pal, Chemical Reviews 107 (2007) 4797-4862.

[36] R. Kaul, B. Pal, Journal of Molecular Catalysis A: Chemistry 355 (2012) 39-43.

[37] B. Tahir, M. Tahir, N.A. Saidina Amin, Clean Technology and Environmental Policy 18 (2016) 2147-2160.

[38] C. Silva, R. Juarez, T. Marino, R. Molinari, H. Garcia, Journal of American Chemical Society 133 (2011) 595-602.

[39] A. Primo, A. Corma, H. Garcìa, Physical Chemistry Chemical Physics 13 (2011) 886-910.

[40] D. Crisan, N. Dragan, M. Raileanu, M. Crisan, A. Ianculescu, D. Luca, A. Nastuta, D. Mandare, Applied Surface Science 257 (2011) 4227-4231.

[41] C.A. Korologos, M.D. Nikolaki, C.N. Zerva, C.J. Philippopoulos, S.G. Poupoulos, Journal of Photochemistry and Photobiology A: Chemistry 244 (2012) 24-31.

[42] M. Daous, V. Iliev, L. Petrov, Journal of Molecular Catalysis A: Chemistry 392 (2014) 194-201.

[43] A. Fujishima, X. Zhang, D. Tryk, International Journal of Hydrogen Energy 32 (2007) 2664,2672.

[44] M. Ni, M. Leung, D. Leung, K. Sumathy, Renewable and Sustainable Energy Reviews 11 (2007) 401-425.

[45] A. Naldoni, F. Fabbri, M. Altomare, M. Marelli, R. Psaro, E. Selli, G. Salviati, V. Del Santo, Physical Chemistry Chemical Physics 17 (2015) 4864-4869.

[46] A. Corma, H. Garcia, Journal of Catalysis 308 (2013) 168-175.

[47] C.J. Orendorff, T.K. Sau, C.J. Murphy, Small 2 (2006) 636–639.

[48] L. Du, A. Furube, K. Yamamoto, K. Hara, R. Katoh, M. Tachiya, Journal of Physical Chemistry C 113 (2009) 6454–6462.

[49] E. Yasun, H. Kang, H. Erdal, S. Cansiz, I. Ocsoy, Y.F. Huang, W. Tan, Interface focus 3 (2013) 1-9.

[50] R. Zanella, S. Giorgio, C.R. Henry, C. Louis, Journal of Physical Chemistry B 106 (2002) 7634-7642.

[51] F. Menegazzo, M. Signoretto, F. Pinna, M. Manzoli, V. Aina, G. Cerrato, B. Flora, Journal of Catalysis 309 (2014) 241-247.

[52] M. Haruta, T. Kobayashi, H. Sano. N. Yamada, Chemistry Letters 16 (1987) 405-408.

[53] M. Haruta, The Chemical Recors 3 (2003) 75-78.

[54] S. Brunauer, P.H. Emmett, E. Teller, Journal of American Chemical Society 60 (1938) 309-319.

[55] E.P. Barrett, L.S. Joyner, P.P. Halenda, Journal of American Chemical Society 73 (1951), 373-380.

[56] D.A. Skoog, F.J. Holler, S.R. Crouch, Principles of Instrumental Analysis, 6th ed. Thomson Brooks/Cole 2007 Stanford CT USA.

[57] J.W. Niemantsverdriet, Spectroscopy in Catalysis, 3rd ed. Wiley 2007 New York USA.

[58] P. Kubelka, F. Munk, Zeitschrift für Physik 12 (1931) 593-601.

[59] V. Štengl, S. Bakardjieva, N. Murafa, Materials Chemistry and Physiscs 114 (2009) 217-226.

[60] J. Goldstein, D. Newbury, D. Joy, C. Lyman, P. Echlin, E. Fifshin, L. Sawyer, J. Michael, Scanning Electron Microscopy and X-ray Microanalysis, 3rd ed. Springer 2003 New York USA.

[61] I.H. Tseng, W.C. Chang, J.C.S. Wu, Applied Catalysis B: Environmental 37 (2002) 37-48.

[62] D. Liu. Y. Fernandez, O. Ola, S. Mackintosh, C.M.A. Parlett, A.F. Lee, J.C.S. Wu, Catalysis Communications 25 (2012) 78-82.

[63] A. Olivo, V. Trevisan, E. Ghedini, F. Pinna, C.L. Bianchi, A. Naldoni, G. Cruciani, M. Signoretto, Journal of CO_2 Utilization 12 (2015) 86-94.

[64] M. Murdoch, G.I.N. Waterhouse, M.A. Nadeem, J.B. Metson, M.A. Keane, R.F: Howe, J. Llorca, H. Idriss, Nature Chemistry 3 (2011) 489-492.

[65] V. Jovic, W.T. Chen, D. Sun-Waterhouse, M.G. Blackford, H. Idriss, G.I.N. Waterhouse, Journal of Catalysis 305 (2013) 307-317.

[66] M. Zhou, J. Zhang, B. Cheng, H. Yu, International Journal of Photoenergy 2012 (2012) 1-10.

[67] X. Yu, N. Wu, Y. Xie, Y. Tang, Journal of Materials Chemistry 10 (2000) 1629-1634.

[68] I. Tseng, J. Wu, H. Chou, Journal of Catalysis 221 (2004) 432-440.

[69] F. Menegazzo, M. Signoretto, D. Marchese, F. Pinna, M. Manzoli, Journal of Catalysis 326 (2015) 1-8.

[70] M. Manzoli, F. Menegazzo, M. Signoretto, G. Cruciani, F. Pinna, Journal of Catalysis 330 (2015) 465-473.

[71] S. Yashnik, Z. Ismagilov, V. Anufrienko, Catalysis Today 110 (2005) 310–322.

[72] J. J. Bravo-Suárez, B. Subramaniam, R. V. Chaudhari, Journal of Physical Chemistry C 116 (2012) 18207–18221.

[73] M. Anpo, H Yamashita, Y. Ichihashi, S. Ehara, Journal of Electroanalytical Chemistry 396 (1995) 21-26.

[74] J.T. Carneiro, C.C. Yang, J.A. Moma, J.A. Moulijin, G. Mul, Catalysis Letters 129 (2009) 12-19.

[75] G. Martra, Applied Catalysis A: General 200 (2000) 275-285.

[76] C. Morterra, Journal of Chemical Society Faraday Transactions 84 (1988) 1617.

[77] G. Cerrato, L. Marchese, C. Morterra, Applied Surface Science 70/71 (1993) 200.

[78] C. Morterra, G. Cerrato, C. Emanuel, Materials Chemistry and Physics 29 (1991) 447.

[79] G. Busca, V. Lorenzelli, Materials Chemistry 7 (1982) 89-126.

[80] J. Baltrusaitis, J. Schuttlefield, E. Zeitler, V.H. Grassian, Chemical Engineering Journal 170 (2011) 471-481.

[81] G. Ramis, G. Busca, V. Lorenzelli, Materials Chemistry and Physics 29 (1991) 425-435.

[82] S.K. Ghosh, T. Pal, Chemical Reviews 107 (2007) 4797-4862.

5 CO_2 photoreduction in liquid phase

Throughout this chapter the most promising materials developed in the previous chapters of this thesis will be employed to carbon dioxide photoreduction in a different medium, i.e. aqueous solution. On one side, as reported in chapter two, handling these conditions is more complicated than vapour phase. On the other, materials physicochemical properties and their interaction with reaction medium and light might lead to different results. Therefore, after a careful consideration of three-phases photocatalytic systems, developed materials will be tested and their photoactivity will be compared to results obtained in gas-solid systems, focusing both on activity and products distribution.

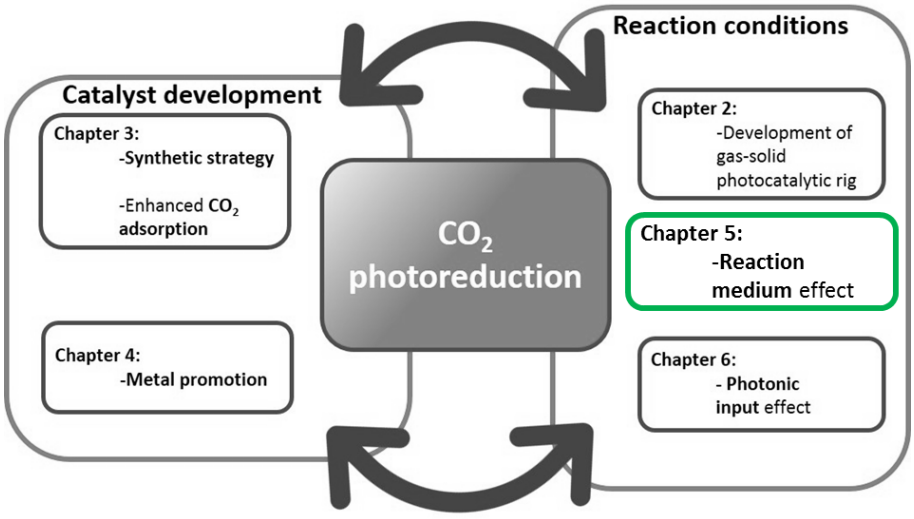

Figure 5.1 Sketch representing this chapter connection to the others in this thesis.

5.1 CO_2 photoreduction in liquid phase: prospects and challenges

Among CO_2 photoreduction scientific community, the main research topic is the development of efficient materials to enhance light harvesting through various synthetic strategies. However, in order to make carbon dioxide photoreduction an efficient technology to abate carbon dioxide and convert it into valuable fuels, an efficient photocatalyst, though necessary, is not the only feature to be considered [1].

Recently photoreactor design has gained more and more importance since it determines how efficiently reagents mix together, mass transfer from/to the catalyst and light harvesting. Due to the novelty of this technology and the flourishing of publications on this topic, different rig configurations are reported in the literature. In fact, if we consider reported photoactivity data for a worldwide benchmark photocatalyst, such as Evonik's P25, in the same conditions of temperature, pressure and light intensity, performances might change either in terms of activity and products distribution [2-4]. In fact, materials' critical physicochemical properties affect differently photoactivity according to reaction conditions, and among them, the most important is reaction medium.

For this reason, it was chosen to test best performing materials in a different photocatalytic rig, and attention was focused in three phases systems, which are the most commonly used for carbon dioxide photoreduction. In fact, from the first study by Inoue and co-workers [5], three phases systems, in which gaseous CO_2, liquid water and solid catalyst are used, have been extensively studied. Water in this configuration is used both as a reagent and a solvent, and these kinds of systems have been deeply investigated.

However, as mentioned in Chapter 2, two main drawbacks must be overcome, which are extremely low carbon dioxide solubility in water and inefficient light harvesting by medium scattering [6,7]. For the first one, most commonly used strategies, such as the substitution of water with organic solvents [8-9], alkali solutions as reaction media [10-13] improved photoactivity indeed despite great issues both in terms of sustainability and economic feasibility. Whereas, for light harvesting, a variety of photoreactors geometries, aimed at maximising catalyst photoactivation, were reported. In the liquid phase, most commonly-used systems are featured by a quartz window that allows light to enter [14-16]. More recently, some papers in the literature reported the use of an annular design that allows a homogeneous light transfer to the catalyst, mainly in the radial direction [17].

In addition to that, very recently, Prof. Ilenia Rossetti's group at University of Milan developed an efficient three phases photoreactor for CO_2 photoreduction tuning pressure, temperature, medium acidity/basicity [18]. Indeed, the increase of pressure enhance carbon dioxide dissolution in reaction medium to increase reduction products

and overall process productivity, but it was observed that reaction thermodynamics hindered photocatalytic performances for values higher than 10 bars [19]. Even tuning temperature represents a challenge, since its increase positively influences kinetics and mass transfer, but it reduces CO_2 solubility and favours electron-hole recombination.

In collaboration with Prof. Rossetti's group, photocatalytic test with already developed materials were performed and results were compared to those obtained in gas phase rig developed in previous chapters.

Differently from the majority of papers available in literature, which report tests conducted at high irradiance conditions [20-25], it was chosen to perform CO_2 photoreduction in low irradiance conditions. In fact, at the best of our knowledge, papers reporting CO_2 photoreduction tests using an irradiance below 100 $W \cdot m^{-2}$ have not been published yet, except papers from this research group and those from Prof. Rossetti's one [18,26]. The promising performances even at low irradiance conditions is an important step towards the use of the most sustainable and inexpensive light source, i.e., sunlight. In fact, world average sunlight irradiance on Earth's surface is roughly 1000 $W \cdot m^{-2}$, but only 5 % ca. is UV irradiation, which is the fraction necessary for this application [27].

From this overview, it is clear that, among reaction conditions, reaction medium tremendously affects catalysts effectiveness in light harvesting and reactant interaction with it, thus playing a crucial role. Moreover, in literature several photocatalysts and photoreactors have been reported [2,28] but reaction medium effect on materials performances is still unclear and this topic has not been experimentally investigated yet. Therefore, the goal of the work is to investigate the effect of reaction medium on CO_2 photoreduction. To do so, titanium dioxide-based materials were tested both in the liquid and vapour phases for a direct comparison under extremely low irradiance conditions to understand the reaction medium effect on process efficiency. Also metal promoted samples, which seemed to be the most promising catalysts in gas-solid photoreactors, will be tested as well. Attention will be focused on activity and selectivity to consider whether there are possible modifications in reaction mechanism or not.

5.2 Materials synthesis

For the comparison of vapour and liquid phase tests, alongside with commercial benchmark Evonik's P25 and Eurosupport's MIRKAT 211, lab- made $TiO_{2\text{-PREC}}$, $CuO\text{-}TiO_{2\text{-PREC}}$ and $Au\text{-}TiO_{2\text{-PREC}}$ were tested in both rigs. Synthetic procedure is reported in Section 4.2. Briefly, unpromoted $TiO_{2\text{-PREC}}$ was obtained by precipitation method using titanium oxysulphate as a precursor and sodium hydroxide as a precipitating agent. Titanium hydroxide was dried at 110 °C and calcined at 400 °C for four hours under air flow.

Cupper (II) oxide was introduced as titanium dioxide to obtain $CuO\text{-}TiO_{2\text{-PREC}}$ by incipient wetness impregnation using $Cu(NO_3)_2{\cdot}3H_2O$ as a precursor. Whereas, gold was introduced by deposition-precipitation method [29] with $HAuCl_4$ as a precursor and sodium hydroxide as a precipitating agent. Both samples were calcined at 400 °C under air flow. In both cases, metal content is 0.2 wt. %.

5.3 Characterisations

5.3.1 X-Ray diffraction

This technique was used to obtain several information on materials morphological structures and their differences in crystallographic properties. XRD analyses were performed at the Department of Earth Sciences at the University of Ferrara in collaboration with Prof. Giuseppe Cruciani. A Bruker D8 Advance powder diffractometer, whose emitted radiation is $CuK\alpha_{1,2}$, that works at 40 kV and 40 mA, was used. Instrumental parameters are reported here: stepsize: 0,02 °; antiscatter: 1/2 °, 0,1 mm, 1/2 °; 2θ range: 5-80 °; time/step: 3 s.

5.3.2 Nitrogen physisorption

Surface properties were investigated by N_2 adsorption–desorption at -196 °C analyses, which were carried out using a MICROMERITICS ASAP 2000. Preliminarily to all measurements, samples were outgassed at 200 °C for two hours in vacuum. The surface

area was calculated by BET equation [30] and the pore size distribution was obtained using the BJH method [31] applied to the isotherm desorption branch.

5.3.3 Diffuse reflectance UV–Visible-NearInfraRed (UV-Vis-NIR) Spectroscopy

By diffuse reflectance UV–Vis-NearInfraRed (UV-Vis-NIR) spectroscopy, an indication of materials interaction with light was obtained and, most importantly, semiconductors' band gap can be measured. In addition to that, it is possible to observe metal promoters' interaction with titanium dioxide and to esteem whether the modify TiO_2's band gap or not. Analyses were performed at Department of Chemistry of University of Turin and Doc. Maela Manzoli is acknowledged for her collaboration.

To collect spectra at run temperature, a Varian Cary 5000 spectrophotometer was used, which was equipped with an integrating sphere using $BaSO_4$ powder as an internal reference, working in the 50000-4000 cm^{-1} range, i.e. 200-2500 nm. UV–Vis-NIR spectra of the as prepared samples are reported in the Kubelka-Munk function (KM) [32]. The band gap energy (BG) of the catalysts were determined by the intercept of a linear fit to the absorption edge and they can be estimated using Equation 5.1.

$$\boldsymbol{BG\ (eV) = h\nu = \frac{h \cdot c}{\lambda} = \frac{1240}{\lambda(nm)}}$$

Equation 5.1

5.4 Photocatalytic tests

5.4.1 CO_2 photoreduction in vapour phase

Catalytic CO_2 reduction tests were carried out in the photocatalytic gas-solid rig developed in the Chapter 2. Reactor configuration and reaction conditions are briefly reported in Figure 5.2 and Table 5.1.

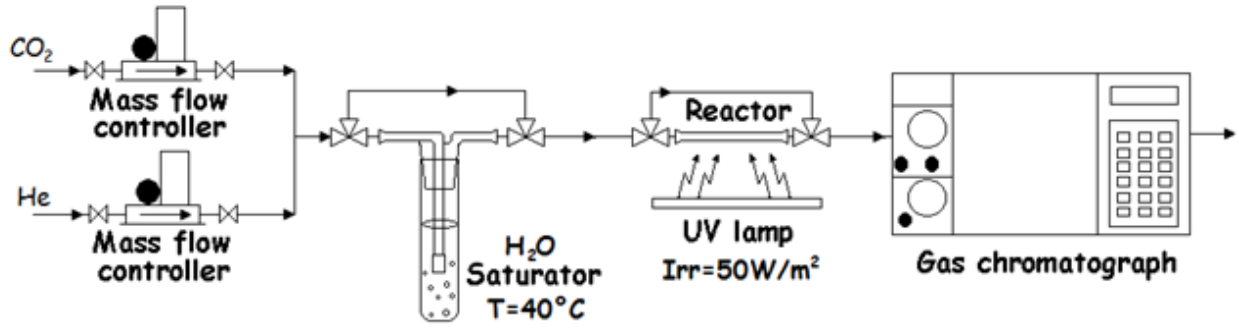

Figure 5.2 Gas phase photoreduction rig.

Reactants phase	**both gaseous**
water introduction method	bubbler at 40 °C
reactor	thin film
reaction temperature	40 °C
pressure	1 atm
irradiance	50 $W \cdot m^{-2}$

Table 5.1 Experimental conditions for CO_2 photoreduction tests in vapour phase rig.

For a more efficient comparison between the two rigs, turn over frequency (TOF) was used as a comparison metric, since it normalises photoactivity for reaction time. To assure repeatability and reproducibility, each photocatalytic test was performed at least three times to assure a significant error analysis. For all samples, error margin is about ± 10 % of obtained value both for TON and TOF results.

$$TOF = \frac{\mu mol_{PRODUCT}}{g_{cat} \cdot h}$$

Equation 5.2

5.4.2 CO_2 photoreduction tests in liquid phase

Liquid phase CO_2 photoreduction tests were performed at Department of Chemistry of University of Milan by Prof. Ilenia Rossetti's group. Tests were carried out in a 1.7 L

pressurised reactor, as sketched in Figure 5.3. This reactor is characterised by annular configuration: in fact, a medium pressure mercury lamp (3) is placed in the centre of the reactor irradiating homogeneously the whole reactor. Mass transfer limitations are also avoided by magnetic stirring (1) and thermal homogeneity was reached by external heating (4). This reactor is also equipped with gas inlet (1), both liquid and gaseous products collection lines (2 and 5). Temperature indicator (TI) and pressure indicator (PI) allowed to control both parameters.

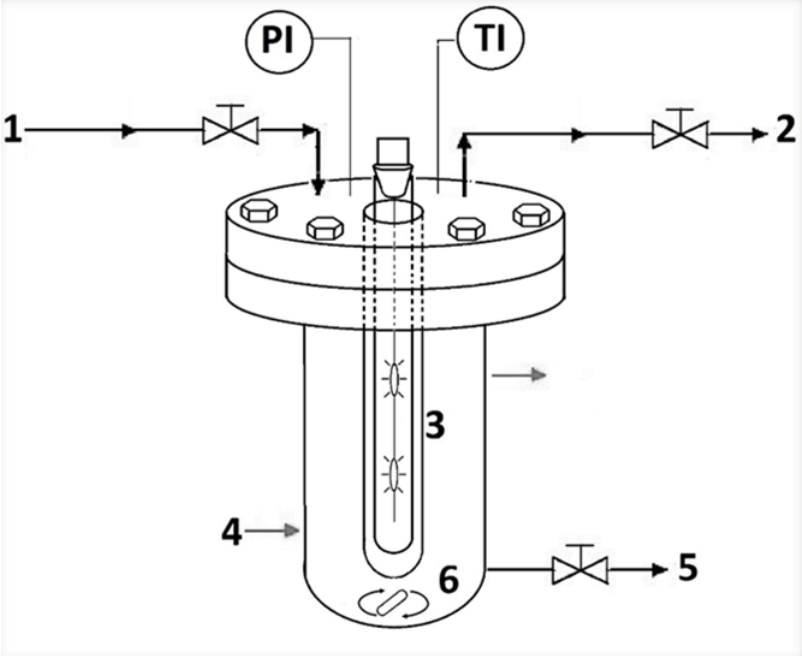

Figure 5.3 Schematisation of pressurised rig for CO_2 photoreduction in liquid phase.

Catalysts were suspended in water with a concentration of 0.3 $g \cdot L^{-1}$ at pH 7. Na_2SO_3 (Sigma Aldrich, 98%) was used as a hole scavenger, with a concentration of 1.7 $g \cdot L^{-1}$. Photocatalytic reduction of CO_2 with H_2O was performed at constant pressure of 7 bar, at a constant temperature of 80 °C for 24 h. This innovative pressurised batch photoreactor is irradiated by a medium-pressure Hg lamp as the source of radiation with an emission range between 254 nm and 364 nm. The lamp was cooled using an inner internal air flow of 2000 $L \cdot h^{-1}$. This air flow was selected to tune the average measured irradiance in the reactor to 50 $W \cdot m^{-2}$, for comparison with testing in the gas phase. The emitted power was periodically measured by means of a photoradiometer (Delta OHM HD2102.2).

Reactants phase	**both gaseous**
water introduction method	liquid reaction medium
CO_2/H_2O ratio	13.3
reactor	pressurised batch reactor
reaction temperature	70 °C
pressure	7 bar
irradiance	50 $W \cdot m^{-2}$

Table 5.2 Experimental conditions for CO_2 photoreduction tests in pressurised liquid phase rig.

Before starting the irradiation of the reaction mixture, the system was outgassed at constant CO_2 flow of 15 $mL \cdot min^{-1}$ at a pressure of 13 bar with the aim to eliminate air from the reactor head space. Then, in order to saturate water with CO_2, a static pressure of 7 bar of CO_2 was applied overnight. The gas phase products mixture was analysed by using a gas chromatography employing a thermal conductivity detector (TCD) to identify and quantify H_2, CH_4, CO, and polar/non-polar light gases.

The liquid mixture was analysed using an Agilent 1220 Infinity HPLC, equipped with an Alltech OA-10308, 300 mm_7.8 mm column with UV and refractive index detectors. Aqueous H_3PO_4 solution (0.1 wt. %) was used as the eluent. The consumption of Na_2SO_3 was measured by iodometric titration, which is based on the oxidation of sulphites (SO_3^{2-}) into sulphates (SO_4^{2-}) by iodine produced from a solution potassium iodate (KIO_3, Sigma Aldrich, 98 wt. % purity) and potassium iodide (KI, Sigma Aldrich, 99 wt. % purity) in acid aqueous medium and the subsequent titration of the iodine excess with sodium thiosulphate ($Na_2S_2O_3$, Sigma Aldrich, 98 wt. % purity) with starch solution as an indicator.

5.5 Results and discussion

5.5.1 Unpromoted titanium dioxide

Like in tests performed in the gas-solid rig, preliminary blank tests were performed. No trace of activity under dark conditions nor in the absence of catalyst or CO_2 was

observed, proving that carbon dioxide, catalyst, and light are necessary for the reaction to happen and that all residual carbonaceous species from sample manipulation are completely removed. Moreover, catalysts are photostable at high pressures and do not contain any trace of carbon from their manipulation, and collected data are not affected by carbonaceous species on the photocatalytic surface. Results are reported in Figure 5.4.

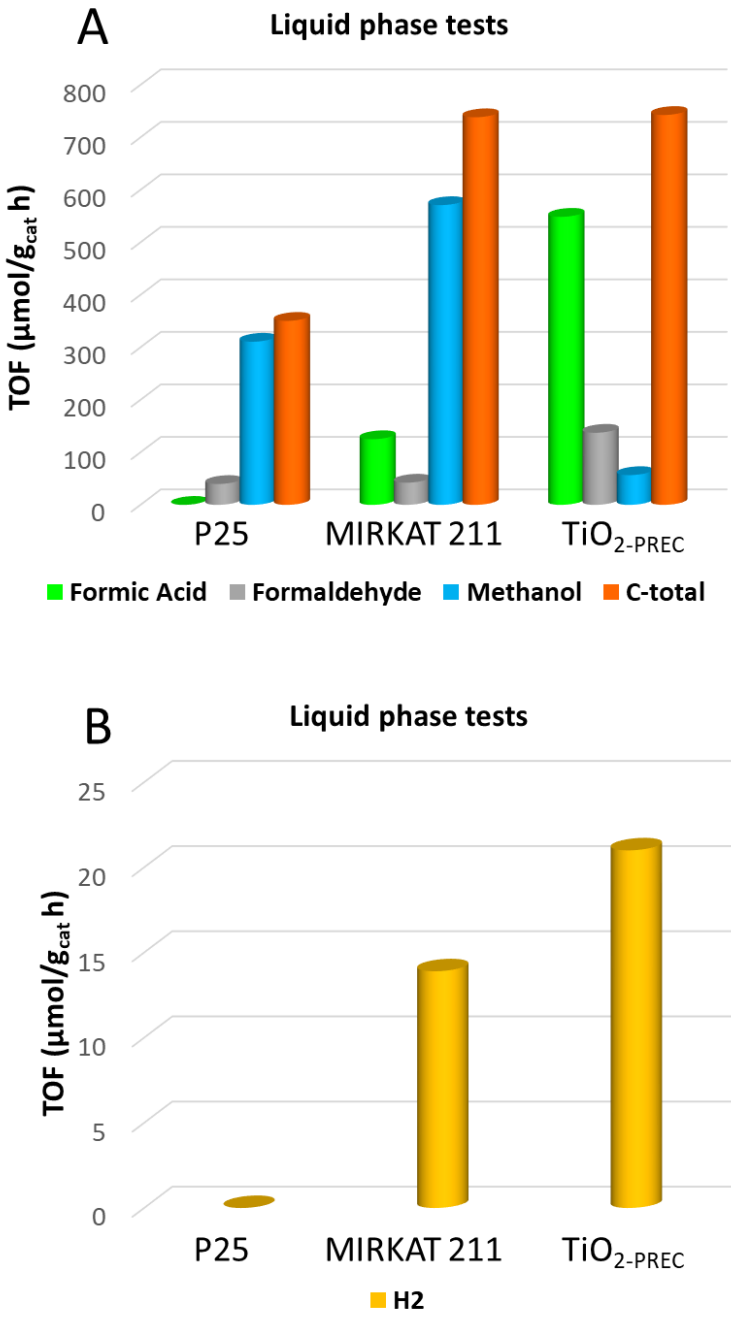

*Figure 5.4 P25, MIRKAT 211, and $TiO_{2\text{-PREC}}$ photocatalytic tests in liquid phase: (**A**) liquid phase C-containing compounds; and (**B**) hydrogen productivities.*

From reported data (Figure 5.4, sections A and B respectively), it is evident that liquid phase products are predominant to gas phase ones. In fact, the most abundant products are methanol, formaldehyde and formic acid, indicating that, in these conditions titanium dioxide is not efficient in a complete carbon dioxide photoreduction to methane, differently from vapour phase results (reported for reference in Figure 5.5). In that, case, all samples were able to reduce completely carbon dioxide into methane and hydrogen was the only observed co-product, providing a selectivity to methane higher than 90 %.

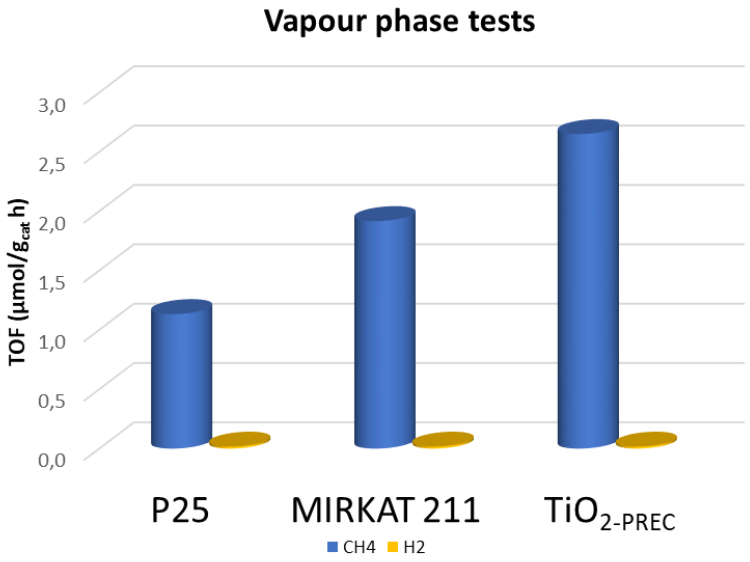

Figure 5.5 P25, MIRKAT 211, and $TiO_{2\text{-PREC}}$ photocatalytic tests in vapour phase: methane and hydrogen productivities.

Comparing these three different materials performances in liquid phase tests, similar C-total productivities of the liquid products were obtained for the TiO_2 and the MIRKAT 211 samples, which is roughly double than P25's results, similarly to what observed in CH_4 production observed in the gas phase testing rig.

Whereas, only detected product in gas phase is hydrogen and lab-made provided the highest yield and, between the two commercial benchmark materials, P25 gave the lowest hydrogen productivity.

To correlate photocatalytic performances with physicochemical properties, in first place surface area was considered, the lowest photoactivity provided by P25 is ascribed to the lowest surface area, 50 $m^2 \cdot g^{-1}$ compared to the other samples (217 $m^2 \cdot g^{-1}$ for MIRKAT

211 and 110 $m^2 \cdot g^{-1}$ for $TiO_{2\text{-PREC}}$) as observable from N_2 physisorption isotherms in Figure 5.6.

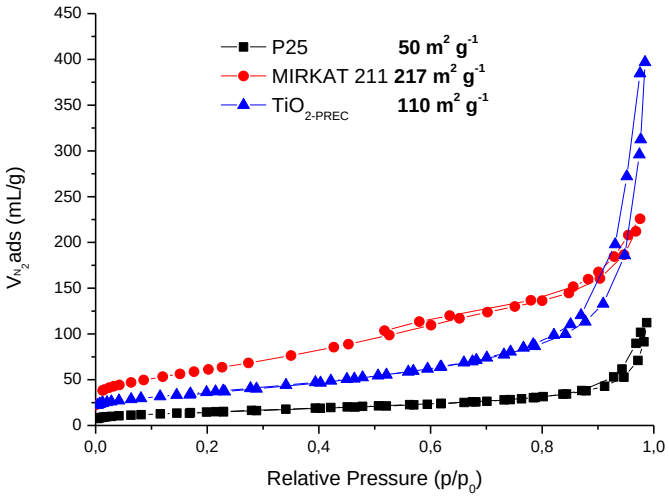

Figure 5.6 P25, MIRKAT 211, and $TiO_{2\text{-PREC}}$ N_2 physisorption isotherms.

The two high surface area samples provided the highest C-total productivity due to enhanced charge separation. However, differences in surface properties are not satisfactory to understand differences in both products distribution.

In fact, also in this case crystallinity plays a crucial role. In fact, as observed by XRD analyses (reported in Figure 5.7), P25 shows anatase-related peaks (JCPDS card No. 00-002-0387), but also diffraction peaks due to rutile (JCPDS card No. 76-1940).

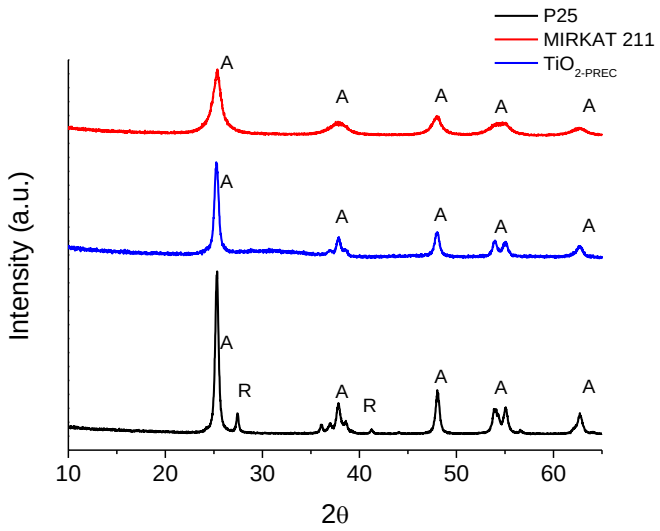

Figure 5.7 P25, MIRKAT 211, and $TiO_{2\text{-PREC}}$ XRD spectra.

This material is made up of a mixture of the two crystal structures in a ca. 75/25 anatase to rutile ratio [33], which creates an electronic circulation from the photoexcited rutile lattice trapping sites, the most easily excitable, yet unstable, to anatase ones which are the most resistant to electron-hole recombination [34].

Conversely, MIRKAT 211's and $TiO_{2\text{-PREC}}$'s only crystal phase is anatase, the most suitable for photocatalytic applications, since it is characterised by the highest electron-hole life among titanium dioxide polymorphs [35]. These differences are also observable in the diffuse reflectance spectroscopy (DRS) spectra reported in Figure 5.8 and they are often correlated to the enhanced lifetime of the photogenerated charges.

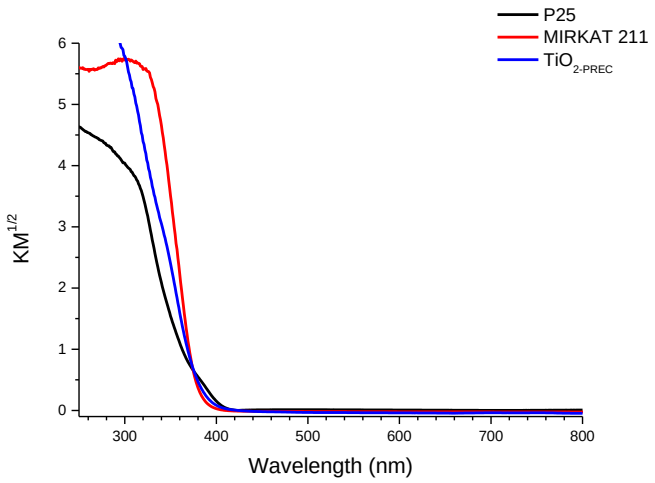

Figure 5.8 P25, MIRKAT 211, and $TiO_{2\text{-PREC}}$ DRS spectra.

MIRKAT 211 and the $TiO_{2\text{-PREC}}$ sample provide a typical sharp absorption below 388 nm, corresponding to a 3.21 eV band gap (typical of anatase), in accordance to the XRD patterns and data reported in the literature [36]. As already mentioned, crystalline features affect photoactivity: anatase conduction band is more reductive than rutile, thus, in principle, being thus more efficient in highly energy-demanding CO_2 reduction [37,38]. Among these two, sharper peaks in lab-made $TiO_{2\text{-PREC}}$'s pattern indicates a higher crystallinity than MIRKAT 211: in fact, while the former is 98 % crystalline, the other is only 40 % crystalline.

Differently from these two samples, in DRS analysis P25 provides a small absorption between 390 and 410 nm due to the small fraction of rutile and below 390 nm absorption due to anatase: thus, P25 overall band gap is 3.10 eV.

Therefore, the two samples made up of anatase provided the highest C-total productivity due to enhanced charge separation by the presence of anatase phase. Moreover, the most crystalline material, i.e. $TiO_{2\text{-PREC}}$, provided the highest hydrogen production.

However, performed physicochemical characterisations were not able to explain why the least crystalline sample provided the highest yield in the most reduced product, i.e. methanol, whereas the most crystalline gives formic acid, the least reduced one, as main product. For this reason, reaction mechanism was investigated to provide an explanation for differences in activity related both to reaction phase and materials properties.

5.5.2 Reaction medium effect on CO_2 photoreduction

Product distribution in liquid phase tests indicates that carbon dioxide photoreduction occurs by consecutive reaction steps at neutral pH [39] (Equation 5.3 to Equation 5.7), while a direct reduction to methane was not observed.

$$VB: 2H_2O + 4h^+ \longrightarrow 4H^+ + O_2$$

Equation 5.3

$$CB: H^+ + e^- \rightarrow \cdot H$$

Equation 5.4

$$CO_2 + 2 \cdot H \rightarrow HCOOH$$

Equation 5.5

$$HCOOH + 2 \cdot H \rightarrow HCHO + H_2O$$

Equation 5.6

$$HCHO + 2 \cdot H \rightarrow CH_3OH$$

Equation 5.7

In literature, it is reported that in similar photocatalytic systems [40-42] reaction's first step is the formation of peroxocarbonate species, that are reduced to formic acid, formaldehyde, and methanol afterwards. Due to the high H_2O/CO_2 ratio, $\cdot CO_2^-$ undergoes hydrogenation faster than deoxygenation, leading to all oxygenated products found in the liquid phase. However, as reported by Liu and Li [43], peroxide species in water are characterised by a high redox potential, that makes them extremely unstable and, thus, unreliably detectable. Therefore, in these conditions the unstable peroxocarbonates are the first intermediates, then directly converted into formate ions, formic acid, and further reduction products. Formaldehyde is, instead, the first forming product when basic aqueous solutions are adopted, and further reduction to methanol or oxidation to formic acid may occur.

Furthermore, hydrogen formation reaction is consecutive to the accumulation of organic compounds in the liquid phase and the depletion of Na_2SO_3, used as a hole scavenger [44]. Indeed, after sulphite consumption, the formed organic compounds start acting as hole scavenger themselves in a photoreforming reaction (Equation 5.8) [36].

$$CH_3OH + H_2O \rightleftharpoons CO_2 + 3H_2$$

Equation 5.8

This reaction is very likely to happen with methanol [45,46], explaining its low yield with highly active $TiO_{2\text{-PREC}}$) and maximum concentration for formic acid in liquid phase compared to commercial samples.

For the same reason among gas phase products, hydrogen by photoreforming was the only observed product; comparing different materials, P25 provided the lowest hydrogen production, whereas crystalline yet high surface area $TiO_{2\text{-PREC}}$ yielded the highest hydrogen production. Moreover, considering both gas and liquid products (in Figure 5.4 section B), this sample provided the highest H_2 productivity, and the lowest of methanol. This can be explained remembering that the most active materials lead to the oxidation of the organic products through photoreforming of the newly-reduced organic compounds (Equation 5.8). This indicates high selectivity to the full reoxidation to CO_2 of the organic compounds in the photoreforming step.

Considering the liquid phase activity results, no methane was detected for all three samples, which is the extreme opposite of what observed in gas phase tests (reported in Figure 5.5), where the only detected products were methane and hydrogen and the former was the most abundant product, indicating probably a different reaction pathway. Karamian and co-workers [43], reported that, in most cases, in gaseous systems CO is the first intermediate product of CO_2 photoreduction by water vapour. However, reaction conditions, and in particular temperature, irradiance, and reaction time modify reaction pathway and product distribution as a consequence. In detail, if CO_2 deoxygenation is faster than dehydrogenation, methane production is favoured with respect to oxygenated compounds [47]. This is the case of vapour phase reaction, characterised by CO_2 excess. This mechanism involves the formation of ·C radicals that recombine with ·H originated from water [48].

In both experimental conditions, despite surface area being important, crystallinity and suitable crystal phase (i.e., anatase) represent the most important physicochemical properties for an efficient TiO_2 photocatalyst. Performing under equal and extremely low irradiance allows the even greater appreciation of these differences in the effectiveness of the different materials in light harvesting and, thus, in carbon dioxide conversion.

From all these considerations, activity and selectivity is affected by the reaction medium. From all experimental evidence, it is possible to suppose that a reduction undergoes two different pathways, as shown in Figure 5.9. In gas phase, fast deoxygenation leads to ·C species that are reduced afterwards whereas, in the liquid phase, peroxo species undergo hydrogenation preferentially [49], yielding to possible intermediate products. The liquid phase product distribution of sample $TiO_{2\text{-PREC}}$ confirms the proposed mechanism (74% formic acid, 18% formaldehyde, 8% methanol).

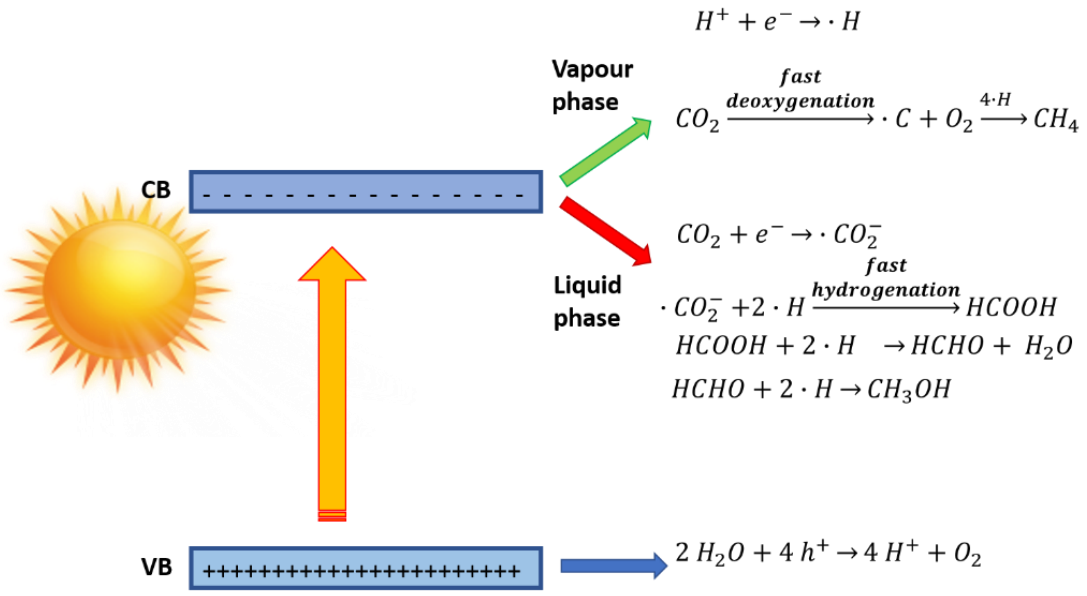

Figure 5.9 Different reaction mechanisms in vapour and liquid phases.

Therefore, different reaction pathways occur in these two different media, yielding to direct production of the most reduced product (methane) in the gas phase system whereas, in the liquid phase, intermediate reduction products are formed together with H_2. However, in liquid phase, tested materials were not sufficiently performing to obtain methane from carbon dioxide and further modification is required to do so.

5.5.3 Metal promoted titanium dioxide

Since unpromoted titanium dioxide materials were not able to catalyse CO_2 conversion into methane in liquid phase, the most desired product, this study progressed testing metal-modified samples, namely CuO-$TiO_{2\text{-PREC}}$ and Au-$TiO_{2\text{-PREC}}$, and comparing their performances with those obtained with unpromoted samples. Results are reported in Figure 5.10.

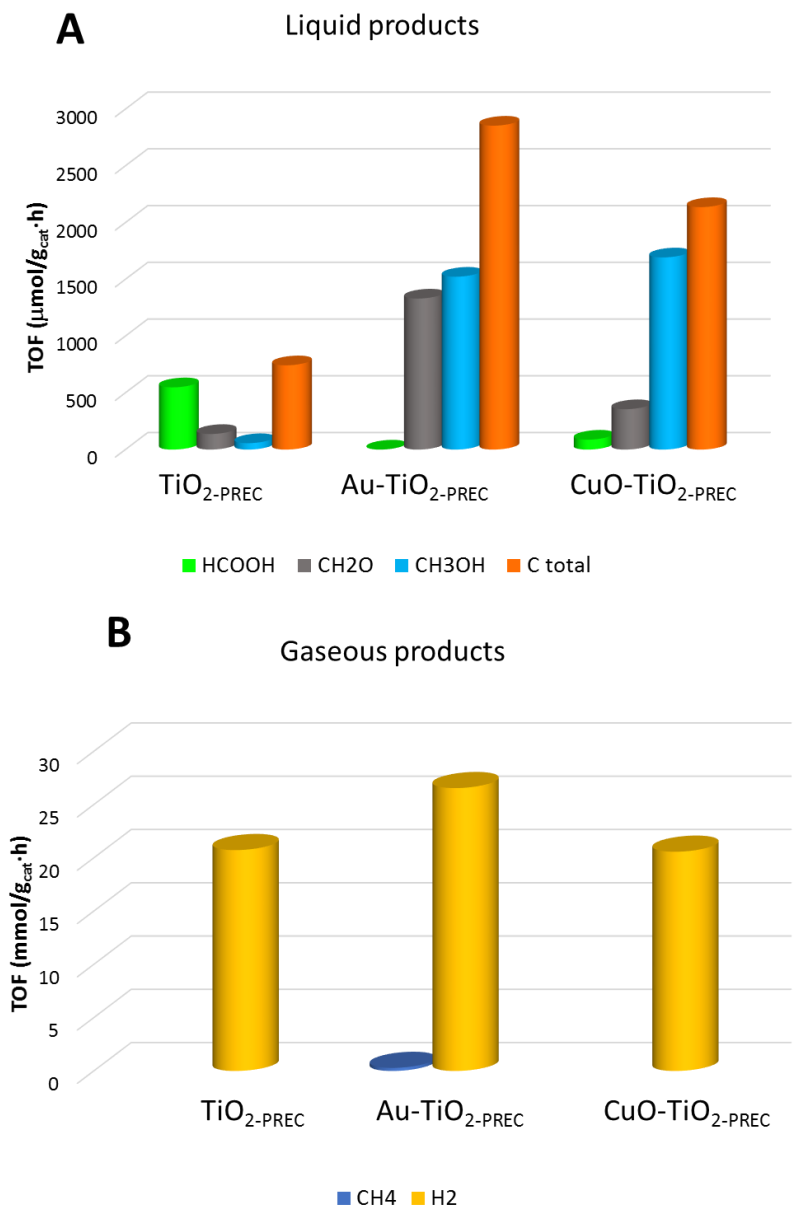

*Figure 5.10 P25, MIRKAT 211, and $TiO_{2\text{-}PREC}$ photocatalytic tests in liquid phase: (**A**) liquid phase C-containing compounds; and (**B**) gas phase productivities.*

Considering total carbon products formation in liquid phase, it is extremely clear that both metal promotions not only improved photoactivity significantly, but also modified products distribution. In fact, in three-phases systems, light harvesting is deeply affected by light scattering in reaction medium decreasing effectiveness of incident photons [2,50]: therefore, metal promotion, which proved to improve and stabilise charge carriers, is pivotal to improve materials activity in CO_2 photoreduction. Nonetheless, like

is gas-solid systems, the choice of metal dopant is important and modifies product distribution, even if experimental evidences are substantially different from those observed in gas phase systems.

In fact, whilst $TiO_{2\text{-PREC}}$ provided formic acid as main product, for both $CuO\text{-}TiO_{2\text{-PREC}}$ and $Au\text{-}TiO_{2\text{-PREC}}$ products distribution is shifted toward formaldehyde and methanol. Among the two metal promotions, gold nanoparticles proved to be more efficient in carbon dioxide photoreduction: in fact, in liquid phase $Au\text{-}TiO_{2\text{-PREC}}$ sample provides the highest yield in C-based products. If also gaseous products are considered, only with this latter sample methane was observed and provided the highest hydrogen production by photoreforming. Whereas $CuO\text{-}TiO_{2\text{-PREC}}$ tests did not show any trace of methane and hydrogen yield is similar to unpromoted sample. These results are completely different to those obtained in gas phase tests, where $CuO\text{-}TiO_{2\text{-PREC}}$ was the most performing and the most selective and $Au\text{-}TiO_{2\text{-PREC}}$ was the least performing in methane production yet providing the highest hydrogen production (for reference, results are reported again in Figure 5.11).

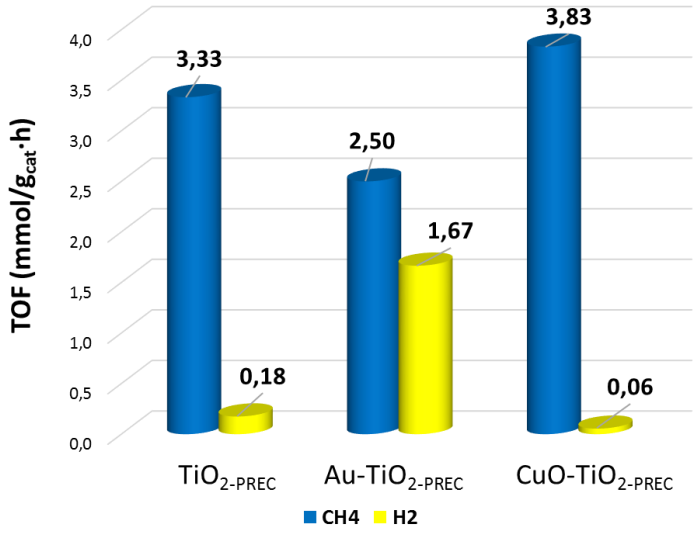

Figure 5.11 Photoactivity tests in the CO_2 photoreduction provided by $TiO_{2\text{-PREC}}$, $Au\text{-}TiO_{2\text{-PREC}}$ and $CuO\text{-}TiO_{2\text{-PREC}}$.

To understand these differences, it must be remembered that, as reported in section 5.5.2, reaction mechanism varies with reaction medium: therefore, metal promotion

effect might be different leading to differences in activity enhancement and product distribution.

In the case of CuO-$TiO_{2\text{-PREC}}$, as reported in the previous chapter and also in literature [51-53], copper oxide is efficient retarding photoinduced electron-hole pairs and/or trapping photoexcited electrons increasing electron-hole life. Moreover, as reported by Slamet *et al.*, reported that higher Cu(II) reducibility (compared to Cu(0) and Cu(I) is correlated to a greater effect as an electron trap, favouring a ·H intermediate production [54], which is a critical step in CO_2 photoreduction in liquid phase. The enhancement of the production of these radicals yields, as a consequence, to an improvement in hydrogenation. According to supposed reaction mechanism in liquid phase, this phenomenon favours methanol production, which is the leading product for CuO-$TiO_{2\text{-PREC}}$.

Different Au-$TiO_{2\text{-PREC}}$ photocatalytic behaviour must be ascribed to different physicochemical properties and thus different promotion mechanisms. Collado and co-workers reported that gold nanoparticles are effective at increasing the lifetime of charge separated states by means of interfacial electron transfer [55]. In fact, under irradiation gold promoted photocatalysts proved to be more active in the production of high electron demanding products. Moreover, as recently observed by Kar *et al.* [56], gold nanoparticles favour what the authors call "*carbene pathway*", which consists in a fast deoxygenation: this phenomenon is triggered by gold nanoparticles excitation, which provided available excited electrons for carbon dioxide reduction. In this way reaction mechanism becomes more similar to what generally occurs in gas phase systems, where pure deoxygenation was observed.

5.6 Conclusions

Throughout this chapter, it was reported that reaction conditions choice is not a trivial matter but it dramatically affects appreciation of differences in materials photocatalytic performances: evidences from experimental work and references from literature were brought up to make this point clear. CO_2 photoreduction was performed in two different rigs and two different media (gas and liquid phase), maintaining irradiance as common reaction conditions: in other terms, the same primary energy input was used in both

systems. Moreover, the choice of low-irradiance conditions allowed, on one side, to appreciate the differences in photocatalytic behaviour and, on the other, to minimise the energetic input.

From experiments run in both reaction media, it was established that the anatase crystal phase and crystallinity improve titanium dioxide photoactivity. The co-presence of both features in $TiO_{2\text{-PREC}}$ explained its best photoactivity, despite the expression "*best photoactivity*" has two different implications according to reaction media. In fact, in gas phase, this material provided the highest methane production, whereas in liquid phase it provided a wider distribution of oxygenated compounds. The choice of reaction medium determines reaction pathway with consequences on process selectivity: in vapour phase, deoxygenation drives selectivity towards methane whereas, in the liquid phase, carbon dioxide hydrogenation allows to obtain intermediate oxidation state products, i.e., formic acid, formaldehyde, and methanol.

Indeed, also in three-phases systems, metal promotion is pivotal to improve titanium dioxide's photoactivity: however, the choice of metal promoter is strictly dependent on reaction mechanism and might lead, products distribution wise, to opposite results. In fact, most performing material in liquid phase, Au-$TiO_{2\text{-PREC}}$ had not performed equally in gas phase and this difference was explained indicating that two different phenomena. In fact, while in gas phase poor carbon dioxide adsorption was crucial, in this case enhanced light harvesting and charge transfer considerably improved photocatalytic performances.

5.7 Reference

[1] R. de Richter, T. Ming, S. Caillol, Renewable and Sustainable Energy Reviews 19 (2013) 82-106.

[2] S. Das, W. Wan Daud, Renewable and Sustainable Energy Reviews 39 (2014) 765-805.

[3] M. Tahir, N. Amin, Renewable and Sustainable Energy Reviews 25 (2013) 560-579.

[4] K. Li, X. An, K. Park, M. Khraisheh, J. Tang, Catalysis Today 224 (2014) 3-12.

[5] T. Inoue, A. Fujishima, S. Konishi, K. Honda, Nature 277 (1979) 637–638.

[6] M. Anpo, H. Yamashita, K. Ikeue, Y. Fujii, S.G. Zhang, Y. Ichihashi, D.R. Park, Y. Suzuki, K. Koyano, T. Tatsumi, Catalysis Today 44 (1998) 327–331.

[7] P.L. Richardson, M.L.N. Perdigoto, W. Wang, R.J.G. Lopes, Applied Catalysis B: Environmental 132-133 (2013) 408–415.

[8] N. Ulagappan, H. Frei, Journal Physical Chemistry 104 (2000) 7834–7839.

[9] B. Liu, T. Torimoto, H. Matsumoto, H. Yoneyama, Journal of Photochemistry and Photobiology A: Chemistry 108 (1997) 187–192.

[10] C. Ampelli, G. Centi, R. Passalacqua, S. Perathoner, Energy and Environmental Science 3 (2010) 292–301.

[11] Z. Zhao, J. Fan, M. Xie, Z. Wang, Journal of Cleaner Production 17 (2009) 1025–1029.

[12] M. Reli, M. Šihor, K. Kočí, P. Praus, O. Kozák, L. Obalová, GeoScience Engineering 58 (2012) 34–42.

[13] W.S. Dodds, L.S. Stutzman, B.J. Sollami, Industrial and Engineering Chemistry and Chemical Engineering Data Series 1 (1956) 92–95.

[14] M. Anpo, H. Yamashita, Y. Ichihashi, S. Ehara, Journal of Electroanalytical Chemistry 396 (1995) 21–26.

[15] Q. Zhang, T. Gao, J.M. Andino, Y. Li, Applied Catalysis B: Environmental 123-124 (2012) 257–267.

[16] M. Tahir, N. Amin, Applied Catalysis B: Environmental 142-143 (2013) 512–522.

[17] L. Matějová, K. Kočí, M. Reli, L. Čapek, A. Hospodková, P. Peikertová, Z. Matěj, L. Obalová, A. Wach, P. Kuśtrowski, Applied Catalysis B: Environmental 152-153 (2014) 172–183.

[18] I. Rossetti, A. Villa, M. Compagnoni, L. Prati, G. Ramis, C. Pirola, C.L. Bianchi, W. Wang, D. Wang, Catalysis Science and Technology 5 (2015) 4481–4487.

[19] M. Compagnoni, G. Ramis, F.S. Reyria, M. Armandi, B. Bonelli, I. Rossetti, Rendiconti Lincei 28 (2017) S151-S158.

[20] O.K. Varghese, M. Paulose, T.J. LaTempa, C. Grimes, Nano Letters 9 (2009) 731-737.

[21] K. Ikeue, H. Yamashita, M. Anpo, Journal of Physical Chemistry B 105 (2001) 8350–8355.

[22] J.C.S. Wu, H.M. Lin, C.L. Lai, Applied Catalysis A: General 296 (2005) 194–200.

[23] B. Vijayan, N.M. Dimitrijevic, T. Rajh, K. Gray, Journal of Physical Chemistry C 114 (2010) 12994–13002.

[24] T.W. Woolerton, S. Sheard, E. Reisner, E. Pierce, S.W. Ragsdale, F.A. Armstrong, Journal of American Chemical Society 132 (2010) 2132–2133.

[25] M. Tahir, B. Tahir, N. Amin, Applied Catalysis B: Environmental 204 (2017) 548–560.

[26] A. Olivo, V. Trevisan, E. Ghedini, F. Pinna, C.L. Bianchi, A. Naldoni, G. Cruciani, M. Signoretto, Journal of CO_2 Utilization 12 (2015) 86-94.

[27] S. Malato, J. Blanco, A. Vidal, D. Alarcòn, M.I. Maldonado, J. Càceres, W. Gernjak, Solar Energy 75 (2003) 329-336.

[28] M. Tahir, N. Amin, Energy Conversion Management 76 (2013) 194-214.

[29] F. Pinna, A. Olivo, V. Trevisan, F. Menegazzo, M. Signoretto, M. Manzoli, F. Boccuzzi, Catalysis Today 203 (2013) 196-201.

[30] S. Brunauer, P.H. Emmett, E. Teller, Journal of American Chemical Society 60 (1938) 309-319.

[31] E.P. Barrett, L.S. Joyner, P.P. Halenda, Journal of American Chemical Society 73 (1951), 373-380.

[32] P. Kubelka, F. Munk, Zeitschrift für Physik 12 (1931) 593-601.

[33] Z. Ding, G.Q. Lu, P.F. Greenfield, Journal of Physical Chemistry B 104 (2000) 4815–4820.

[34] D.C. Hurum, A.G. Agrios, K.A. Gray, T. Rajh, M.C. Thurnauer, Journal of Physical Chemistry B 107 (2003) 4545–4549.

[35] S. Bagheri, Z.A. Mohd Hir, A. Termeh Yousefi, S. Bee, A. Hamid, Microporous and Mesoporous Materials 218 (2014) 206–222.

[36] G.Jr. Carini, F. Parrino, G. Palmisano, G. Scandura, I. Citro, G. Calogero, A. Bartolotta, G. Di Marco, Photochemistry and Photobiological Science 14 (2015) 1685–1693.

[37] A. Di Paola, M. Bellardita, L. Palmisano, Catalysts 3 (2013) 36–73.

[38] O. Ola, M. Maroto-Valer, Journal of Photochemistry and Photobiology C: Photochemistry Reviews 24 (2015) 16–42.

[39] F. Galli, M. Compagnoni, D. Vitali, C. Pirola, C.L. Bianchi, A. Villa, L. Prati, I. Rossetti, Applied Catalysis B: Environmental 200 (2017) 386–391.

[40] T. Baran, S. Wojtyła, A. Dibenedetto, M. Aresta, W. Macyk, Applied Catalysis B: Environmental 178 (2015) 170–176.

[41] K. Kočí, L. Obalová, L. Matějová, D. Plachá, Z. Lacný, J. Jirkovský, O. Šolková, Applied Catalysis B: Environmental 89 (2009) 494–502.

[42] E. Karamian, S. Sharafina, Journal of CO_2 Utilization 16 (2016) 194-103.

[43]L. Liu, Aerosol and Air Quality Research 2 (2014) 453–469.

[44] X. Chen, S. Shen, L. Guo, S.S. Mao, Chemical Reviews 110 (2010) 6503–6570.

[45] N.M. Dimitrijevic, I.A. Shkrob, D.J. Gosztola, T. Raji, Journal of Physical Chemistry C 116 (2012) 878-885.

[46] L. Clarizia, I. Di Somma, L. Onotri, R. Andreozzi, R. Marotta, Catalysis Today 281 (2017) 117-123.

[47] L. Liu, Aerosol and Air Quality Research 2 (2014) 453–469.

[48] S. Tan, L. Zou, E. Hu, Catalysis Today 115 (2006) 269–273.

[49] L. Matějová, M. Šihor, J. Lang, I. Troppová, N. Ambrožová, M. Reli, T. Brunátová, L. Čapek, A. Kotarba, K. Kočí, Journal of Sol-Gel Science and Technology 84 (2017) 158-168.

[50] M. Tahir, N. Amin, Energy Conversion and Management 76 (2013) 194-214.

[51] I.H. Tseng, W.C. Chang, J.C.S. Wu, Applied Catalysis B: Environmental 37 (2002) 37-48.

[52] N. Singhal, A. Ali, A. Vorontsov, C. Pendem, U. Kumar, Applied Catalysis A: General 523 (2016) 107-117.

[53] H.C. Yang, H.Y. Lin, Y.S. Chien, J.C.S. Wu, H.H. Wu, Catalysis Letters 131 (2009) 381-387.

[54] Slamet, H.W. Nasution, E. Purnama, S. Kosela, J. Gunlazuardi, Catalysis Communications 6 (2005) 313-319.

[55] L. Collado, A. Reynal, J.M. Coronado, D.P. Serrano, J.R. Durrant, V.A. de la Peña O'Shea, Applied Catalysis B: Environmental 178 (2015) 177-185.

[56] P. Kar, S. Farsinezhad, N. Mahsi, Y. Zhang, U. Obuekwe, H. Sharma, J. Shen, N: Semagina, K. Shankar, Nano Research 9 (2016) 3478-3493.

6 Investigation of irradiance effect on photocatalytic performances

From extensive literature review on carbon dioxide photoreduction with water, the optimisation of innovative and efficient materials has been extensively reported, whilst there is still a nonnegligible lack of information about the effect of reaction conditions. For this reason, in this final chapter, the effect of primary energy input, i.e. light irradiance, will be considered comparing performances provided by the same materials (developed in chapters 3 and 4) in two different gas-solid rigs, a configuration which proved to be the most promising in the previous chapter. Moreover, to deeply understand the results, in collaboration with Prof. Maroto-Valer's research group at Heriot Watt Unversity in Edinburgh (UK), a design of experiments (DoE) approach will be used aimed at assessing the effect of irradiance and reaction time on photocatalytic efficiency.

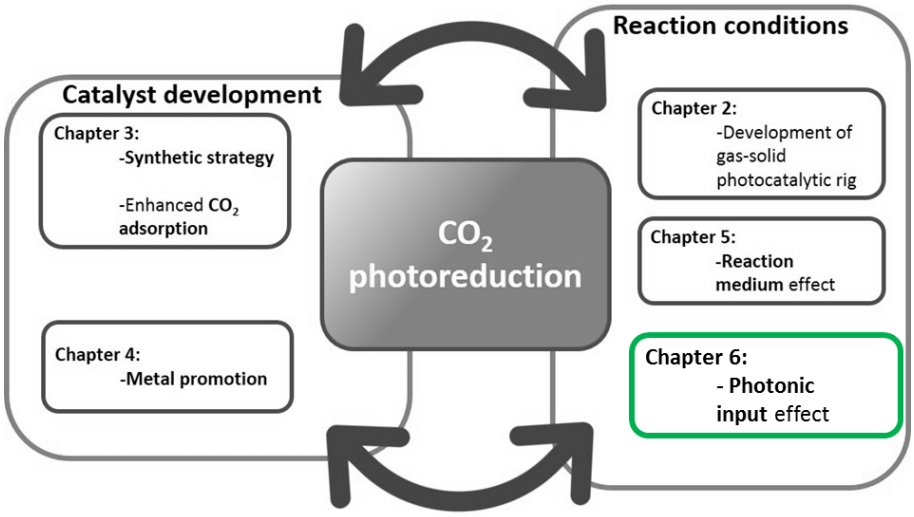

Figure 6.1 Sketch representing this chapter connection to the others in this thesis.

6.1 Photons input effect: a parameter to be considered

6.1.1 Shining a light on irradiance conditions

In any photocatalytic reaction, primary energy input, i.e. irradiation, drives the whole photocatalytic process and thus it covers pivotal importance. Up to now, irradiance effect on reactor design and catalytic conditions for CO_2 photoreduction has not been systematically investigated yet. In fact, several reviews in literature report a wide variety of photocatalytic systems configurations characterised by different light sources [1,2] but, due to substantial differences in experimental procedures, reaction regimes, data collection and processing, it is difficult to compare results from different groups. Despite recently gas phase systems have been used to overcome limitations by photons and mass transfer [3,4], and to perform photoreduction at room temperature and atmospheric pressure [5-7], there are still much differences in irradiation features.

Generally speaking, UV light is more common than visible light, even though the latter one should be more promising for a future application using sunlight directly. In fact, bare titanium dioxide excitation requires, in the case of anatase phase, a radiation whose wavelength is equal to or lower than 388 nm [8]. Indeed, materials modification is effective in reducing semiconductors band gap by means of the introduction of non-metal elements, such as boron, carbon, nitrogen, sulphur, bromine and iodine [9-13]. However, this band gap reduction, due to the introduction of intra band gap electronic states [14,15], reduces valence and conduction bands' oxidising and reducing power respectively [16]. In the case of carbon dioxide photoreduction, this feature negatively affects activity, limiting materials application under visible light [17,18].

Radiation wavelength aside, an important metric to compare energy input is irradiance, which is defined by IUPAC as "*Radiant power (P) of all wavelengths incident from all upward directions on a small element of surface containing the point under consideration divided by the area of the element (S)*" (Equation 6.1) [19].

$$Irr = \frac{dP}{dS}$$

Equation 6.1

On Earth's surface average irradiance provided by the sun is 1000 $W \cdot m^{-2}$, but only 5 % ca. is UV irradiation [20], but in CO_2 photoreduction tests, energy input is way higher that available solar energy. In fact, irradiance value is usually in the range of 1000–3000 $W \cdot m^{-2}$, which is extremely higher than UV light fraction in sunlight [21-24]. In very few papers results from tests performed at lower irradiances are reported: for instance, Woolerton *et al.* performed CO_2 photoreduction tests in the aqueous phase under 450 $W \cdot m^{-2}$ irradiance [25], whilst, more recently Tahir *et al.* reported tests conducted at 200 $W \cdot m^{-2}$ in the vapour phase conditions [26]. Nonetheless, at the moment, papers reporting CO_2 photoreduction tests using an irradiance below this value have not been published yet, except those from Signoretto's group and Rossetti's one. [27,28].

As observed in the previous chapter, same materials can perform differently according to reaction environment conditions. For this reason, the most performing developed materials will be tested using high irradiance conditions, in order to verify whether they perform similarly under difference irradiation input or not. To do so, materials were tested at the Centre for Innovation in Carbon Capture and Storage (CICCS) at Heriot Watt University (Endinburgh, UK), in conditions much closer to those generally reported in literature and results will be reported here and compared to those obtained in low irradiance conditions.

6.1.2 Design of Experiments for CO_2 photoreduction

In the field of CO_2 photoreduction, the investigation of photons input effect has not provided unanimously accepted results yet, while common catalysis parameters (e.g. catalyst amount, reaction time, reagents concentrations) have been already investigated [29-31]. Indeed, light harvesting considerably affects surface activation and, as a consequence, the number of activated sites to the photocatalytic reaction. In fact, photons input determines experimental regime: in particular, according to what is reported by Herrmann for photooxidations, at low irradiances, reaction rate is linearly proportional to photons flux, whereas, at high irradiance, it becomes proportional to

photons flux's square root, due to a consistent growth in electron-hole recombination rate [32].

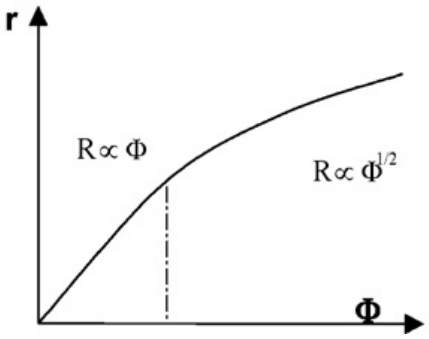

Figure 6.2Dependence of photooxidation reactions rate from radiant photons flux [32].

To investigate the effect of irradiance in consistently different CO_2 photoreduction reaction, design of Experiments (DoE) offers a systematic non-biased approach. This to evaluate the response of inputs (factors) on a given system. Design of experiments was refined throughout the 20th century and some milestones were achieved by the efforts of Box *et al.*, whose rationalisation work was published in 2005 [33]. More recently, Antony provided practical guidelines for scientists to use DoE approach [34].

In detail, this approach allows to study both independent and dependent variables contemporaneously, saving time and redundant experiments [35], providing, in the case of two variables, a model described by the general equation:

$$y = a_0 + a_1 x_1 + a_2 x_2 + a_{1,2} x_1 x_2 + \varepsilon$$

Equation 6.2

where y is experimental response, x_1 and x_2 are considered parameters a_0 a_1 and a_2 are parameters coefficients and ε is residual error. In this way, by the term $a_{1,2}x_1x_2$, it is possible to consider also the interaction between considered variables, which is not achievable by single-variable analysis. From an experimental point of view, once chosen considered variables and range of investigation, central and axial points are defined

(Figure 6.3). By these points, conditions for experimental test are obtained and randomly ordered to provide the experimental design.

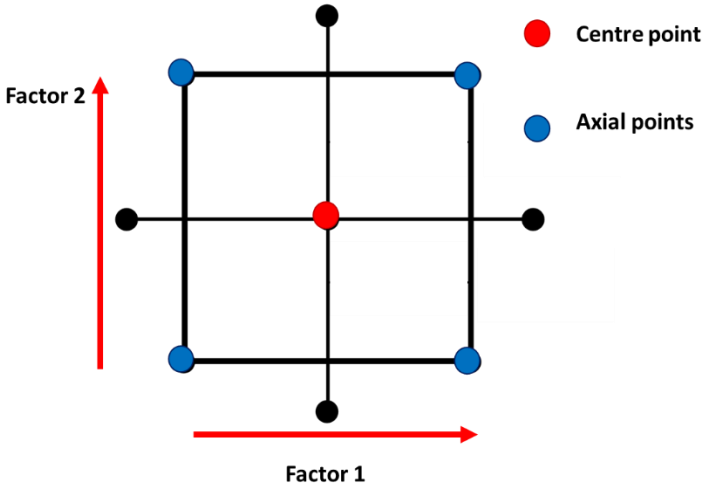

Figure 6.3 Schematisation of a two-variable full factorial design.

Finally, from collected data, by analysis of variance (ANOVA), it is possible to obtain indications on how investigated variables affect the whole process.

This statistical approach has been already applied to many catalytic processes, such as alkanes isomerisation [36], hydroconversion of Fischer-Tropsch waxes [37], biodiesel production [38], ethanol steam reforming [39] and pharmaceutical processes [40]. Despite great advantages, in photocatalysis the use of this approach is extremely rare. For example, for photocatalytic methane dry reforming, Delavari and co-workers evaluated some experimental factors and optimised them to improve CO_2 conversion [41]. Moreover, papers using DoE to investigate carbon dioxide photoreduction with water have not reported yet.

For these reasons, the effect of the most varying parameters, namely reaction time and irradiance, on conversion will be evaluated by a full factorial design of experiments approach. Chosen variables are correlated to photons input in the catalytic system, so it would be possible to evaluate the effect of energetic input, whose effect has not been thoroughly investigated yet for this reaction. This novel approach in photocatalysis was used to elaborate data obtained in two different setups: the rig developed in chapter 2

and the rig used at Heriot Watt University to compare results. Due to the great difference in irradiances values, it was investigated whether experimental conditions can affect both selectivity and conversion for CO_2 photoreduction.

6.2 Materials

For the comparison of vapour and liquid phase tests, alongside with commercial benchmark Eurosupport's MIRKAT 211 and lab- made $TiO_{2\text{-PREC}}$, $CuO\text{-}TiO_{2\text{-PREC}}$ and $Au\text{-}TiO_{2\text{-PREC}}$ were tested in both rigs. Synthetic procedure is reported in Section 4.2. Briefly, unpromoted $TiO_{2\text{-PREC}}$ was obtained by precipitation method using titanium oxysulphate as a precursor and sodium hydroxide as a precipitating agent. Titanium hydroxide suspension was aged at 60 °C for 20 hours, then washed, dried at 110 °C and calcined at 400 °C for four hours under air flow.

Cupper (II) oxide was introduced as titanium dioxide to obtain $CuO\text{-}TiO_{2\text{-PREC}}$ by incipient wetness impregnation using $Cu(NO_3)_2{\cdot}3H_2O$ as a precursor. Gold was introduced by deposition-precipitation method [42] with $HAuCl_4$ as a precursor and sodium hydroxide as a precipitating agent. Samples were calcined at 400 °C under air flow. In both cases, metal content is 0.2 wt. %.

6.3 Photocatalytic tests

6.3.1 Low irradiance reactor

Catalytic CO_2 reduction tests were carried out in the photocatalytic gas-solid rig developed in the chapter 2. Reactor configuration and reaction conditions are briefly reported in Figure 6.4 and Table 6.1.

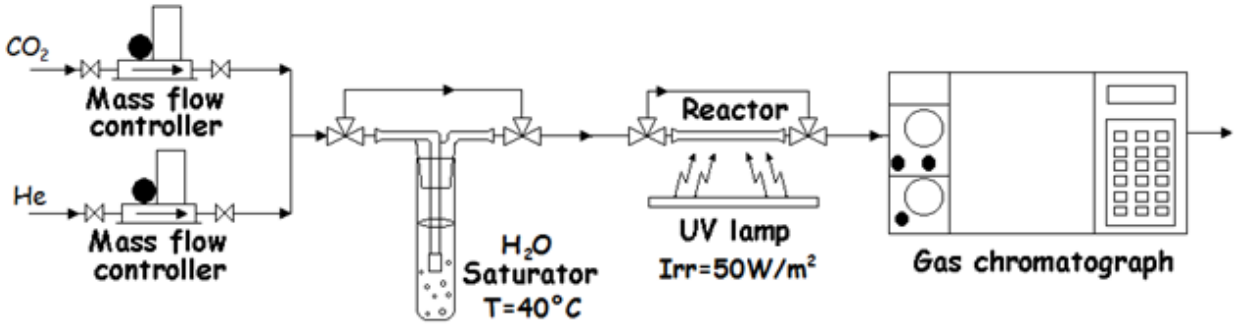

Figure 6.4 Gas phase low irradiance photoreduction rig.

To compare the two rigs, turn over number (TON) was used instead of turnover frequency (TOF) in order not to include time, one of chosen variables, in performance metric.

$$TON = \frac{\mu mol_{PRODUCT}}{g_{cat}}$$

Equation 6.3

Reactants phase	**both gaseous**
water introduction method	bubbler at 40 °C
reactor	thin film on reactor's surface
reaction temperature	room temperature
pressure	1 atm
irradiance	50 $W \cdot m^{-2}$
reaction time	6 hours

Table 6.1 Experimental conditions for CO_2 photoreduction tests in low irradiance rig.

For DoE analysis, reaction time ranged between four and eight hours, while irradiance between 40 and 60 $W \cdot m^{-2}$). First four tests represent the corner points of the model,

whereas the last three are the centre points. Test at centre point conditions was performed three times to improve significance of obtained results and estimate pure error. Experimental ranges for reaction time and irradiance were chosen to use as centre point conditions used for materials screening.

LOW IRRADIANCE DOE TESTS

Std. Order	Time (h)	Irradiance ($W \cdot m^{-2}$)	Photons (einstein)
1	4	60	0.011
2	8	60	0.021
3	8	40	0.014
4	4	40	0.007
5	6	50	0.013
6	6	50	0.013
7	6	50	0.013

Table 6.2 Experimental conditions varied during low irradiance design of experiments tests.

For the statistical analysis of data from DoE experiments, Minitab 17 Statistical Software (2010) developed by Minitab, Inc. (PA, USA) [43] was used to create Pareto Charts and to assess statistically significant effect of irradiance and reaction time on photocatalytic performances.

6.3.2 High irradiance reactor

High irradiance tests rig is represented in Figure 6.5.

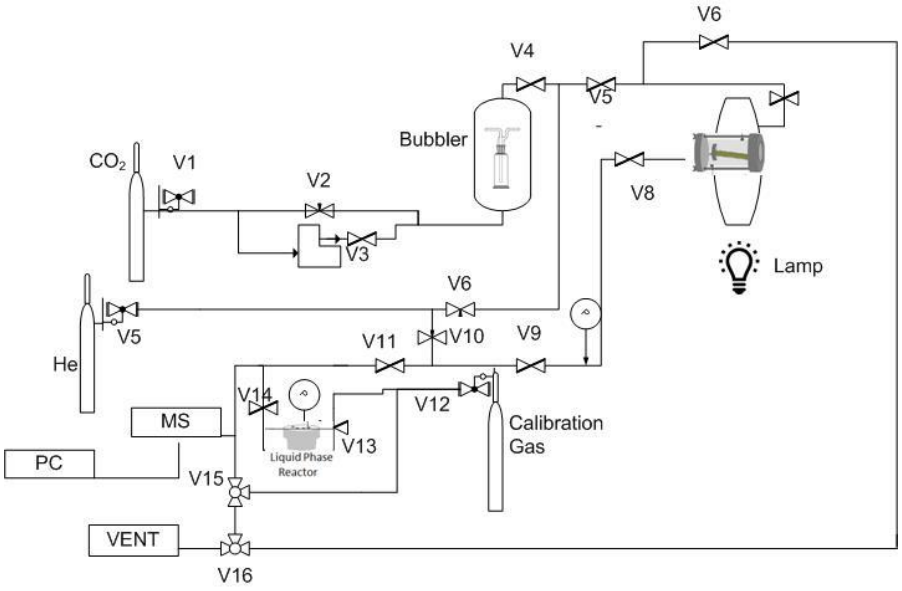

Figure 6.5 Setup for high irradiance tests at Centre Centre for Innovation in Carbon Capture and Storage (CICCS) at Heriot Watt University (Endinburgh, UK).

CO_2 photoreduction with H_2O was performed in a cylindrical Pyrex glass reactor (Figure 6.6), which consisted of two stainless steel lids (one of which was equipped with a quartz window) and a cylindrical Pyrex vessel (diameter 5.5 cm, length 11 cm, i.e. a volume of 216 mL). The vessel was sealed with O-rings in Viton and four stainless steel rods secured with wing nuts. A quartz plate, angled by a Teflon ring, was introduced to support for the catalyst. To introduce the catalyst (20 mg), it was suspended in 2-propanol (1 mL) for one hour in ultrasonic bath and then deposited on the central part of quartz plate until complete evaporation. Impregnated area was kept constant during tests and equal to 12 cm^2. Impregnated plate was left for another hour at 110 °C to eliminate completely any trace of dispersing agent.

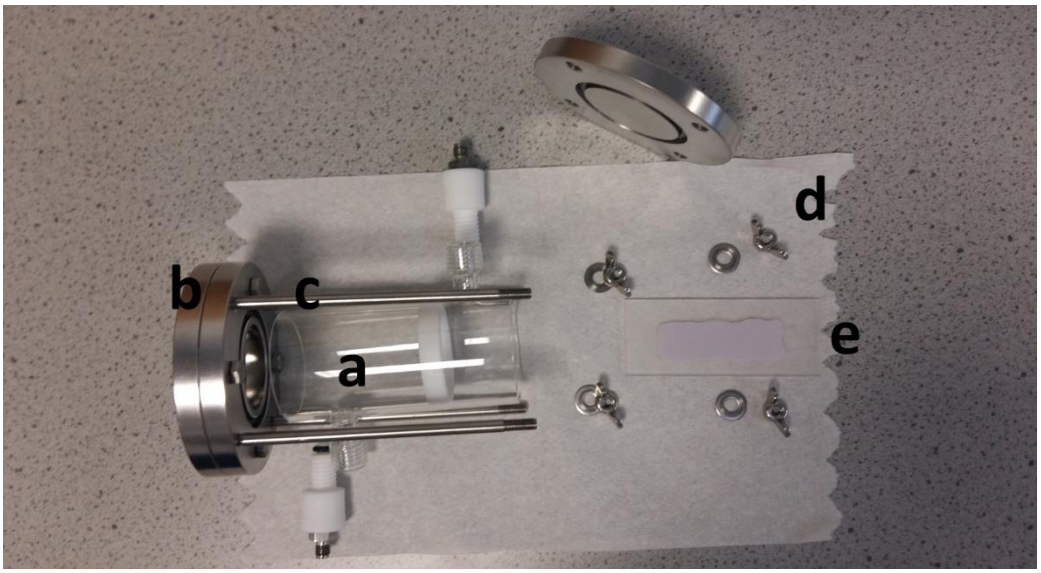

Figure 6.6 Photoreactor used for high irradiance tests (a is the Pyrex vessel, b one of the lids, c the rods, d the wing nuts and e the quartz plate for catalyst deposition).

Similar to low irradiance rig, a saturator was used to introduce water vapour in gas inlet and the temperature and pressure were monitored by means of a thermocouple and a pressure gauge respectively. Irradiation was provided by an OmniCure Series 2000 with a 365 nm filter by Lumen Dynamics and irradiance was controlled by UV/Vis OmniCure Radiometer after the optical fibres light guide.

Reagents and products were detected using a Hyden Analytical Quadrupole Mass Spectrometer (HPR-20 QIC) equipped with both a Faraday cup and secondary electron multiplier (SEM) detectors. For a quantitative analysis, before any photocatalytic tests, a calibrated gas mixture (purchased by BOC Industrial Gases) containing 100 ppm each of hydrogen H_2, oxygen O_2, methane CH_4, methanol CH_3OH, C_2H_6, ethylene C_2H_4, acetaldehyde CH_3CHO, ethanol CH_3CH_2OH while carbon dioxide is the remaining part.

Experimentally, before each test, catalyst was introduced into the reactor and let overnight under a small helium flow to keep surface clean and avoid the presence of atmospheric oxygen within the reactor. Carbon dioxide was introduced into the reactor by mass flow controller (8 $mL \cdot min^{-1}$ flow) and gas inlet was saturated with water vapour by means of the bubbler at room temperature. From flow rate and temperature, it was calculated CO_2/H_2O ratio, which was equal to 40. Once reactor was filled with reaction mixture at 1.5 bar, reactor was closed and lamp was switched on. Irradiance was

measured for each test and it was kept at 1000 W·m^{-2} for tests aimed at comparing different materials, whereas for DoE analysis irradiance was varied between 60 and 1200 W·m^{-2}. Reaction time was two hours for materials comparison and it was changed between 2 and it ranged from one to three hours for the DoE. Reaction conditions are summarised in Table 6.3.

Reactants phase	**both gaseous**
water introduction method	bubbler at 40 °C
reactor	thin film on a quartz plate
reaction temperature	room temperature
pressure	1 atm
irradiance	1000 W·m^{-2}
reaction time	1 - 3 h

Table 6.3 Experimental conditions for CO_2 photoreduction tests in high irradiance rig.

HIGH IRRADIANCE DOE TESTS

Std. Order	Time (h)	Irradiance (W·m^{-2})	Photons (einstein)
1	1	60	0.008
2	3	60	0.024
3	1	2400	0.316
4	3	2400	0.948
5	2	1200	0.316
6	2	1200	0.316
7	2	1200	0.316

Table 6.4 Experimental conditions varied during high irradiance design of experiments tests.

Also in this case, statistical interpretation of collected data was using Minitab 17 Statistical Software (2010).

6.4 Results and discussion

6.4.1 Materials photoactivity under high irradiance conditions

Before, testing materials in high irradiance conditions, blank tests were performed. In fact, in this particular case, high irradiance conditions might affect both photocatalyst and reagents stability, affecting collected results. Therefore, to overcome biased results, preliminary tests were performed without either reagents, light or catalyst. In none of these cases, products formation was observed, indicating that catalyst and reagents are stable in reaction conditions and that also in this case that this is not a photochemical reaction, but a photocatalytic one.

The most performing lab made materials developed in chapters 3 and 4 (namely $TiO_{2\text{-PREC}}$, $CuO\text{-}TiO_{2\text{-PREC}}$ and $Au\text{-}TiO_{2\text{-PREC}}$) were tested in high irradiance conditions and results were compared with those obtained using MIRAKT 211 as a reference material. Results from two hours long tests under 1000 $W \cdot m^{-2}$ UV irradiance are reported in Figure 6.7 and Table 6.5.

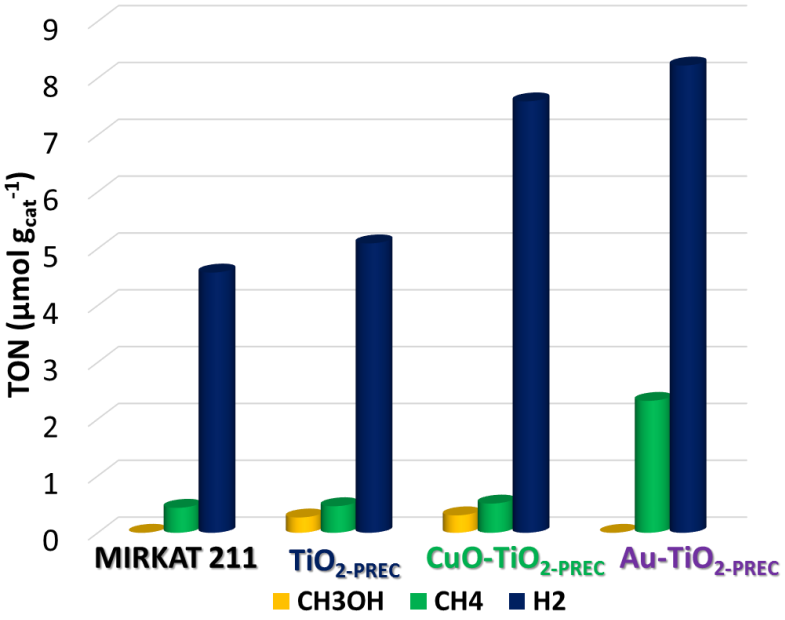

Figure 6.7 Photocatalytic results of commercial MIRKAT 211, lab-made $TiO_{2\text{-PREC}}$ and promoted CuO- $TiO_{2\text{-PREC}}$ and Au- $TiO_{2\text{-PREC}}$.

	METHANOL PRODUCTION ($\mu mol \cdot g_{cat}^{-1}$)	METHANE PRODUCTION ($\mu mol \cdot g_{cat}^{-1}$)	HYDROGEN PRODUCTION ($\mu mol \cdot g_{cat}^{-1}$)
MIRKAT 211	0.0	0.4	4.6
$TIO_{2\text{-PREC}}$	0.3	0.5	5.1
$CuO\text{-}TIO_{2\text{-PREC}}$	0.3	0.5	7.6
$Au\text{-}TIO_{2\text{-PREC}}$	0.0	2.3	8.2

Table 6.5 Methanol, methane and hydrogen productivity of investigated samples in high irradiance conditions.

From these results, with all investigated samples hydrogen is the most abundant product, whereas carbon-based products represent only a small fraction of reaction mixture: in fact, selectivity to C-based products ranges between 6 % and 22 %. Products distribution data are completely opposite to those obtained in low irradiance conditions, where the most abundant product was methane and hydrogen was the only detected side product (for reference, see Figure 6.8).

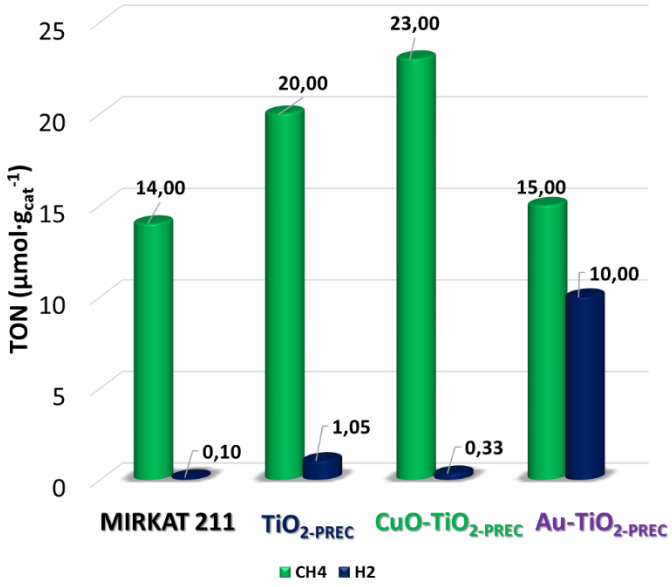

Figure 6.8 Photocatalytic tests in the low irradiance conditions: methane and hydrogen productivities.

Hydrogen might be due to two different processes: water splitting or photoreforming of reduced products. All literature papers reporting tests in similar conditions, state that hydrogen derives by water reduction by water splitting, whereas photoreforming is improbable due to short reaction time and low concentration of reduced products [18,44-46]. For this reason, it is very likely that water splitting happened the same in this high irradiance rig.

Reactions involved in semiconductors' light harvesting indicate that a high photons input, from a kinetic point of view, enhances the formation of photocatalytically active sites [47] (Equation 6.4).

$$TiO_2 + h\nu \rightleftharpoons h^+_{VB} + e^-_{CB}$$

Equation 6.4

However, also the reverse reaction can happen and, according to Liu and Li [50], the recombination rate of e^-–h^+ pairs is nearly two or three orders of magnitude faster than the rate of charge separation/transport and chemical reaction itself. Therefore, at high irradiance conditions, where surface is saturated with photons, it was observed that the rate of charge carrier recombination becomes higher than both light adsorption and surface reaction rates [48].

For these reasons, fast recombination rates under high irradiance explain why product distribution is shifted toward hydrogen. In fact, water reduction to hydrogen requires only a two-electrons transfer, whereas carbon dioxide reduction to methanol or methane requires six or eight electrons respectively [49]. For this reason, from a kinetic point of view, hydrogen production is preferred to carbon dioxide photoreduction.

Considering carbon based products, in both low and high irradiance conditions, only most reduced products (i.e. methanol and methane) were detected whereas formic acid and formaldehyde were not detected. This evidence is in accordance with what was observed and proposed in the previous chapter about reaction mechanism in gas phase. In fact, also in this case deoxygenation seems to occur faster than hydrogenation [50, 51], but, differently from low irradiance conditions, not fast enough to prevent the

formation of methanol, which some author report as main product in similar conditions [52,53].

Comparing different catalysts under high irradiance (Figure 6.7), performances obtained using unpromoted titanium dioxide materials, namely commercial MIRKAT 211 and lab-made $TiO_{2\text{-}PREC}$, are very similar both in activity and selectivity. In the case of these two unpromoted materials, both made up of anatase, as shown in Figure 3.12, recombination rate depends only on crystal phase capacity to stabilise excited electrons and holes, leading to similar photocatalytic performances, regardless other physicochemical properties.

Since recombination reaction regulates activity and hinders further photoactivity, electron-hole stabilisers are required to reach this goal. In fact, metal promotion effect is still observable both for copper oxide and gold nanoparticles, despite the introduction of these promoters provides different effects. In the case of CuO, an increase of hydrogen production was observed, whereas gold nanoparticles maximised both methane and hydrogen production. It must be remembered that, in terms of methane production, the same promoters in low irradiance conditions had provided the opposite result, i.e. CuO promoted sample had given the highest methane production.

In the case of copper, Wu and Huang reported that, in similar conditions, hydrogen reduced atoms migrate from titanium dioxide to copper species, and the Cu-H sites enhance hydrogenation reaction to methanol rather than deoxygenation reaction to methane [54]. According to their study, in presence of copper species, an increase in dioxymethylene transient species was observed by *in situ* DRIFT. These species, according to the authors, are the intermediate for methanol production.

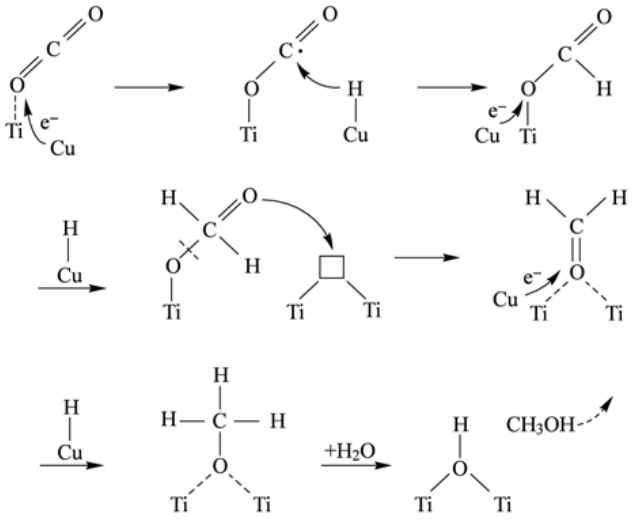

Figure 6.9 Proposed mechanism for CO_2 photoreduction on CuO promoted TiO_2 [54]

This indicates that copper species are not only promoter for excited electrons stability, but also, they can be truly considered as photocatalytic sites different from TiO_2, as also indicated by Slamet and co-workers [55]. In fact, CuO has a narrow band gap of 1.2 eV, so used 365 nm irradiation is sufficiently energetic to excite co-catalyst as well [56].

On the other side, different considerations on material physicochemical properties must be made to explain Au-$TiO_{2\text{-PREC}}$ photocatalytic behaviour. In fact, as pointed out by tests with unpromoted samples, the main effect to control under high irradiance condition is recombination. Under UV irradiation, gold is nanoparticles do not inject electrons in titanium dioxide conduction band by plasmonic resonance, but diminish the recombination rate of photoinduced e^--h^+ pairs effectively, improving their stability [57-59]. This enhancement of active sites improves the activity in multielectron transfer reactions and, drives reaction to the most reduced product, i.e. methane, which requires an eight electrons transfer. Moreover, it is reported that in similar reaction conditions, gold nanoparticles drive reaction pathway to deoxygenation, improving non-oxygenated product, i.e. methane [57].

For this reason, gold nanoparticles promotions proved to be the most effective in methane formation from carbon dioxide photoreduction under high irradiance and therefore this sample was employed to investigate the effect of photons input by design of experiments in the following chapter.

6.4.2 Design of Experiments Results

To investigate the effect of photons input by DoE, the effect of two experimental parameters were considered, namely irradiance and reaction time, since the number of incident photons is dependent on these two variables, as described in Equation 6.5.

$$Photons\ (Einstein) = \frac{Irr \cdot illuminated\ area \cdot time \cdot \lambda}{N_A \cdot h \cdot c}$$

Equation 6.5

In this case, full factorial design was chosen as only two factors were tested, meaning only 2^k experiments were needed, where k is the number of factors, thus four experiments. Three midpoints tests were also included in the full factorial design to evaluate experimental error and reproducibility. Random order of performed tests is reported in Table 6.2 and Table 6.4. As a response, methane turnover number (TON), since both this metric is not dependent on time, which is one of the investigated parameters.

$$TON\ (CH_4) = \frac{CH_4(\mu mol)}{cat\ (g)}$$

Equation 6.6

In first place, design of experiments tests were performed in low irradiance conditions, aimed at investigating how chosen photocatalyst, Au-$TiO_{2\text{-PREC}}$, in a relatively small range of different irradiances. Despite DoE could be performed using any photocatalyst, the choice of this material was made since it provided promising results at low irradiance and provided the best results under high irradiance conditions.

Std. Order	*Time (h)*	*Irradiance ($W \cdot m^{-2}$)*	*Methane ($\mu mol \cdot g_{cat}^{-1}$)*
1	4	60	20.8
2	8	60	28.5
3	8	40	20.9
4	4	40	12.7
5	6	50	19.5
6	6	50	17.3
7	6	50	21.0

Table 6.6 Experimental points and responses used for factorial design collected in low irradiance conditions.

Analysis of variance (ANOVA) was performed to separate the variability of collected results into assignable causes and assess parameters significance. For these calculations, it was assumed that significance level α, a parameter for the sensitivity of measurements, was equal to 0.05 to cut-off statistically unreliable data [60]. Results are reported in Pareto charts (in Figure 6.10), which show standardised effect for each parameter.

In each graph, there is a red line that indicates the margin of error (ME), that is defined as:

$$ME = t \cdot PSE$$

Equation 6.7

where t is the (1-α/2) quantile of a t-distribution and PSE is Lenth's Pseudo Standard Error [61]. In simple words, if standardised effect is higher than ME, parameters effect on the output is statically significant for the process; otherwise, investigated parameter is not significant. In the case of tests performed in low irradiance conditions, both investigated parameters' standardised effect bars (Figure 6.10) exceed margin of error. This result indicates that both time and irradiance have a statistically significant effect on methane productivity and that they not dependent one to the other.

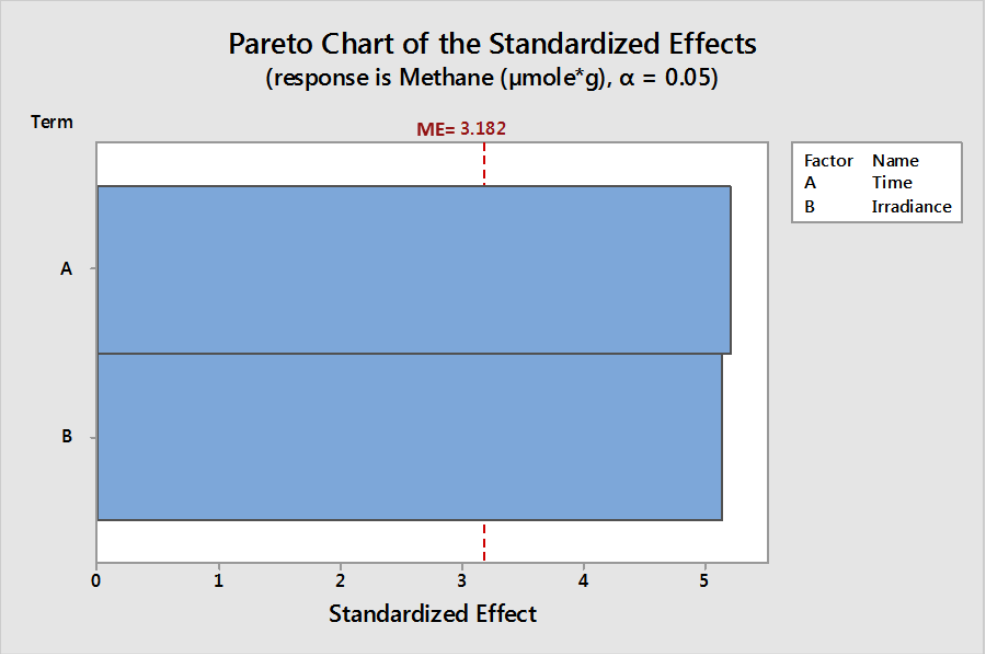

Figure 6.10 Pareto Charts from ANOVA analysis of results from low irradiance DoE tests.

If methane production is plotted in a 3-D space as a function of irradiance and reaction time, all experimental points are set on a plane with a 0.92 R correlation value (Figure 6.11). This indicates that methane production is linearly dependent on both reaction time and irradiance and confirms the independence of these parameters on the final output. This statistical elaboration of experimental data has several implications that clarify the effect of irradiance and time on CO_2 photoreduction process.

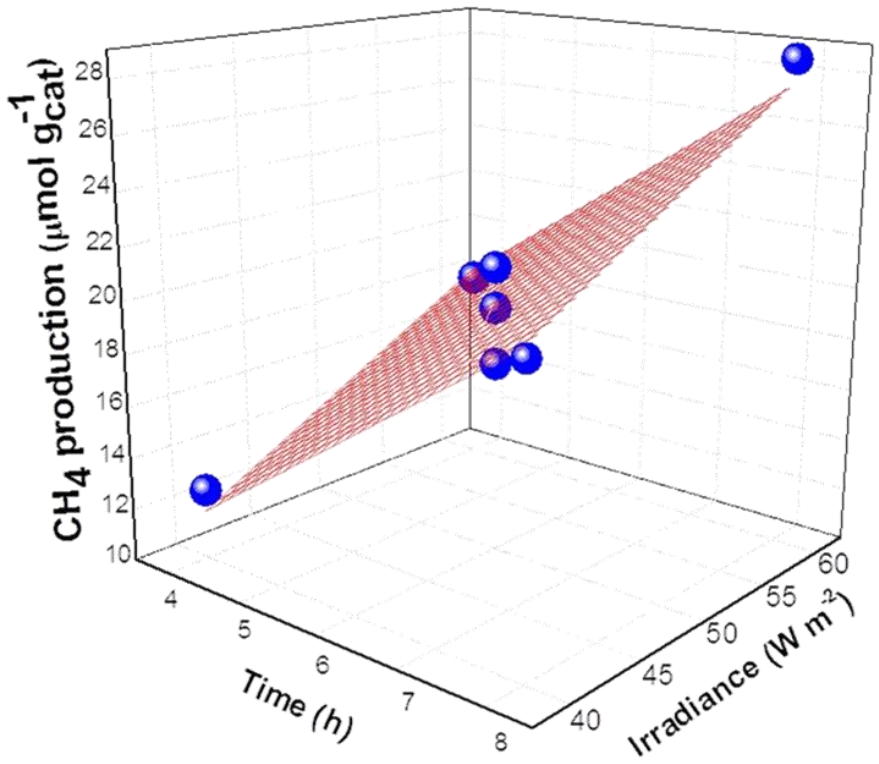

Figure 6.11 3-D plot of methane production vs. time and irradiance.

From these data, methane production is also linearly dependent from irradiance. This evidence is in accordance to general assumptions on photocatalysis reported by Hermann [32]. In fact, for low irradiances, products formation is proportional to photons input, while, for higher irradiances, the increase in recombination rate complicates the overall phenomenon. In the field of photoreduction, this reported result is particularly relevant because, up to now, irradiance effect not have been thoroughly investigated for carbon dioxide photoreduction. In fact, only Tan *et al.* reported the effect of irradiance on methane formation [62]: in their paper, they reported that, between 650 $W \cdot m^{-2}$ and 1800 $W \cdot m^{-2}$, which is a range way higher than the one considered in this part of the work, methane production increased with irradiance, despite growth was not linear and the subject was not further investigated. Therefore, this is the first study that finally assess the effect of irradiance on carbon dioxide photoreduction for methane.

Considering reaction time, it seems that, in the investigated experimental range, methane production linearly increases with time and that any sign of activity loss with time was observed. Confronting these findings with literature, this behaviour is

apparently different to what is generally reported. For instance, Bazzo and Urawaka reported CO_2 photoreduction tests in relatively stressed conditions (80 °C and 150 °C) using a time-resolved mass-spectrometry as a detector and observed that methane production for short reaction times, following further deactivation [63]; similar results were found also by Tan *et al.* [64] and Anpo and co-workers [65]. Therefore, it is probable that experimental range investigated a time region where no (or little) deactivation occurs in investigated experimental range.

Finally, considering that incident photons is a linear function of both reaction time and irradiance (Equation 6.5), the overall effect of primary energetic input on methane formation was considered, as observable in

Figure *6.12*.

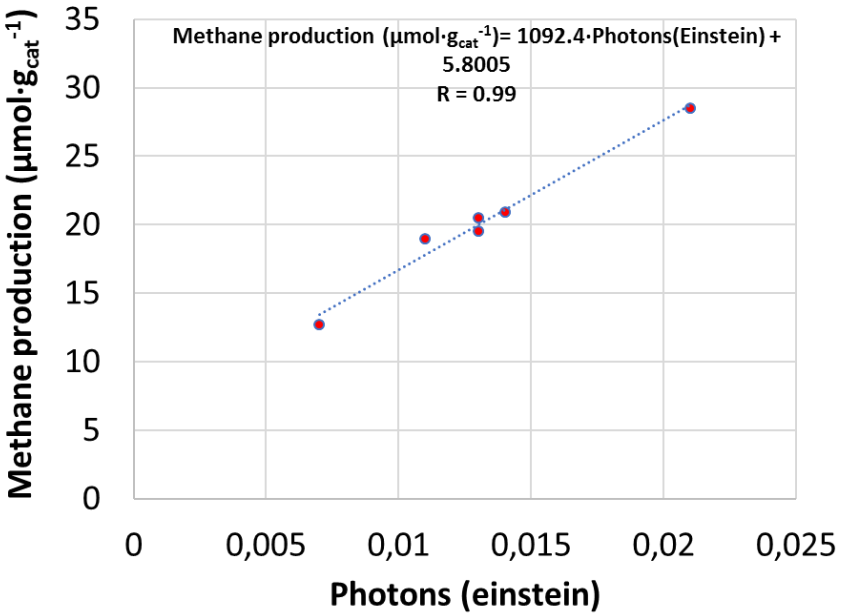

Figure 6.12 Methane production as a function of photons input.

From this graph, it is possible to state that methane production is linearly dependent, as assured by R value from photons input, no matter if irradiance or reaction time is varied. Therefore, to boost methane production by carbon dioxide photoreduction increasing

irradiance and/or lengthening reaction time can be used, opening to different strategies to pursue this aim.

If we consider photon input effect on a wider range of irradiances, the photocatalytic behavior is completely different, as observable in Table 6.7.

Std. Order	***Time (h)***	***Irradiance ($W \cdot m^{-2}$)***	***Methane ($\mu mol \cdot g_{cat}^{-1}$)***
1	1	60	0.004
2	3	60	0.916
3	1	2400	0.024
4	3	2400	0.274
5	2	1200	0.066
6	2	1200	0.085
7	2	1200	0.190

Table 6.7 Experimental points and responses used for factorial design collected in high irradiance conditions.

Looking at statistical analysis of collected data in Pareto chart of Standardised Effects (in Figure 6.13), only time is a statistically significant parameter in carbon dioxide photoreduction under high irradiance. This means that, in the investigated experimental range, photonic input wise, only prolonged reaction times enhance methane production, whereas an irradiance increase does not significantly improve photocatalytic performances. In terms of reaction time, observed trend is similar to what observed in low irradiance conditions and in accordance with literature data

reported by Dimitrijevic *et al.* [66] and already mentioned papers [63-65], who showed an increase in photoactivity with time, though not considering irradiance effect.

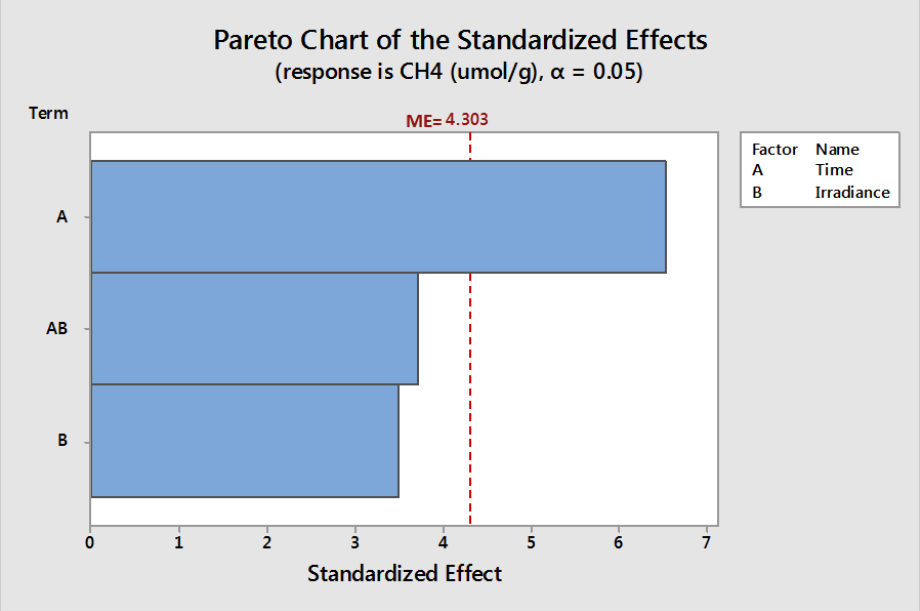

Figure 6.13 Pareto Charts from ANOVA analysis of results from high irradiance DoE tests.

Conversely, obtained results on irradiance effect are completely different from what had been previously observed at low irradiances, where both investigated parameters were significant. This experimental evidence can be explained remembering that a higher number of photons is able to activate all available photocatalytic sites, so, in this way, a further increase in photonic input does not provide an increase in methane formation. In CO_2 photoreduction literature, there is not any paper reporting the effect of irradiance, but some comparisons can be made with more established photooxidative processes. For example, Vorontsov and Dubovitskaya reported that ethanol photocatalytic oxidation rate reached a steady state for high irradiance, thus not being a significant parameter for the process [67]. This phenomenon was also observed by Strini and Schiavi for toluene oxidation [68] and Ching and co-workers for formaldehyde oxidation [69]. From this comparison with available papers on photooxidations, it is possible to sustain proposed explanation for irradiance irrelevance in these conditions, since they allow to saturate photocatalytic surface with photons already.

6.5 Conclusion

Throughout this chapter, it was fully proved that assessing irradiance conditions is fundamental to understand results from photocatalytic carbon dioxide photoreduction, despite lack of concern on this topic by most researchers in this field. In fact, photons represent the primary energetic input and any change in this parameter has an effect on final materials performances.

By available literature references and provided experimental data, it was shown that the same materials, in different rigs, whose most consistent difference is irradiance, behaved in a completely different way giving different results in both activity and products distribution. In fact, the best performing catalyst in low irradiance conditions, namely CuO-$TiO_{2\text{-PREC}}$, proved not to enhance much photoactivity due to improved hydrogenation activity, whereas gold improved significantly photoactivity due to electrons injection in titanium dioxide's conduction band.

Finally, the different effect of photonic input was assessed by design of experiments approach, considering the experimental parameters affecting photons input, i.e. irradiance and reaction time. The effect of these variables proved to be different according to experimental regimes. At low irradiance, where surface is not saturated with photons, both reaction time and irradiance proved to influence significantly methane production, whereas, at high irradiance, due to photonic saturation of the surface, irradiance increase does not affect photocatalytic performances but prolonged time proved to be important still.

6.6 References

[1] S. Das, W. Wan Daud, Renewable and Sustainable Energy Reviews 39 (2014) 765-805.

[2] M. Tahir, N. Amin, Renewable and Sustainable Energy Reviews 25 (2013) 560-579.

[3] S. Kaneco, H. Kurimoto, K. Ohta, T. Mizuno, A. Saji, Journal of Photochemistry and Photobiology A: Chemistry 109 (1997) 59-63.

[4] H. Kawanami, D.C. Grills, T. Ishizaka, M. Chatterjee, A. Suzuki, Journal of CO_2 Utilization 3-4 (2013) 93-97.

[5] P. Richardson, M. Perdigoto, W. Wang, R.J.G. Lopes, Applied Catalysis B. Environmental 132-133 (2013) 408-415.

[6] L. Liu, F. Gao, H. Zhao, Y. Li, Applied Catalysis B: Environmental 134-135 (2013) 349-358.

[7] M. Tahir, N. Amin, Applied Catalysis B: Environmental 162 (2015) 98-109.

[8] S. Sakthivel, M.C. Hidalgo, D.W. Bahnemann, S.U. Geissen, V. Murugesan, A. Vogelpohl, Applied Catalysis B: Environmental 63 (2006) 31-40.

[9] Q.Y. Zhang, Y. Li, E.A. Ackerman, M. Gajdardziska-Josifovska, H.L. Li, Applied Catalysis A: General 400 (2011) 195–202.

[10] M. Hamadanian, A. Rieisi-Vanani, A. Majedi, Materials Chemistry and Physics 116 (2009) 376-382.

[11] V. Trevisan, A. Olivo, F. Pinna, M. Signoretto, F. Vindigni, G. Cerrato, C.L. Bianchi, Applied Catalysis B: Environmental 319 (2014) 61-70.

[12] V. Trevisan, E. Ghedini, M. Signoretto, F. Pinna, Microchemical Journal 113 (2014) 186-189.

[13] J. Ju, X. Chen, Y. Shi, J. Miao, D. Wu, Powder technology 237 (2013) 616-622.

[14] M. Pelaez, N.T. Nolan, S.C. Pillai, M.K. Seery, P. Falaras, A.G. Kontos, P.S.M. Dunlop, J.W.J. Hamilton, J.A. Byrne, K. O'Shea, M.H. Entezari, D.D. Dionysiou, Applied Catalysis B: Environmental 125 (2012) 331-349.

[15] Q. Zhang, T. Gao, J.M. Andino, Y. Li, Applied Catalysis B: Environmental 123-124 (2012) 257-264.

[16] O. Ola, M. Maroto-Valer, Journal of Photochemistry and Photobiology C: Chemistry Reviews 24 (2015) 16-42.

[17] L. Tan, W. Ong, S. Chai, A. Rahman, Chemical Engineering Journal 308 (2017) 248-255.

[18] M. Tahir, N. Amin, Energy Conversion Management 76 (2013) 194-214.

[19] S.E. Braslavsky, A.M. Braun, A.E. Cassano, A.V. Emeline, M.I. Litter, L. Palmisano, V.N. Parmon, N. Serpone, Pure and Applied Chemistry 83 (2011) 931-1014.

[20] S. Malato, J. Blanco, A. Vidal, D. Alarcòn, M.I. Maldonado, J. Càceres, W. Gernjak, Solar Energy 75 (2003) 329-336.

[21] O.K. Varghese, M. Paulose, T.J. LaTempa, C. Grimes, Nano Letters 9 (2009) 731-737.

[22] J.C.S. Wu, H.M. Lin, C.L. Lai, Applied Catalysis A: General 296 (2005) 194-200.

[23] K. Ikeue, H. Yamashita, M. Anpo, Journal of Physical Chemistry B 105 (2001) 8350-8355.

[24] B. Vijayan, N.M. Dimitrijevic, T. Rajh, K. Gray, Journal of Physical Chemistry C 114 (2010) 12994-13002.

[25] T.W. Woolerton, S. Sheard, E. Reisner, E. Pierce, S.W. Ragsdale, F.A. Armstrong, Journal of American Chemical Society 132 (2010) 2132-2133.

[26] M. Tahir, B. Tahir, N. Amin, Applied Catalysis B: Environmental 204 (2017) 548-560.

[27] A. Olivo, V. Trevisan, E. Ghedini, F. Pinna, C.L. Bianchi, A. Naldoni, G. Cruciani, M. Signoretto, Journal of CO_2 Utilization 12 (2015) 86-94.

[28] I. Rossetti, A. Villa, M. Compagnoni, L. Prati, G. Ramis, C. Pirola. C.L. Bianchi, Catalysis Science and Technology 5 (2015) 4481-4487.

[29] B. Michalkiewicz, J. Majewska, G. Kasziolka, K. Bubacz, S. Mozia, A.W. Morawski, Journal of CO_2 Utilization 5 (2014) 47-52.

[30] M. Tahir, B. Tahir, N. Amin, Chemical Engineering Transactions 56 (2017) 319-324.

[31] T.V. Nguyen, J.C.S. Wu, Applied Catalysis A: General 335 (2008) 112-120.

[32] J.M. Hermann, Applied Catalysis B: Environmental 99 (2010) 461-468.

[33] G.E.P. Box, J.S. Hunter, W.G. Hunter, Statistics for experimenters: design, innovation, and discovery, 1st ed. 2005 Wiley New York USA.

[34] J. Antony, Design of Experiments for Engineers and Scientists, 1st ed. Elsevier 2014 Oxford UK.

[35] S.A. Schunk, N. Böhmer, C. Futter, A. Kuschel, E. Prasetyo, T. Roussiere, Catalysis 25 (2013) 172-215

[36] A. Rüfer, W. Reschetilowski, Chemical Engineering Science 75 (2012) 364-375.

[37] V. Calemma, S. Correra, C. Perego, P. Pollesel, L. Pellegrini, Catalysis Today 106 (2005) 282-287.

[38] G. Vicente, A. Coteron, M. Martinez, J. Aracil, Industrial Crops Production 8 (1998) 29-35.

[39] M. Compagnoni, A. Tripodi, I. Rossetti, Applied Catalysis B: Environmental 203 (2017) 899-909.

[40] S.A. Wessman, N.G. Anderson, Organic Process Research & Development 19 (2015) 1605-1633.

[41] S. Delavari, N. Amin, Applied Energy 162 (2016) 1171-1185.

[42] F. Pinna, A. Olivo, V. Trevisan, F. Menegazzo, M. Signoretto, M. Manzoli, F. Boccuzzi, Catalysis Today 203 (2013) 196-201.

[43] Minitab Inc. Official Website: https://www.minitab.com.

[44] A. Corma, H. Garcia, Journal of Catalysis 308 (2013) 168-175.

[45] L. Tan, W. Ong, S. Chai, A. Rahman, Chemical Engineering Journal 308 (2017) 248-255.

[46] S. Protti, A. Albini, N. Serpone, Physical Chemistry Chemical Physics 16 (2014) 19790-19827.

[47] E. Karamian, S. Sharifnia, Journal of CO_2 Utilization 16 (2016) 194-203.

[48] J.M. Hermann, Catalysis Today 53 (1999) 115-129.

[49] A. Dhakshinamoorthy, S. Navalon, A. Corma, H. Garcia, Energy & Environmental Science 5 (2012) 9217-9233.

[50] L. Liu, Y. Li, Aerosol and Air Quality Research 14 (2014) 453–469.

[51] S. Tan, L. Zou, E. Hu, Catalysis Today 115 (2006) 269–273.

[52] S.N. Habitsreutinger, L. Schmidt-Mende, J.K. Stolarczyk, Angewandte Chemie International Edition 52 (2013) 7372-7408.

[53] Y. Izumi, Coordination Chemistry Reviews 257 (2013) 171-186.

[54] J.C.S. Wu, C. Huang, Frontiers in Chemical Engineering in China 4 (2010) 120-126.

[55] Slamet, H.W. Nasution, E. Purnama, S. Kosela, J. Gunlazuardi, Catalysis Communications 6 (2005) 313-319.

[56] J. Ghijsen, L.H. Tjeng, J. van Elp, H. Eskes, J. Westerink, G.A. Sawatzky, M.T. Czyzyk, Physical Reviews B 38 (1998) 11322-11-330.

[57] L. Collado, A. Reynal, J.M. Coronado, D.P. Serrano, J.R. Durrant, V.A. de la Peña O'Shea, Applied Catalysis B: Environmental 178 (2015) 177-185.

[58] S. Neatu, J.A. Macia-Agullò, H. Garcia, International Journal of Molecular Sciences 15 (2014) 5246-5262.

[59] J.Jiao, Y. Wei, Z. Zhao, W. Zhong, J. Liu, J. Li, Catalysis Today 258 (2015) 319-329.

[60] NIST/SEMATECH e-Handbook of Statistical Methods website: https://www.itl.nist.gov/div898/handbook/

[61] M. Hazewinkel, Encyclopedia of Mathematics, 1st ed. Springer 1997 Oxford UK.

[62] L. Tan, W. Ong, S. Chai, A. Rahman, Chemical Engineering Journal 308 (2017) 248-255.

[63] A. Bazzo, A. Urawaka, ChemSusChem 6 (2013) 2095-2102.

[64] J. Tan, Y. Fernàndez, D. Liu, M. Maroto-Valer, J. Bian, X. Zhang, Chemical Physics Letters 531 (2012) 149-154.

[65] M. Anpo, H. Yamashita, Y. Ichihashi, S. Ehara, Journal of Electroanalytical Chemistry 396 (1995) 21-26.

[66] N.D. Dimitrtijevic, B.K. Vijayan, O.G. Poluktov, T. Rajh, K.A. Gray, H. He, P. Zapol, Journal of American Chemical Society 133 (2010) 3964-3971.

[67] A.V. Vorontsov, V.P. Dubovitskaya, Journal of Catalysis 221 (2004) 102-109.

[68] A. Strini, L. Schiavi, Applied Catalysis B: Environmental 103 (2011) 226-231.

[69] W.H. Ching. M. Leung, D.Y.C. Leung, Solar Energy 77 (2004) 129-135.

7. Final remarks

The conversion of carbon dioxide into solar fuels requires a paradigm shift in how this gas is considered: in fact, from an undesired pollutant, it can be turned into a valuable feedstock. Among possible technologies, application of titanium dioxide as a photocatalyst in carbon dioxide photoreduction with water represents a promising strategy since solar radiation can be exploited under mild conditions. Considering the state of the art on this topic, the most representing word for carbon dioxide photoreduction is potential: potential to reduce anthropogenic carbon dioxide emissions, potential to obtain sustainable carbon-based fuels from a renewable source.

Throughout this thesis, from this reaction's physicochemical features, main challenges involved in this process were brought up, providing possible routes to improve the overall effectiveness. Presented work relied on an integrated *catalysis by design* approach, which is still lacking in research on CO_2 photoreduction, covering different expertise areas, focusing, in particular, on materials science for catalyst design and applied engineering to tune reaction conditions. In both cases, two most critical issues were considered, namely poor CO_2 adsorption on TiO_2 and light harvesting.

Titanium dioxide physicochemical properties proved to be a relevant feature for a catalyst: similarly to other processes, high surface area and high crystallinity in anatase phase is beneficial to carbon dioxide photoreduction, as shown in chapter 2 and 3, but it is not sufficient to increase photoactivity. Improvement of carbon dioxide adsorption on the catalyst by material design proved to be particularly intricate to be dealt with: basic alkaline-earth oxides promotion, discussed in chapter 3, proved to be effective yet suppressing photocatalytic activity due to the formation of particularly stable carbonates. Conversely, light harvesting proved to be effective in enhancing photoreduction, as extensively showed in chapter 4. Both copper oxide, a co-catalyst, and gold nanoparticles, an electron trap, improved stability of photocatalytically active electron-hole couples. However, they proved to affect photoactivity differently, leading to either methane or hydrogen as a main product. Observed different behaviour was related to different modification in different selectivity toward either carbon dioxide photoreduction and water splitting side reaction. In addition to that, it was observed

that metal promoters modified carbon dioxide adsorption as well. The potentiality of semiconductors coupling in C-based solar fuels production is a topic that can be addressed in next step of the research toward an efficient CO_2 photoreduction process. In particular the choice of a suitable, reliable and affordable semiconductor to boost photoactivity, selectivity and stability at the same time.

Even if the catalyst is the core of the whole process, reactor design and process conditions heavily affect materials activity: in fact, completely different results were obtained testing the same photocatalysts in different conditions. Considering reaction medium, which was discussed in chapter 5, reaction pathway is profoundly modified. In aqueous systems, fast hydrogenation occurs leading to the production of all oxygenated carbon-based products, whilst in gas phase fast deoxygenation improves selectivity to methane, which is the most desired product. Reactants introduction in gas phase proved to have several advantages, such as low light scattering, high CO_2/H_2O ratio and maximised catalyst exposure to light by its introduction in the reactor as a thin film. Finally, primary energetic input was investigated in chapter 6 and, thanks to design of experiments approach, it proved to affect significantly activity and products distribution, determining different experimental regimes. Variation of energy source by either irradiance or reaction time proved to be a pursuable strategy when irradiance is low, whereas in more stressed conditions, a further increase in photonic input is effective only by lengthening reaction time. Despite efforts and promising results reported in literature and obtained in this thesis, still improvements can be achieved modifying reactor geometry aiming at maximising the contact between the three main components, i.e. photons, catalyst and reagents.

From all these considerations, it is clear that a deep understanding of physicochemical fundamentals of photocatalytic carbon dioxide reduction by water to identify issues to face. From there the complexity of carbon dioxide photoreduction can be challenged by a wide variety of approaches to turn this process into a solid sustainable technology.

8 Acknowledgements

Three years ago, I could not imagine myself at the end of my PhD: in perspective, I think that I have grown tremendously both personally and professionally, but in this journey, I was accompanied by many people, which I would like to acknowledge.

My deep gratitude goes to Prof. Michela Signoretto, for believing in my capabilities from day one, for letting me put my own personal interests into this work and for the tons of chances to do as many activities as I could to gain precious extra-curricular skills, such as in supervising and in tutoring. I would also like to thank her for pushing me hard to become a better scientist and to be more effective in presenting my results. I would like to thank all the scientists that helped me to develop this work: Prof. Giuseppe Cruciani at University of Ferrara for TG/DTA and XRD analysis, Doc. Maela Manzoli at University of Turin for DRS and FTIR analysis and Prof. Ilenia Rossetti and Matteo Compagnoni at University of Milan for photocatalytic tests in liquid phase. My gratitude goes also to Prof. Mercedes Maroto-Valer for hosting me in CICCS group at Heriot Watt University in Edinburgh for high irradiance tests: this was a great opportunity to work in a large multicultural group. Many thanks to fellow students at Heriot Watt, in particular Elizabeth Bay for training me to working with high irradiance photocatalytic rig and Warren Thompson for explaining me the potentialities of DoE.

My overwhelming gratefulness goes to all CATMAT team members. First of all, I'd like to thank Elena for helping me in understanding materials science and finding silver linings even when things got hard. Then I'd like to thank Federica for her precious and constructive criticisms to improve my work. Then Tania for welcoming her every morning and her amazing help in the lab to solve little and big experimental problems. I'd like to thank the other PhD students, hurricane Cristina and Danny, and the newbies in the team, Enrica and Sebastiano for the time spent together and all the B.Sc. and M.Sc. students that worked in the lab with me in these three years.

Finally, I would like to thank my parents for supporting me in my choice to continue my studies without understanding it completely, my sister, my brother in law, my nephew and niece for pushing me to pursue my dreams.

9 Appendix

Curriculum Vitae et Studiorum:

Born in 1988, I obtained my Master *cum laude* in Science in Sustainable Chemistry and Technologies (curriculum: Industrial Chemistry) in March 2014 defending a thesis on the development of promoted carbon dioxide photocatalysts for carbon dioxide photoreduction. From May 2011 to September 2011 I worked as a research fellow at Venice Research Unit of National Interuniversity Consortium of Materials Science and Technology (INSTM) on the formulation of innovative photocatalysts for NO_x oxidation for applications in green building. In 2016, I spent five months at Heriot Watt University (Edinburgh, UK) as a visiting Ph.D. student. Since November 2017, I am Honorary Fellow at Dept. of Molecular Sciences and Nanosystems at Ca' Foscari University of Venice.

During my Ph.D. studies, I also got the chance to serve as laboratory tutor for Industrial Chemistry II course (M.Sc.) and twice for Formulation Technology (B.Sc.) and also to be secondary supervisor of both an undergraduate and a postgraduate student in Sustainable Chemistry and Technologies.

My research interests lie in the study of innovative processes for light utilisation. The core of the work involves solar fuels production by carbon dioxide photoreduction, covering all relevant aspects such as catalysts design, their characterisation and process conditions investigation. More recently, I have got involved in photoreforming to obtain hydrogen from biomass. Beside solar fuels production, I am also interested in the formulation of multifunctional materials for sustainable architecture both for insulation and photocatalytic abatement of environmental pollutants. Research activity results have been proved by papers published on peer-reviewed international journals and contributions presented at national and international congresses.

Awards

Quality of presented research at congresses and conferences was twice awarded:

- Highly commended poster: *The search for the golden age of CO_2 photoreduction*, presented at 4th IMPEE Conference, Edinburgh (UK) 02/09/2016;
- Highly commended poster: *Metal modified TiO_2 for CO_2 photoreduction in unconventional conditions*, presented at NOVACAM Green Catalysis by Design Scientific Meeting, Padua (Italy) 22/02/2017-23/02/2017.

List of Publications

From this thesis, several papers were produced and published on peer-reviewed journals, while few are still under review or in preparation.

- Chapter 1

A. Olivo, D. Zanardo, E. Ghedini, F. Menegazzo, M. Signoretto*, Solar Fuels: from chemical bases understanding to process development,* manuscript in preparation.

- Chapter 2

A. Olivo, V. Trevisan, E. Ghedini, F. Pinna, C.L. Bianchi, A. Naldoni, G. Cruciani, M. Signoretto, *CO_2 photoreduction with water: catalyst and process investigation*, **Journal of CO_2 Utilization** 12 (2015) 86-94.

- Chapter 3

A. Olivo, M.Signoretto, E. Ghedini, *CO_2 Photoreduction to Solar Fuels: Basis Effect on TiO_2 Photocatalysts,* **DGMK Tagungsbericht** 2 (2017) 137-143 (Conference Paper DGMK International Conference on Petrochemistry and Refining in a Changing Raw Materials Landscape; Dresden; Germany; 9 October 2017 through 11; ISBN 978-3-941721-74-6).

- Chapter 4

A. Olivo, E. Ghedini, P. Pascalicchio, M. Manzoli, G. Cruciani, M. Signoretto, *Sustainable carbon dioxide photoreduction by a cooperative effect of reactor design and titania metal promotion*, accepted for **Catalysts** *in press doi:10.3390/catal8010041*.

- Chapter 5

A. Olivo, E. Ghedini, M. Signoretto, M. Compagnoni, I. Rossetti, *Liquid vs. gas phase CO_2 photoreduction process: which is the effect of reaction medium?*, **Energies** 10 (2017) 1394-1407.

- Chapter 6

A. Olivo, E. Ghedini, F. Menegazzo, M. Signoretto, W. Thompson, M. Maroto-Valer, *CO_2 photoreduction in context: process parameters assessment via Design of Experiments*, manuscript in preparation

Other publications from the candidate:

A. Olivo, M. Signoretto, E. Ghedini, F. Pinna, D. Marchese, G. Cruciani, M. Manzoli, *Tuning the Synthetic Parameters to Obtain Smart C-N Co-Doped Titania Photocatalysts for NOx Abatement*, **Chemistry Select** 2 (2017) 728-739.

V. Trevisan, A. Olivo, F. Pinna, M. Signoretto, F. Vindigni, G. Cerrato, C.L. Bianchi, *C-N/TiO_2 photocatalysts: Effect of co-doping on the catalytic performance under visible light*, **Applied Catalysis B: Environmental** 319 (2014) 61-70.

F. Pinna, A. Olivo, V. Trevisan, F. Menegazzo, M. Signoretto, M. Manzoli, F. Boccuzzi, *The effects of gold nanosize for the exploitation of furfural by selective oxidation*, **Catalysis Today** 203 (2013) 196-201.

List of Conferences Proceedings

- Chapter 2

A. Olivo, E. Ghedini, M. Signoretto, F. Pinna, V. Trevisan, G. Cruciani, *Photoreactor design for sustainable carbon dioxide photoreduction*, Proceeding of XIX National Congress of Industrial Chemistry Division of Italian Chemical Society, Salerno (Italy) 14/09/2015 – 17/09/2015

- Chapter 3

A. Olivo, M.Signoretto, E. Ghedini, (2017, October 9-11) *CO_2 Photoreduction to Solar Fuels: Basis Effect on TiO_2 Photocatalysts,* Proceeding of Petrochemistry and Refining in a Changing Raw Materials Landscape DGMK Conference, Dresden (Germany) 09/10/2017 – 11/10/2017

- Chapter 4

A. Olivo, E. Ghedini, M. Singoretto, M. Compagnoni, I. Rossetti, *Metal modified TiO_2 for CO_2 photoreduction in unconventional conditions*, Proceeding of NOVACAM Green Catalysis by Design Scientific Meeting, Padua (Italy) 22/02/2017-23/02/2017

- Chapter 5

A. Olivo, M. Signoretto, E. Ghedini, M. Manzoli, I. Rossetti, M. Maroto-Valer, *CO_2 photoreduction in context: catalyst modification and reaction condition investigations*, Proceeding of Catalysis: Fundamentals and Practice Summer School, Liverpool (UK) 17/06/2018 – 21/07/2017

M. Compagnoni, A. Olivo, F. Galli, A. Villa, C. Pirola, L. Prati, M. Signoretto, N. Dimitratos, I. Rossetti, *CO_2 Photoconversion to Fuels and Chemicals under High Pressure*, Proceeding of 6th EuChemMS Chemistry Congress, Seville (Spain) 11/09/2016-15/06/2016

- Chapter 6

A. Olivo, E.R.B. Bay, E. Sanchez Fernandez, W. Thompson, M. Maroto Valer, E. Ghedini, M. Signoretto, *The search for the golden age of CO_2 photoreduction*, Proceeding of 4th IMPEE Conference, Edinburgh (UK) 02/09/2016

A. Olivo, M. Signoretto, E.R.B. Bay, W.A. Thompson, M. Maroto-Valer, *CO_2 conversion to solar fuels: importance of reaction conditions for significant assessment of photocatalytic performances*, Proceeding of EUROPACAT 2017, Florence (Italy) 27/08/2017-31/08/2017

M. Signoretto, A. Olivo, M. Manzoli, I. Rossetti, M. Maroto-Valer, *Looking at the bigger picture in carbon dioxide photoreduction*, Proceeding of XXVI Congresso Nazionale della Società Chimica Italiana, Paestum (Italy) 10/09/2017 – 14/09/2017

Other conference proceedings from the candidate:

- S. Tieuli, M. Signoretto, E. Ghedini, A. Olivo, *ELPIS- Enhancement of Lignocellulose Processing for Innovation and Sustainability*, Proceeding of 17th Edition of Merck Young Chemists Symposium (MYCS), Milano Marittima (Italy) 13/11/2017 – 15/11/2017

- D. Zanardo, M. Signoretto, A. Olivo, G. Cruciani, *CuO promoted TiO_2 catalysts for ethanol photoreforming*, Proceeding of 17th Edition of Merck Young Chemists Symposium (MYCS), Milano Marittima (Italy) 13/11/2017 – 15/11/2017

- A. Olivo, M. Signoretto, E. Ghedini, G. Cruciani, A. Di Michele*, Innovative multifunctional TiO_2-SiO_2 materials for green building*, Proceeding of Advanced inorganic materials: green and unconventional synthesis approaches and functional assessment, Padua (Italy) 08/09/2017

- E. Ghedini, M. Signoretto, A. Olivo, G. Cruciani, M. Manzoli, A. Di Michele, High *Surface Area TiO_2-SiO2 catalysts: a multifunctional and environmentally friendly material for building applications*, Proceeding of EUROPACAT 2017, Florence (Italy) 27/08/2017-31/08/2017

- E. Sanchez Fernandez, W. Thompson, X. Luo, E. R. B. Bay, A. Olivo, M. Maroto-Valer, *The impact of kinetics on catalysts benchmarking in CO_2 photoreduction*, 15th International Conference on Carbon Dioxide Utilization, Shanghai (China) 17/07/2017-21/07/2017

- A. Olivo, E.R.B. Bay, W. Thompson, E. Sanchez Fernandez, E. Lesnik, X. Luo, M. Maroto-Valer, *Solar Fuels from Photocatalytic Reduction of CO_2 via Engineering Innovation*, Proceeding of CRITICAT Advanced Photocatalysis, Edinburgh (UK) 12/12/2016-13/12/2016

- A. Olivo, E.R.B. Bay, W. Thompson, E. Sanchez-Fernandez, M. Maroto-Valer, R. Trofimovaite, S. Kumar, A.F. Lee, *Solar Fuels from Photocatalytic Reduction of CO_2 via Engineering Innovation*, Proceeding of 14th International Conference on Carbon Dioxide Utilisation, Sheffield (UK) 11/09/2016-15/06/2016

- D. Marchese, E. Ghedini, A. Olivo, M. Signoretto, *Innovative and sustainable multifunctional materials for green building industry*, Proceeding of XIX National Congress on Catalysis, Bressanone (Italy) 11/06/2016-14/09/2016

- M. Manzoli, A. Olivo, E. Ghedini, G. Cruciani, M. Signoretto, *An effective one-pot synthesis for C-N co-doped titania photocatalysts for NO_x abatement*, Proceeding of XIX National Congress on Catalysis, Bressanone (Italy) 11/06/2016-14/09/2016

- W. Thompson, E.R.B. Bay, E. Sanchez Fernandez, M. Maroto Valer, A. Olivo, *Reactor design, kinetics and process optimization towards solar fuels*, Proceeding of 4th IMPEE Conference, Edinburgh (UK) 02/09/2016

- F. Menegazzo, A. Olivo, M. Signoretto, F. Pinna, M. Manzoli, *Selective oxidations of biomass resources on Au/ZrO_2 catalysts doped by sulphates*, Proceeding of XIX National Congress of Industrial Chemistry Division of Italian Chemical Society, Salerno (Italy) 14/09/2015 – 17/09/2015

- A. Olivo, M. Signoretto, V. Trevisan, E. Ghedini, G. Cruciani, *Sustainable approach for visible light active titania photocatalysts for NO_x abatement*, Proceeding of VI Workshop Nazionale AICing, Rome (Italy) 22/06/2015-23/06/2015

- A. Olivo, M. Signoretto, V. Trevisan, E. Ghedini, G. Cruciani, *Innovative and sustainable synthesis for C-N-doped titania photocatalysts for NO_x removal under visible light*, Proceeding of 6th Czech-Italian-Spanish Conference on Molecular Sieves and Catalysis, Amantea (Italy) 14/07/2015-17/07/2015

- V. Trevisan, M. Signoretto, A. Olivo, E. Ghedini, F. Pinna, A. Naldoni, *CO_2 photoreduction via promoted titania photocatalysts*, Proceeding of Italian Photochemistry Meeting 2014, Abbiategrasso (Italy) 27/11/2014-29/11/2014

- V. Trevisan, F. Pinna, M. Signoretto, E. Ghedini, A. Olivo, G. Cruciani, *Nanostructured titania as an efficient material for organic and inorganic pollutants abatement*, Proceeding of NanotechItaly 2014 International Conference, Venice (Italy) 26/11/2014-28/11/2014

- E. Ghedini, M. Signoretto, A. Olivo, V. Trevisan, F. Pinna, C. Guerretta, *Chitosan Assisted Synthesis of Efficient TiO_2 photocatalysts*, Proceeding of NanotechItaly 2014 International Conference, Venice (Italy) 26/11/2014-28/11/2014

- A. Olivo, M. Signoretto, V. Trevisan, E. Ghedini, F. Pinna, C.L. Bianchi, A. Naldoni, *CO_2 to fuels via N and Cu co-doped titania photocatalysts*, XXV Congress of Italian Chemical Society, Rende (Italy) 07/09/2014-12/09/2014

- F. Pinna, A. Olivo, V. Trevisan, F. Menegazzo, M. Signoretto, M. Manzoli, F. Boccuzzi, *The effects of gold nanosize for the exploitation of furfural by selective oxidation*, Proceeding of EUROPACAT X, Glasgow (UK) 28/08/2011-02/09/2011

Abstract

Student	*Alberto Olivo*	**Ph.D. Course**	*Chemistry*
Registration No.	s225440	**Cycle**	*XXX*

Title: *Development of titanium dioxide based photocatalytic systems for CO_2 photoreduction*

Abstract: In this thesis, different aspects related to carbon dioxide photoreduction with water, focusing are discussed, focusing in particular on the two most important issues: catalyst design and reaction conditions investigation.

On one side, catalyst formulation was considered and several titanium dioxide based materials were synthesised by different techniques to tune physicochemical properties. Considering reaction mechanism, modifications on this material were performed aimed at improving carbon dioxide adsorption introducing alkali-earth oxides on catalytic surface, reaching total selectivity to methane avoiding water splitting side reaction. Furthermore, to lengthen electron-hole life on titania surface, metal promotion was investigated introducing, in one case, copper oxide as a co-catalyst and, in the other, gold nanoparticles for their plasmon resonance properties. In this way, it was possible to obtain an increase in photoactivity and a modification in products distribution, which was explained by an in-depth characterisation by a wide range of analytical techniques.

On the other side, reaction conditions effect was investigated. Titanium dioxide effectiveness in CO_2 photoreduction in gas phase was increased by three orders of magnitude developing a thin film reactor which maximised light harvesting providing promising results even in mild conditions. Furthermore, developed materials were tested in different photocatalytic systems to investigate the effect of experimental conditions. Reaction medium proved to be an important feature: in fact, performing CO_2 photoreduction in liquid phase using the same catalysts provided a much wider products distribution, indicating a strong effect on reaction mechanism and products distribution as a consequence. Finally, reaction was performed in high irradiance conditions and, by a design of experiments approach, the effect of irradiance and reaction time differs according to experimental regime was assessed.

Titolo: *Sviluppo di sistemi fotocatalitica a base di biossido di titanio per la fotoriduzione di CO_2*

Abstract: In questa tesi, vengono approfonditi gli aspetti salienti riguardanti la fotoriduzione di CO_2, ponendo particolare attenzione sui due più importanti: lo sviluppo del catalizzatore e lo studio delle condizioni di reazione.

Da un lato, è stata considerata la formulazione del catalizzatore e, attraverso diversi approcci sintetici, sono stati sintetizzati diversi campioni di biossido di titanio, in modo tale da modulare le loro proprietà chimico-fisiche. Considerando attentamente il meccanismo di reazione, i materiali sono stati modificati per migliorare l'assorbimento di CO_2 introducendo ossidi alcalino-terrosi sulla superficie catalitica, ottenendo una selettività totale a metano ed evitando la reazione parallela di *water splitting*. Inoltre, per allungare il tempo di vita della coppia buca-elettrone sulla superficie del catalizzatore, è stata studiata la promozione con metalli introducendo, in un caso, ossido di rame come co-catalizzatore e, nell'altro, nanoparticelle di oro per le loro proprietà di risonanza plasmonica. In questo modo, è stato possibile incrementare l'attività fotocatalitica e modificare la distribuzione dei prodotti, che è stata spiegata attraverso un'approfondita caratterizzazione utilizzando numerose tecniche analitiche.

D'altra parte, è stato approfondito l'effetto delle condizioni di reazione. Lo sviluppo di un reattore a film sottile ha migliorato l'irraggiamento del catalizzatore, incrementando l'efficienza del biossido di titanio nella fotoriduzione di CO_2 in fase gas di tre ordini di grandezza, con risultati promettenti anche in condizioni blande. Inoltre, i materiali sviluppati sono stati testati in diversi impianti fotocatalitici per valutare l'effetto delle condizioni di reazioni, ovvero il mezzo di reazione (fase liquida e fase gas) e l'input energetico (bassa e alta irradianza). È stato osservato che il mezzo di reazione riveste particolare importanza: infatti nei test in fase liquida, con gli stessi fotocatalizzatori, è stata osservata una distribuzione di prodotti più ampia rispetto alla fase gas, indicando che la reazione procede attraverso due distinti meccanismi di reazione. Infine, l'effetto dell'energia luminosa incidente è stato valutato, attraverso l'approccio del *design of experiments*, il quale ha permesso di stabilire il diverso effetto di tempo di reazione ed irradianza sul processo.